INVESTIGATING THE INTERPLAY BETWEEN CHROMOSOME AXES AND HOMOLOGOUS RECOMBINATION IN *ARABIDOPSIS* MEIOSIS

by

CHRISTOPHE LAMBING

A thesis submitted to

The University of Birmingham

for the degree of

DOCTOR OF PHILOSOPHY

School of Biosciences

University of Birmingham

March 2014

UNIVERSITY OF BIRMINGHAM

University of Birmingham Research Archive

e-theses repository

Abstract

During meiosis and mitosis, the chromatin is organised stochastically in loop arrays. The formation and stabilisation of chromatin loop arrays is dependent on both cohesin and condensin but independent on the presence of a chromosome axis. The meiotic chromosome axes differ significantly from the mitotic axes. Components of the meiotic chromosome axes are thought to localise on the chromatin during S-phase and G2 in budding yeast and *Arabidopsis*, respectively, and promote the formation of meiotic DNA double-strand breaks (DSBs). In addition, several evidences suggest that the chromosome axes are required for the repair of SPO11-dependent DSBs off the sister. The status of the meiotic axes may also have an important role in the designation of future crossover sites and crossover interference. However, the composition of the chromosome axes, the regulation of its morphology and its function during meiosis are poorly understood in plants.

The aims of this study consisted at further investigating the function of the axis-associated protein AtASY1 during DSB formation and DSB repair. The interaction between AtASY1 and the structural axis component AtASY3 was tested. In addition, the interplay between chromosome axes and the localisation of the AtSPO11-accessory protein AtPRD3 was analysed. This study showed that the formation of meiotic DSBs is spatially and temporally regulated by the formation of a nascent axis in *Arabidopsis*. The formation of the axes was independent on the formation of DSBs. However, the repair of DSBs off the sister and the formation of inter-homologue crossovers led to the remodelling of the axes in a pathway dependent on AtPCH2, an AAA ATPase family member. In addition, the phosphorylation level of AtASY1 T295 was increased in response to DSB formation. These highlight the coordination between the formation of DSBs/progression of DSB repair by homologous recombination and the remodelling of the chromosome axes.

Acknowledgements

I would like to thank my supervisor Professor Chris Franklin for giving me the opportunity to conduct this project and for guiding me throughout my PhD.

I would like to thank Doctor Sue Armstrong for helping me with the cytology.

I would like to thank James, Kim and Elaine for their support and help. I also would like to thank Steve and Karen for their technical support throughout the program of my PhD and all members of the laboratory for their kindness. I also would like to thank the Biotechnological and Biological Sciences Research Council (BBSRC) for supporting my PhD.

I would especially like to thank my family for their love.

List of contents

Chapter 1

Introduction

Chapter 3

AtASY1 physically interacts with the coiled-coil domain of AtASY3 to form a

List of figures

List of tables

Chapter 1

Introduction

1.1. Overview of meiosis

Meiosis is a key event essential for all sexually reproducing organisms. During meiosis, each chromatid is duplicated to form an identical sister chromatid during a single round of DNA replication. This is followed by two successive rounds of chromosome segregation defined as meiosis I and meiosis II, respectively. The outcome of meiosis I is a reductional division where homologous chromosomes segregate towards opposite poles of the mother cell resulting in the reduction by two of the number of chromosomes present in the sister cells. In contrast, the outcome of meiosis II is an equational division characterized by the loss of sister chromatid cohesion at the centromeres and the segregation of sister chromatids towards opposite poles of the cell. Meiosis occupies a central role in sexual reproduction among most eukaryotes by halving the chromosome content in the eggs and sperm cells. During fertilisation, the egg and sperm cells fuse, restoring the diploid content of the cell. The halving of chromosome in gametes is essential to prevent the doubling of chromosomal material in the zygote during each generation, which would be deleterious for the cell (Roeder, 1997; Zickler & Kleckner, 1998).

Meiosis shares some biochemical features with mitosis such as the presence of a single round of DNA replication during S-phase and the use of spindle fibres to move the chromosomes towards opposite poles of the cell (Figure 1.1). The observation of similar features between mitosis and meiosis led to the hypothesis that meiosis evolved from mitosis during evolution (Cavalier-Smith, 2002; Wilkins & Holliday, 2009). However, meiosis is a more complex type of cell division than mitosis and has key additional characteristics. Among them, the homologous chromosomes pair and recombine, the sister

chromatid cohesion is maintained at the centromere during the first meiotic cell division until anaphase II and the absence of DNA replication and cytokinesis between the first and second meiotic cell divisions (Figure 1.2) (Cavalier-Smith, 2002; Wilkins & Holliday, 2009).
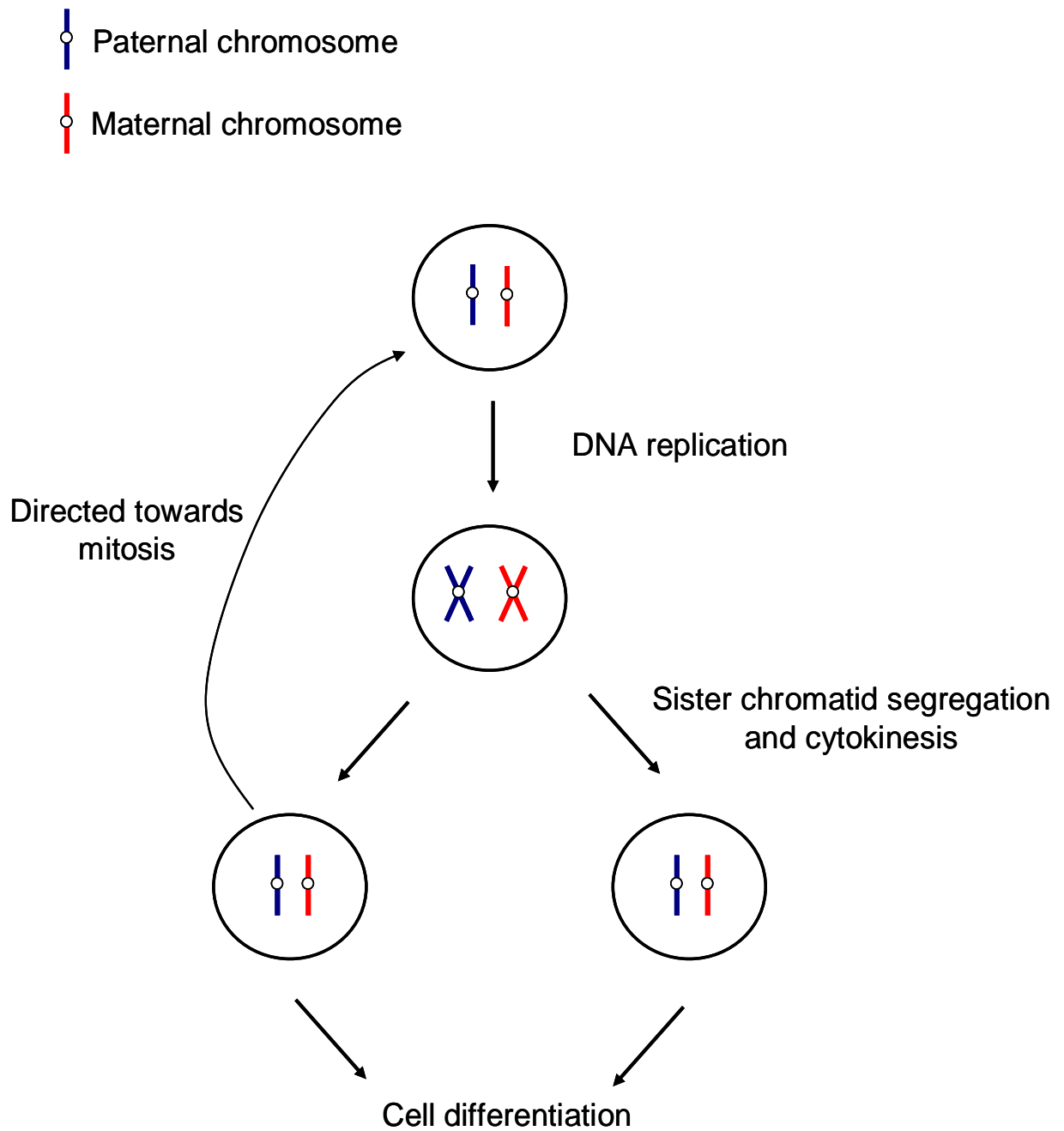
Figure 1.1. Schematic representation of mitosis.

Cells entering mitosis have their DNA replicated during S-phase. Loss of sister chromatid cohesion and segregation of sister chromatids towards opposite poles of the cells are observed during anaphase. Then, cytokinesis occurs with the formation of two diploid daughter cells. The daughter cells can either enter a new mitotic cycle or become differentiated. Centromeres are represented by a white circle.
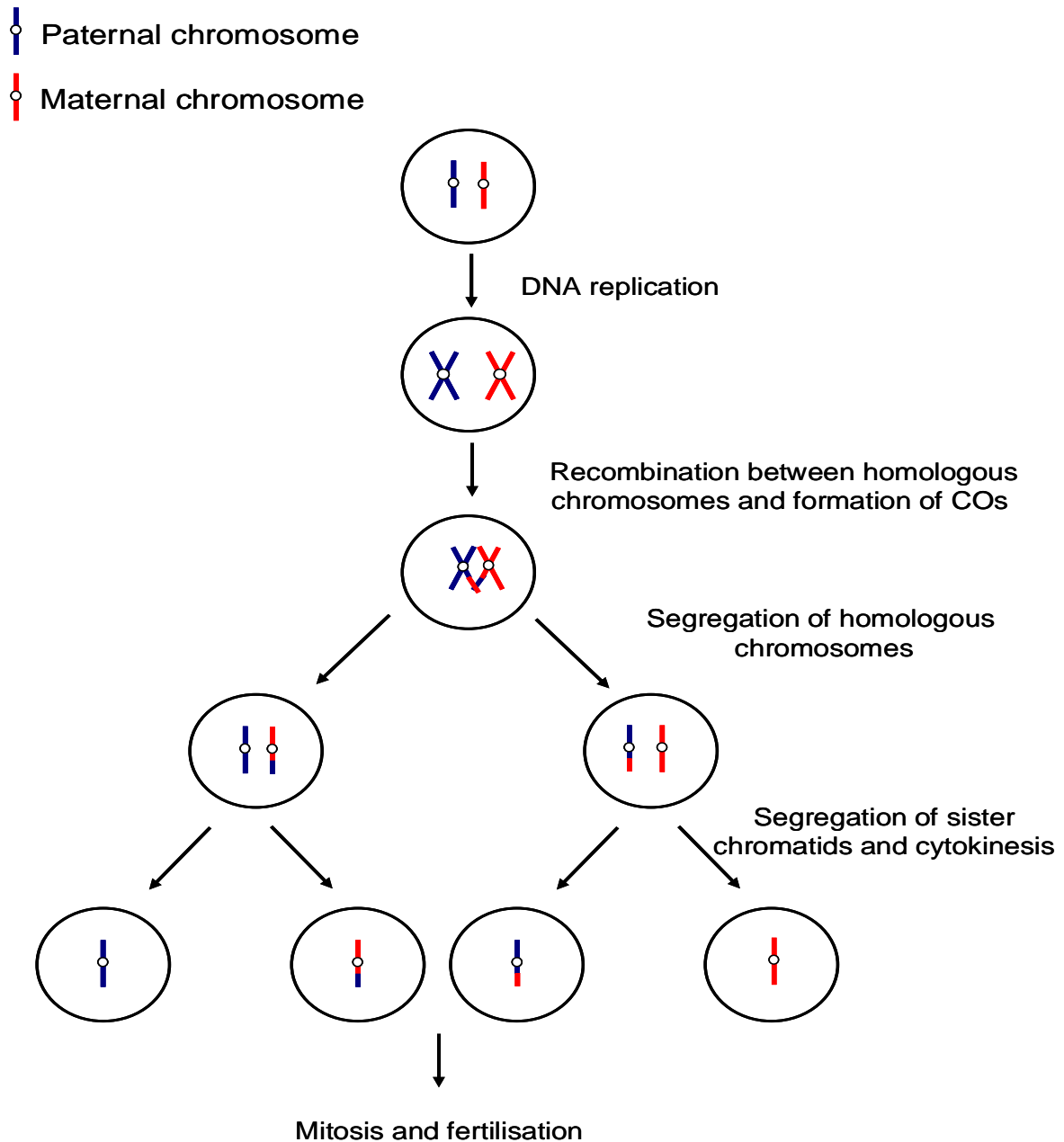
Figure 1.2. Schematic representation of meiosis.

Following replication of the DNA content, homologous chromosomes undergo a reciprocal exchange of genetic information, also called a crossing-over (CO). The resolution of COs is followed by two rounds of chromosome segregation resulting in the formation of four haploid gametes. Each gamete will then undergo mitosis and some gametes will be involved in fertilisation.

Meiosis is thought to have originated in an ancestor lineage of eukaryotes and has been maintained in most of the eukaryotes. The primarily advantage of the origin of meiosis probably relies on the requirement for the ancestor lineage of eukaryotes to possess a biological response towards adverse environmental conditions and the formation of highly toxic DSBs. By inducing meiosis, the ancestoral lineage of eukaryotes could repair the DSBs by using the genetic information present on the homologous chromosome. The maintenance of meiosis in eukaryotic cells is probably related to the evolution of sexual reproduction. Meiosis presents several advantages for sexually reproducing organisms. The reciprocal exchange of a portion of DNA molecules between homologous chromosomes favours the genetic diversity of species. Budding yeast and fission yeast induce meiosis in response to stress such as nitrogen starvation (Kassir et al, 1988; Strudwick et al, 2010; Yamamoto, 1996a; Yamamoto, 1996b). The induction of meiosis in response to adverse environmental changes results in the reshuffling of genes, an increase of the genetic diversity and potentially, an increase in the survival rate of the progeny. In addition, the maintenance of sexual reproduction in most eukaryotes has the advantage that it limits the spreading of deleterious traits to the offspring compared to asexual eukaryotic cells (Solari, 2002; Wilkins & Holliday, 2009).

The basic understanding of meiosis in model organisms such as the plant *Arabidopsis thaliana* is essential to transfer the knowledge to crop species and eventually to modulate meiosis in economically important crops. For instance, moderating the distribution of reciprocal DNA exchange between the parental chromosomes could help adapting new varieties that are more sustainable to climate change. In addition, controlling the distribution of genetic exchange between homologous chromosomes is essential for plant

breeders when new traits are introduced in crops. During breeding of crops, the introduction of desirable traits is often accompanied by the integration of undesirable segment of DNA in the host genome by a mechanism called linkage drag. By modulating the distribution or increasing the genetic exchange between homologous chromosomes, it could be possible to remove more rapidly the undesirable DNA fragment from the crop genome.

1.2. Meiotic stages in *Arabidopsis thaliana*

Improvement in chromosome-spreading procedure combined with the development of fluorescence microscopes facilitated the analysis of chromosome morphogenesis in meiotic cells. Meiosis is composed of a meiotic interphase followed by two rounds of chromosome segregation called meiosis I and meiosis II. Meiosis I and meiosis II can be cytologically divided into four stages: prophase, metaphase, anaphase and telophase. The meiotic duration from S-phase onward was estimated at 34 hours in *Arabidopsis thaliana* (Armstrong et al, 2003). Prophase I is the predominant stage of meiosis with a duration estimated at 22-23 hours. Prophase I is an essential and very dynamic stage were homologous chromosome pair, synapse and recombine. Therefore, prophase I was divided into five sub-stages: leptotene, zygotene, pachytene, diplotene and diakinesis based on cytological observations of chromosome spreading of pollen mother cells (PMCs) and embryo-sac mother cells (EMCs) in *Arabidopsis*. The development of PMCs and EMCs is fairly synchronous in anthers and ovules and is linked to the development of the female reproductive organ of a flower (Armstrong & Jones, 2003; Ross et al, 1996).

7

1.2.1. Interphase

Meiotic interphase is composed of an unreplicated G1-phase followed by S-phase and G2-phase. During meiotic S-phase, the DNA content of the cell is replicated and each chromosome will consist of two sister chromatids after replication. DNA synthesis occurs concomitantly with the establishment of cohesin between sister chromatids. The duration of meiotic S-phase is significantly extended compared to mitotic S-phase in plant and yeast (Armstrong et al, 2003; Cha et al, 2000; John, 1990). Meiotic cells in G1-, S- and G2-phase have a similar appearance with the presence of a large nucleolus and a size bigger than the surrounding somatic cells (Armstrong & Jones, 2003). G1 cells have a more condense pericentromeric heterochromatin compared to S and G2 cells. In addition, G2 cells present short stretches of chromosome thread that may correspond to the formation of the meiotic chromosome axes as suggested by chromosomes staining and immunocytochemistry studies using an antibody raised against the axis-associated protein AtASY1 (Figure 1.3A) (Armstrong & Jones, 2003; Sanchez-Moran et al, 2007b; Zickler & Kleckner, 1998).
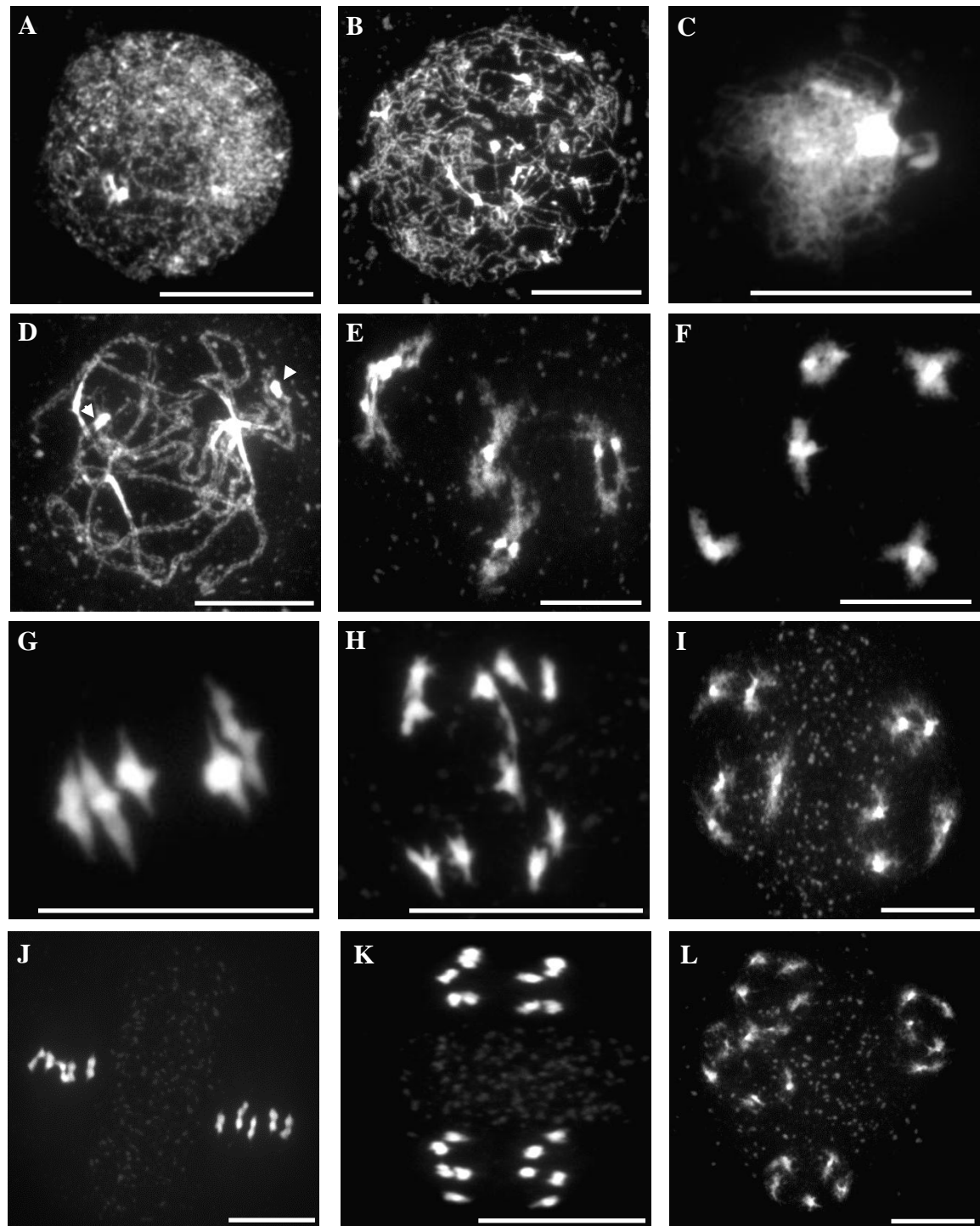
Figure 1.3. Meiotic stages from *Arabidopsis* pollen mother cells.

(A) G2, (B) leptotene, (C) zygotene, (D) pachytene, (E) late diplotene, (F) diakinesis, (G) metaphase I, (H) anaphase I, (I) dyad, (J) metaphase II, (K) anaphase II, (L) tetrad. Nuclei are stained using DAPI (blue). Note the nucleolus organizer regions (arrowheads). Scale bar, 10 μM.

1.2.2. Early to mid-prophase

G2-leptotene transition is characterized by the extension of the chromosome axes that will ultimately mark the entire chromosomes length. The pericentromeric heterochromatin regions are more condensed and both centromeres and nucleolus organizer regions (NORs) are visualised with the presence of 4, 6-diaminido-2-phenylinidole (DAPI)-bright stains (Figure 1.3B,D). The nucleolus forms a large structure in the centre of the nucleus and will progressively move towards the nuclear periphery at the end of leptotene. At this stage, the centromeres are dispersed in the nucleus while the telomeres are clustered and associated with the nucleolus (Armstrong et al, 2001; Armstrong & Jones, 2003; Da Ines et al, 2012; Ross et al, 1996). At zygotene, chromosomes are polarized and clumped towards one side of the nucleus (Figure 1.3C). Homologous chromosomes start to synapse and the formation of the synaptonemal complex (SC) initiates, as suggested by the thicker staining of the chromosome threads and immunocytochemistry study using an antibody raised against the SC transverse filament AtZYP1 (Higgins et al, 2005). The telomeres lose their nucleolus association and the pericentromeric heterochromatin aggregate into a variable number of clumps (Armstrong et al, 2001; Armstrong & Jones, 2003). At pachytene, homologous chromosomes are shorter, fully synapsed and form a double structure along the entire chromosomes (Figure 1.3D).

1.2.3. Late prophase and beyond

At the onset of diplotene, the chromatin is more diffuse and the homologous chromosomes progressively separate from each other apart from the site of COs. A CO is defined when

two homologous chromosomes have reciprocally exchanged genetic information. Formation of a CO can be cytologically visualised on chromosomes as a discrete structural connection between two chromosomes and is called a chiasma. COs have an important impact on the genetic diversity of species by generating new combination of parental alleles. In addition, COs together with sister chromatid cohesion are essential to physically connect homologous chromosomes until the onset of anaphase I (Buonomo et al, 2000; Kudo et al, 2006; Lacefield and Murray, 2007; Sanchez Moran et al, 2001). At late diplotene, homologous chromosomes gradually condense to form five discrete bivalent structures. The centromeres are unpaired (Da Ines et al, 2012) and each chromosome presents a prominent pericentromeric heterochromatin block. The two *Arabidopsis* acrocentric chromosomes, chromosomes 2 and 4, are often observed associated by their NORs (Figure 1.3E). At diakinesis, the condensation and shortening of the bivalents is more pronounced (Figure 1.3F). During metaphase I, the five bivalents are co-oriented on the spindle and the homologous centromeres are directed towards opposite poles. Each bivalent contains between one and three chiasmata. Cytoplasmic organelles are excluded from the spindle (Figure 1.3G). During anaphase I, the cohesion between homologous chromosomes is lost and the homologous chromosomes are migrating towards opposite poles of the cell. The presence of cohesin at the centromeric regions maintains the cohesion between sister chromatids (Figure 1.3H). Telophase I is characterised by the presence of two polar groups of five condensed chromosomes that will partially decondense during dyad stage. At this stage, the two polar groups of chromosomes are separated by a band of cytoplasmic organelles (Figure 1.3I). The transition between meiosis I and meiosis II is rapid and characterised by the absence of DNA replication and cytokinesis. During prophase II, the five chromosomes present in each polar group

progressively condense until metaphase II. At this stage, the chromosomes are very condensed and individual chromosomes are aligned on the metaphase II spindle (Figure 1.3J). At anaphase II, the cohesion maintaining the association between the sister chromatids at the centromeric regions is lost and the sister chromatids migrate towards opposite poles of the cell (Figure 1.3K). At late anaphase II-early telophase II, four polar groups of chromosomes within a common cytoplasm are visualised. Finally, cytokinesis occurs and the cytoplasm becomes partitioned and a tetrad of four haploids gametes is formed (Figure 1.3L) (Armstrong & Jones, 2003; Ross et al, 1996).

1.3. Homologous recombination pathway

The formation of DSBs can be deleterious for the cell and they need to be accurately repaired. The repair of DSBs depends on the stage of the cell. DSBs formed during G0/G1 are predominantly repaired by non-homologous-end-joining pathway while the formation of programmed DSBs during meiosis activates the homologous recombination pathway (Goedecke et al, 1999; Lemmens et al, 2013). The homologous recombination pathway has been studied in several model organisms and the biochemical steps described from budding yeast studies are likely similar across species (Figure 1.4) (Grabarz et al, 2012; Mimitou & Symington, 2011; Osman et al, 2011).

ds DNA

ds DNA

DSB formation
AtSPO11-1/2, AtPRD1/2/3/4, AtDFO

5' end resection
AtMRE11, AtRAD50, AtNBS1, AtCOM1

Single strand DNA invasion
AtRAD51, AtDMC1, AtRAD51C, AtXRCC3
AtMND1, AtHOP2

Synthesis-dependent strand annealing

Homologous recombination and formation of double Holliday junctions

3' end extension

3' end extension

D-loop dissociation

D-loop stabilization, further 3' end extension
AtRFC1, AtMSH4/5, AtMER3, AtMLH1/3, AtRPA1, AtZIP2/3/4

Annealing

Second end capture, formation of dHJs

Formation of hemi-catenate intermediate, dHJ resolution
AtRMI1, AtTOP3a
AtFANCM, AtMUS81, AtEME1

dHj resolution
AtMLH1/3?

DNA synthesis and ligation

NCO

NCO

CO

Figure 1.4. Schematic representation of the meiotic homologous recombination pathway. Homologous recombination initiates by the formation of DSBs. The 5' ends of the DSBs are then resected prior to the loading of RAD51/DMC1 recombinases to form the presynaptic nucleofilament. The presynaptic nucleofilament can then invade the homologous chromosome to form a displacement-loop (D-loop) structure. The D-loop can either be dissociated or stabilised. Unstable D-loop will release the invading 3' single-stranded DNA (ssDNA) which can anneal with the sister chromatid to form a non crossover (NCO) by the SDSA pathway. In contrast, stable D-loop undergoes DNA synthesis, second-end capture and dHJ formation. dHJs can either be resolved to form a crossover (CO) or a NCO. Orange circles represent SPO11 protein covalently bounds to the DSB ends.

1.3.1. SPO11-dependent DSB formation initiates meiotic recombination

In all sexually reproducing organisms, meiotic recombination events are initiated by the formation of programmed-DSBs that are thought to be catalysed by the topoisomerase II-like transesterase SPO11 protein. SPO11 is a well conserved protein among lower and higher eukaryotes and shares homology with the catalytic subunit A of the archaeal topoisomerase VI from *Sulfolobus shibatae* (Bergerat et al, 1997; Grelon et al, 2001; Yu et al, 2010). So far it has not been possible to purify a functionally active form of SPO11 and hence not possible to assess the putative enzymatic activity of the protein. However, several studies suggest that SPO11 protein cleaves DNA in a topoisomerase-like transesterification reaction to form DSBs. Topoisomerases are involved in the change of topology of closed DNA molecules by forming an ATP-dependent transient DSB (Keeney, 2008). The DSB is formed by transesterification of a conserved tyrosine residue of the topoisomerase to the DNA phosphodiester backbone and the topoisomerase becomes covalently linked to the DNA end after reaction (Bergerat et al, 1997; Keeney, 2008). The DNA break repair function, which resides in the subunit B of the type VI topoisomerase, seems to be missing in SPO11 protein but the DSB activity is present (Hartung & Puchta, 2000). Keeney *et al.* (1997) first identified SPO11 as a protein covalently attached to unresected DSB ends in *rad50* budding yeast mutant (Keeney et al, 1997). This indicates that the protein may have a biochemical function similar to topoisomerase rather than having a hydrolytic cleavage activity towards DNA molecules (Cole et al, 2010). More recently, two other studies showed that mice (Neale et al, 2005) and fission yeast (Milman et al, 2009) SPO11 orthologues were also found covalently attached to unresected meiotic DSB ends. In addition, a conserved tyrosine residue found in SPO11 proteins from fungi

(Bergerat et al, 1997; Sharif et al, 2002) and plants (Hartung et al, 2007) is required for the formation of DSBs in meiosis, which further emphasises the potential topoisomerase-like-transesterification activity of SPO11.

Only mono- and dicotyledonous plants possess more than one SPO11 paralogue in their genome (An et al, 2011; Yu et al, 2010). However, Bellani et al. (2010) reported the presence of two SPO11 isoforms resulting from an alternative splicing in both spermatocytes and oocytes of mouse. A similar alternative splicing was also found in human (Bellani et al, 2010; Romanienko and Camerini-Otero, 1999; Shannon et al, 1999). In *Arabidopsis thaliana*, three SPO11 paralogues have been characterised; AtSPO11-1, AtSPO11-2 and AtSPO11-3 (Hartung & Puchta, 2000; Hartung & Puchta, 2001). Two independent studies showed that AtSPO11-3 is involved in the decatenation of chromosomes during endoreduplication cycles and does not have a role in meiotic DSB formation (Sugimoto-Shirasu et al, 2002; Yin et al, 2002). In contrast, many studies have provided strong evidence that AtSPO11-1 and AtSPO11-2 are both involved in DSB formation. This is suggested by the observation that a T-DNA insertion in either of these two genes is sufficient to abolish the formation of meiotic DSBs (Grelon et al, 2001; Sanchez-Moran et al, 2007a; Shingu et al, 2012; Stacey et al, 2006). Malik *et al.* (2007) proposed that two gene duplication events occurred during evolution. The first event separated *AtSPO11-3* from the ancestor of the *SPO11* meiotic gene and the second gene duplication event separated the meiotic *SPO11* ancestor gene into *AtSPO11-1* and *AtSPO11-2* (Malik et al, 2007).

At least eleven proteins (Sae2, Rad50, Mre11, Xrs2, Rec102, Rec104, Rec114, Ski8, Mer2, Mei4 and Spo11) are involved in the formation of meiotic DSBs in budding yeast *Saccharomyces cerevisiae*. Very little information concerning the respective molecular function of these proteins exists despite several investigations (Keeney, 2008). Nevertheless, two studies established a network of protein interactions using a yeast two hybrid system (Arora et al, 2004; Maleki et al, 2007). Both studies revealed that Spo11 accessory proteins form three sub-complexes to form a larger pre-DSB complex that bind to the chromatin (Arora et al, 2004; Maleki et al, 2007). Ski8, Rec102, Rec104 and Spo11 form the first sub-complex. Ski8 has a role in both meiotic and vegetative cells. However, the meiotic role of Ski8 seems to be distinct from its cytoplasmic function in RNA metabolism (Arora et al, 2004). Arora *et al.*, (2004) and Tessé et al. (2003) suggested that Ski8 may have a scaffold function to favour the interaction between Spo11 and Rec102/Rec104 (Arora et al, 2004; Tesse et al, 2003). Interestingly, ChIP analysis showed that Rec102 preferentially localises on the chromatin loop rather than on the chromosome axes (Kee et al, 2004). Moreover, the absence of Rec102, Rec104 or Rec114 prevents the localisation of Spo11 on the chromatin (Prieler et al, 2005). This indicates that Spo11 may form a complex with Rec102, Rec104 and eventually Ski8 prior to its recruitment to the pre-DSB sites (Prieler et al, 2005). In addition, Sasanuma *et al.* (2007) suggested that Spo11 forms a homo-dimer and that the conserved active tyrosine residues of both Spo11 molecules are involved in the formation of meiotic DSBs (Sasanuma et al, 2007). This is consistent with two recent works of Shingu et al. (2010) and Hartung *et al.* (2007). The authors suggested that AtSPO11-1 and AtSPO11-2 may need to form a hetero-dimer to be functionally active in *Arabidopsis thaliana* (Hartung et al, 2007; Shingu et al, 2010). More recently, Vrielynck and Grelon (personal communication) characterised a new AtSPO11

accessory protein called AtPRD4. AtPRD4 is required for DSB formation and promotes the formation of a hetero-dimer AtSPO11-1/AtSPO11-2. The biological relevance of this interaction remains to be investigated.

The second pre-DSB sub-complex is composed of Mei4, Mer2 and Rec114. ChIPchip analysis indicated that these proteins mostly localise on the chromosome axes, in regions adjacent to the site of DSB hotspots (Carballo et al, 2013; Panizza et al, 2011). Immunocytochemistry study suggests that all three proteins localise adjacent to Mre11 and Spo11 foci which is consistent with ChIPchip experiment (Li et al, 2006). In addition, Mei4, Mer2 and Rec114 interact with each other in yeast two hybrid and co-immunoprecipitation studies (Arora et al, 2004; Li et al, 2006; Maleki et al, 2007). Althought, Mei4 was found to interact with Rec102 and Rec104 in a yeast two hybrid assay, the localisation of Mei4 on the chromatin is only dependent on Mer2 and Rec114 (Li et al, 2006; Maleki et al, 2007). The function of these three proteins is unclear. The differential localisation of the two pre-DSB sub-complexes suggests that Mei4/Mer2/Rec114 may interact with some components of Spo11/Ski8/Rec102/Rec104 complex and tether the chromatin loop to the chromosome axes to activate Spo11 activity and form meiotic DSBs.

The last group of proteins is composed of Mre11, Rad50 and Xrs2. The proteins are found in a complex and are involved in various aspects of DNA metabolism in both vegetative and meiotic cells (Arora et al, 2004). Mre11 is involved in meiotic DSB formation in *S. cerevisiae* (Keeney, 2008) and *C. elegans* (Chin & Villeneuve, 2001) but is not required for the formation of meiotic DSBs in *Coprinus cinerus* (Gerecke & Zolan, 2000) and *S.*

pombe (Keeney, 2008). A mutation in Mre11 is sufficient to abolish the formation of meiotic double strand breaks in budding yeast (Furuse et al, 1998; Johzuka & Ogawa, 1995). The homologue of the Mre11, Rad50, Xrs2 complex has been identified in *Arabidopsis thaliana* (AtMRE11, AtRAD50, AtNBS1) but the complex appears to have a role in DSB repair rather than a role in the formation of meiotic DSBs (Puizina et al, 2004; Uanschou et al, 2007). However, the full analysis of *Atmre11* T-DNA insertion mutant line has not been carried out. Therefore, it is not excluded that a reduction of SPO11-dependent DSBs occurs in *Atmre11*.

In *Arabidopsis thaliana*, the regulation of meiotic DSB formation is poorly understood. The meiotic role of SPO11-accessory proteins is conserved in some but not all organism. For instance, Ski8 is required for meiotic recombination in *Schizosaccharomyces pombe* (Evans et al, 1997) but not in *Arabidopsis thaliana* (Jolivet et al, 2006). Recently, AtPRD1 was identified as an AtSPO11-1 interacting protein and a mutation in *AtPRD1* abolishes the formation of DSBs (De Muyt et al, 2007; Shingu et al, 2010). More recently, three other proteins, AtPRD2 (De Muyt et al, 2009), AtPRD3 (De Muyt et al, 2009) and AtDFO (Zhang et al, 2012) were characterised as being involved in the formation of meiotic DSBs. The lack of sequence similarity of SPO11-accessory proteins among kingdoms and the absence of domain in their structure make the analysis of their function particularly difficult (Cole et al, 2010). Kumar *et al.* (2010) identified some similarities at the amino acid level between AtPRD2 and Mei4 and between AtPHS1 and Rec114 by using single signature motifs (Kumar et al, 2010). However, the function of these pre-DSB proteins remains elusive. In addition, a role for AtPHS1 in the formation of DSBs has not been demonstrated (Ronceret et al, 2009).

Lastly, several other factors regulate the formation of meiotic DSBs. The local remodelling of the chromatin by histone modifications (Acquaviva et al, 2013; Reddy & Villeneuve, 2004, Sommermeyer et al, 2013; Yamada et al, 2013) and the cyclin-dependent phosphorylation of Mer2 (Henderson et al, 2006, Sasanuma et al, 2008) temporally regulate the formation of meiotic DSBs in regard to the progression of the pre-meiotic DNA replication and the progression of meiosis (Blitzblau & Hochwagen, 2013; Borde et al, 2000; Keeney, 2008; Murakami & Nurse, 2001). The regulation of meiotic DSB formation does not only occur at the time of its initiation. The formation of too many DSBs can be deleterious for the cell. Therefore a mechanism must exist to negatively regulate the formation of DSBs after some DSBs are formed. Four independent studies showed that such a feedback loop exists during meiosis (Carballo et al, 2013; Joyce et al, 2011; Lange et al, 2011; Zhang et al, 2011). Lange *et al.* (2011) and Carballo *et al.* (2013) speculated that Mec1 and Tel1 are involved in a negative feedback loop to control the number of Spo11-dependent DSBs by phosphorylating Rec114 (Carballo et al, 2013; Lange et al, 2011). Zhang *et al.* (2011) extended the study and showed that Tel1 and Mec1 activities are involved in the inhibition of Spo11-dependent DSB to ensure that, at a given locus, only one pair of sister chromatids undergoes meiotic DSB. Finally, Farmer *et al.* (2012) proposed a role for Pch2 in the formation of DSBs. This highlights the complexity of the network of proteins involved in the initiation of meiotic recombination (Farmer et al, 2012).

1.3.2. Endonucleolytic release of SPO11 and generation of 3' single-stranded DNA tails

The formation of DSBs can potentially lead to genetic instability if incorrectly repaired. Two main pathways exist to repair DSBs: the error-prone non-homologous end joining pathway, which requires little or no sequence homology between the donor and the receiver DNA strands, and the homologous recombination pathway. The choice between the two DSB repair pathways depends on the nature of the DSBs and the timing of their formation. DSBs formed during G0/G1-phase are predominantly repaired by the non-homologous end joining pathway while DSBs arose from collapsed replication forks during S-phase and meiotic SPO11-dependent DSBs are principally repaired by the homologous recombination pathway (Grabarz et al, 2012; Mimitou & Symington, 2010). The repair of DSBs by homologous recombination requires the processing of the DSB ends to generate a long 3' end single-stranded DNA (ssDNA) that will subsequently invade the homologous chromosome for repair. During meiosis, the covalent binding of SPO11 to the DSB ends prevents the processing of the DSB ends by exonucleases. Several studies indicate that the removal of SPO11 from the DSB ends occurs by endonucleolytic cleavage dependent on the evolutionary conserved MRN/MRX (Mre11-Rad50-NBS1/Xrs2) complex in association with Sae2/COM1. The MRN/MRX complex is involved in various biological processes such as telomere maintenance and genome stability (Deng et al, 2009; Langerak et al, 2011). Following SPO11-dependent DSB formation, the MRX complex is recruited to the DSB ends. It is thought that the coiled-coil domain of two RAD50 molecules bridges the two ends of a DSB (Hopfner et al, 2002; Mockel et al, 2012). This is followed by the deposition of cohesin to maintain the sister chromatids in close contact

(Strom et al, 2004; Unal et al, 2004). In budding yeast (Lengsfeld et al, 2007; Manfrini et al, 2010; Zakharyevich et al, 2010) and fission yeast (Farah et al, 2009), Sae2/Ctp1 and Mre11 have an endonuclease activity and the absence of either of the two nuclease activities abolishes the initial resection of the DSB ends. The role of the nuclease activities of Mre11 and Sae2/Ctp1 in the initial resection of the DSBs remains elusive (Farah et al, 2009; Manfrini et al, 2010). Conversely, in higher eukaryotes, CtIP, the human functional orthologue of the yeast Sae2/Ctp1, lacks a nuclease activity (Sartori et al, 2007). The authors proposed that CtIP may promote the endonucleolytic activity of MRE11. In plants, the absence of AtMRE11 or AtCOM1, the functional orthologues of Mre11 and Sae2, respectively, leads to the extensive fragmentation of chromosomes and the persistence of AtSPO11-1 on the chromatin during meiotic prophase I (Uanschou et al, 2007). The persistence of AtSPO11-1 localisation in *Atcom1* and *Atmre11* prophase I likely accounts for the absence of DSB end resection and the persistence of covalently attached AtSPO11-1 to the DSB ends. This suggests that AtMRE11 and AtCOM1 share similar function with their budding yeast orthologues (Ji et al, 2012; Puizina et al, 2004; Uanschou et al, 2007).

The initial resection of the DSB ends forms a single-stranded break. The ends of the nascent breaks are sensitive to exonuclease activity and will be further resected. During meiotic homologous recombination, the exonuclease Exo1 and the helicase/endonuclease Sgs1/Dna2 complex are involved in the processing of most DSB ends through two distinct pathways in budding yeast (Manfrini et al, 2010; Zakharyevich et al, 2010). Two recent studies showed that the exonuclease activity of Mre11 and Exo1 contribute to the resection of the DSB ends in a bidirectional direction (Garcia et al, 2011; Zakharyevich et al, 2010). Exo1 processes the DSB ends with a 5' to 3' exonuclease activity while Mre11 processes

the DSB ends with a 3' to 5' exonuclease activity (Garcia et al, 2011; Zakharyevich et al, 2010). Zakharyevich *et al.* (2010) showed that the absence of Exo1 resulted in a reduction of the resection tract length. The authors reported that Exo1 processed most DSB ends but some DSB ends were normally processed in its absence. Interestingly, the reduction of the 5'-3' resection tract length did not significantly affect the homology search of the ssDNA tail and the formation of COs (Manfrini et al, 2010; Zakharyevich et al, 2010). In budding yeast mitotic cells, Sgs1 has a helicase activity and can unwind the two strands of a DSB end to facilitate access of the exonucleases Dna2 and Exo1. Dna2 is involved in the formation of long range resection tracts (> 3 kb) (Manfrini et al, 2010).

Two models can explain the DSB end resection step and the formation of Spo11-oligonucleotides in budding yeast. The initial resection of the DSB ends by Mre11/Sae2 could release a short Spo11-oligonucleotide. The ssDNA ends would then be sensitive to the exonuclease activities of Mre11 and Exo1. However, the similar kinetics of the DSB end resolution and the detection of Spo11-oligonucleotides is in disaccord with this model (Neale et al, 2005). Alternatively, Spo11-oligonucleotides formed after the initial resection by Mre11/Sae2 could remain associated with the complementary unresected 3' end ssDNA until completion of the processing of the 5' end (Neale et al, 2005). Several studies indicate that the MRX complex in association with Sae2 can tether DNA molecules (Bhaskara et al, 2007; Clerici et al, 2005; de Jager et al, 2001; Kaye et al, 2004; Lobachev et al, 2004) and could have a role in maintaining Spo11-oligonucleotides associated with the complementary ssDNA. However, further analysis is required to elucidate this mechanism.

Nucleosome repositioning and histone modifications are important events required for the processing of the DSBs and their subsequent repair by homologous recombination. Chromatin remodelers are recruited at site of DSBs to displace the nucleosomes and promote the loading of nucleases (Adkins et al, 2013; Chai et al, 2005; Chen et al, 2012; Costelloe et al, 2012; Shim et al, 2007; Tsukuda et al, 2009). In addition, sumoylation of H2A.Z (Kalocsay et al, 2009) and phosphorylation of the histone variant H2AX (Rogakou et al, 1998) at the residue serine 129 and serine 139 in yeast and mice, respectively, occur in response to the formation of DSBs and induce conformational changes of the chromatin surrounding the DSBs to direct DSB processing and repair (Chapman et al, 2012;; Lukas et al, 2011).

1.3.3. ssDNA invasion

In most reproductive organisms, two RecA recombinase related proteins, RAD51 and DMC1, are involved in the repair of SPO11-dependent DSBs (Bishop et al, 1992; Pittman et al, 1998; Shinohara et al, 1992). In *Arabidopsis,* AtRAD51 is involved in the repair of DNA damage during both mitosis and meiosis while the function of AtDMC1 is restricted to meiosis. In an *Atdmc1* T-DNA insertion mutant line, ten univalent chromosomes are observed during metaphase I (Couteau et al, 1999; Doutriaux et al, 1998). It is thought that DSBs are repaired by using the sister chromatid as template in a pathway dependent on AtRAD51. In contrast, chromosome fragmentation is observed in an *Atrad51* T-DNA insertion mutant line, which suggests that DSBs remain unrepaired (Li et al, 2004). In budding yeast, meiotic DSBs are preferentially repaired using the homologous chromosome (Kim et al, 2010; Schwacha and Kleckner, 1994). This barrier to repair off

the sister chromatids, depends on the interplay between components of the chromosome axes and the recombination machinery (further explain in Section 1.7) (Hong et al, 2013; Niu et al, 2009).

Following the resection of DSBs and the generation of 3' end ssDNA, RAD51 and DMC1 protomers are loaded onto the ssDNA to form a pre-synaptic nucleofilament. Formation of the pre-synaptic nucleofilament requires the presence of accessory proteins. In budding yeast, Rad51 (Cloud et al, 2012), Rad54 (Nimonkar et al, 2012), Tid1/Rdh54 (Nimonkar et al, 2012), Mei5-Sae3 (Ferrari et al, 2009; Hayase et al, 2004) and Hop2-Mnd1 (Chan et al, 2014) complexes are involved in the formation of Dmc1 pre-synaptic nucleofilaments. Stable Dmc1/Rad51 pre-synaptic nucleofilaments invade the homologous chromosomes and anneal with the complementary ssDNA of the homologous chromosomes to form a heterologous duplex. Pezza *et al.* (2007) suggested that the loading of DMC1 onto the chromatin did not require the presence of HOP2/MND1. However, the DMC1 pre-synaptic nucleofilament was unstable in-vitro and the authors reported that the complex HOP2/MND1 was necessary to stabilise the pre-synaptic nucleofilament (Pezza et al, 2007). HOP2/MND1 complex stabilises the dsDNA heteroduplex by acting on the condensation of DNA molecules (Pezza et al, 2010; Pezza et al, 2007; Pezza et al, 2013). Interestingly, Morozumi *et al.* (2012) reported that human PSF can interact with DMC1 and RAD51 and is involved in the aggregation of DNA molecules. The authors showed that PSF stimulates the formation of dsDNA heteroduplexes (Morozumi et al, 2012).

In *Arabidopsis*, several proteins have been characterised as epistatic to AtRAD51 and AtDMC1 in their role during DSB repair. AtBRCA2a and AtBRCA2b can interact with

AtRAD51 and AtDMC1 and are required for the recruitment of both recombinases on the chromatin (Seeliger et al, 2012; Siaud et al, 2004). In addition, the localisation of AtDMC1 on the chromatin is partially dependent on AtRAD51 and the number of AtDMC1 foci is reduced in *Atrad51* T-DNA insertion mutant line (Kurzbauer et al, 2012; Vignard et al, 2007). A role for AtRAD51 in the loading of AtDMC1 onto the chromatin is reminiscent with the role of Rad51 as a Dmc1 accessory protein in budding yeast (Cloud et al, 2012). Moreover, the localisation of Dmc1 on the chromatin is dependent on Rad51 (Bishop, 1994).

A complex of two proteins sharing sequence similarities with Hop2-Mnd1 complex was identified in *Arabidopsis.* The absence of AtHOP2 or AtMND1 prevented the pairing between homologous chromosomes and led to chromosome fragmentation at metaphase I (Uanschou et al, 2013; Vignard et al, 2007). In higher eukaryotes, five RAD51 paralogues have been characterised: RAD51B, RAD51C, RAD51D, XRCC2 and XRCC3. In *Arabidopsis*, *Atxrcc3* (Bleuyard et al, 2004; Bleuyard et al, 2005) and *Atrad51C* (Abe et al, 2005; Bleuyard et al, 2005) mutants are epistatic to *Atrad51* mutant with regard to the presence of chromosome fragmentation. The function of RAD51B, RAD51D and XRCC2 during meiosis is poorly understood. Bleuyard *et al.* (2005) reported the absence of meiotic defect in *Atrad51b* and *Atxrcc2*. Both T-DNA insertion mutant lines showed hypersensitivity to the DNA cross-linking agent Mitomycin C suggesting that both proteins may be involved in the repair of DNA damage (Bleuyard et al, 2005). In addition, analysis of *Atrad51b*/*Atrad51d*/*Atxrcc2* triple mutant revealed no apparent meiotic defect (Wang et al, 2013) However, Da Ines *et al.* (2013) showed that RAD51B, RAD51D and XRCC2 are involved in somatic homologous recombination. The authors reported that the absence of

any of the three proteins resulted in an increased rate of meiotic COs. The authors hypothesised that RAD51B, RAD51D and XRCC2 may regulate the function of DMC1 during the strand invasion step (Da Ines et al, 2013a), although further analysis is required to confirm this result.

Recently, two additional proteins, AtRFC1 and AtMCM8, involved in the early step of homologous recombination were identified (Crismani et al, 2013; Liu et al, 2012; Wang et al, 2012b). *Atrfc1* (Liu et al, 2012; Wang et al, 2012b) and *Atmcm8* (Crismani et al, 2013) T-DNA insertion mutant lines presented chromosome fragmentation from anaphase I onwards. Wang *et al.*, (2012) proposed that AtRFC1 may be involved in the extension of the invading ssDNA by DNA-synthesis, while the function of AtMCM8 in DSB repair is more elusive (Crismani et al, 2013; Wang et al, 2012b).

1.3.4. DSB repair

1.3.4.1. Synthesis-dependent strand annealing pathway

Following formation of SPO11-dependent DSBs and their subsequent resection, DMC1/RAD51 pre-synaptic nucleofilaments invade the homologous chromosomes. Annealing between the invading pre-synaptic nucleofilament (receiver chromatid) and the complementary non-sister chromatid (donor chromatid) forms a dsDNA heteroduplex and a D-loop structure (Figure 1.4). The 3' end of the invading chromatid is then extended by DNA-synthesis, which further enlarges the D-loop. The heterologous duplexes are thought to be very unstable and McMahill *et al.* (2007) suggested that most heterologous duplexes

dissociate after a short elongation of the receiver chromatid by DNA-synthesis. The authors proposed that invading chromatids can repeat the step of strand invasion/DNA synthesis/dissociation several times before being repaired by the SDSA pathway (Danilowicz et al, 2013; McMahill et al, 2007).

Components of the SDSA pathway are largely unknown. However, it is thought that DSBs repaired by the SDSA pathway can only lead to the formation of NCOs (Figure 1.4). The presence of nucleotide polymorphisms between the locus of the receiver chromatid and the donor chromatid results in the transfer of genetic information from the donor chromatid towards the receiver chromatid by DNA synthesis. After dissociation of the D-loop structure and re-association of the invading ssDNA with the non-invading complementary ssDNA, the newly synthesised region of the invading ssDNA can be used as template to repair the break of the complementary strand. Therefore, any transfer of genetic information between the donor chromatid and the receiver chromatid, called gene conversion, will also be transferred to the non-invading ssDNA. In contrast, annealing between the newly synthesised nucleotide region of the invading ssDNA and the undamaged region of the non-invading ssDNA will result in the formation of a dsDNA heteroduplex, if a nucleotide polymorphism exists at this locus between homologous chromosomes. The dsDNA heteroduplex can be recognised by the mismatch repair system. The non-invading and the invading ssDNAs can be used as DNA template to repair the mismatch. Hence, the mismatch repair system can either keep the converted genotype or restore the parental genotype (Berchowitz & Copenhaver, 2010). Yang *et al.* (2012) crossed two *Arabidopsis* inbred ecotypes, Columbia and Landsberg erecta, and analysed 40 F2 plants by sequencing. The authors reported that over 90 % of the recombination events

were GC events and that the average GC track length was 402 base pairs (Yang et al, 2012a). In a separate study, Sun *et al.* (2012) used a tetrad pollen assay and estimated the average frequency of GC events per locus per meiosis at 3.5×10^{-4}. The authors also showed that the frequency of GC was variable between locus-to-locus (Sun et al, 2012).

1.3.4.2. Formation of COs

Stabilisation of the D-loop structure and extension of the invading chromatid by DNA synthesis lead to the formation of a Holliday junction (HJ). Further extension of the 3' end ssDNA can result in its association with the quiescent end of the DSB to form a second HJ in a process called second-end capture (Figure 1.4). The resolution of a double Holliday junction (dHJ) by cleavage and ligation of DNA molecules determine the formation of a CO or a NCO. Symmetrical cleavage of a dHJ forms a NCO while asymmetrical cleavage of a dHJ forms a CO (Figure 1.4) (Heyer, 2004; Hollingsworth & Brill, 2004). It is thought that dHJs are predominantly resolved towards the formation of COs in meiosis (Allers & Lichten, 2001; Hunter & Kleckner, 2001; Jessop & Lichten, 2008). At least two classes of COs have been characterised in most sexually reproductive organisms. COs of class I are sensitive to interference, which implies that the formation of one CO limits the formation of an additional CO in the adjacent chromosomal region. The strength of interference is maximum at the region surrounding the CO site and is proportionally reduced towards distal regions (further explained in Section 1.4). In contrast, COs of class II are interference-independent and the COs are randomly distributed along the chromosomes (Berchowitz et al, 2007; Higgins et al, 2008a; Hollingsworth & Brill, 2004; Holloway et al, 2008).

1.3.4.2.1. Formation of interference-dependent COs

Several proteins are involved in the formation of COs of class I in budding yeast; Zip1, Zip2, Zip3, Zip4, Mer3, Msh4, Msh5, Spo16 and Pph3. These proteins localise on the chromatin and presumably mark at least some of the early recombination nodules, which are thought to be the cytological representation of DSBs undergoing recombination events during leptotene-zygotene. Intermediate joint molecules are sensitive to the anti-recombinase activity of helicases such as Sgs1 (Lorenz et al, 2012) and AtFANCM (Crismani et al, 2012; Knoll et al, 2012), in budding yeast and *Arabidopsis*, respectively. Anti-recombinases can dissolve dHJ intermediates and prevent inter-homologue recombination and CO formation (Bugreev et al, 2007; Chelysheva et al, 2008; De Muyt et al, 2012; Hartung et al, 2008; Wu & Burgess, 2006). The designation and implementation of a DSB to be repaired towards the formation of a CO are not very well understood. However, it is thought that the ZMM complex implements the decision to repair a CO-designated DSB site towards inter-homologue recombination and CO formation by counter-acting the anti-recombinase activities of helicases (Crismani et al, 2012; Knoll et al, 2012).

In mammals and plants, MSH4 localises as numerous foci during early leptotene and the number of foci progressively decreases through prophase I. Snowden *et al.* (2004) showed that hMSH4-hMSH5 complex clamps HJs (Snowden et al, 2004). Higgins *et al.* (2008) suggested that AtMSH4-AtMSH5 complex has a similar function and stabilises HJs in *Arabidopsis* (Higgins et al, 2008b). The number of MSH4 foci observed in early prophase I of mammalian and plant nuclei is similar to the number of RAD51 foci and presumably

mark most DSB sites. The number of AtMSH4 foci outnumbers the number of the late recombination protein AtMLH1 and the number of chiasmata observed at metaphase I of *Arabidopsis* PMCs (Ferdous et al, 2012). Interestingly, Goldfarb and Lichten (2010) reported that Msh4 was required for normal levels of intersister joint molecules in budding yeast (Goldfarb & Lichten, 2010). In addition, the frequency of NCO events is reduced in *Atmsh4* mutant in *Arabidopsis* (Drouaud et al, 2013). This suggests that Msh4 is important to stabilise joint molecules between both homologue chromosomes and sister chromatids. This is consistent with the abundant localisation of the protein on the chromatin in mammals and plants (Higgins et al, 2008b) during early prophase I (Guiraldelli et al, 2013; Kneitz et al, 2000; Luo et al, 2013).

In budding yeast, Zip1-Zip2-Zip3-Zip4 localise at the sites of future COs. The absence of any of these components significantly reduces the level of COs. Zip2, Zip3 and Zip4 are required for the proper nucleation of Zip1 and the elongation of the SC. The function of Zip2 and Zip4 are unknown. However, Zip2 and Zip4 are mutually dependent for their localisation (Tsubouchi et al, 2006). Zip3 regulates the spatiotemporal formation of the SC. In addition, Zip3 is a putative SUMO ligase and interacts with several recombination proteins (Agarwal & Roeder, 2000; Cheng et al, 2006; Macqueen & Roeder, 2009). In mice, HEI10/ CCNB1IP1 and RNF212 share structural homologies with Zip3 (Perry et al, 2005; Strong & Schimenti, 2010). SC formation occurred normally but the late recombination events were defective in *rnf212* and *hei10* mutants. The number of TEX11 foci, the mice functional orthologue of Zip4, and MSH4 foci were reduced in *rnf212* mutant (Reynolds et al, 2013). In contrast, the number of MSH4 and RNF212 foci remains abnormally high during mid-prophase I in *hei10* mutant. However, the late recombination

protein MLH1 was not detected in the mutant (Qiao et al, 2014; Ward et al, 2007). Although, RNF212 and HEI10 share a N-terminal RING-finger domain, a similar meiotic defect in the formation of COs and are dosage sensitive, they present striking differences in the localisation pattern of early recombination proteins. This led to the attractive model where RNF212-mediated sumoylation of MSH4 stabilises the protein at the CO-designated sites. These sites mature into late recombination nodules, recruit MLH1/MLH3 complex and form COs. In contrast, HEI10 mediates the ubiquitination of MSH4 at DSB sites that are not designated to become CO sites. MSH4 and possibly other factors are destabilised from these DSB sites that subsequently fail to mature into late recombination nodules (Lake & Hawley, 2013; Qiao et al, 2014). In *Arabidopsis* and rice, the functional orthologue of HEI10 has been characterised. Similarly to mammals, HEI10 is dispensable for SC formation but essential for the formation of MLH1-dependent COs (Chelysheva et al, 2012; Wang et al, 2012a)

Mer3 is a component of the ZMM complex and has a helicase activity. The protein promotes the single end invasion (SEI) probably by unwinding DNA duplexes in the 3' to 5' direction. Interestingly, Mer3 helicase can also block the extension of DNA heteroduplexes in the 5' to 3' direction (Guiraldelli et al, 2013; Mazina et al, 2004; Mercier et al, 2005; Nakagawa et al, 2001; Nakagawa & Kolodner, 2002a; Nakagawa & Kolodner, 2002b).

The resolvase involved in the resolution of dHJs towards the formation of COs of class I is unknown. Zakharyevich *et al.* (2012) recently showed that Exo1, Mlh1 and Mlh3 are required for the formation of interference-dependent COs (Zakharyevich et al, 2012). Exo1

and Mlh3 have a nuclease activity (Nishant et al, 2008; Ranjha et al, 2014; Rogacheva et al, 2014). However, Zakharyevich *et al.* (2012) showed that the nuclease activity of Exo1 was dispensable for the resolution of dHJs (Zakharyevich et al, 2012). Further study is required to understand the role of Exo1, Mlh1 and Mlh3 in the resolution of dHJs.

In *Arabidopsis*, the spatiotemporal localisation of AtMLH1 and AtMLH3 differs from the spatiotemporal localisation of ZMM proteins. AtMLH1 and AtMLH3 form few foci (around 10 foci) in late pachytene of *Arabidopsis* PMCs (Ferdous et al, 2012; Jackson et al, 2006). These foci presumably mark the late recombination nodules, which are the cytological representation of the intermediate joint molecules undergoing resolution to form a CO. The number of MLH1 foci observed on chromosome spread preparation (Ferdous et al, 2012; Jackson et al, 2006) is consistent with the number of chiasmata observed at metaphase I of *Arabidopsis* PMCs (Sanchez-Moran et al, 2002) and the rate of COs per genome identified by genome wide sequencing of 1,505 F1 plants from crosses between *Arabidopsis* Columbia and *Arabidopsis* Landsberg *erecta* (Giraut et al, 2011). Jackson *et al.* (2006) showed that loss of AtMLH3 resulted in the presence of residual COs of class I (Jackson et al, 2006). Conversely, in *Atmsh4* (Higgins et al, 2004) or *Atmsh5* (Higgins et al, 2008b) T-DNA insertion mutant lines, the formation of COs of class I was abolished. This indicates that additional components of the late recombination nodules account for the resolution of dHJs and formation of CO sensitive to interference, independently of AtMLH3. *Arabidopsis* genome lacks a functional orthologue of Exo1 and the significance of the residual level of COs of class I formed in *Atmlh3* remains to be investigated.

1.3.4.2.2. Formation of interference-independent COs

COs of class II are distributed randomly along the chromosomes and are not sensitive to interference. Recent studies suggest that three proteins with an endonuclease activity, Mus81, Yen1 and Slx1, are involved in the resolution of dHJs and the formation of COs of class II. It is thought that these nucleases cleave dHJs both symmetrically and asymmetrically (Nishino et al, 2005). Hence, dHJs resolved by these nucleases lead to the formation of COs and NCOs in statistically identical proportions. Zakharyevich *et al.* (2012) and De Muyt *et al.* (2012) showed that the joint molecule resolution activities of Mus81-Mms4 and Yen1 are partially redundant in budding yeast (De Muyt et al, 2012; Zakharyevich et al, 2012). In the absence of Mus81 or Mms4, Yen1 and Slx1-Slx4 promote joint molecule resolution, although not as efficiently as Mus81. Matos *et al.* (2011) reported that the endonuclease activity of Yen1 and Mus81 are differentially regulated by phosphorylation (Matos et al, 2011). Mus81 activity is promoted by Cdc5-mediated phosphorylation of its regulator Mms4. In contrast, phosphorylation of Yen1, by an as yet unknown kinase, inhibits its endonuclease activity during meiosis I. The authors suggested that Yen1 acts as a safeguard system. In this model, the dephosphorylation of Yen1 at meiosis 2 activates its endonuclease activity. Joint molecules unresolved by Mus81 during meiosis I can be processed by Yen1 during meiosis II. Oh *et al.* (2008) showed that Mus81 has an additional role by resolving aberrant joint molecules, such as multichromatid joint molecules, in *sgs1* mutant (Oh et al, 2008).

In plants, homologues of Yen1 and Mus81 have been identified as AtGEN1 and AtMUS81. In *Arabidopsis*, COs of class II represent 15 % of the total number of COs

(Higgins et al, 2004; Higgins et al, 2008a). In *Atmsh4/Atmus81* double mutant, the mean chiasma frequency is reduced to 0.85 per nucleus, suggesting that some dHJs are resolved to form COs of class II, independently of the endonuclease activity of AtMUS81 (Higgins et al, 2008a). A similar observation was reported in budding yeast (De Muyt et al, 2012; Zakharyevich et al, 2012). Investigation of *Atmus81/Atgen1* and *Atmsh4/Atmus81/Atgen1* mutants may reveal additional functions of these nucleases in the resolution of dHJs and the formation of COs during meiosis. Yang *et al*. (2012) reported that OsGEN-L, a component of the class 4 RAD2/XPG family nucleases in rice, has a 5'-flap endonuclease activity and a HJ resolvase activity. However, the role of OsGEN-L during meiosis has not been studied (Yang et al, 2012b).

The difference of sensitivity of COs of class I and II towards interference is poorly understood, partially because of the poor understanding of the implementation and spreading of interference along chromosomes. The resolution of joint molecules towards COs of class I and II involves different resolvases. This suggests that different forms of joint molecules may exist. One type of joint molecules will be resolved by a complex composed of Exo1-Mlh1-Mlh3-unknown resolvase and hence forms COs of class I. The other type of joint molecules will be resolved by the Mus81-Mms4-Yen1-Slx1-Slx4 pathway and forms COs of class II. Alternatively, similar joint molecules are sensitive to the two types of resolvases but are under the control of different factors and therefore will be resolved to form one of the two classes of COs. In this model, the MUS81 pathway is inactive under wild-type condition (Berchowitz et al, 2007; Higgins et al, 2008a). In contrast, in the absence of factors involved in the inter-homologue recombination pathway

and the formation of COs of class I, MUS81 pathway becomes active and processes dHJs to form COs of class II (Ferdous et al, 2012; Franklin et al, 2006; Higgins et al, 2004).

1.4. CO interference

In most reproductive organisms, COs are not randomly distributed along the chromosomes. For instance, the distribution of COs is biased towards the distal regions in *Arabidopsis* (Sanchez Moran et al, 2002). In addition, the formation of one CO inhibits the formation of an additional CO in the adjacent genomic region. This phenomenon is called interference. The strength of interference is not constant. The interference is stronger close to the CO site and become weaker with increasing distance outwards from the CO site. It was initially thought that interference does not cross the centromeres. However, the majority of the COs is distributed in centromeric-distal regions. A CO forms close to the centromere is associated with elevated rate of chromosome mis-segregation in budding yeast (Obeso & Dawson, 2010; Rockmill et al, 2006), *Drosophila* (Koehler et al, 1996) and humans (Koehler et al, 1996). Therefore, CO formation is inhibited in regions proximal to the centromeres. This led Colombo and Jones to reassess a large set of chiasma data from the grasshoppers *Leptysma argentina* and *Chorthippus brunneus*. The authors showed that interference spreads across the centromeres and that the propencity for chiasmata to form at centromeric-distal regions had led to a mis-interpretation of the role of centromeres in the spreading of interference (Berchowitz & Copenhaver, 2010; Colombo & Jones, 1997; Weinstein, 1918).

The mechanism responsible for interference is unknown. Several physical and mathematical models explaining the phenomenon of interference exist. The counting model is a mathematical based model suggesting that CO events are separated by a fixed number of NCO events (Foss et al, 1993). King and Mortimer (1990) proposed the polymerisation model where a factor would be bi-directionally spread from a CO-designated site along the chromosomes. This factor would then prevent other DSB sites to be designated as future COs. This factor remains to be identified. It could be a protein or a post-translational modification such as phosphorylation of proteins or methylation/acetylation of histones (King & Mortimer, 1990). More recently, Hulten (2011) suggested a model where CO interference is imposed by the oscillatory movement of the telomeres and the kinetochores (Hulten, 2011). Lastly, Kleckner *et al.* (2004) proposed that interference is a representation of a mechanical stress relief starting from the CO-designated site and propagating outwards from that point. The authors suggested that the chromatin undergoes cycle of expansion and contraction. The expansion of the chromatin generates compression forces against the chromosome axes that will eventually buckle under the stress. Axis buckling is important to implement the sites of CO and generate local axis relaxation that will spread along the chromosome axes. The bi-directional spreading of the stress relief disfavours subsequent buckling of the chromosome axes at DSB sites and thus prevents other DSB to be committed to become a CO (Berchowitz & Copenhaver, 2010; Kleckner et al, 2004).

The strength of interference and the number of COs per chromosome is variable between organisms. For instance, a high number of DSBs and COs are formed in *S. cerevisiae*. In contrast, *Arabidopsis* and mice meiocytes form a high number of DSBs and a low number

of COs while *C. elegans* form few DSBs and few COs. This suggests that the mechanism implementing interference has evolutionary diverged during evolution. *S. pombe* forms only COs insensitive to interference. *S. pombe* genome lacks all components of the ZMM complex. In addition, the axial element and the SC are not formed. Instead, the chromatin is organised into chromatin loops array on a primitive linear element (Kohli & Bahler, 1994; Lorenz et al, 2004a). *S. pombe* contains three large chromosomes and presents an average of 12.7 COs per chromosome (Berchowitz & Copenhaver, 2010). Although the COs are distributed randomly along the chromosomes, the high number of COs ensure that each bivalent forms at least the obligate CO. The low number of chromosomes ensures that a high proportion of meiotic products will receive at least one copy of each chromosome if the chromosomes were segregating randomly due to the absence of CO. In addition, the presence of a catalytically inactive Rec12, the fission yeast orthologue of Spo11, increases the proper segregation of achiasmatic chromosomes during meiosis I. A similar backup system, preventing random segregation of achiasmatic chromosomes during meiosis I, was also suggested in budding yeast (Newnham et al, 2010), mice (Bisig et al, 2012; Qiao et al, 2012) and *Arabidopsis* (Pradillo et al, 2007).

In contrast, *C. elegans* forms only interference-dependent COs and present an absolute interference under wild-type conditions (Youds et al, 2010). *C. elegans* forms an average of 2.1 meiotic DSBs per chromosome. One DSB site will be committed to form a CO while the other DSB sites, on the same chromosome, will be repaired as NCOs in a pathway dependent on RTEL-1 (Mets & Meyer, 2009; Youds et al, 2010). The absolute interference can be partially explained by the absence of CO in the end of the chromosomes. Interference will then spread on both sides of the CO sites and inhibits the

formation of a second CO along the chromosomes. Formation of the obligate CO is followed by an important remodeling of the chromosome axes (Martinez-Perez et al, 2008). The CO is usually distributed off-center on the chromosomes, resulting in the presence of a short axis and a long axis. HTP1, HTP2 and LAB2 localise on the long axis and maintain the cohesion between the sister chromatids until anaphase II. In contrast, these proteins are depleted from the short axis which favour the segregation of the homologous chromosomes during anaphase I (Martinez-Perez et al, 2008; Schvarzstein et al, 2010). The formation of a second CO will presumably affect the remodeling of the chromosome axes and the subsequent segregation of the homologous chromosomes at anaphase I. Homologous chromosomes pair and synapse before the formation of SPO11-dependent DSBs in *C. elegans*. Although it is conceivable that the establishment of the SC may have a role in the absolute interference (Libuda et al, 2013), studies from yeast (Borner et al, 2004) and *Arabidopsis* (Higgins et al, 2005) suggest that the SC does not mediate interference.

Arabidopsis, S. cerevisiae and mice differ from *S. pombe* and *C. elegans*. A high number of interference-sensitive COs is formed, representing 85 % - 90 % of the overall number of COs. *S. cerevisiae* has a relatively high number of COs per bivalents with an average of 5.6 while *Arabidopsis* and mice have an average of 2.0 and 1.4 COs per bivalent, respectively. The discrepancy in the strength of interference between organisms probably relies in the divergence of the proteins involved in crossover homeostasis and in the difference of chromosomal features (Berchowitz & Copenhaver, 2010).

1.5. Obligate crossover and crossover homeostasis

Repair of SPO11-dependent DSBs using the homologous chromosome as template results in the formation of COs. COs are essential to physically connect homologous chromosomes until the onset of anaphase I. Physical links between homologous chromosomes ensure their proper disjunction at anaphase I. Several studies from yeasts (Borner et al, 2004; Buonomo et al, 2000; Kan et al, 2011), mammals (Kudo et al, 2006) and plants suggest that the formation of at least one CO per bivalent, the obligate CO, is required to prevent mis-segregation of chromosomes during anaphase I (Jones & Franklin, 2006; Page & Hawley, 2003). The number of COs per homologous chromosomes is relatively low, constant among cells of an individual organism, and estimated between 1 and 5 for most organisms studied (Kotwaliwale, 2012). This implies that a control over the formation of COs must exist to regulate the number of COs formed along the chromosomes. It is thought that the formation of too many and too few COs is detrimental for the cell, although there is no evidence suggesting that an excess of COs affects the normal progression of meiosis (Cole et al, 2012; Crismani et al, 2012; de Boer et al, 2006; Martini et al, 2006; Nishant et al, 2010). CO homeostasis and obligate CO, two aspects of the control over the formation of COs, are not very well understood. CO homeostasis maintains the number of CO constants in the nuclei even if the number or early inter-homologue recombination events are reduced (Henderson & Keeney, 2004). CO homeostasis and interference may be related processes. It is possible that chromosomes are free of constraints until one CO is formed. Following, the formation of the obligate CO, interference is spread along the chromosome thus limiting the formation of additional COs.

The obligate CO and CO homeostasis are maintained until a threshold CO level is reached. Nishant et al. (2010) analysed various mutant Msh4 and Msh5 alleles. The authors showed that the wild-type level of COs is not required to maintain meiotic viability. Below a threshold CO level, meiotic viability is reduced. In addition, mutant Msh4 and Msh5 alleles differentially affect the formation of COs on chromosomes, with smaller chromosomes less affected by the overall reduction of COs (Nishant et al, 2010). In most organisms studied, there is an excess of DSBs over the number of COs. In mammals (Cole et al, 2012) and plants (Ferdous et al, 2012), the number of early recombination nodules, visualised by immunocytological analysis of RAD51, DMC1 and MSH4, is 6-9 and 11 times higher than the number of late recombination nodules, visualised by immunocytological analysis of MLH1. In mice, CO homeostasis and interference are progressively implemented during meiosis. The first control occurs after the formation of early recombination intermediates with the presence of non-random MSH4 foci. The second control occurs when some of these early recombination intermediates matures to late recombination intermediates (Cole et al, 2012; de Boer et al, 2006; Martini et al, 2006). A reduction and an augmentation of DSBs, to respectively 55-60% and 180-240 % wild-type level of DSBs, does not significantly affect the number of COs (Cole et al, 2012; Henderson & Keeney, 2004). The authors proposed that CO homeostasis maintains the number of COs at the expense of the number of NCOs, when the formation of DSBs is increased or decreased. These observations are in disaccord with the counting model, proposed by Foss *et al.*, (1993), to explain the spreading of interference. In addition, CO homeostasis is lost when the number of DSBs is reduced to less than 60 % the wild-type level of DSBs (Henderson & Keeney, 2004). This phenomenon seems to be conserved among yeasts (Martini et al, 2006), nematodes (Rosu et al, 2011) and plants (Roberts,

2009). The imposition of the two levels of CO implementation may be related with the expansion of the chromatin. Kleckner *et al.* (2004) proposed that the global structure of the chromatin varies between an expansion and a contraction stage (Kleckner et al, 2004). The authors showed that chromatin undergoes three cycles of expansion/contraction during early prophase I of meiosis and that the chromatin expands at the time where DSBs, SEIs and dHJs are formed. This phenomenon was also reported in Barley (Higgins et al, 2012). The expansion of the chromatin probably makes the chromatin more accessible to proteins involved in all three steps of the homologous recombination pathway mentioned above. Additionally, the expansion of the chromatin generates compression forces against the chromosome axes that will in turn commit some DSBs sites to become COs and reinforces the CO-designated-SEIs and CO-designated-dHJs to become COs. In this model, the second expansion of the chromatin, at the time of SEI, would explain the interference-dependent distribution of MSH4 foci observed in mice (Cole et al, 2012). In addition, the third expansion of the chromatin, occurring at the time when dHJs are formed, correlates with a stronger interference observed in the distribution of MLH1 foci (Cole et al, 2012; de Boer et al, 2006; Martini et al, 2006).

1.6. Chromosome axis morphogenesis and meiotic DSB formation

Ultrastructural analysis of early meiotic prophase I nuclei from *Bombyx mori* showed that the chromatin is organised in a loop array along a structural axis (Rattner et al, 1981). This feature of the chromatin organisation was also observed in pachytene nuclei of *Hyalophora columbia* (Moens and Pearlman, 1988) and *Saccharomyces cerevisiae* (Moens and Pearlman, 1988). The chromatin is arranged in a loop-spacer-loop structure and the

chromatin loops are closed at their bases (Zickler & Kleckner, 1999). It is thought that the chromatin organises in a loop array at or soon after the pre-meiotic S-phase (Zickler & Kleckner, 1999). Sister chromatids are organised in two distinct linear loop arrays that lie in a parallel configuration, one above the other, and perpendicular to the plane of the SC in pachytene nuclei. The two sister chromatid axes form a single morphological unit and the chromatid loops emanate outwards from the SC (Figure 1.5A) (Kleckner, 2006; Zickler & Kleckner, 1999). The control over the organisation of the chromatin is unknown. However, Naumova *et al.* (2013) used conformation capture methods and polymer simulation to show that the mitotic chromatin is organised stochastically in chromatin loop array in prometaphase of human cells (Naumova et al, 2013). In addition, the organisation of the chromatin in a loop array is independent on the presence of the sister chromatid and independent of the formation of the meiotic axial element (Kleckner, 2006; Zickler & Kleckner, 1999). Furthermore, the data obtained from chromatin conformation capture by Naumova *et al.* (2013) can be reproduced using polymer simulation with or without the presence of a scaffold (Naumova et al, 2013). Klecker (2006) suggested that proteins involved in the formation of the mitotic chromosome axis may also mediate the formation of the linear axis structure which forms the basis where the chromatin loops emanate. The formation of chromatin loops arrays occurs along all the chromosomes with minimal variation in chromatin loop size along a chromosome. The density of chromatin loops along the SC is conserved across organisms suggesting that the basis of the linear chromatin loop array is evolutionary conserved (Zickler & Kleckner, 1999). This is interesting as the length of the SC can vary considerably within same species between male and female and during pachytene meiotic stage (Drouaud et al, 2007; Giraut et al, 2011;

Kleckner, 2006; Kleckner et al, 2003;). This implies that the size of the chromatin loop is inversely correlated with the length of the SC.

During meiosis, formation of the axial element can be monitored by immunolocalisation study of axis components. The axial element is a proteinaceous structure where proteins localise on the chromatin fibre and are involved in several steps of homologous recombination (see below) (Zickler & Kleckner, 1999). At mid-prophase I of meiosis, the axis of each homologous chromosome are closely aligned and become linked by a central structure to form the SC. The SC is a tripartite structure as observed by electron microscopy and is composed of two lateral elements, formed from the two homologous axial elements, and a central element (Figure 1.5A) (Zickler & Kleckner, 1999). Components of the axial element are thought to localise on the chromatin fibre in multiple horizontal layers. Cohesin subunits such as Smc1, Smc3, Stag3 and the meiotic specific kleisin Rec8 forms the first layer of the chromosome axes and are involved in the cohesion of the sister chromatids and DSB repair (Kim et al, 2010). The deposition of cohesin along the chromosome axes is thought to occur during DNA replication in the pre-meiotic S-phase. ChIPchip analysis of chromosome axes components from budding yeast nuclei revealed that the distribution of the kleisin Rec8 is not constant along the chromosomes (Glynn et al, 2004). In contrast, the protein preferentially binds to specific sites. Rec8 localises abundantly at the centromeric regions, which is in accord with its role in sister chromatid cohesion. It also forms domains of higher and lower abundance along the chromosome axes (Glynn et al, 2004; Ishiguro et al, 2010; Panizza et al, 2011; Watanabe & Nurse, 1999). Several other components of the chromosome axes have been identified and form a second layer of proteins. In budding yeast, Red1 and Hop1 are two components

of the lateral/axial element. Red1 protein is thought to have a structural function and forms a complex with Hop1, while Hop1 is a sensor protein favouring recombination events towards the homologous chromosome (see below) (Carballo et al, 2008; Woltering et al, 2000). Panizza *et al.* (2011) showed that Red1 and Hop1 are organised in domains of hyper and lower abundance along the chromosome axes, similarly to Rec8 domainal localisation (Panizza et al, 2011). In addition, Blat *et al.* (2002) showed that Red1 domainal localisation is determined by the bulk of chromatin status. The chromosomes can be divided in units with GC-rich contents, called R-bands, and AT-rich contents, called G-bands. These distinct chromosomal units differ in physical properties (Blat et al, 2002; Dekker et al, 2002). Red1 localisation is more abundant on R-band isochores and shows a similar localisation pattern with Mcd1/Scc1 mitotic cohesin and Rec8 meiotic cohesin along the chromosome 3 of budding yeast. However, this is in disaccord with the work of Kim *et al.* (2010) where the authors showed Red1 localisation was distinct from Rec8 localisation. Blat *et al.* (2002) proposed that the status of the chromatin fibre influences the localisation of the chromosome axis components (Blat et al, 2002). In addition, the hyper abundant domains of the meiotic cohesin correlates with the hyper abundant domains of the mitotic cohesin which reinforce the idea that the organisation of the linear chromatin loop array may be mediated by mitotic components during the pre-meiotic S-phase (Blat et al, 2002).

Components of the meiotic chromosome axes have been identified across all organisms. AtASY3 (Ferdous et al, 2012) and AtASY1 (Caryl et al, 2000) share functional similarities with Red1 and Hop1, respectively, in *Arabidopsis*. Both proteins present a low sequence similarity with their functional orthologues. AtASY1 and AtASY3 were identified based

on their meiotic defect rather than based on their sequence homology with their budding yeast counterpart (Caryl et al, 2000; Ferdous et al, 2012). Chambon and Grelon recently identified AtASY4 as a new axis component interacting with AtASY3 (personal communication). In addition, several cohesin subunits have been characterised and immunocytochemistry studies suggested that these proteins localise along the chromosome axes during mid-prophase I of *Arabidopsis* meiosis (Cai et al, 2003; Chelysheva et al, 2005; Lam et al, 2005; Yuan et al, 2012). In mice, SYCP2, SYCP3, COR1/SCP3 and HORMAD1/2 were characterised as axes proteins. HORMAD1/2 share structural and functional homologies with Hop1 and AtASY1 (Fukuda et al, 2010; Fukuda et al, 2012;; Schalk et al, 1998; Wojtasz et al, 2012; Wojtasz et al, 2009). In fission yeast, several axes proteins have been characterised. Rec10 and Hop1 have a similar function to Red1 and Hop1, respectively. In addition, three additional coiled-coil proteins were recently identified; Rec25 (Davis et al, 2008), Rec27 (Davis et al, 2008) and Mug20 (Estreicher et al, 2012). The localisation of these proteins was mostly dependent on Rec10 (Davis et al, 2008; Estreicher et al, 2012; Fowler et al, 2013).

Several lines of evidence suggest that meiotic DSBs occur on the chromatin loops when the chromatin loops are tethered to the chromosome axes (Blat et al, 2002; Fowler et al, 2013; Panizza et al, 2011). Formation of the chromosome axes occurs during/after the pre-meiotic S-phase but prior to the formation of meiotic DSBs, as suggested by immunocytochemistry study of Rec8 and Red1 in a meiotic time course experiment carried out on budding yeast nuclei (Kim et al, 2010). Thus, the nascent chromosome axes presumably determine the site of future DSBs. Panizza *et al.* (2011) showed that the cohesin Rec8 and the axis structural component Red1 regulate the localisation of Hop1 and

the two Spo11-accessory proteins Mer2 and Rec114, along the chromosome axes in budding yeast (Panizza et al, 2011). Similarly, Rec8 regulates the localisation of the axes component Rec27 along the chromosome axes in fission yeast. Rec27 likely determines the sites of DSB as suggested by the positive correlation between the distribution of the higher abundant domains of Rec27 and the distribution of the DSBs along the chromosomes (Fowler et al, 2013). Physical analysis of meiotic DSB formation in the absence of components of the chromosome axes has mostly been carried out in budding and fission yeast. The absence of Rec10 (Fowler et al, 2013; Mallela et al, 2011) and Red1 (Blat et al, 2002; Kim et al, 2010) drastically reduce the formation of DSBs, with some studies reporting the abolition of DSB formation. In addition, Hop1 is essential for the formation of a large proportion of DSBs in budding yeast (Carballo et al, 2008). Ferdous *et al.* (2012) analysed the formation of meiotic DSBs in the context of the chromosome axes in *Arabidopsis*. The authors assumed that the number of DSBs can be inferred by the number of γH2AX foci, the phosphorylated form of the histone variant H2A at residue serine 139. The authors reported that the number of DSBs was reduced to 70 % the WT level in *Atasy3* and that it was not significantly reduced in *Atasy1* (Ferdous et al, 2012).

A

Recombination complex

Sister chromatids

Axis-associated protein ASY1

Homologous chromosomes

Lateral element ASY3/ASY4

Central element

Axial elements

Transverse filament ZYP1a/b

Interphase   Leptotene   Zygotene   Pachytene

B

DAPI ZYP1

A   B   C
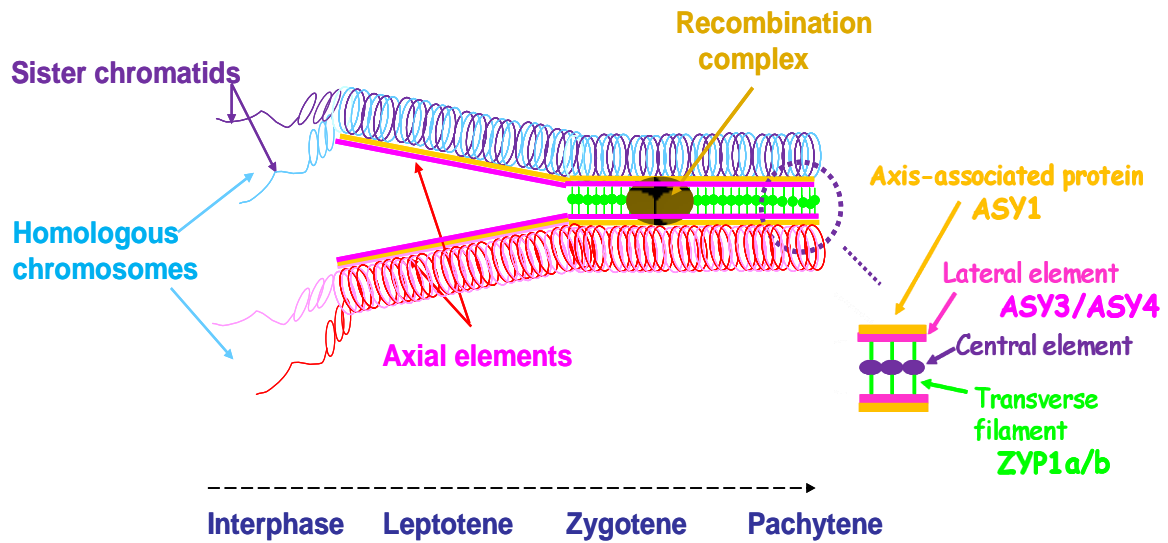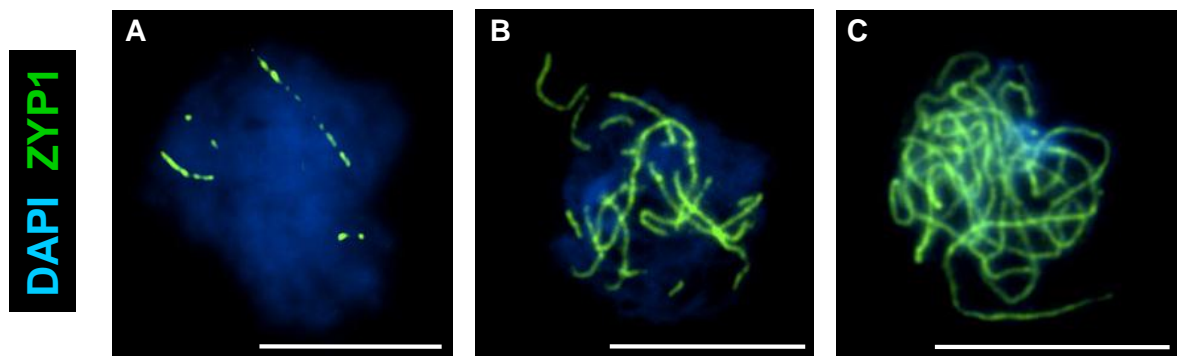
<u>Figure 1.5.</u> **Formation of the synaptonemal complex during prophase I in *Arabidopsis*.**

A. Schematic representation of the synaptonemal complex formation during prophase I. The formation of the synaptonemal complex initiates at the transition leptotene/zygotene, when homologous chromosomes are paired and the recombination machinery is present at the site of DSBs.

B. Immunolcalisation of ZYP1 (green) in *Arabidopsis* pollen mother cells during prophase I. (A) early zygotene, (B) mid-zygotene, (C) pachytene. Nuclei are stained with DAPI (blue). Scale bar, 10 μM.

1.7. Chromosome axes and interhomologue recombination bias

In budding yeast (Bishop, 1994; Bishop et al, 1992) and mice (Pittman et al, 1998), DSBs remain unrepaired in the absence of DMC1. This phenomenon, also called, barrier to the sister chromatid, blocks the invasion of the nascent 3' ssDNA towards the sister chromatid. Accumulation of unrepaired DSBs activates the pachytene checkpoint and stops the progression of meiosis (Wu & Burgess, 2006). In budding yeast, meiosis initiates in response to nitrogen starvation (Su et al, 1996). Meiotic cells arrested at pachytene are not committed to meiosis and can return to mitotic growth if the environment becomes rich in nutrients (Honigberg & Esposito, 1994). In the absence of Dmc1, the barrier to the sister chromatid prevents the repair of DSBs. This may impede the formation of ectopic recombination that can be deleterious for the cell if it reverses back to mitotic growth.

The mechanism responsible for the inter-homologue recombination bias integrates multiple layers of controls involving structural controls and recombination-mediated events. Inter-homologue bias is thought to occur during early prophase I when the chromatin is expending. Kleckner *et al.* (2004) proposed that the expansion of the chromatin generates compression stress along the chromosome axes that could drive conformational changes of the axes and promote DNA recombination. The authors suggested that the expansion of the chromatin mass could generate subtle separation of the sister chromatids. This phenomenon could occur locally where the sister cohesion is already loose, such as at the sites of SPO11-dependent DSBs and hence favour inter-homologue recombination (Kim et al, 2010; Kleckner et al, 2004).

The formation of the chromosome axes initiates before the formation of the meiotic DSBs. Components of the chromosome axes, such as Hop1, Red1 and Rec8, are required to pre-condition the homologue bias (Hong et al, 2013; Kim et al, 2010; Niu et al, 2005). Blat *et al.* (2002) showed that the localisation of Red1 along the chromosome axes is regulated by the presence of R-band and G-band isochores. The authors proposed that R-band isochores disfavour the loading of Dmc1, although the explanation for this observation is unclear. The localisation of Red1 at R-band isochores counteracts the inhibitory effect towards the localisation of Dmc1 and thus favour repair of DSBs by inter-homologue recombination. In contrast, in the absence of Red1, Dmc1 fails to localise at the sites of DSB in R-bands isochores and the DSBs are repaired by inter-sister recombination (Blat et al, 2002). Similarly, AtASY1, the functional homologue of Hop1, stabilises the loading of DMC1 on the chromatin in *Arabidopsis* (Sanchez-Moran et al, 2007a). AtASY1 forms a complex with AtASY3, similarly to their functional orthologue Hop1/Red1 and mediates inter-homologue CO formation (Ferdous et al, 2012). It is possible that the structure of the axial element and the components of the chromosome axes form a first layer of control over the inter-homologue bias. Following DSBs, additional controls will then be super-imposed to form the so-called barrier against the sister chromatid. In *C. elegans*, the SC is formed before the formation of meiotic DSBs and the tripartite structure maintains the homologous chromosome in close alignment thus favouring inter-homologue recombination. *C. elegans* lacks the recombinase DMC1. RAD51 recombinase activity probably accounts for the repair of the DSBs. In this scenario, the SC conditions the RAD51 pre-synaptic filament to invade the homologous chromosome and thus favours inter-homologue recombination. However, if an artificial DSB is generated before formation of the SC, RAD51 pre-synaptic filament is not directed towards the homologous chromosome and the DSB is

repaired by inter-sister recombination (Rosu et al, 2011; Youds et al, 2010). There are several differences between the homologous recombination pathway between nematode and budding yeast. In budding yeast, the formation of the SC is dependent on the early recombination events while SC formation is independent on the early recombination events in nematode (Dernburg et al, 1998; Padmore et al, 1991). However, it is possible that the axial/lateral element pre-conditions the inter-homologue bias in higher eukaryotes. The presence of the two recombinases Rad51 and Dmc1 in yeasts, mammals and plants implies that additional controls must exist to impose the inter-homologue bias (Abdu et al, 2003).

Hollingsworth's lab showed that Hop1 and Red1 form a complex with the forkhead kinase Mek1 in budding yeast. The absence of any of these proteins alleviates the meiotic arrest and restores the Rad54-dependent repair of meiotic DSBs in a *dmc1* mutant (Wan et al, 2004). This suggests that the complex Hop1-Red1-Mek1 is involved in the inter-homologue bias. Rad54 is a Rad51 accessory protein and promotes Rad51 recombinase activity. It is thought that in the absence of Dmc1 and one of the components of the Hop1-Red1-Mek1 complex, a Rad51-Rad54 pre-synaptic nucleofilament is formed, resulting in the repair of most DSBs by inter-sister recombination (Carballo et al, 2008; Hong et al, 2013; Kim et al, 2010; Woltering et al, 2000). The formation of the complex Hop1-Red1 promotes the dimerization of Mek1 protein and activates its kinase acitivity (Niu et al, 2009). Mek1 kinase activity mediates Rad54 phosphorylation thus inhibiting the formation of a Rad51-Rad54 complex and reducing the recombinase activity of Rad51. An additional pathway restricting the recombinase activity of Rad51 and dependent on Hed1 was reported (Tsubouchi & Roeder, 2006). Recently Busygina *et al.*, (2012) showed that Hed1 interacts with Rad51. Biochemical analysis suggests that the major function of Hed1

consists of restricting the interaction between Rad54 and Rad51 and thus limiting the inter-sister recombinase activity of Rad51 (Busygina et al, 2008). However, biochemical analysis does not predict if one end or both ends of a DSB are bound by Hed1. *hed1* mutant cells display slight reduction in spore viability and CO numbers. The formation of the remaining COs is dependent on the other controls mediating the inter-homologue bias, such as Red1 and Mek1 (Hong et al, 2013). Hed1 could act on the invading DSB end to favour inter-homologue bias, already pre-conditioned by Hop1-Red1-Mek1. Hed1 could also act on the non-invading DSB end to inhibit Rad51 recombinase activity and maintain this DSB end in a quiescent state (Busygina et al, 2012; Lao et al, 2013; Tsubouchi & Roeder, 2006).

The deposition of cohesin between sister chromatid must be tightly regulated during meiosis. Too little cohesin between sister chromatid can result in premature sister chromatid separation and aneuploidy, while too much cohesin prevents inter-homologue recombination. Storlazzi *et al.* (2008) showed that the late recombination nodules were poor in SPO76 cohesin and sister axes were locally separated at these sites in *rec8* mutant in Sordaria (Storlazzi et al, 2008). Two recent studies indicate that Rec8 promotes inter-sister bias at the SEI step (Hong et al, 2013; Kim et al, 2010). The function of Rec8, mostly dependent on its cohesin activity, is counteracted by Mek1 kinase activity and Red1. In addition, in the absence of Rec8, IH-SEIs occur more often than inter-sister SEIs (IS-SEIs). This is consistent with the model where Red1 and Mek1 mediate inter-homologue SEI formation. However, the ratio IH-dHJs:IS-dHJs is reduced from 5 to 1 in *rec8* mutant compared to wild-type. The authors suggested that Rec8 mediates a bias towards IS-SEI. In addition, Rec8 has a later role in promoting IH-dHJ formation at the transition SEI-dHJ

(Hong et al, 2013). It is conceivable that the deposition of Rec8 is differentially regulated between the two ends of a DSB. If the invading DSB end is poor in Rec8 deposition and rich in Red1-Mek1 deposition, this will favour IH-SEI. In addition, if the quiescent DSB end is rich in Rec8 deposition and poor in Red1-Mek1 deposition, this will maintain the association of the DSB end with the sister chromatid and maintain the DSB end in a quiescent state. Loss of cohesin at the quiescent DSB end can lead to the invasion of the DSB end towards the homologous chromosome and the formation of a four way molecule which will form an IS-dHJ (Hong et al, 2013). This is consistent with the observation of an increase in IS-dHJs in *rec8* mutant reported by Kim *et al.* (2010). Interestingly, inter-homologue joint-molecules are formed at the expense of inter-sister joint molecules in *rec8/red1* double mutant. This suggests that inter-homologue recombination is the default recombination event (Hong et al, 2013; Kim et al, 2010).

In *Arabidopsis Atdmc1* mutant, meiotic progression is not arrested and DSBs are repaired in a pathway dependent on AtRAD51 (Couteau et al, 1999; Li et al, 2004). *Arabidopsis* genome lacks an orthologue for Hed1 and Mek1. The absence of orthologues could be the result of a rapid evolution of the two proteins or the presence of a different mechanism promoting inter-homologue bias. Several studies suggest that AtDMC1 may repair DSBs by using the sister chromatid as template, under certain conditions such as in the absence of AtASY1 and AtATR (Crismani et al, 2013; Kurzbauer et al, 2012). This indicates that AtASY1 and AtATR are two essential components to favour a bias towards inter-homologue CO formation in *Arabidopsis*.

1.8. Role of the synaptonemal complex in homologous recombination

The formation of a SC and the control over its formation is variable across organisms. *S. pombe* (Lorenz et al, 2004a) and *Tetrahymena thermophila* (Howard-Till et al, 2013) lack a proper SC. Instead, *S. pombe* has a primitive linear element while further analysis is required to clarify the structure of the chromosome axes in *Tetrahymena thermophila*. Formation of the SC occurs prior to and independently of the formation of meiotic DSBs in *Drosophila melanogaster* (McKim et al, 1998), *Caenorhabditis elegans* (Dernburg et al, 1998)*, and females *Bombyx mori* (Rasmussen, 1976). In contrast, formation of the SC is dependent on the formation of DSBs in the other organisms (Baudat et al, 2000; Grelon et al, 2001; Henderson & Keeney, 2004; Romanienko & Camerini-Otero, 2000). The SC is composed of a central element linked with the two lateral elements by transverse filaments. The molecular characterisation of the SC components remains largely incomplete. The conserved transverse filament protein Zip1 has been identified in most organisms studied (Higgins et al, 2005; Liu et al, 1996; MacQueen et al, 2002; Sym et al, 1993). Recently, two components of the SC have been identified in budding yeast; Ecm11 and Gmc2 (Humphryes et al, 2013). The authors proposed that these proteins promote the formation of the SC. In mice, SYCE1 (Hamer et al, 2006), SYCE2 (Hamer et al, 2006), SYCE3 (Schramm et al, 2011) and TEX12 (Hamer et al, 2006) form the central element of the SC (Costa et al, 2005). In *C. elegans*, SYP2 (Colaiacovo et al, 2003) was characterised as a component of the central element while SYP1 (MacQueen et al, 2002) and SYP4 (Smolikov et al, 2009) form the transverse filaments and SYP3 (Smolikov et al, 2007) links the transverse filaments with the lateral elements.

Electron-microscopy analysis of *Drosophila* prophase I nuclei revealed the presence of electron-dense ovoid structures associated with the chromosome axes and the nascent SC (Carpenter, 1975). These ovoid structures were later identified as recombination nodules. Two classes of recombination nodules were characterised; the early recombination nodules are thought to be the cytological representation of the sites of DSB, while the second class of recombination nodules, called late recombination nodules, are thought to be the cytological representation of the sites of dHJ and future COs. The number of early nodules exceeds the number of late nodules. This is consistent with the observation that there is an excess of DSBs over the number of COs (Cole et al, 2012; Ferdous et al, 2012). An electron-microscopy study of early meiotic prophase I nuclei from *Allium* showed bridges or axial connections between homologous axes (Albini & Jones, 1988). It is thought that early nodules are first associated with one chromosome axes before forming a bridge between the two homologous axes. The bridges will then de-evolve back to nodule where the SC nucleates (Albini & Jones, 1988; Zickler & Kleckner, 1999). Storlazzi *et al.* (2010) analysed the dynamics of Mer3-GFP tagged proteins, a protein involved early in the recombination pathway, in Sordaria. The authors showed that Mer3 localisation evolved from an on-axis localisation at leptotene to a between-axis localisation at the onset of synapsis. In contrast, localisation of Msh4-GFP tagged proteins, localising at a later time point as Mer3, show only a between-axis localisation (Storlazzi et al, 2010). The change of configuration from axial connections to recombination nodules, as observed by electron microscopy in *Allium,* can be explained by the progression of the homologous recombination events and the formation of intermediate joint molecules as well as the rapprochement of the homologous axes and the nucleation of the SC. In organisms where the formation of the SC depends on the formation of DSBs, it is essential that DSBs are

processed by a recombinase that mediates ssDNA invasion towards the homologous recombination. This process will ensure connections between homologous chromosomes and their subsequent pairing. In the absence of these axial connections, the homologous chromosomes fail to pair, recombine and synapse. These observations also explain the requirement to have a high number of DSBs in yeasts, mammals and plants. In contrast, meiotic DSBs are formed after the formation of the SC in *C. elegans.* In addition, an average of 2.1 DSBs is formed per chromosome which ensures the formation of the obligate CO. The synapsis between the homologous chromosomes before the formation of DSBs alleviates the need to form a high number of DSBs (Mets & Meyer, 2009; Zickler & Kleckner, 1999).

Storlazzi *et al.* (2010) estimated the width between the homologous axes at 400 nm at the onset of leptotene, 200 nm at zygotene, when Mer3 foci change from an on-axis to a between-axis localisation, and 100 nm between synaptic regions in Sordaria (Storlazzi et al, 2010). This highlights the coupling between the progression of the homologous recombination events and the pairing/synapsis of homologous chromosomes. Interestingly, the width of the SC is similar to the dimensions of the late recombination nodules observed by EM studies and it is evolutionary conserved across organisms (Goldstein, 1997; Page & Hawley, 2003; Schild-Prufert et al, 2011; Sym et al, 1993; Zickler & Kleckner, 1999). The most detailed model of the molecular organisation of the SC was described in *C. elegans*. Components of the SC interact with each other to form a "puzzle" bridge emanating from the central element of the SC towards each lateral element (Hawley, 2011; Schild-Prufert et al, 2011). The width of the SC is determined by the assembly of these components in a specific order and a biomechanical constraint limits the width of the SC. A mutation

increasing the length of the predicted coiled-coil domain of ZIP1 and SCP1 proteins results in an increase of the width of the SC in budding yeasts (Sym & Roeder, 1995) and the width of the polycomplexes in mice (Ollinger et al, 2005).

Initiation and progression of the SC formation can be monitored by immunolocalisation studies of ZIP1/ZYP1 protein (Figure 1.5B). In budding yeast, SC initiates at distinct sites, called synpasis initiation sites (SIS) (Chua & Roeder, 1998). The number of SIS outnumbers the number of COs. In *S. cerevisiae*, the initial loading of Zip1 occurs at non-centromeric region, where the COs form, as well as at the centromeres (Tsubouchi et al, 2008). Gladstone *et al.* (2009) and Newnham *et al.* (2010) proposed that Zip1 localisation at the centromeres favours the association between the homologous centromeres and segregation of homologous chromosomes at anaphase I. The association between centromeres limits the mis-segregation of achiasmatic chromosomes (Gladstone et al, 2009; Newnham et al, 2010). A similar role for the transverse filament SYCP1 was reported in mice (Bisig et al, 2012; Qiao et al, 2012). However, similar localisation of AtZYP1a/b at the centromeric regions was not reported in *Arabidopsis* (Higgins et al, 2005). In maize, ZYP1 appears to localise at the centromeres but after the centromeres form associations (Zhang et al, 2013). The asynchronous nucleation of the SC does not permit an accurate determination of the number of SIS in mammals and plants. COs are mostly located at the sub-telomeric regions in plants. Hence it is likely that additional SIS, located at more centromeric proximal regions, occurs to ensure the elongation of a stable SC. Components of the SC can self-assemble and if the initiation of the SC is not regulated, aberrant structures called polycomplexes can be observed on the chromatin and in the nucleus (Ollinger et al, 2005; Sym & Roeder, 1995; Zickler & Kleckner, 1999). In

addition, formation of the SC can occur between homologous chromosomes, non-homologous chromosomes and fold-back chromosomes. It is thus important to regulate the formation of the SC and couple its initiation with the progression of the homologous recombination events (Golubovskaya et al, 2011). Zickler and Klecker (1999) proposed a model for the formation of the SC that incorporates two phases of synapsis (Zickler & Kleckner, 1999). The first phase of synapsis would occur at the SIS and between homologous chromosomes. The nascent SC structures will undergo a transitional stress that will destabilise some of the SIS and the SC formed between non-homologous chromosomes. During the second phase of synapsis, SC cannot initiate at de-novo SIS. However, the control over the formation of the SC is less stringent and the SC can polymerise and depolymerise between homologous and non homologous chromosomes in an attempt to minimise the absence of SC along the chromosome length. This phenomenon is called synaptic adjustment and was reported in *C. elegans* (Henzel et al, 2011; Rog & Dernburg, 2013) and more recently in mice (Kauppi et al, 2013).

The role of the SC in homologous recombination is unclear. The absence of SC in *S. pombe* (Kohli & Bahler, 1994; Lorenz et al, 2004b), where only interference-independent COs are formed, suggests that the SC may be involved in interference. However, this does not explain the presence of interference in *Tetrahymena thermophilas*, an organism that does not form a SC (Howard-Till et al, 2013; Loidl & Scherthan, 2004). Furthermore, recent studies showed that sites of DSB are designated to become a CO before the formation of the SC and the distribution of the SIS show interference in budding yeasts (Fung et al, 2004) and mice (Cole et al, 2012; de Boer et al, 2006). In addition, CO interference is maintained in an RNAi knockdown of AtZYP1 gene expression in

Arabidopsis (Higgins et al, 2005). The SC may only have a structural role in maintaining the homologous chromosomes in close contact to ensure resolution of dHJ into COs (Borner et al, 2004; Kleckner, 2006). The SC can assemble and disassemble. It is possible that initial assembly of the SC between non-homologous recombination activates a checkpoint mechanism that disassembles the SC and dissolves ectopic recombinations. Interestingly, Higgins *et al.* (2005) reported the presence of high levels of multivalents in an RNAi knockdown of AtZYP1 gene expression (Higgins et al, 2005). Furthermore, dissociation of homeologous association occurs after the formation of the SC in allohexaploid wheat (Zickler & Kleckner, 1999). However, a decreased in ectopic recombination was observed in budding yeast *zip1* mutant. This may represent a discrepancy of ZIP1 function between organisms (Shinohara & Shinohara, 2013).

1.9. Aim and objectives of my PhD project

Components of the chromosome axes are essential for inter-homologue CO formation. Absence of the cohesin subunit AtSYN1 (Bai et al, 1999) or the axial structural component AtASY3 (Ferdous et al, 2012) affects the repair of DSBs towards inter-homologue CO formation. AtASY1 is an axis associated protein localising on the chromatin prior to the formation of DSBs (Armstrong et al, 2002). In budding yeast and mice, Hop1 (Schwacha & Kleckner, 1994) and HORMAD1 (Daniel et al, 2011), the functional orthologues of AtASY1, are thought to be involved in the formation of meiotic DSBs. The early localisation of AtASY1 at G2 phase (Armstrong et al, 2002) suggests that AtASY1 may have a role in the formation of DSBs and/or the determination of the future DSB sites. Several proteins have been identified as required for the formation of DSBs. However, the

function of these proteins and the interplay between these AtSPO11-accessory proteins and the chromosome axes is largely unknown.

In addition, recent observations from an *Atasy3* mutant suggest that AtASY1 has an important role in the formation of inter-homologue COs during prophase I of meiosis (Ferdous et al, 2012). Based on this study and on budding yeast studies, AtASY1 and Hop1 likely act as sensor proteins where their association with the chromosome axes and their function may be tightly regulated (Carballo et al, 2008). During prophase I of meiosis, the chromosome axes undergo structural changes in response to the formation of DSBs. Several lines of evidence from fungi indicate that following the formation of DSBs, multiple mechanisms govern the remodeling of the chromosome axes and the degree of condensation of the higher chromatin structure. These modifications are timely regulated with the progression of meiosis and the recombination events (Kleckner et al, 2004). Higgins *et al.* (2012) proposed that the chromatin undergoes cycles of expansion/contraction through prophase I and that these conformational changes occur during key steps of the homologous recombination such as the formation of DSBs and the formation of intermediate joint molecules (Higgins et al, 2012).

The aim of my project consists at further investigating the role of AtASY1 during meiosis. AtASY1 and AtASY3 share functional similarities with Hop1 and Red1, respectively. In budding yeast, Hop1 and Red1 form a complex to establish the inter-homologue bias. The first part of my project will assess the interaction between AtASY1 and the newly characterised axis component AtASY3. The interaction between these two proteins will be assessed by yeast two hybrid and immunoprecipitation studies from yeast crude extract.

To shed light on additional functions of AtASY1, it is important to identify new AtASY1 interacting partners. An immunoprecipation study from *Brassica* crude extract, using an anti-AtASY1 antibody, identified several meiotic specific proteins (Osman and Franklin, personal communication). One of these proteins is AtPRD3. AtPRD3 was previously characterised as an AtSPO11-accessory protein. The function of AtPRD3 will be further studied and the link between AtSPO11-accessory proteins and AtASY1/axis components will be investigated. Immunocytochemistry analysis of AtASY1 using an anti-AtAY1 antibody showed that the staining intensity of AtASY1 is different between unsynapsed and synapsed regions. This is representative of a remodeling of the chromosome axes occurring during the progression of the recombination events and the formation of the SC. Additionally, several (S/T)Q sites of BoASY1 were found phosphorylated by mass spectrometry analysis (Osman and Franklin, personal communication). One of these phospho-sites, BoASY1 T294 (corresponding to AtASY1 T295), is conserved across organisms. In budding yeast, Hop1 T318, which corresponds to BoASY1 T294, is phosphorylated by Mec1/Tel1 kinases in response to the formation of Spo11-dependent DSBs (Carballo et al, 2008). Phosphorylation of Hop1 T318 is essential to favour inter-homologue recombination. Therefore, the dynamic of AtASY1 phosphorylation at the residue T295 during prophase I of meiosis and the biological significance of this post-translational modification will be analysed.

Chapter II

Materials and Methods

2.1. Plant material and growth conditions

Seeds were sown on soil based compost and grown in a glasshouse at 18 °C to 25 °C with a 16 h light cycle. The ecotype *Arabidopsis thaliana* Columbia 0 (Col-0) and *Brassica oleracea* A12 were used as a wild-type control in all experiments. T-DNA insertion mutant lines were obtained from NASC and their accession number were specified in Appendix 1.

2.2 Plant manipulation

2.2.1. Bromodeoxyuridine treatment

Stems from 6 week old *Arabidopsis thaliana* plants were cut under water to a length of 5 cm and were rapidly immersed in a solution of 10 mM bromodeoxyuridine (BrdU) (SIGMA). The stems were left for 2 hours in the immersion solution and under the glasshouse condition to allow the BrdU to be incorporated into nuclear DNA of cells during S-phase via the transpiration stream (Armstrong et al., 2003). After 2 hours, the stems were transferred to water. Inflorescences were fixed in a solution of 3:1 ethanol-acetic acid at different time points.

2.2.2. Crossing *Arabidopsis thaliana* plants

Arabidopsis plants of 5-6 week old, at a stage when they have developed few inflorescences, were used for crossing. Siliques, open flowers and open buds were removed from the inflorescence of the mother plant. The three biggest unopened buds were

63

kept for emasculation while the smaller buds were removed. The flower buds were then opened with the help of a forceps and a needle and the immature anthers were removed. A flower from an *Arabidopsis* plant with a different genetic background was opened and a mature anther was taken and rubbed onto the stigma of the emasculated plant until the stigma was fully covered with pollen. The emasculated plant was then bagged and the hybrid seeds were harvested 2 to 3 weeks after the crossing.

2.2.3. Plant transformation by floral dipping

2-3 colonies of transformed Agrobacterium tumefaciens GV3101 were used to inoculate 20 ml of luria broth (LB) + rifampicin (25 µg/ml). The culture was incubated at 28 °C under agitation (multitron infors, 200 rpm) overnight. 125 µL of the overnight liquid culture was transferred to 500 ml of LB + rifampicin (12.5 µg/ml) until the OD_{600} reaches 1.5-2.0. The liquid culture was divided into two sterile buckets and centrifuged for 10 minutes at 1500 g and 4 °C. The supernatant was discarded and the pellet in each tube was re-suspended in 25 ml of a solution of 5 % sucrose (w/v). The two samples were pooled and the solution of 5 % sucrose was added to the re-suspended solution until the OD_{600} reaches 0.8.

Subsequently to this, 50 µl of Silwet L-77 was added per 100 ml of 5 % sucrose solution. The 6 week old plants to be transformed were dipped into the solution for 30 seconds. The plants were then dripped of any excess of bacterial culture, covered with cling film and

kept under low light for 24 hours. After this, the cling film was removed and the plants were grown under normal glasshouse conditions (Zhang et al., 2006).

2.2.4. Sterilisation of *Arabidopsis* seeds for plating on Murashige and Skoog agar plates

Seeds were sterilised in 20 % Parozone bleach (v/v) for 10 minutes and then washed four times in sterile distilled water (SDW) for 5 minutes each. Seeds were then left to dry on a filter paper (Fisher Scientific) in a laminar flow workstation before plating on Murashige and Skoog (MS) (SIGMA) agar plate supplemented with 25 µg/ml of glufosinate ammonium.

2.3. Bacterial and yeast strains and growth conditions

2.3.1. Bacterial and yeast strains

2.3.1.1. Bacterial strains

Agrobacterium tumefaciens (*A. tumefaciens*) GV3101

Escherichia coli (*E. coli*) DH5α

*Sup*E44, ∆*lac*U169 (Φ*lac*Z∆M15), *hsd*R17, *rec*A1, *end*A1, *gyr*A96, *thi*-1, *rel*A1.

2.3.1.2. Yeast strains

Saccharomyces cerevisiae (*S. cerevisiae*) Y2H Gold (Clontech)

2.3.2. Bacterial and yeast growth conditions

Recipes for growth media are specified in Appendix 2.

2.3.2.1. *A. tumefaciens*

A. tumefaciens liquid cultures were grown on LB containing rifampicin (25 µg/ml) and kanamycin (50 µg/ml) on a rotary shaker (multitron infors) at 200 rpm for 16 hours at 28 °C. *A. tumefaciens* cells were placed on luria agar (LA) plates with 25 µg/ml of rifampicin and 50 µg/ml of kanamycin. Plates were incubated inverted for 2 to 3 days at 28 °C. Inoculations of liquid culture and agar plates were carried out under aseptic conditions.

2.3.2.2. *E. coli*

E. coli liquid cultures were grown on LB with appropriate selective antibiotic on a rotary shaker at 200 rpm (multitron infors) for 16 hours at 37 °C. *E. coli* cells were placed on LA agar plates with appropriate selective antibiotic and the plates were incubated inverted for 16 h to 20 h at 37 °C. Inoculations of liquid culture and agar plates were carried out under aseptic conditions.

2.3.2.3. *S. cerevisiae*

S. cerevisiae liquid cultures were grown on yeast peptone dextrose adenine (YPDA) broth medium or the appropriate synthetic defined dropout amino acids broth medium (SD) on a rotary shaker at 250 rpm (multitron infors) for about 18 hours at 30 °C. *S. cerevisiae* cells were placed on YPDA agar plates or the appropriate SD dropout amino acids agar plates. Plates were incubated inverted for up to 5 days at 37 °C. Inoculations of liquid culture and agar plates were carried out under aseptic conditions.

2.4. Nucleic acid manipulation

Recipes for reagents are specified in Appendix 3.

2.4.1. DNA extraction from plant

The edge of a leave was cut using the cap of a 0.5 ml microfuge tube. 50 μl of extraction buffer was added and the leave was broken up by taping with a tip of a pipette until the solution turned lightly green. The tube was incubated at 95 °C for 10 minutes and then cooled on ice for 2 minutes. 50 μl of dilution buffer was added to the solution and the sample was briefly vortex to mix the solution. Subsequently to this, the tube was centrifuged at 15.7 g for 1 minute prior to storage at -20 °C. The supernatant contained the extracted DNA.

2.4.2. Polymerase Chain Reaction (PCR)

PCR was used for genotyping transgenic plants and cloning procedures.

2.4.2.1. PCR for genotyping plants

Extracted DNA from *Arabidopsis* leaves were amplified with two different primer sets to identify plants homozygote for the T-DNA insertion. WT primer set amplified a genomic region of the gene of interest only if it does not contain a T-DNA inserted. T-DNA primer set amplified a region comprising the left border of the T-DNA and the sequence of the gene of interest adjacent to the left border of the T-DNA inserted (see appendices 1 and 4 for primer combinations and nucleotide sequences). The ThermoPrime *Taq* DNA polymerase from Thermo Scientific was used. Primer sequences were obtained from the T-DNA Express: Arabidopsis gene mapping tool website (http://signal.salk.edu/cgi-bin/tdnaexpress). Lyophilized oligonucleotides were supplied by Eurofins MWG Operon and were re-suspended in Biotechnology Performance Certified (BPC) water grade (Sigma) to a final concentration of 100 μM. Reaction mixtures were made up to a 25 μl volume as follow:

BPC water grade (Sigma)	9 μl
ReddyMix	12.5 μl
DNA template (100 ng/μl)	1.0 μl
Primer 1 (10 μM)	1.25 μl
Primer 2 (10 μM)	1.25 μl

A general profile of a PCR reaction is shown in Table 2.1. The optimal annealing temperature (Tm) of each primers used is presented in Appendix 4.

Table 2.1. PCR cycling parameters for genotyping transgenic plants. Annealing temperature and extension time of the segment 2 were variable, depending on both the primer pair used and the length of the DNA fragment to be amplified.

Step	Number of cycles	Temperature	Duration
1	1	95 °C	2 minutes
2	35	95 °C	25 seconds
		Primer Tm – 5 °C	35 seconds
		72 °C	1 minute per kb
3	1	72C	5 minutes

2.4.2.2. PCR for cloning procedures

cDNA synthesised from mRNA template extracted from *Arabidopsis* buds were amplified with the high fidelity *PfuUltra* II Fusion HS DNA polymerase (Agilent) to produce error-free amplification of DNA fragments. Primers were designed by hand and analysed using the tool OligoAnalyzer 3.1 of the Integrated DNA Technologies (http://eu.idtdna.com/analyzer/Applications/OligoAnalyzer/).

Lyophilized oligonucleotides were supplied by Eurofins MWG Operon and were re-suspended in BPC water grade (Sigma) to a final concentration of 100 μM. Reaction mixtures were made up, as recommended by the manufacturer's protocol, to a 50 μl volume as follow:

BPC water grade (Sigma)	40.5 μl
10X Pfu Ultra II reaction buffer	5.0 μl
dNTP mix (25 mM each dNTP)	0.5 μl
cDNA template (100 ng/μl)	1.0 μl
Primer 1 (10 μM)	1.0 μl
Primer 2 (10 μM)	1.0 μl
PfuUltra II fusion HS DNA polymerase	1.0 μl

A general profile of a PCR reaction is shown in Table 2.2. The optimal annealing temperature (Tm) of each primers used is presented in Appendix 4.

Table 2.2. PCR cycling parameters for cloning procedure using Pfu Ultra I fusion HS DNA polymerase.

Annealing temperature and extension time of the segment 2 were variable, depending on both the primer pair used and the length of the DNA fragment to be amplified.

Segment	Number of cycles	Temperature	Duration
1	1	95 °C	2 minutes
2	40	95 °C	20 seconds
		Primer Tm – 5 °C	20 seconds
		72 °C	15 seconds per kb
3	1	72 °C	3 minutes

2.4.3. DNA agarose gel electrophoresis

The concentration of agarose used to make a gel depends on the nucleotide length of the DNA fragments to be visualised. In all cases, 1 % agarose gels were used unless otherwise specified. Agarose was dissolved in 0.5X TBE in microwave. The molten solution was then cooled and ethidium bromide was added to a final concentration of 0.5 μg/ml prior to setting in Hybaid electrophoresis kits. DNA sample was mixed with 1X DNA loading buffer prior to loading. A 100 bp or 1 kb DNA ladder from New England BioLabs was also loaded to determine the molecular weight of the nucleic acid products analysed. Small and long gels, with a dimension of 7 cm X 8 cm or 11 cm X 14 cm, were respectively run at 90 V and 110 V in 0.5X TBE for an hour.

2.4.4. DNA detection

Images of DNA gel electrophoresis were captured using a FluorS Multi-imager (BioRad) and DNA fragments were analysed using Quantity One Software (BioRad).

2.4.5. Digestion of DNA by restriction enzymes

Digestions were carried out using the appropriate buffer and restriction enzymes supplied by New England Biolabs. The temperature of incubation and the incubation time were depending on the type of restriction enzyme used and both the amount of enzyme and DNA used. Typically, digestions were carried out at 37 °C for 3 hours.

2.4.6. Purification of digested DNA

Digested DNA were purified using the QIAQuick PCR purification kit (Qiagen) as stated in the manufacturer's protocol.

2.4.7. Extraction and purification of amplified DNA from agarose gel

Amplified DNA fragments were separated onto agarose electrophoresis gels and visualised under minimal UV light. The portion of the gel containing the desired DNA fragment was cut and DNA was then extracted and purified using the Qiagen gel extraction kit as stated in the manufacturer's protocol.

2.4.8. Ligation of DNA fragments into vectors

Ligation reactions were carried out using the In-Fusion™ advantage PCR cloning kit (Clontech). Vectors and inserts DNA were mix together in a 1:2 molar ratio. The cloning reaction was then set up as recommended by the manufacturer's protocol (Clontech).

2.4.9. Colony PCR

To rapidly screen *E. coli* resistant cells for the presence of the vector of interest, half of the colony was plated on a LA plate supplemented with appropriate antibiotics while the another half of the colony was mixed with 100 µl of BPC water grade (Sigma) and boiled at 95 °C for 10 minutes. 1 µl of the solution was then used with the addition of a primer set to identify the presence of the gene of interest in the DNA content of the bacterium. The solution was mixed with the PCR reaction mixture and the PCR was performed as mentioned in Section 2.4.2.1.

2.4.10. Extraction and purification of plasmid DNA from bacterial culture

Isolation of plasmid DNA was carried out using the Wizard *Plus* SV Minipreps DNA Purification System from Promega. The volume of *E. coli* overnight liquid culture used was depending on the type of vector to be isolated. Typically, 7 ml of *E. coli* DH5α liquid culture was used. The purification step was prepared as recommended by the manufacturer's protocol.

2.4.11. DNA sequencing

Sequencing of DNA was carried out using the dideoxy chain termination method by the Functional Genomics Laboratory of the University of Birmingham. DNA samples were prepared as described below and loaded onto a sequencing plate:

Plasmid DNA template   200-500 ng

Primer   3.2 pM

BPC water grade (Sigma)   Up to 10 μl

2.4.12. Sequencing analysis

Sequences obtained from the Functional Genomics Laboratory of the University of Birmingham were analysed using the software Chromas. Homology search of nucleic acid sequences was performed by using the programme BLAST, available from the National Centre for Biotechnology Information (www.ncbi.nlm.nih.gov).

2.5. Transformation of bacterial and yeast cells

Recipes for growth media are specified in appendix 2.

2.5.1. Preparation of bacterial and yeast competent cells

2.5.1.1. Preparation of *E. Coli* DH5α competent cells

5 µl of *E. coli* DH5α glycerol stock was spread on a LA plate. The plate was incubated inverted at 37 °C for 16 hours. A single colony of *E.*coli DH5α was used to inoculate 100 ml of Super Optimal Broth medium (SOB) in a 1 L flask (37 °C, 200 rpm, multitron infors) until the OD_{600nm} reaches 0.3. The culture was transferred into two ice-cold 50 ml centrifuge tubes and the cells were recovered by centrifugation (4 °C, 2 700 g, 10 minutes). The supernatant was poured off and the tubes were drained off for 1 minute. The pellet was re-suspended in 10 ml of ice-cold 0.1 M $CaCl_2$ and the cells were recovered at 2 700 g for 10 minutes at 4 °C. The supernatant was poured off and the pellet was re-suspended in 2 ml of ice-cold 0.1 M $CaCl_2$. Aliquots of 50 µl of competent cells were prepared. The competent cells were snap frozen in liquid nitrogen and were stored at - 80 °C.

2.5.1.2. Preparation of *A. tumefaciens* GV3101 competent cells

5 µl of *A. tumefaciens* GV3101 glycerol stock was spread on a LA plate supplemented with 25 µg/ml of rifampicin. The plate was incubated inverted at 28 °C for 3 days. A single colony of *A. tumefaciens* was inoculated in 3 ml of LB containing 25 µg/ml of rifampicin overnight (200 rpm, multitron infors, 28 °C). Subsequently to this, two flasks each containing 100 ml of LB (+ 25 µg/ml rifampicin) were inoculated with 0.5 ml of the overnight liquid culture and grew under agitation (200 rpm, multitron infors) at 28 °C until the OD_{600} reached 0.5-1.0. The liquid culture was then cooled down on ice and transferred to six 30 ml Corex tubes prior to centrifugation at 2 700 g at 4 °C for 5 minutes. The supernatant was then poured off and the tubes were inverted for 1 minute to drain the excess of liquid. Cells in each tube were re-suspended with 15 ml of ice-cold 10 % glycerol (v/v) then centrifuged as above. The pellet in each tube was re-suspended in 4 ml

of ice-cold 10 % glycerol before repeating the centrifugation step. Cells were re-suspended in each tube with 2 ml of ice-cold 10 % glycerol prior to centrifugation. Finally, the pellet was re-suspended in 1.5 ml of ice-cold 10 % glycerol. Aliquots of 50 μl of competent cells were prepared. The competent cells were snap frozen in liquid nitrogen and were stored at - 80 °C.

2.5.1.3. Preparation of *S. cerevisiae* Y2H Gold competent cells

S. cerevisiae Y2H Gold competent cells were prepared by using the Yeastmaker Yeast transformation System 2 according to the manufacturer's instructions (Clontech).

2.5.2. Transformation of bacterial and yeast cells

2.5.2.1. Transformation of *E. Coli* DH5α by heat shock

100 ng of plasmid DNA was added to a pre-thawed 50 μl aliquot of *E. coli* DH5α competent cells with a pre-chilled pipette tip and the mixture was gently stirred. The mixture was incubated on ice for 30 minutes and then heat-shocked at 42 °C for 90 seconds. The mixture was immediately returned on ice for 3 minutes prior to the addition of 800 μl of Super Optimal broth with Catabolite repression medium (SOC). The solution was then incubated at 37 °C (200 rpm, multitron infors, 1 h) for a recovery step. 200 μl of the solution was spread onto a LA plate supplemented with appropriate antibiotic. Plates were incubated inverted at 37 °C for 16 hours.

2.5.2.2. Transformation of *A. tumefaciens* GV3101 by electroporation

100-150 ng of plasmid DNA was added to a pre-thawed 50 μl aliquot of *A. tumefaciens* competent cells with a pre-chilled pipette tip and the mixture was gently stirred. The mixture was then transferred to a pre-cooled electroporation cuvette (Bio-Rad). The cuvette was gently tap to remove any air bubbles and set in an electroporator (Bio-Rad) with the setting 25 uF capacitance, 200 Ω resistance, 2.4 V voltage for 2 seconds. The cuvette was then left at 4 °C for 5 minutes and 500 μl of pre-cooled LB was added. The sample was gently mixed and transferred to a 1.5 ml eppendorf tube. The sample was incubated at room temperature for 10 minutes and then incubated under agitation (200 rpm, multitron infors) at 28 °C for 2.5 hours. Subsequently to the recovery step, 100 μl of the solution was spread on a fresh LA plate supplemented with appropriate antibiotic. Agar plates were incubated inverted at 28 °C for 3-4 days.

2.5.2.3. Transformation of *S. cerevisiae* Y2H Gold competent cells by polyethylene glycol/lithium acetate-based method

The transformation of *S. cerevisiae* competent cells was performed by using the high-efficiency polyethylene glycol/lithium acetate-based method of the Yeastmaker Yeast transformation System 2 according to the manufacturer's instructions (Clontech).

S. cerevisiae competent cells were transformed with 200-500 ng of appropriate plasmid DNA. Fresh competent cell were rapidly transformed to avoid any significant loss in efficiency. Unused competent cells were discarded. Approximately 100 μl of 1/10 and

1/100 dilutions of transformed cells were spread on appropriate SD dropout amino acids agar plates and the plates were incubated inverted at 30 °C for 2-5 days.

2.6. Protein manipulation

Recipes for reagents are specified in Appendix 3.

2.6.1. Protein extraction

2.6.1.1. Protein extraction from *S. cerevisiae* using YeastBuster

5 µl of *S. cerevisiae* glycerol stock was spreaded onto the appropriate SD dropout amino acids agar plate. The plate was incubated inverted at 30 °C for 3 days. A single colony of *S. cerevisiae* was used to inoculate 5 ml of the appropriate SD broth dropout amino acids medium and the culture was incubated overnight (30 °C, 225 rpm, multitron infors). The overnight culture was vortexed for 1 minute to disperse the clump of cells and the whole volume of culture was used to inoculate 50 ml of YPDA broth medium. The culture was grown at 30 °C under agitation (250 rpm, multitron infors) until an OD_{600nm} of 0.4-0.6 was reached. The culture was quickly chilled by pouring it into a pre-chilled 100 ml centrifuge tube halfway filled with ice-cold SDW. Then, the tube was centrifuged at 1000 g for 5 minutes at 4 °C. The supernatant was poured off and the pellet was re-suspended in 50 ml of ice-cold SDW. The pellet was recovered by centrifugation at 1,000 g for 5 minutes at 4 °C. The pellet was re-suspended in 1.5 ml of ice-cold SDW and stored at -70 °C. The extraction of proteins from yeast cells was performed by using YeastBuster protein

extraction kit as stated by the manufacturer's recommendations (Novagen). The protein extract was stored at 4 °C, to avoid inactivation of proteins by freeze-thaw cycles, before loading onto SDS-polyacrylamide gel.

2.6.1.2. Protein extraction from *S. cerevisiae* using TCA precipitation

The preparation of yeast cultures for protein extraction was performed as described in the Section 2.6.1.1. Each cell pellet was re-suspended in 100 µl of ice-cold TCA buffer per 7.5 OD_{600nm} units of cell culture (the total number of OD_{600nm} units for a liquid culture is defined by multiplying the OD_{600nm} by the volume of culture). The re-suspension solution was transferred to a pre-chilled tube containing 100 µl of 425-600 microns glass beads (SIGMA) and 100 µl of ice-cold 20 % TCA (w/v) per 7.5 OD_{600nm} units of cells. The tube was vortexed for 10 minutes at 4 °C and then put on ice for 1 minute. The supernatant above the settled glass beads was transferred to a new tube and left on ice (first cell extract). The glass beads were washed with 500 µl of an ice-cold 1:1 solution of 20 % TCA and TCA buffer. The tube was vortexed for 5 minutes at 4 °C and then put on ice for 1 minute. The supernatant above the settled glass beads was transferred to the first cell extract. The tube containing the two cell extracts was centrifuged at 15.7 g, 4 °C for 10 minutes. The supernatant was discarded and the pellet was re-suspended in TCA-Laemmli loading buffer (10 µl of TCA-Laemmli loading buffer, defined in Appendix 3, per OD_{600nm} units of cells).

2.6.1.3. Protein extraction from plant

Plant tissue was collected in an eppendorf and snap froze in liquid nitrogen before being stored at - 80 °C until required. Plant material was ground to a powder with a blue pestle for 5 minutes. The tissue was not allowed to thaw by continually refreezing the tube in liquid nitrogen. One volume of IP buffer was then added and the plant material was grounded for 10 minutes. After this, one volume of IP buffer was added and the sample was briefly vortexed. Then, the sample was centrifuged for 20 minutes, 4.5 g at 4 °C. The supernatant containing the protein extract was further analysed.

2.6.2. Estimating protein concentration

Protein concentration was estimated using the BioRad assay according to the manufacturer's instructions. Bradford reagent was added to the protein samples and the absorbance was measured at 595_{nm} using a Jenway 6305 UV/Vis spectrophotometer. A solution of BSA 10 mg/ml (New England Biolabs) was used as a standard.

2.6.3. Sodium-dodecyl-sulfate polyacrylamide gel electrophoresis.

Proteins were analysed by sodium-dodecyl-sulfate polyacrylamide gel electrophoresis (SDS-PAGE) using Bio-Rad self-assembly kits. The percentage of polyacrylamide used depended on the molecular weight of the protein being studied. Proteins of low molecular weights were analysed on 12 % SDS-polyacrylamide gels whereas high molecular weight proteins (over 60 kDA) were analysed on 10 % SDS-polyacrylamide gels. After pouring 7

ml of resolving gel into the glass plates, a layer of absolute butanol was added to level the top of the gel. After the resolving gel had set, the butanol was rinsed off with SDW. The stacking gel was then cast on the top of the resolving gel and a comb containing wells of the appropriate size was inserted. For both gel, TEMED was added just prior to pouring as this cause the polyacrylamide to polymerise. After polymerisation of the stacking gel, the comb was removed and the gel was assembled to the electrophoresis apparatus as described in the manufacturer's instructions. Proteins to be loaded were mixed with 1X SDS-loading dye and boiled for 5 minutes prior to loading. The protein molecular weight marker PageRuler^{TM} Plus (fermentas) was loaded to estimate the molecular weight of the proteins being studied. Gels were run in 1X Electrode Buffer at 70 V for 30 minutes and 100 V until the dye reached the bottom of the gel.

2.6.4. Two dimensional gel electrophoresis

Plant crude extract was precipitated with 7 volumes of ice-cold acetone + 20 mM dithiothreitol (DTT) overnight at − 20 °C. The solution was centrifuged at 4.5 g, 4 °C for 2 minutes. The supernatant was discarded and the pellet was washed two times with 7 volumes of ice-cold acetone + 20 mM DTT. Following the final centrifugation, the supernatant was discarded and the pellet was dried at room temperature for 5 minutes before being incubated at − 20 °C for 1 hour. The rehydratation step and the first-dimension isoelectric focusing step were performed using Ettan^{TM} IPGphor^{TM} Isoelectric Focusing System and 7 cm immobiline DryStrips pH 3-5.6 NL according to the manufacturer's instructions (Amersham Biosciences). Following equilibration of the immobiline DryStrips, a 10 % SDS page was prepared as mentioned in the Section 2.6.3 at

the exception that the comb containing wells was not used. Instead, the immobiline DryStrip was placed in contact to the stacking gel and a small well was cut out in the resolving gel and was used to load the protein molecular weight marker PageRuler[TM] Plus (fermentas) on the side of the immobiline DryStrip. Gels were run in 1X Electrode Buffer at 50 V for 30 minutes. The immobiline DryStrips were then removed and the gels were run at 100 V until the dye reached the bottom of the gel.

2.6.5. Western blotting

2.6.5.1. Transfer of proteins to nitrocellulose membrane

Proteins were resolved by SDS-PAGE and the stacking gel was removed. The western blot apparatus was then assembled with the gel according to the manufacturer's instructions (Bio-Rad). Four sheets of Whatman 3M filter papers and two sponges were cut to the size of the gel and were soaked in protein transfer buffer for 10 minutes. The gel was placed in contact to a nitrocellulose membrane pre-soaked in protein transfer and two Whatmans paper and a sponge were added on the top of the membrane. Two additional Whatman papers and a sponge were placed directly in contact to the back side of the gel. Great care was taken to ensure that no air bubble was in this stack of membranes. The layered arrangement was then placed between two electroblotting pads (Bio-Rads) and inserted into an electroblotting tank (Bio-Rad). An ice block was added to prevent the solution to over-heat and the tank was filled with protein transfer buffer. Bio-Rad power packs were used to blot the gel at 400 mA under agitation for 1.5 h at 4 °C. Following to transfer, the

nitrocellulose membrane was removed and placed in blocking buffer at 4 °C under agitation for subsequent blotting.

2.6.5.2. Antibody blotting

The nitrocellulose membrane was placed in blocking buffer under agitation on a desk top shaker at 4 °C overnight. All subsequent steps were performed at room temperature and under agitation using a desk top shaker. The membrane was incubated for 2 hours in blocking buffer containing the primary antiserum. The membrane was washed three times 10 minutes in 1X TBST buffer and then incubated with a blocking buffer containing the secondary antibody conjugated with horseradish-peroxidase for 1 hour. The membrane was then washed four times 10 minutes in 1X TBST buffer before detection.

2.6.5.3. Enhanced chemiluminescence detection

Proteins were detected with ECL blotting reagents according to the manufacturer's instructions (GE Healthcare). Blots were placed on Hyperfilm-ECL (Amersham) and developed using an X-o-Graph (Fuji).

2.6.6. Coomassie staining of protein gels

Gels were stained in Coomasie stain solution under agitation (AOS rocking platform) at 100 rpm for 1h30 and then destained overnight in Coomasie destain solution under the same agitation. Gels were then washed in SDW and stored between cellophane sheets.

2.6.7. Ponceau S staining of protein gels

Nitrocellulose membranes were stained two times 5minutes in Ponceau S stain solution under agitation (AOS rocking platform) at 100 rpm. The membranes were then washed two times in SDW under agitation (AOS rocking platform) at 100 rpm for 5 minutes.

2.6.8. Antiserum purification

2.6.8.1. Antiserum purification by blotted antigen

The same recombinant protein used to generate an antiserum was loaded onto a SDS polyacrylamide gel and transferred to a nitrocellulose membrane. Proteins were visualized by Ponceau S staining and the band corresponding to the predicted molecular weight of the recombinant protein was cut. The part of nitrocellulose containing the recombinant protein was then incubated two times 30 minutes with a blocking buffer before incubation with 2 ml of a solution 1:1 antiserum/blocking buffer on a roll overnight and at 4 °C. The nitrocellulose membrane was washed four times 5 minutes with a solution of 1X TBST buffer on a roll at room temperature. The supernatant was discarded and 1 ml of elution buffer was added. The solution was mixed for 30 seconds and the supernatant, containing the purified antibody, was transferred to a new tube with 70 µl of 1.5M Tris. The elution step was repeated 2 more times and both supernatants were pooled in the tube containing the first supernatant solution.

2.6.8.2. Antiserum purification by *E. Coli*-reactive protein column purification

Antiserum was purified by using the immobilized *E. coli* lysate kit (pierce thermo scientific) as stated in the manufacturer's protocol.

2.6.9. Immunoprecipitation

2.6.9.1. Binding antibodies to protein A beads

One volume of protein A beads (bv) (Bio-Rad) was briefly washed two times with 10 bv of a solution of 1X TBST. The solution was centrifuged for 2 minutes, 4.5 g at 4 °C. The supernatant was discarded. Then, a volume of antibody was added to the protein A beads to reach a ratio of 1 mg of antibody per ml of beads. The solution was mixed on a rotator for 1 hour at room temperature. The beads were then washed three times briefly with 10 bv of 1X TBST on a rotator at 4 °C. The solution was centrifuged for 2 minutes, 4.5 g at 4 °C and the supernatant was discarded.

2.6.9.2. Cross-linking of antibodies to beads

Beads bound with the antibody were washed briefly three times with a solution of 0.2 M sodium borate (pH 9.2). The solution was centrifuged for 2 minutes, 4.5 g at 4 °C and the supernatant was discarded. Beads were then mixed with a solution of 20 mM dimethyl pimelimidate dihydrochloride (SIGMA) in 0.2 M sodium borate (pH 9.2) on a rotator for 30 minutes at room temperature. The reaction of cross-linking was stopped by washing the

beads two times with 10 bv of 0.2 M Tris-HCl, pH 8.0 on a rotator for 10 minutes at room temperature. The solution was centrifuged for 2 minutes, 4.5 g at 4 °C and the supernatant was discarded. The beads were then washed two times briefly with 10 bv of 1X TBST on a rotator for 10 minutes at room temperature. The solution was centrifuged for 2 minutes, 4.5 g at 4 °C and the supernatant was discarded.

2.6.9.3. Pre-elution with glycine

To remove non-crosslinked antibodies, beads were washed two times briefly with 10 bv of a solution of 0.1 M glycine, pH 2.0. Beads were then washed three times briefly with 10 bv of 1X TBST at 4 °C. Antibody-coupled beads were stored at 4 °C in 1X TBST + 0.05 % of sodium azide.

2.6.9.4. Pre-clearing of the protein extract

Protein extraction from plant tissue was performed as described above. The crude extract was incubated with a solution of non-specific antibody-coupled beads (1 μl of antibody-coupled bead for 150 μg of protein) on a rotator for 30 minutes at 4 °C. The solution was centrifuged for 2 minutes, 4.5 g at 4 °C and the supernatant was used for further steps.

2.6.9.5. Immunoprecipitation

The supernatant containing the pre-cleared protein extract was incubated with a solution of specific antibody-coupled beads (1 μl of antibody-coupled bead for 150 μg of protein) on a

rotator for 30 minutes at 4 °C. The solution was centrifuged for 2 minutes, 4.5 g at 4 °C and the supernatant was discarded. Beads were re-suspended in a solution of 50 bv ice-cold IPW buffer (IP buffer + 0.1 % NP-40 (SIGMA), 1X PIM, 0.1 mM phenylmethylsulfonyl fluoride) and incubated on a rotator for 5 minutes at 4 °C. The solution was centrifuged for 2 minutes, 4.5 g at 4 °C and the supernatant was discarded. Two more washed with 50 bv ice-cold IPW buffer were performed.

2.6.9.6. Elution of immunoprecipitated proteins from beads

Beads were re-suspended with 100 μl of a solution of 150 mM NaCl. The solution was transferred to an Axygen low-retention 0.2 ml PCR tube. The solution was centrifuged for 2 minutes, 4.5 g at 4 °C and the supernatant was discarded. Beads were then incubated with 40 μ of 0.1 M glycine (pH 2.0) and the solution was mixed by flicking the tube for 1 minute at 4 °C. The solution was centrifuged for 2 minutes, 4.5 g at 4 °C and the supernatant was transferred to a new Axygen low-retention 0.2 ml PCR tube. Beads were incubated a second time with 20 μ of 0.1 M glycine (pH 2.0) and the solution was mixed by flicking the tube for 1 minute at 4 °C. The solution was centrifuged for 2 minutes, 4.5 g at 4 °C and the supernatant was pooled with the previous supernatant. Beads were briefly washed three times with 10 bv of 1X TBST before storage. The solutions of immunoprecipitated proteins were kept overnight at 4 °C before analysis.

2.7. Cytological procedures

Recipes for reagents are specified in Appendix 3.

All microscopic slides (SuperFrost VWR) were washed with acetone then water and finally with ethanol for 10 minutes each wash. The slides were left at room temperature to dry and were recovered with cling film.

2.7.1. Alexander's staining of *Arabidopsis* pollen

Arabidopsis inflorescences were fixed in a solution of 10 % ethanol (v/v) overnight at room temperature. Mature anthers were dissected and placed in a drop of water on a microscopic slide. The anthers were squashed with the edge of a forceps to release the pollen grains and 2-3 drops of Alexander's stain solution were added. The slides were then covered with a cover slip which was sealed with a rubber solution. Slides were incubated on a hot block at 50 °C for 1.5 hours.

2.7.2. DAPI-stained chromosome spread

Arabidopsis inflorescences were fixed in a fixative solution composed of 3:1 ethanol-acetic acid for 3 hours on ice. The inflorescences were then incubated in a fresh solution of fixative for 5 hours at room temperature before changing the fixative solution one more time. Fix buds with a length of approximately 0.2-0.7 mm, corresponding to the floral stages 8 to 10 as defined by Smyth *et al.* (1990) and linked with meiotic stages by

Armstrong and Jones (2003), were dissected with a pair of forceps in a fresh solution of fixative solution in a black jar under a Nikon SMZ 800 stereomicroscope (Armstrong & Jones, 2003; Smyth et al, 1990). Buds were then washed three times in a solution of citrate buffer for 2 minutes. Buds were then incubated with an enzyme solution in a moist box for 1.5 hours at 37 °C. Following this, the reaction was stopped by replacing the enzyme solution with a solution of citrate buffer. One or two buds, depending on their respective size, were transferred to a drop of SDW on a slide and were gently tapped with a brass rod and two times 5 µl of 60 % acetic acid was added. The mixture containing the meiocytes was then mixed with a needle and the slides were placed on a hot block at 48 °C for 1 minute. 125 µL of ice-cold fixative solution was added on the slides, which were subsequently dried inverted using a hairdryer. The slides were counterstained with 14 µl of a solution containing DAPI/Vectashield.

2.7.3. Fluorescence In-Situ Hybridisation

Chromosome spreading was prepared using the method as previously described in Section 2.7.2. Slides with the desirable meiotic stages were washed with absolute ethanol until the cover slip could be easily removed from the slide. The slides were then washed in 2X SSC for 10 minutes at room temperature. The slides were then incubated in a solution of pepsin for 1.30 minutes at 37 °C. Following this, the slides were washed with 2X SSC for 10 minutes and with 4 % paraformaldehyde (w/v) for 10 minutes at room temperature. The slides were briefly rinsed in SDW prior to an alcohol series washes with 70 %, 85 % and absolute ethanol (v/v) for 2 minutes incubation each wash. 19 µl of hybridisation solution was applied onto each slide. A cover slip was added to each slide and sealed with rubber

solution. The slides were then placed on a hot block for 4 minutes at 75 °C and then incubated in a moist box for 1-2 days at 37 °C. Following hybridisation, the cover slips were removed and the slides were washed three times with 50 % formamide in 2X SSC, one time with 2X SSC and one time with 4T. Each wash was performed in a fume cupboard at 45 °C for 5 minutes. The slides were then washed with 4T at room temperature for 5 minutes before applying 50 μl of a solution containing the secondary antibodies. The slides were incubated in a moist box for 30 minutes at 37 °C. The slides were then washed three times with 4T for 5 minutes at room temperature and the slides were counterstained with 14 μl of a solution containing DAPI/Vectashield (Sanchez Moran et al, 2001).

2.7.4. BrdU detection

Chromosome spreading was prepared using the method as previously described in Section 2.7.2 at the exemption that the slides were not counterstained with DAPI/Vectashield. The slides were washed 3 times with a solution of PBST at room temperature for 5 minutes. BrdU labelling of nuclear cells was detected by probing the slides with an anti-BrdU antibody (Roche) as mentioned by the manufacturer's recommendations. The slides were counterstained with 14 μl of a solution containing DAPI/Vectashield.

2.7.5. Immunolocalisation

Immature anthers from fresh buds with a length of approximately 0.2-0.5 mm, corresponding to the floral stages 8 and 9 as defined by Smyth *et al.* (1990) and linked with meiotic stages by Armstrong and Jones (2003), were dissected, on a damp filter paper

(Fisher Scientific), using a forceps and a needle under a Nikon SMZ 800 stereomicroscope (Armstrong & Jones, 2003; Smyth et al, 1990). 6 buds were dissected for each slide prepared and the anthers were collected in 5 µl of EM digestion mix. After dissection, 5 µl of EM digestion mix was applied on the anthers and the slides were incubated in a moist box on a hot block at 37 °C for 1 minute. Following this, the anthers were gently tapped with a brass rod to release meiocytes. 10 µl of EM digestion mix was added and the slides were incubated in a moist box on a hot block at 37 °C for 2 minutes. 10 µl of 1 % lipsol (v/v) was then applied on each slide and the solution was mixed for 1 minute with a needle to individualise the meiocytes (Armstrong et al, 2002). Before the slides started to dry, 20 µl of 4 % paraformaldehyde (w/v) was added on each slide and the slides were placed in a fume cupboard. After the slides were dried, they were briefly washed in PBST and 50 µl of a solution containing the primary antibodies in EM block was applied on each slide. The slides were then incubated in a moist box for 1 or 2 days, depending on the antibodies being used, at 4 °C. After incubation, the slides were washed three times with PBST for 5 minutes at room temperature. 50 µl of a solution containing the secondary antibodies diluted in EM block were applied on the slides. The slides were then incubated in a moist box at 37 °C for 30 minutes. After incubation, the slides were washed three times with PBST for 5 minutes at room temperature and were counterstained with 7 µl of a solution containing DAPI/Vectashield.

2.7.6. Microscopy and image analysis

For scoring pollen viability, slides were prepared using Alexander's staining method and were examined by using a Leitz Dialux 22 microscope binocular. Images were captures by

a photometrics sensys camera on a Nikon eclipse E600 fluorescence microscope. Images were analysed using Smart Capture 3 software.

Slides prepared for DAPI staining and FISH labelling were examined by fluorescence microscopy using an Olympus BX61. Images were captured by a Hamamatsu C8484 digital camera and were analysed using Smart Capture 3 software.

Slides prepared for immunolocalisation studies were examined by fluorescence microscopy using a Nikon eclipse 90i. Images were captured by a Nikon DS-Qi1Mc digital camera and were analysed using NIS-Elements AR 3.2 software. Images were deconvolved by the Mexican hat function.

2.8. Yeast two hybrid assay

Yeast two hybrid assay was performed using the Matchmaker Gold Yeast Two-Hybrid Sytem, as recommended by the manufacturer's protocol (Clontech). Co-transformed yeast cells, expressing respectively a bait protein fused to the Gal4 DNA-binding domain and a prey protein fused to the Gal4 DNA activation domain, were grown on SD dropout leucine (Leu), tryptophan (Trp), histidine (His), adenine (Ade) agar plates and SD dropout -Leu, -Trp, -His agar plates to test for protein-protein interaction. Agar plates were inverted incubated at 30 °C for up to 6 days. To confirm the interaction and assess the strength of interaction between two proteins, a colony was used to inoculate 5 ml of SD broth dropout -Leu, -Trp. The culture was incubated at 30 °C under agitation (multitron infors) at 250 rpm for 15 hours. Liquid cultures with a similar OD_{600nm} of approximately 0.5, were used

for the drop dilution assay. 3 µl of the liquid culture with no dilution, 1/10 and 1/100 dilutions in 0.9 % NaCl (w/v) solution were dropped on the appropriate SD dropout amino acids agar plates. Agar plates were inverted incubated at 30 °C for 2 days. Images were captured by a FinePix S20 Pro digital camera.

2.9. Statistical procedures

All statistical procedures were carried out using Microsoft Office Excel.

Chapter III

AtASY1 physically interacts with the coiled-coil

domain of AtASY3 to form a complex that favours

inter-homologue CO formation

3.1. Introduction

In budding yeast, Spo11-dependent DSBs are principally repaired by inter-homologue recombination. It is though that Red1 and Hop1 form a complex with the forkhead kinase Mek1 to establish a barrier to inter-sister recombination (Hong et al, 2013; Kim et al, 2010; Niu et al, 2005; Wan et al, 2004; Woltering et al, 2000).

Caryl *et al.* (2000) identified AtASY1, a HORMA protein, required for synapsis and inter-homologue CO formation. The authors proposed that the protein is the functional orthologue of the budding yeast Hop1 (Armstrong et al, 2002; Caryl et al, 2000; Sanchez-Moran et al, 2007a). More recently, a new component of the chromosome axis sharing some functional similarities with Red1 was identified as AtASY3. AtASY3 is essential for the proper localisation of AtASY1, synapsis between homologous chromosomes and the formation of inter-homologue COs (Ferdous et al, 2012).

The initial aim of this project consisted at analysing the amino acid sequence of AtASY3 to gain more information about the function of the protein. A database search using the Conserved Domain Search Service from the National Center for Biotechnology Information revealed that a putative coiled-coil domain located towards the C-terminus of the protein is the only conserved predicted secondary structure found between AtASY3 and its functional orthologues. In *S. cerevisiae*, Woltering *et al.*, (2000) showed that the regions upstream of the first coiled-coil domain and the second coiled-coil domain of Red1 are involved in the interaction with Hop1. Therefore, the second part of the project consisted of testing the interaction between AtASY1 and AtASY3. A yeast two-hybrid

assay showed that the two proteins physically interact in the same manner as their functional orthologues in budding yeast. To confirm the interaction between the two proteins, an anti-AtASY3 antiserum was purified and used to immunoprecipitate AtASY1 from yeast crude extracts. Additionally, Osman and Franklin found that BoASY3, the homologue of AtASY3 in *Brassica oleracea,* was pulled down with an anti-AtASY1 antibody. Overall these results suggest that ASY1 forms a complex with ASY3 in plant. The coiled-coil domain conserved between AtASY3 and its functional orthologues seems to be particularly important for the function of the protein in several model organisms. For instance in *S. cerevisiae*, the coiled-coil domain located towards the C-terminus of Red1 is involved in the homo-dimerization of the protein, the interaction with Zip1 and contains a lysine rich motif that undergoes SUMO modification (Eichinger & Jentsch, 2010; Woltering et al, 2000).

Yeast two-hybrid assay and co-immunoprecipitation study showed that AtASY3 interacts with AtASY1 via its coiled-coil domain. AtASY3 can also form a homo-dimer through the coiled-coil domain. The similarity of function between AtASY1/AtASY3 and their functional orthologues in budding yeast suggests that the two proteins may form a complex to prevent the use of the sister chromatid during the repair of AtSPO11-dependent DSBs in *Arabidopsis*.

3.2. Comparative analysis and structure prediction of AtASY3 with its functional orthologues in other model organisms

A blast search of sequence similarity between budding yeast meiotic proteins and the *Arabidopsis* proteome is a powerful method to identify new proteins involved in *Arabidopsis* meiosis. However, the degree of similarity at the amino acid level between proteins across kingdoms is often low. Therefore, the secondary and tertiary structures of proteins are analysed to detect homology of structure (Kumar et al, 2010).

3.2.1. Comparative analysis of AtASY3 and its functional orthologues

The full length amino acid sequence of AtASY3 was successively aligned with the full length amino acid sequence of six functional orthologues; among them, three belong to the kingdom *Fungi* and three belong to the kingdom *Planta*. Comparative analysis between amino acid sequences was carried out using the sequence similarity search of the European Bioinformatics Institute (www.ebi.ac.uk) and the amino acid sequence of the different proteins were obtained from the National Center for Biotechnology Information (ww.ncbi.nlm.nih.gov).

The degree of conservation between the amino acid sequence of AtASY3 and its fungal orthologues is relatively low with less than 17% amino acid identity and between 19% and 41% amino acid similarity. AtASY3 shares about 25 % identity with OsPAIR3 and HvASY3. In contrast, AtASY3 has 74% identity and 82% similarity with BoASY3 (Table 3.1).

The low degree of sequence similarity between AtASY3 and its functional orthologues from yeasts and monocotyledon plants is not surprising and a similar lack of sequence similarity between meiotic proteins and their functional orthologues from different organisms was previously reported (Kumar et al, 2010). Additionally, the high level of sequence identity between AtASY3 and BoASY3 is in accord with the recent separation of the lineages between *Arabidopsis* and *Brassica* (Town et al, 2006). The overall low homology between AtASY3 and its functional orthologues suggests that the proteins may share a similar structural role rather than a similar enzymatic function.

3.2.2. Structural analysis of AtASY3 and its functional orthologues

Woltering *et al.* (2000) predicted the presence of two putative coiled-coil domains in Red1. Coiled-coil is a supersecondary structure, in which two to five helices are wrapped around each other. Coiled-coil domains are important structures involved in protein-protein interactions (Mason & Arndt, 2004). A database search, using the coiled-coil prediction tool of the Pôle BioInformatique Lyonnais (npsa-pbil.ibcp.fr) and the tool of the European Molecular Biology network (www.embnet.org), revealed that RED1 has two putative coiled-coil domains at the positions 359-400 and 750-808. One coiled-coil domain was predicted towards the C-terminus of all AtASY3 functional orthologues apart from its *K. lactis* orthologue.

The Search for Conserved Domain of the National Center for Biotechnology Information (http://www.ncbi.nlm.nih.gov/Structure/cdd/wrpsb.cgi) was used to identify additional predicted domains of AtASY3 and its functional orthologues. A predicted P-loop NTPase

was predicted at the position 155-273 (P = 0.05) and a condensin domain was predicted at the position 391-616 (P = 0.02) of AtASY3. Interestingly, a condensin domain was also predicted for its budding yeast orthologue Red1 at the position 429-704 (P = 0.04) (Figure 3.1). However, no predicted domain with a P value under 0.05 was found for the other AtASY3 functional orthologues.

Species	Degree of identity (%)	Degree of similarity (%)
ScRed1	16.4	30
KlRed1	11.5	19.3
SpRec10	14.9	41
OsPAIR3	25.6	25.5
BoASY3	73.6	82
HvASY3	23.3	39.1

Table 3.1. Sequence homology between AtASY3 and its functional orthologues
The whole amino acid sequence of AtASY3 was successively aligned with the whole amino acid sequence of each of its functional orthologues to determine the degree of identity and similarity. Sc: *Saccharomyces cerevisiae*, Kl: *Kluyveromyces lactis*, Sp: *Schizosaccharomyces pombe*, Os: *Oryza sativa*, Bo: *Brassica oleracea*, Hv: *Hordeum vulgare*.

A

AtASY3

B
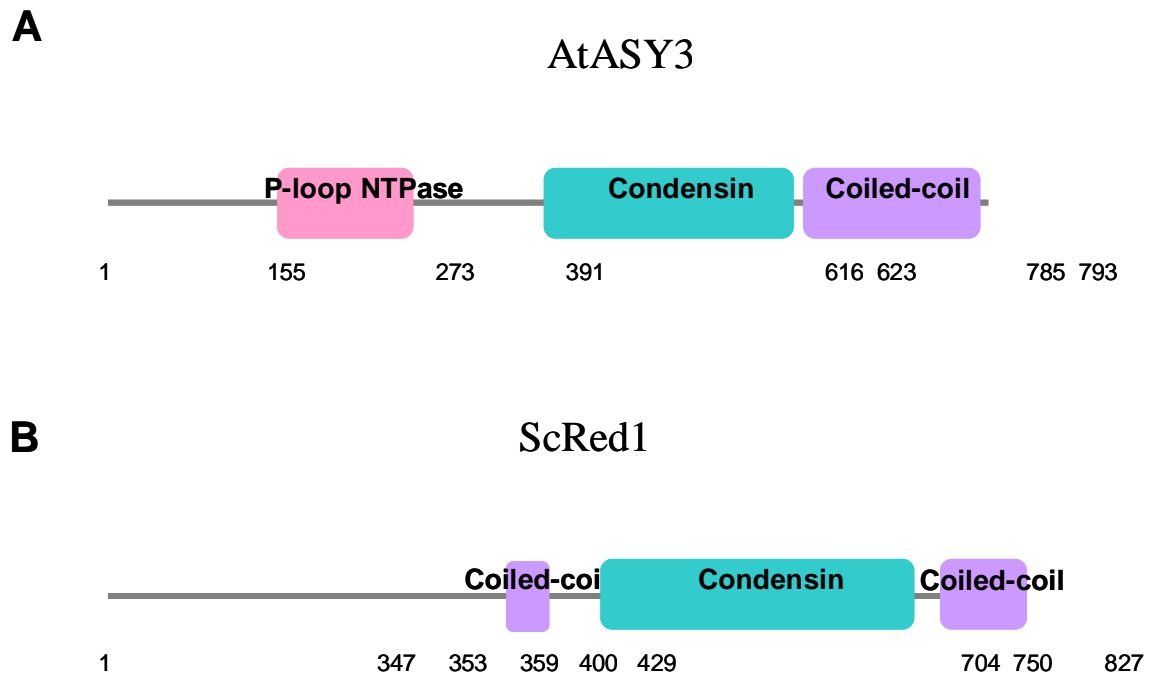
ScRed1

Figure 3.1. Schematic illustration of the predicted domains of AtASY3 (A) and ScRed1 (B) and their relative position

AtASY3 and budding yeast ScRed1 have similar predicted domains located towards the C-terminus region of both proteins. The P loop NTPase and the condensin domain of AtASY3 are predicted with a P value of $P = 0.05$ and $P = 0.02$, respectively. The condensin domain of ScRed1 is predicted with a P value of $P = 0.04$.

3.3. AtASY1 physically interacts with AtASY3 in a yeast two-hybrid assay

In budding yeast, Hop1 and Red1 form a complex that favours inter-homologue recombination (Woltering et al, 2000). Immunocytochemistry analysis of chromosome spread preparations from PMCs of *Arabidopsis* wild-type and an *Atasy3* T-DNA insertion mutant suggested that AtASY3 may be a functional orthologue of RED1 (Ferdous et al, 2012). We hypothesised that if AtASY1 and AtASY3 are the functional orthologues of Hop1 and Red1 respectively, they may also physically interact like their yeast counterparts (Woltering et al, 2000).

To test the potential interaction between AtASY1 and AtASY3, a yeast two-hybrid assay was performed. Amplification of the full length coding sequence of AtASY1 and AtASY3 was carried out by PCR amplification of *Arabidopsis* bud cDNA, using the primer sets pGAD-ASY1 F/pGAD-ASY1 R, pGBK-ASY1 F/pGBK-ASY1 R, pGAD-ASY3$_{1-793}$ F/ pGAD-ASY3$_{1-793}$ R and pGBK-ASY3$_{1-793}$ F/ pGBK-ASY3$_{1-793}$ R (See Appendix for the nucleotide sequences). The corresponding PCR products were then cloned into pGADT7 and pGBKT7 vectors to form in-frame fusions with the GAL4 activating domain (AD) and the GAL4 DNA-binding domain (BD). The DNA-binding domain specifically binds to a binding site in the UAS region, which is present in the G1 and G2 promoters that regulate the expression of the two yeast reporter genes *HIS3* and *ADE2*. *HIS3* and *ADE2* gene products are involved in the histidine and adenine synthesise pathways, respectively. A yeast two-hybrid assay was performed as described in Materials and Methods. Y2HGold yeast cells were co-transformed with vectors encoding AtASY1-AD and AtASY3-BD and

the reciprocal pair of constructs. Co-transformed colonies were screened on SD dropout leucine and tryptophan (SD-LT). The positive co-transformed cells were then incubated on SD dropout media lacking leucine, tryptophan and histidine (SD-LTH) or SD dropout media lacking leucine, tryptophan, histidine and adenine (SD-LTHA) to test for protein-protein interaction through the activation of the two nutritional reporter genes *HIS3* and *ADE2*. In addition, negative controls were generated by co-transforming Y2HGold cells with either the AtASY1 or AtASY3 construct in addition to the empty complementary vector, to ensure that no auto-activation of the reporter genes occurred.

After 4-5 days of incubation, growth of yeast cells expressing AtASY1 and AtASY3 was observed on SD–LTH and SD–LTHA (Figure 3.2). In contrast, yeast cells expressing either AtASY1 or AtASY3 alone were unable to grow on the more stringent media SD–LTHA. A few colonies were observed on the less stringent media SD–LTH for cells co-transformed with pGBKT7-ASY1/pGADT7 and pGADT7-ASY3/pGBKT7. The degree of growth was assessed by serial drop dilutions of mid-exponential-phase cell cultures. Growth of colonies co-transformed with pGBKT7-ASY1/pGADT7 and pGADT7-ASY3/pGBKT7 was observed on SD –LTH at no dilution but not at the 1/10 and 1/100 dilution, suggesting that the expression of the reporter gene *HIS3* was very weak compared to the cells expressing both AtASY1 and AtASY3 (Figure 3.2). The histidine competitor 3-amino-1,2,4-triazole, which is a competitive inhibitor of the *HIS3* gene product, was not used as it was not needed to validate an interaction between AtASY1 and AtASY3. The growth of yeast cells expressing only the fused protein AtASY3-AD on SD–LTH may be due to the DNA-binding property of AtASY3 although it is unlikely that AtASY3 binds to yeast promoters. The growth of yeast cells on the restrictive media is likely due to weak

leaky expression of *HIS3*. Protein extraction and subsequent western blot analysis were performed for all combinations of co-transformed cells to ensure that the recombinant proteins were correctly expressed in yeast cells (Figure 3.3). The recombinant protein AtASY3 was not consistently observed at the expected molecular weight of 105-110 kDA on western blotting using a rabbit anti-AtASY3 antiserum. Instead, several bands were observed with a molecular weight of 70 kDA, 50 kDA and 20 kDA. The proportion of each band was variable between samples. A similar shift of migration was observed with the recombinant protein AtASY1 but to a lesser extent. This may represent a truncated version of the protein that occurred during the procedure of protein extraction.

Overall, the yeast two-hyrbid assay showed that AtASY1 physically interacts with AtASY3 and suggests that the two proteins may also interact in *Arabidopsis*. The interaction between the two proteins was not observed every time the experiment was performed. Several types of media with slight variations in their composition were used to determine the cause of the presence/absence of interaction. It was however not possible to determine the cause of the variations observed in the interaction between AtASY1 and AtASY3. In addition, more cells co-transformed with the vectors encoding the fusion proteins AtASY1-BD and AtASY3-AD grew on the restrictive media SD-LTHA than the cells co-transformed with the reciprocal pair of vectors. It is possible that the interaction between the two proteins is transient and the post-translational modification of at least one of the two proteins is required to stabilize the complex. It is also possible that AtASY1 and or AtASY3 are toxic at some level for the cells. Similarly, the interaction between Red1 and Hop1, the yeast functional orthologues of AtASY3 and AtASY1, was not consistently

observed (Wang TF, personal communication). In order to validate the interaction between AtASY1 and AtASY3, it is important to confirm the interaction by a different technique.
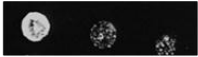
	SD -LT	SD -LTH	SD -LTHA

pGADT7-AtASY1/pGBKT7

pGBKT7-AtASY1/pGADT7

pGADT7-AtASY3/pGBKT7

pGBKT7-AtASY3/pGADT7

pGADT7-AtASY1/pGBKT7-AtASY3

pGADT7-AtASY3/pGBKT7-AtASY1

Figure 3.2. AtASY1 and AtASY3 physically interact in a yeast two-hybrid assay

Full length nucleotide sequence of AtASY1 and AtASY3 were fused with the activating domain (in pGADT7 vector) and the binding domain (in pGBK7 vector) of GAL4. *S. cerevisiae* Y2H Gold cells were co-transformed with a combination of pGADT7/pGBKT7 vectors. Co-transformed yeast cells were screened on the restrictive media SD –LT. Growth of yeast cells expressing AtASY1-AD and AtASY3-BD, or the reciprocal fused proteins, was observed on the restrictive media SD -LTH and SD -LTHA. All negative controls were unable to grow on the most stringent media SD –LTHA. This suggests that AtASY1 and AtASY3 physically interact in a yeast two-hybrid assay. The strength of interaction between the two proteins was assessed by serial drop dilutions of mid-exponential-phase cell cultures. 3μl of undiluted, 1/10 and 1/100 diluted cultures were spotted on the selective agar medium and incubated at 30°C for 2 days.

AF α-AtASY1 AB   **α-AtASY3 AB**

Lane labels (left group, AF α-AtASY1 AB):
- pGADT7-AtASY1/pGBKT7
- pGADT7/pGBKT7-AtASY1
- pGADT7-AtASY1/pGBKT7-AtASY3
- pGADT7-AtASY3/pGBKT7-AtASY1

Lane labels (right group, α-AtASY3 AB):
- pGADT7-AtASY3/pGBKT7
- pGADT7/pGBKT7-AtASY3
- pGADT7-AtASY3/pGBKT7-AtASY1
- pGADT7-AtASY1/pGBKT7-AtASY3
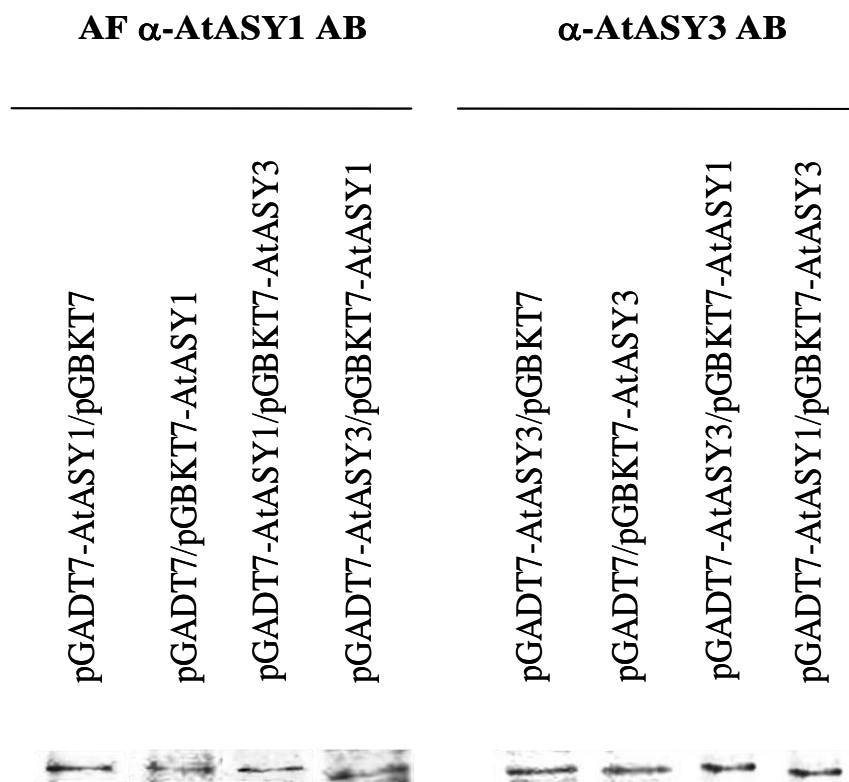
Figure 3.3. Protein expression analysis of AtASY1 and AtASY3 from yeast cells co-transformed with the corresponding vectors

75 μg of protein from each crude extract was loaded onto a 10 % acrylamide gel. C-Myc- and His-tagged-AtASY1 were detected by western blotting using an affinity-purified anti-AtASY1 antibody (AF α-AtASY1 AB) (provided by Osman K.) raised against the full length AtASY1 recombinant protein. C-Myc- and His-tagged-AtASY3 were detected by western blotting using an anti-AtASY3 antiserum raised against the C-terminus region of AtASY3 (α-AtASY3 AB) (provided by Ferdous M.). All fusion proteins were resolved at the correct predicted size; tagged-AtASY1: 85-90 kDA; tagged-AtASY3: 105-110 kDA. Composite photo comprising band images from different gels.

3.4. Purification of AtASY3 antiserum

Immunoprecipitation of proteins from *Arabidopsis* buds extract using an antibody against AtASY1 or AtASY3 would bring additional information on the potential in-vivo interaction between the two proteins. An anti-AtASY3 antiserum specific towards the C-terminus of the protein was produced (provided by Ferdous M.). Several attempts to detect AtASY3 from crude extracts of *Arabidopsis* buds using an anti-AtASY3 antiserum on western blotting were unsuccessful (Osman K, personal communication). Immunocytochemistry using the same antiserum revealed staining of the chromosome axis during prophase I of WT PMCs. The signal is absent in an *Atasy3* T-DNA insertion mutant line suggesting that the antiserum used for both experiments is immuno-reactive to AtASY3 protein (Ferdous et al, 2012). The absence of detection of AtASY3 protein by western blotting could be explained by the low abundance of the protein in the crude extract. In order to improve the detection of AtASY3 in plant extracts, the anti-AtASY3 antiserum was purified using blotted antigen and an *E. coli* column purification as described in Materials and Methods.

To purify anti-AtASY3 antiserum by blotted antigen, 40 μg of crude extract from *E. coli* cell culture, expressing the C-terminus of the protein, was loaded onto a 15% acrylamide gel and stained with Ponceau stain (Figure 3.4A). In addition, 50μg, 25 μg and 10 μg of crude extract was loaded onto a 15% acrylamide gel and stained with Coomassie to confirm the presence of AtASY3 recombinant protein and assess the abundance of the protein in the crude extract (Figure 3.4B). A large band was observed at the molecular weight slightly above 25 kDA which corresponds to the expected molecular weight of the

recombinant protein. To increase the specificity of anti-AtASY3 anti-serum against AtASY3 recombinant protein, the part of the nitrocellulose membrane stained at this molecular weight was cut and used for the purification of the anti-serum as described in Materials and Methods. To determine the efficiency of the purification, 5 μg, 2.5 μg and 1 μg of *E. coli* crude extract were loaded onto three 15% acrylamide gels and transferred to nitrocellulose membranes. The membranes were then incubated with the no purified antiserum, the unbound fraction obtained from the blotted antigen antibody purification procedure or the purified antibody. Purification of the antiserum by blotted antigen resulted in the loss of specificity towards non-specific proteins. The other non-specific cross reacting bands observed in western blotting using the unpurified anti-AtASY3 antiserum were weaker when using the purified antibody (Figure 3.5A,B,C). This suggests that the purification of the antiserum reduced some but not all non-specific signals. A more intense signal corresponding to AtASY3 recombinant protein was observed by western blotting when using the unbound fraction compared to the purified antibody. A significant amount of antibody specific to AtASY3 recombinant protein was lost during the procedure of antiserum purification. However, this was expected as the antiserum was used in excess over the amount of recombinant protein to limit the presence of unspecific polyclonal antibodies in the purified antiserum. The purified antiserum was used for a second round of blotted antigen purification in an attempt to obtain a more specific antiserum. Nevertheless, a similar pattern of unspecific signals was observed.

As an alternative method to purify the anti-AtASY3 antiserum, an *E. coli* column was used to purify 1 ml of anti-AtASY3 antiserum as described in Materials and Methods. Following the purification step, 1 ml of elution solution was recovered. 5 μg, 2.5 μg and 1

μg of *E. coli* crude extract, expressing the C-terminus part of the protein, were loaded onto a 15% acrylamide gel and transferred to a nitrocellulose membrane. Western blotting using the *E. coli* column purified anti-AtASY3 antibody showed a reduction in the intensity of the non-specific signals suggesting that the anti-AtASY3 antibody is less reactive towards *E. coli* proteins (Figure 3.6A,B). The blotted antigen and the *E. coli* column purification procedures increase the specificity of the anti-serums towards AtASY3 recombinant protein. The blotted antigen purified AtASY3 anti-serum appeared more specific towards AtASY3 recombinant proteins than the *E. coli* column purified AtASY3 anti-serum. It was however found that the signal of AtASY3 recombinant protein was blurred when using the blotted-antigen-purified AtASY3 antibody. This may result from a loss of the immuno-reactivity of the anti-AtASY3 antibody due to the acidic pH treatment used during the purification (Figure 3.5C). Therefore, the *E. coli* column-purified anti-AtASY3 antibody was used for subsequent experiments.
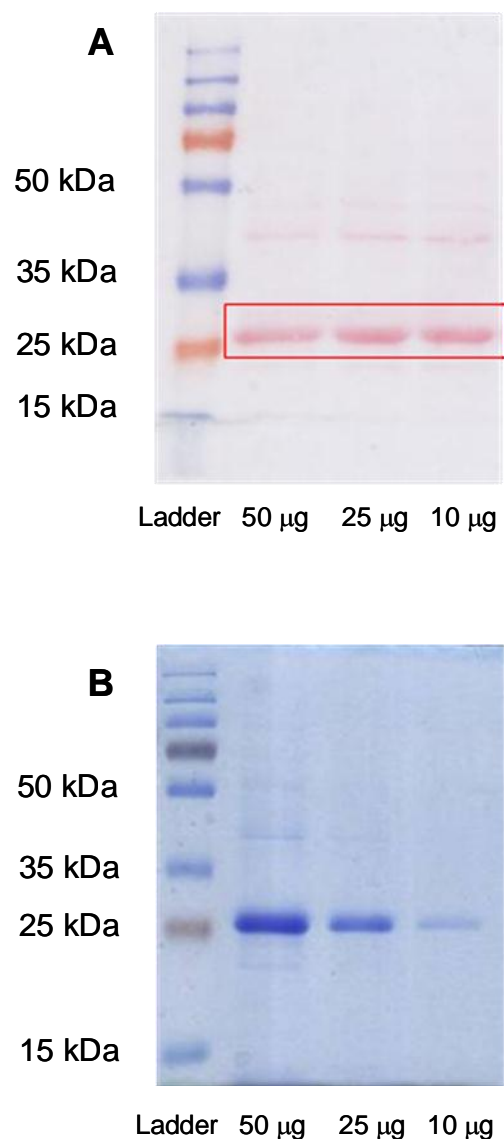
Figure 3.4. Detection of AtASY3 recombinant protein on SDS-page

AtASY3 recombinant protein has an expected molecular weight of 26.6 kDA.

(A) AtASY3 recombinant protein was detected by Ponceau staining. 50 μg, 25 μg and 10 μg of crude extract were loaded onto a 15% acrylamide gel. The portion of the membrane stained at the expected molecular weight of ASY3 recombinant protein and used for anti-serum purification is marked in red.

(B) AtASY3 recombinant protein was detected by Coomassie staining. 50 μg, 25 μg and 10 μg of crude extract were loaded onto a 15% acrylamide gel.
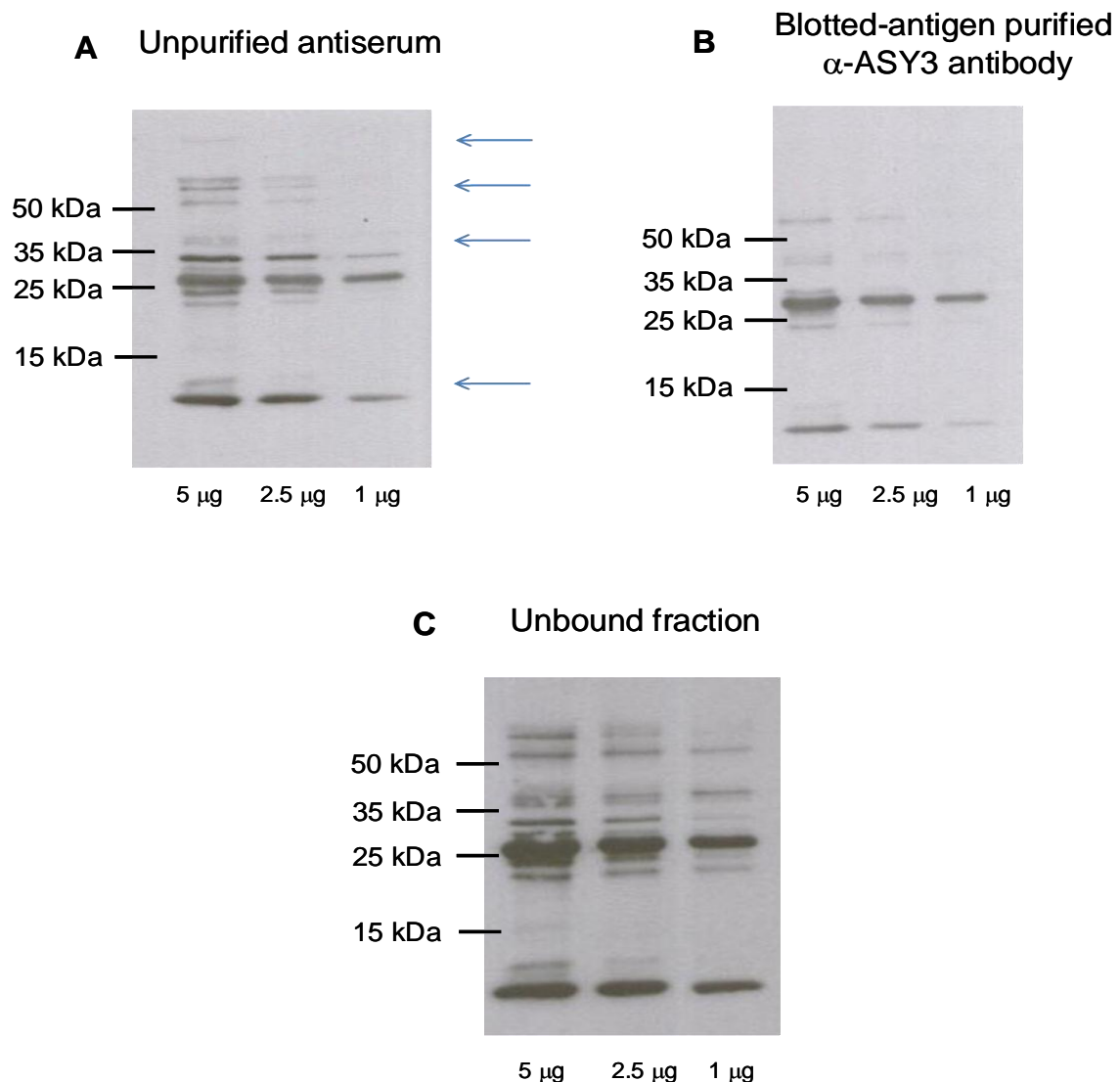
Figure 3.5. Blotted-antigen purification of AtASY3 anti-serum increases its specificity towards AtASY3 recombinant protein

5 μg, 2.5 μg and 1 μg of AtASY3 recombinant protein were loaded onto a 15% acrylamide gel and transferred to a nitrocellulose membrane. AtASY3 recombinant protein has an expected molecular weight of 26.6 kDA.

(A) Western blot using unpurified antiserum (dilution 1/13 300). Blue arrows represent the signals that were not detected with the blotted-antigen-purified anti-AtASY3 antibody

(B) Western blot using blotted-antigen purified anti-AtASY3 antibody (dilution 1/5 000).

(C) Western blot using the unbound fraction obtained during the blotted-antigen purification procedure (dilution 1/13 300).
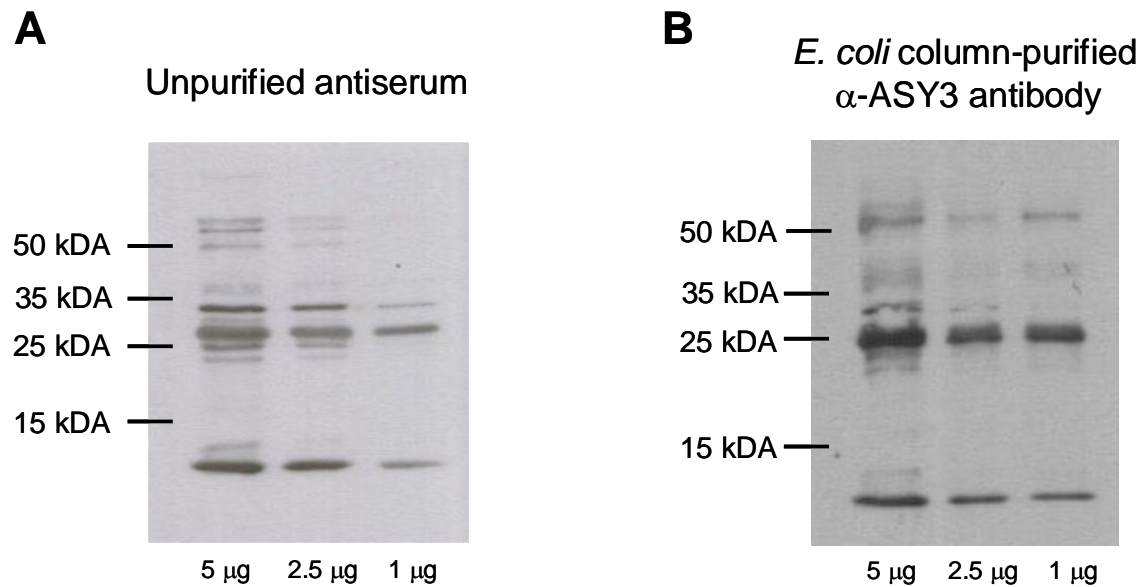
Figure 3.6. *E. coli* **column purification of AtASY3 anti-serum increases its specificity towards AtASY3 recombinant protein**

5 µg, 2.5 µg and 1 µg of AtASY3 recombinant protein were loaded onto a 15% acrylamide gel and transferred to a nitrocellulose membrane. AtASY3 recombinant protein has an expected molecular weight of 26.6 kDA.

(A) Western blot using unpurified antiserum (dilution 1/13 300).

(B) Western blot using *E. coli* column-purified anti-AtASY3 antibody (dilution 1/13 300).

3.5. Co-immunoprecipitation from yeast crude extract confirms the interaction between AtASY1 and AtASY3

To determine if AtASY3 can be extracted in large amount from *Arabidopsis* crude extract, different volumes of *Arabidopsis* crude extract were loaded onto a 10 % acrylamide gel and *E. coli* column purified anti-AtASY3 antibody was used to detect AtASY3. However, no signal corresponding to the molecular weight of AtASY3 was detected. It is possible that the amount of AtASY3 presents in the crude extract is beyond the threshold of detection. AtASY3 is an axis associated protein and it is possible that the protein is not abundant enough to be detected from *Arabidopsis* bud extract. In addition, it has been reported that Red1, the budding yeast functional orthologue of AtASY3, is not easily detectable by biochemical analysis. Lai *et al.* (2011) suggested that Red1 is highly sensitive to proteases such as vacuolar proteases (Lai et al, 2011). AtASY3 was detected at a lower molecular weight in yeast crude extract (Section 3.3.1.). Thus, the incapacity to detect AtASY3 may result from a combination of factors.

Since AtASY3 was not detectable from *Arabidopsis* buds extract, co-immunoprecipitation of AtASY1 and AtASY3 was performed on a yeast crude extract. The yeast two-hybrid assay previously presented, showed that AtASY1 physically interacts with AtASY3 in yeast cells. However, the interaction was not consistently observed and the reason for this is unclear. To prevent any possible cell growth defects due to the co-expression of the two meiotic proteins, two independent yeast cell cultures were prepared. The first culture contained yeast cells expressing pGBKT7-AtASY1 while the other culture contained yeast cells expressing pGADT7-AtASY3. As a control, two liquid cultures containing either

yeast cells transformed with pGADT7-AtASY3 or pGBKT7 empty vector were prepared. This combination of vectors was chosen according to the previous results of the yeast two-hybrid experiment. A higher yield of cells expressing both AtASY1 and AtASY3 and dividing on the restrictive media SD –LTHA was observed when the cells were co-transformed with the vector combination pGADT7-AtASY3/pGBKT7-AtASY1. This observation reflects a weak and/or transient interaction between the two proteins.

Proteins from each liquid culture were extracted using a non denaturing procedure. The crude extract of yeast cells expressing pGBKT7-AtASY1 was pooled with the crude extract of yeast cells expressing pGADT7-AtASY3. Similarly, the crude extract of the two liquid cultures corresponding to the negative control were pooled. AtASY3 was immunoprecipitated from each pooled crude extract using *E. coli* column-purified anti-AtASY3 antibody-coupled beads, as described in Materials and Methods. Proteins pulled down with AtASY3 were eluted and loaded onto a 10% acrylamide gel prior to western blotting with an affinity-purified anti-AtASY1 antibody (provided by Osman K.). A strong band was visualized at 55 kDA and two weaker bands were observed with a molecular weight of about 65 kDa and 95 kDa for the immunoprecipitated crude extract containing pGBKT7-AtASY1 and pGADT7-AtASY3. In contrast, no band was observed for the crude extract containing only pGADT7-AtASY3 (Figure 3.7A). In parallel, the input crude extracts were loaded onto a 10% acrylamide gel and AtASY1 was detected with an affinity-purified anti-AtASY1 antibody. Three bands were observed, which have a similar molecular weight than the three bands observed from the immunoprecipitated solution of the test sample (Figure 3.7A,B). The band with the slower migration rate has a molecular weight close to the predicted molecular weight of the fused protein AtASY1-AD (85-90

kDa). The protein extraction was performed under non-denaturing conditions and it is possible that the recombinant protein AtASY1 was degraded during the process. The band with the lower molecular weight observed before and after immunoprecipitation, is more intense than the two other bands and may represent a degradation product of AtASY1.

In a separate study, BoASY3, the homologue of AtASY3 in *Brassica oleracea,* was pulled down with anti-AtASY1 antibody-coupled beads. This suggests that BoASY1 and BoASY3 form a complex *in-vivo* (Ferdous et al, 2012). Therefore, a second repeat of immunoprecipitation using yeast crude extracts from cells expressing only AtASY1 as a negative control was not carried out. The results obtained from biochemical studies are consistent with the yeast two-hybrid data and confirmed that AtASY1 may physically interact with AtASY3 in *Arabidopsis*.
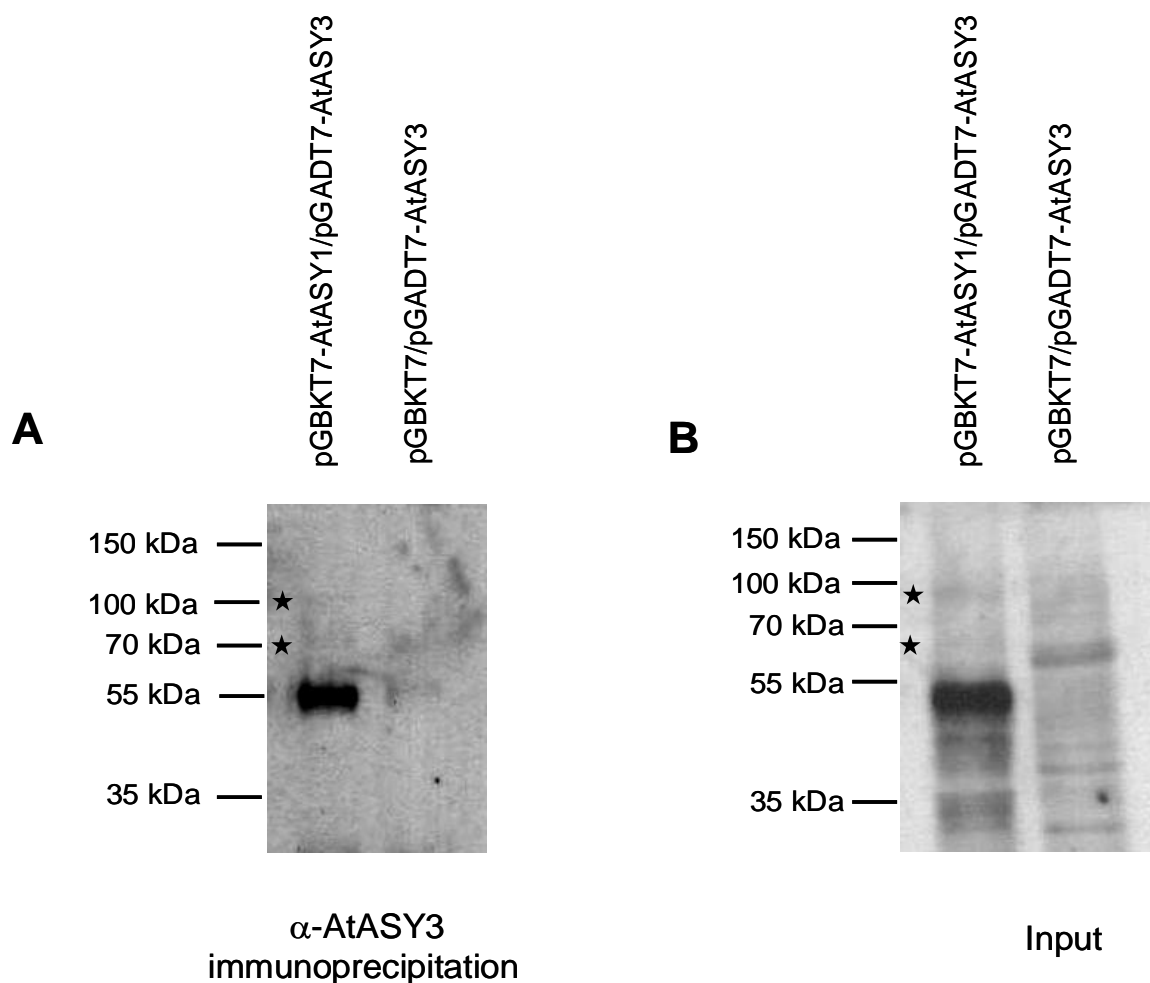
Figure 3.7. AtASY1 co-immunoprecipitates with AtASY3

(A) 7 mg of each pooled crude extract was used and immunoprecipitated with *E. coli*-column-purified-anti-AtASY3 antibody-coupled beads. The eluted solution was loaded onto a 10 % acrylamide gel. The stars represent the two faint bands at the molecular weights of 65 kDa and 95 kDa.

(B) 45 μg of each pooled crude extract was loaded onto a 10 % acrylamide gel to visualise the input protein before immunoprecipitation. The stars represent the two faint bands at the molecular weights of 70 kDa and 100 kDa.

C-Myc-tagged-AtASY1 protein was detected using an affinity-purified anti-AtASY1 antibody (dilution 1/2 500). The predicted molecular weight of c-Myc-tagged-AtASY1is 85-90 kDA.

3.6. The C-terminus region of AtASY3 is required for the interaction with AtASY1

3.6.1. The C-terminus region of AtASY3 interacts with AtASY1 in a yeast two-hybrid assay

Woltering *et al.* (2000) reported that a region upstream of the first coiled-coil domain of Red1 is required to establish an interaction with Hop1, although a low degree of interaction between the C-terminus of Red1 and Hop1 was also observed. The authors identified seven amino acids conserved between Red1 and its orthologue in *K. lactis*. The lysine residue at position 348 of Red1 was found to be critical for the interaction with Hop1 (Figure 3.8).

In order to identify the domain of AtASY3 involved in the interaction with AtASY1, comparative analysis between AtASY3 and Red1 was performed using the tool ClustalW2 of the European Bioinformatics Institute (http://www.ebi.ac.uk/Tools/msa/clustalw2/). However, the comparative analysis did not show conservation of the seven amino acids between the two proteins. The absence of conservation of this motif is not surprising based on the previous comparative analysis between AtASY3 and its functional orthologues across model organisms. Hence, three shorter versions of AtASY3 were designed according to the putative domains of the protein. A shorter version corresponding to the first 510 amino acids (AtASY3$_{1-510}$) was designed to assess the importance of the coiled-coil domain in the interaction between AtASY3 and AtASY1. The presence of a mRNA coding for this truncated version of AtASY3 was found in *Arabidopsis* database. The second version has a length of 280 amino acids (AtASY3$_{1-280}$) and corresponds to the N-

terminus of AtASY3 protein. This version assesses the importance of the N-terminus of the protein as well as the P-loop NTPase domain (Figure 3.8). The third version of AtASY3 truncated protein corresponds to the last 170 amino acids (AtASY3$_{623-793}$) located towards the C-terminus of AtASY3, and is predicted to form a coiled-coil domain.
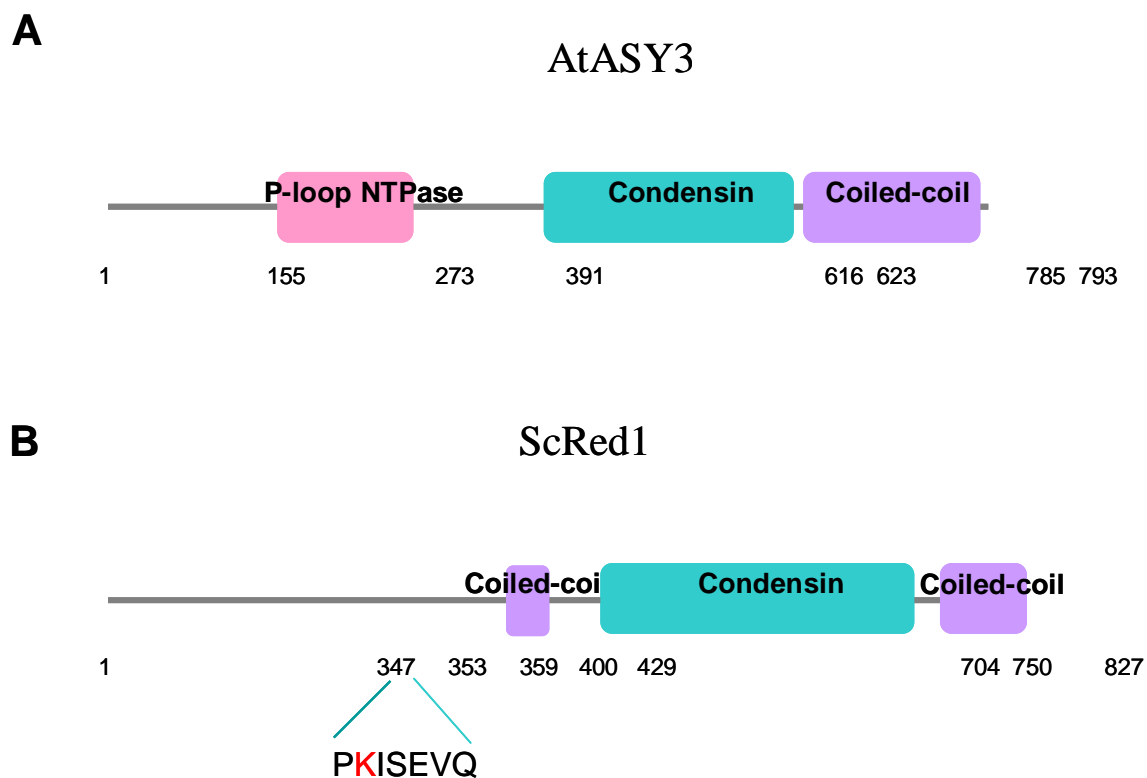
Figure 3.8. Schematic representation of the region of Red1 required for interaction with Hop1 in relation to the predicted domains of AtASY3 (A) and ScRed1 (B)

Seven amino acid residues of ScRed1 are required for interaction with Hop1. These residues are located at the positions 347-353 of ScRed1 protein. The critical lysine residue required for this interaction is highlighted in red.

Amplification of the shorter versions of AtASY3 was carried out by PCR amplification from *Arabidopsis* buds cDNA using the primer sets pGAD-ASY3$_{1-280}$ F/ pGAD-ASY3$_{1-280}$ R, pGAD-ASY3$_{1-510}$ F/ pGAD-ASY3$_{1-510}$ R and pGAD-ASY3$_{623-793}$ F/ pGAD-ASY3$_{623-793}$ R (see Appendix for nucleotide sequences). The corresponding PCR products of AtASY3 were cloned into pGADT7 to form in-frame fusions with the activating domain of GAL4.

A yeast two-hybrid assay was carried out as described above and in Materials and Methods. After 3-4 days of incubation, growth of yeast cells co-transformed with pGADT7-AtASY3/pGBKT7-AtASY1 and pGADT7-AtASY3$_{623-793}$/pGBKT7-AtASY1 was observed on SD –LTH and SD –LTHA. In contrast, yeast cells co-transformed with pGBKT7-AtASY1/ pGADT7-AtASY3$_{1-280}$ and pGBKT7-AtASY1/ pGADT7-AtASY3$_{1-510}$ were unable to grow on the restrictive media SD –LTH and SD –LTHA (Figure 3.9). Negative controls were performed by co-transforming Y2HGold cells with either AtASY1, or a version of AtASY3 and the empty complementary vector, to ensure that no auto-activation of the reporter genes occurred. Yeast cells expressing only one of the two proteins AtASY1/AtASY3 were unable to grow on the more stringent media, SD -LTHA. As described above, some yeast cells expressing only AtASY1 or AtASY3 were able to grow on the less stringent media (Figure 3.9). Protein extraction and subsequent western blot analysis were performed for all combinations of co-transformed cells to ensure that the recombinant proteins were expressed in yeast cells (Figure 3.10). The anti-AtASY3 antibody was raised against the C-terminus of the protein and as a result, the shorter versions of AtASY3 recombinant proteins cannot be detected with this antibody. Recombinant proteins fused with the activating domain GAL4-DNA-AD were also fused with an influenza hemagglutinin (HA) tag. Therefore, an anti-HA antibody was used to

detect AtASY3 recombinant proteins. As mentioned above, the detection of AtASY3 from yeast extract was inconsistent. AtASY3 was not detected at the expected molecular weight on western blotting. A shorter version of AtASY3 was detectable at the molecular weight of 35 kDA which probably corresponds to a degradation product of AtASY3.

Overall, this result suggests that the coiled-coil domain of AtASY3 is involved in the interaction with AtASY1 (Figure 3.11). Interestingly, Woltering *et al.* (2000) also observed an interaction between the coiled-coil domain located towards the C-terminus of Red1 and Hop1. However, this interaction was weaker than for the interaction between Hop1 and the domain of Red1 containing the seven amino acids residues PKISEVQ. The secondary structure of AtASY3 diverges from the secondary structure of Red1. Therefore, it is possible that the region located upstream of the first predicted coiled-coil motif and involved in the interaction between Red1 and Hop1, was lost during evolution. It is also possible that the yeast two-hybrid assay is not sensitive enough to reveal the importance of an additional region of AtASY3 required for interaction with AtASY1.
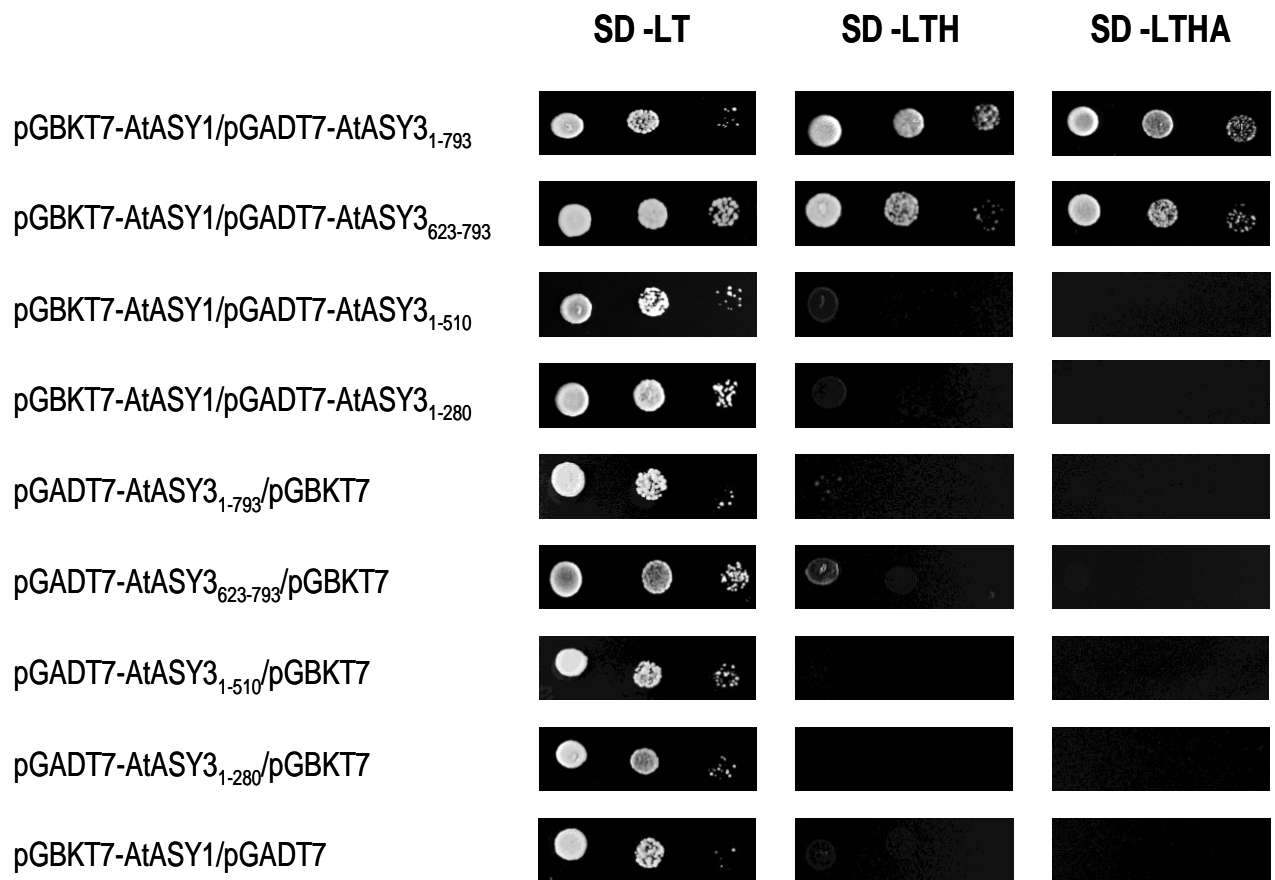
Figure 3.9. AtASY3 coiled-coil domain is required for interaction with AtASY1

Full length coding sequence of AtASY1 and four versions of the coding sequence of AtASY3 were fused with GAL4-BD and GAL4-AD, respectively, and expressed in *S. Cerevisiae* Y2H Gold strain. The media SD –LT allowed the selection of co-transformant cells while the restrictive media SD –LTH and SD –LTHA were used to assess the interaction between the two proteins. Yeast cells co-transformed with pGBKT7-AtASY1/pGADT7-AtASY3$_{623-793}$ grew on the restrictive media SD -LTHA which suggests that AtASY1 physically interacts with the coiled-coil domain of AtASY3 in the GAL4 yeast two-hybrid system. All negative controls were unable to grow on the most stringent media SD –LTHA. The strength of interaction between the two proteins was assessed by serial drop dilutions of mid-exponential-phase cell cultures. 3µl of undiluted, 1/10 and 1/100 diluted cultures were spotted on the selective agar medium and incubated at 30°C for 2 days.

Figure 3.10. Protein expression analysis of AtASY1 and AtASY3 from yeast cells co-transformed with the corresponding vectors

75 μg of protein from each crude extract was loaded onto a 10 % or 15 % acrylamide gel. Anti-Influenza Hemagglutinin antibody (α-HA AB) was used to detect the different versions of HA-tagged-AtASY3 protein. AtASY1 was detected using an affinity-purified anti-AtASY1 antibody (AF α-AtASY1 AB) (provided by Osman K.) raised against the full length AtASY1 recombinant protein. All fusion recombinant proteins were resolved at the correct predicted size apart for $AtASY3_{1-793}$; tagged-AtASY1: 85-90 kDA, tagged-$AtASY3_{1-280}$: 48-55 kDA, tagged-$AtASY3_{1-510}$: 74-80 kDA, tagged-$AtASY3_{623-793}$: 37-43 kDA. Tagged-$AtASY3_{1-793}$ was detected at a molecular weight of 35 kDA. Composite photo comprising band images from different gels.
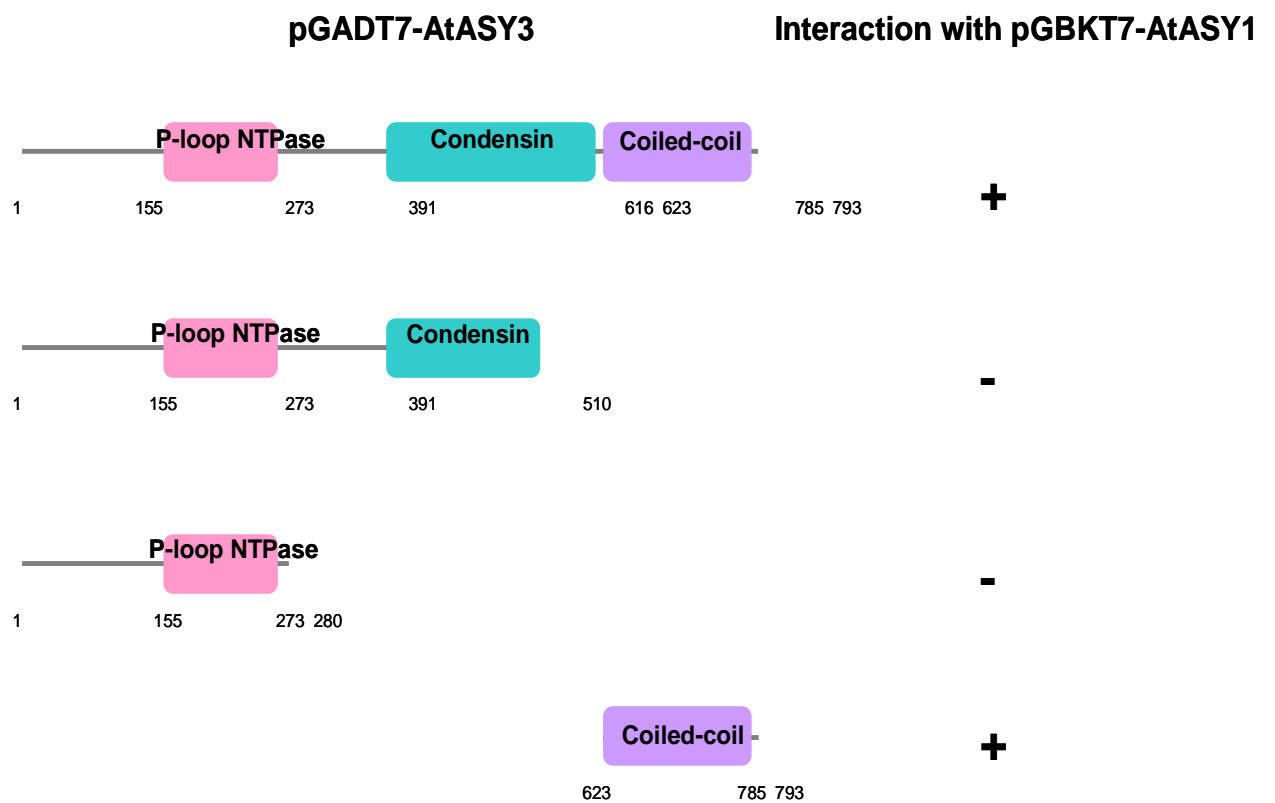
Figure 3.11. Map of the domain of AtASY3 interacting with AtASY1

The coiled-coil domain of AtASY3 interacts with AtASY1.

3.6.2. Co-immunoprecipitation from yeast crude extract confirms the interaction between AtASY3 C-terminus and AtASY1.

To confirm the requirement of the AtASY3 coiled-coil domain in the interaction with AtASY1, AtASY1 was immunoprecipitated, using an affinity-purified-anti-AtASY1 antibody, from a crude extracts containing $AtASY3_{1-280,}$ $AtASY3_{1-510}$ or $AtASY3_{623-793.}$ Each version of AtASY3 protein was fused with an anti-HA tag. The presence of AtASY3 in the eluate following immunoprecipitation was assessed using an anti-HA antibody. As a negative control, a crude extract from yeast cells expressing AtASY3 but not AtASY1, was used.

Two yeast cultures were prepared for each immunoprecipitation and native protein extraction was carried out from these cultures. The crude extract from yeast cells expressing pGBKT7-AtASY1 or pGBKT7 was pooled with the crude extract from yeast cells expressing one of the three shorter versions of AtASY3; pGADT7- $AtASY3_{1-280,}$ pGADT7- $AtASY3_{1-510}$ and pGADT7- $AtASY3_{623-793}$. AtASY3 was not consistently observed on western blotting of yeast crude extract. Therefore, immunoprecipitation of the full length AtASY3 was not attempted. The pooled crude extracts were then immunoprecipitated with affinity-purified anti-AtASY1 antibody-coupled-beads as described in Materials and Methods. The eluates were then loaded on 10 % or 15 % acrylamide gels and the different versions of HA-tagged-AtASY3 proteins were detected using an anti-HA antibody. A strong band at a molecular weight slightly higher than 43 kDa was observed after immunoprecipitation of the crude extract AtASY1- $AtASY3_{623-793}$ and $AtASY3_{623-793}$ (Figure 3.12A,B,C). The signal was more intense in the eluate

containing AtASY1. This band may represent AtASY3$_{623-793}$ although the molecular weight was slightly higher than the predicted molecular weight of the tagged-AtASY3 protein (37-43 kDa). It is also possible that the band is an unspecific cross reacting band and that the difference in intensity results from a difference in protein expression between cultures. Additionally, three bands with smaller molecular weights were observed in the crude extract containing AtASY1- AtASY3$_{623-793}$. The three bands had a range of molecular weights between 25 kDa and 43 kDa. These bands may represent AtASY3$_{623-793}$ and the faster migration bands could be the result of the degradation of AtASY3 by proteases. These bands were not observed in the negative control (AtASY1 protein was absent in the crude extract). Western blotting of the input crude extracts using an anti-HA antibody revealed that the level of protein between both samples is similar (Figure 3.12A). In contrast, no band was observed after immunoprecipitation from crude extracts containing AtASY1 and AtASY3$_{1-280}$ (Figure 3.12B). Lastly, a weak band of a molecular weight between 72 and 95 kDa was observed after immunoprecipitation of AtASY3$_{1-510}$ (predicted molecular weight 74-80 kDa) with AtASY1 (Figure 3.12C). It is possible that AtASY3$_{1-510}$ weakly interacts with AtASY1. However, the band is very weak and no degradation product is observed (Figure 3.12C). The band observed is likely an unspecific cross reacting band and its absence in the negative control is likely due to slight variation of protein level between the two crude extracts.

Overall, the data obtained from the co-immunoprecipitation assay is consistent with the yeast two-hybrid data and suggests that AtASY3 interacts with AtASY1 via its coiled-coil domain. However, the sensitivity of AtASY3 to proteases makes the interpretation of the immunoprecipitation study less reliable.
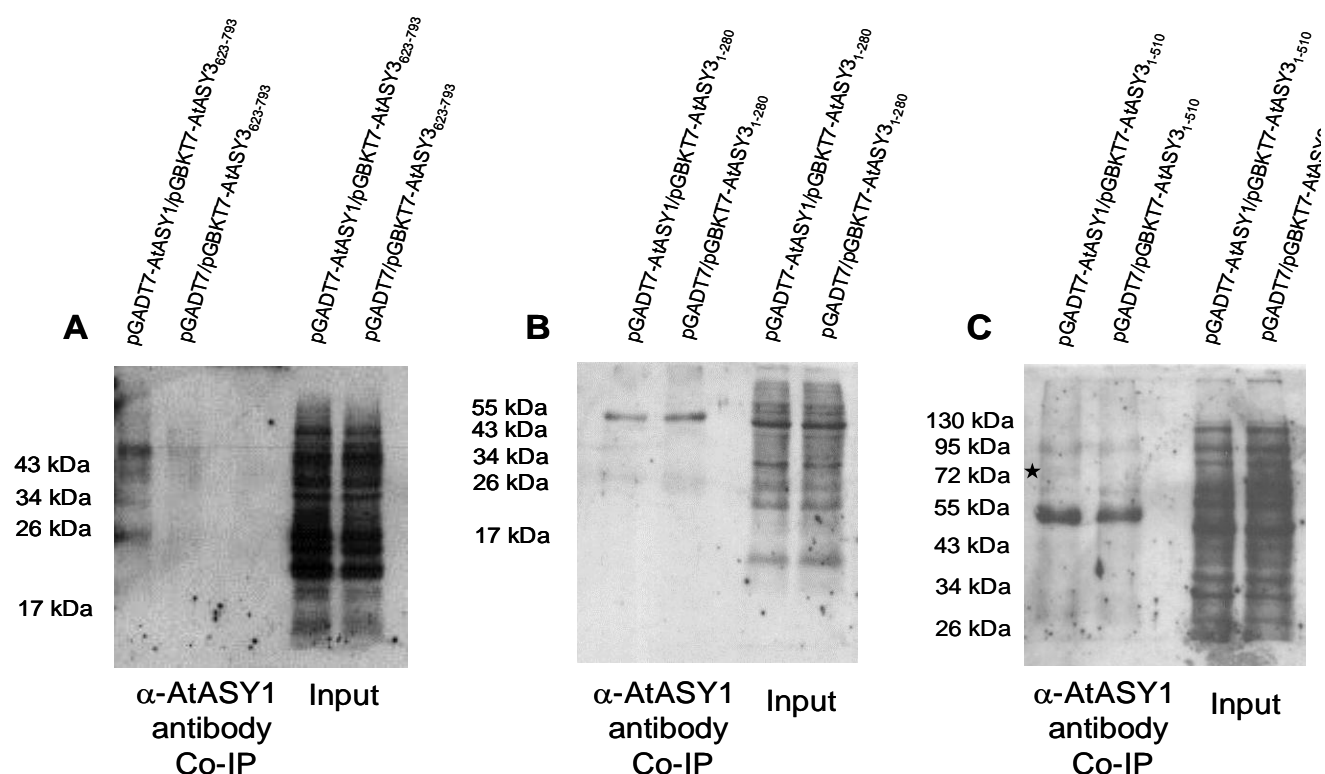
Figure 3.12. AtASY3₆₂₃₋₇₉₃ co-immunoprecipitates with AtASY1

Immunoprecipitation study was carried out using 3 mg of each pooled crude extract and affinity-purified anti-AtASY1 antibody-coupled beads (provided by Osman K.). The eluted solution was loaded onto an acrylamide gel (Co-IP). 40 μg of each pooled crude extract was loaded onto the same acrylamide gel to visualise the input protein before immunoprecipitation (Input). HA-tagged AtASY3 was detected using an anti-HA antibody (1/1 000).

(A) Immunoprecipitation of crude extract containing HA-tagged-AtASY3$_{623-793}$ (predicted molecular weight of 37-43 kDa).

(B) Immunoprecipitation of crude extract containing HA-tagged-AtASY3$_{1-280}$ (predicted molecular weight of 48-55 kDa).

(C) Immunoprecipitation of crude extract containing HA-tagged-AtASY3$_{1-510}$ (predicted molecular weight of 74-80 kDa). The star represents the faint band observed after immunoprecipitation of AtASY1 from a crude extract that contained HA-tagged-AtASY3$_{1-510}$.

127

3.7. The AtASY3 coiled-coil domain is required for homo-dimerisation

A yeast two-hybrid assay was carried out to assess the potential homo-dimerisation of AtASY3. The nucleotide sequence coding for the coiled-coil domain of AtASY3 was amplified with primers pGAD-ASY3$_{623-793}$ F/pGAD-ASY3$_{1-793}$ R, and the amplified product was cloned into pGBKT7 vector (see Appendix for the primer sequences). Y2HGold yeast cells were co-transformed with vectors encoding one version of AtASY3-AD and the full length AtASY3-BD. Yeast two-hybrid assays were carried out as described above and in Materials and Methods.

After 3 days incubation, cells co-transformed with pGBKT7-AtASY3$_{1-793}$-pGADT7-AtASY3$_{1-793}$ were observed on both SD –LTH and SD –LTHA. After 5 days incubation, cells co-transformed with pGBKT7-AtASY3$_{1-793}$-pGADT7-AtASY3$_{623-793}$ were observed on both SD –LTH and SD –LTHA (Figure 3.13). The delay in cell growth observed between the two types of co-transformed cells may result from a difference in the strength of interaction between the homo-dimer AtASY3$_{1-793}$-AtASY3$_{1-793}$ and AtASY3$_{1-793}$-AtASY3$_{623-793.}$ No growth on the restrictive media was observed for colonies co-transformed with pGBKT7-AtASY3$_{1-793}$-pGADT7-AtASY3$_{1-280}$ or pGBKT7-AtASY3$_{1-793}$-pGADT7-AtASY3$_{1-510}$. Yeast cells co-transformed with pGADT7-AtASY3$_{1-793}$-pGBKT7 and with pGADT7-AtASY3$_{623-793}$-pGBKT7 were able to grow on the less stringent media SD –LTH but not on the more stringent media SD –LTHA (Figure 3.13). Growth of the negative control may be due to the capability of the coiled-coil domain of AtASY3 to interact with DNA. Overall, this result showed that AtASY3 is able to homo-dimerise in the yeast two-hybrid system. The interaction required the coiled-coil domain of AtASY3.

The delay in growth observed in cells co-transformed with $pGBKT7\text{-}AtASY3_{1\text{-}793}$-$pGADT7\text{-}AtASY3_{623\text{-}793}$ suggests that an additional region of AtASY3 may be necessary to form a stable homo-dimer.

To confirm the requirement for the coiled-coil domain in the homo-dimerisation of AtASY3, the coding sequence of AtASY3 coiled-coil domain was cloned into pGBKT7 vector using the primer set $pGBK\text{-}ASY3_{623\text{-}793}$ F/$pGBK\text{-} ASY3_{1\text{-}793}$ R (see Appendix for the primer sequences). Growth of yeast cells co-transformed with $pGADT7\text{-}AtASY3_{623\text{-}793}$-$pGBKT7\text{-}AtASY3_{623\text{-}793}$ was observed on the low and high stringent media. However, growth of yeast cells co-transformed with $pGADT7\text{-}AtASY3_{623\text{-}793}$-$pGBKT7\text{-}AtASY3_{1\text{-}793}$ was observed on the stringent media SD –LTHA for all three serial dilutions, while growth of yeast cells co-transformed with $pGADT7\text{-}AtASY3_{623\text{-}793}$-$pGBKT7\text{-}AtASY3_{623\text{-}793}$ was observed on SD –LTHA at no dilution only and after a longer incubation time (Figure 3.13). This suggests that although the coiled-coil domain of AtASY3 is required for the homo-dimerisation of AtASY3, an additional domain located upstream the coiled-coil domain may be involved in the stabilisation of the complex. Protein extraction and subsequent western blot analysis were performed for all combinations of co-transformed cells to ensure that the recombinant proteins were correctly expressed in yeast cells. Recombinant proteins fused with the activating domain GAL4-DNA-AD were also fused with a HA- tag while recombinant proteins fused with the binding domain GAL4-DNA-BD, were fused with a c-MYC- tag. Anti-c-MYC and anti-HA antibodies were used to detect AtASY3 proteins. All fusion recombinant proteins were detected at the correct predicted size apart for $AtASY3_{1\text{-}793}$. Only a truncated form of AtASY3 was observed with the anti-HA antibody (Figure 3.14).

	SD -LT	SD -LTH	SD -LTHA
pGBKT7-AtASY3$_{1-793}$/ pGADT7 –AtASY3$_{1-793}$			
pGBKT7-AtASY3$_{1-793}$/pGADT7-AtASY3$_{623-793}$			
pGBKT7-AtASY3$_{623-793}$/pGADT7-AtASY3$_{623-793}$			
pGBKT7-AtASY3$_{1-793}$/pGADT7-AtASY3$_{1-510}$			
pGBKT7-AtASY3$_{1-793}$/pGADT7-AtASY3$_{1-280}$			
pGADT7-AtASY3$_{1-793}$/pGBKT7			
pGADT7/pGBKT7-AtASY3$_{1-793}$			
pGADT7-AtASY3$_{623-793}$/pGBKT7			
pGADT7-AtASY3$_{1-510}$/pGBKT7			
pGADT7-AtASY3$_{1-280}$/pGBKT7			
pGADT7/pGBKT7-AtASY3$_{623-793}$			

Figure 3.13. AtASY3 coiled-coil domain is required for homo-dimerisation

Full length amino-acid sequence of AtASY3 and the three shorter versions of AtASY3 were fused with GAL4-BD and GAL4-AD, respectively, and expressed in *S. cerevisiae* Y2H Gold. Cells co-transformed with the two plasmids were selected on SD –LT. The restrictive media SD -LTH and SD –LTHA were used to assess the interaction between the two proteins. Yeast cells co-transformed with pGBKT7-AtASY3$_{1-793}$-pGADT7-AtASY3$_{1-793}$, pGBKT7-AtASY3$_{623-793}$-pGADT7-AtASY3$_{1-793}$ and pGBKT7-AtASY3$_{623-793}$-pGADT7-AtASY3$_{623-793}$ were able to grow on the restrictive media SD –LTHA. However, the strength of interaction was variable between the three different types of co-transformed cells. Full length AtASY3 is essential to observe maximum interaction between AtASY3 proteins. In addition, the coiled-coil domain of AtASY3 and a region upstream the coiled-coil domain are required to form a homo-dimer. All negative controls were unable to grow on the stringent media SD–LTHA. The strength of interaction between the two proteins was assayed by serial drop dilutions of mid-exponential-phase cell cultures. 3µl of undiluted, 1/10 and 1/100 diluted cultures were spotted on the selective agar medium and incubated at 30°C for 2 days.
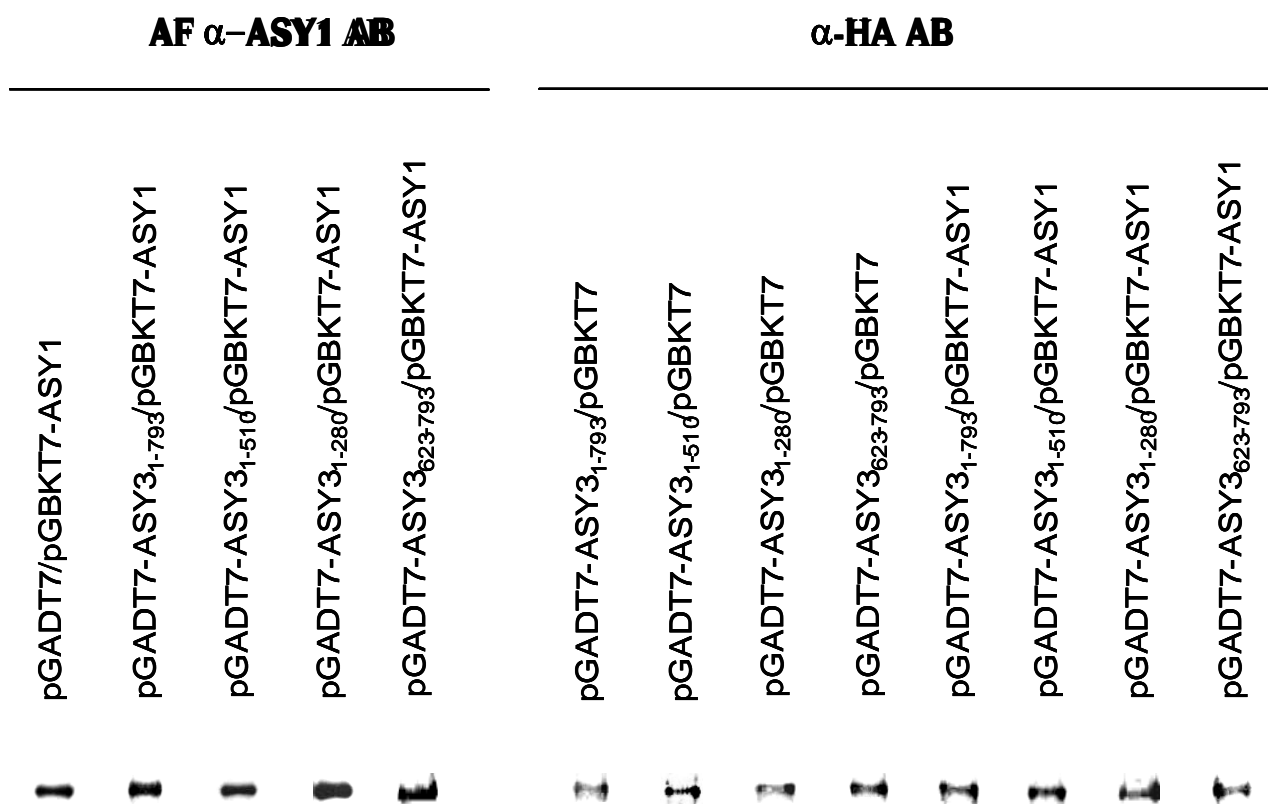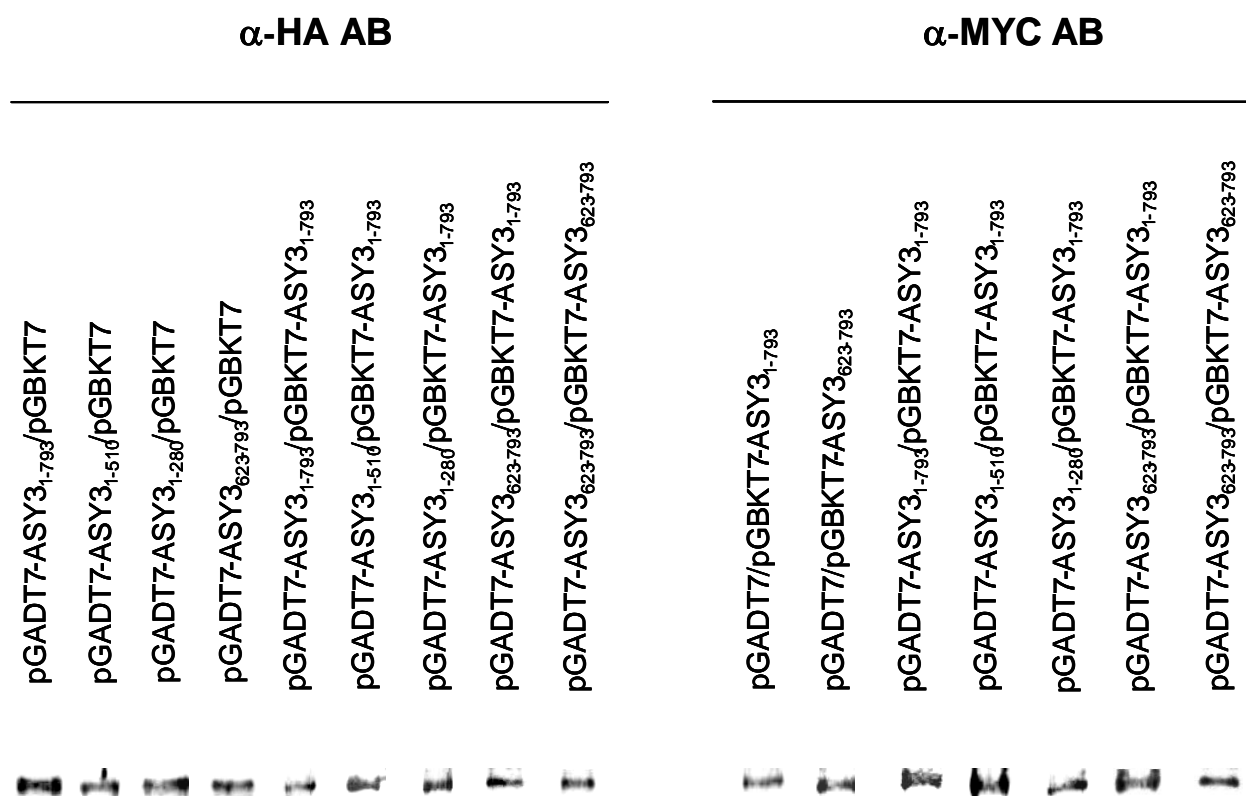
Figure 3.14. Protein expression analysis of AtASY3 from yeast cells co-transformed with the corresponding vectors

75 µg of protein from each crude extract was loaded onto a 10 % or 15 % acrylamide gel. Anti-HA and anti-c-MYC antibodies (α-HA AB and α-c-MYC AB) were used to detect the different versions of HA- and c-MYC-tagged-AtASY3 proteins. All fusion recombinant proteins were resolved at the correct predicted size apart for AtASY3$_{1-793}$. Tagged-AtASY3$_{1-280}$: 48-55 kDA, tagged-AtASY3$_{1-510}$: 74-80 kDA, tagged-AtASY3$_{623-793}$: 37-43 kDA. Tagged-AtASY3$_{1-793}$ was detected at the molecular weight of 35 kDA with α-HA AB and 105-110kDA with α-c-MYC AB. Composite photo comprising band images from different gels.

3.8. Discussion

3.8.1. AtASY3 presents a low degree of amino-acid sequence similarity with its functional orthologues in fungi and plants

Bioinformatic analysis showed that the amino acid sequence of AtASY3 has highly diverged from its distant functional orthologues in other model organisms. The predicted coiled-coil domain located towards the C-terminus of AtASY3 is the only conserved secondary structure among most AtASY3 orthologues. The rapid evolutionary divergence of the amino-acid sequence between AtASY3 and its functional orthologues has been previously reported for other meiotic proteins (Kumar et al, 2010). The divergence observed at the amino-acid level between AtASY3 and its orthologues may indicate a difference of biological function. This may be correlated with the evolution of the meiotic chromosome axis. For instance, Rec10 is a distant orthologue of Red1 and the two proteins have low amino-acid sequence homology and share some similarities in their meiotic functions. Rec10 and Red1 are required for the formation of Spo11-dependent DSBs, formation of the axial/linear element and are found in complex with Hop1. However, *S. pombe* lacks an axial element. Instead a primitive structure, called a linear element was observed by electron microscopy. In addition, the bias towards inter-homologue recombination is weaker in *S. pombe* compared to *S. cerevisiae* (Kim et al, 2010; Lorenz et al, 2004b; Mallela et al, 2011; Spirek et al, 2010). The differences observed in the structure of the chromosome axis between the two yeast species suggest that the structural components of the axial/linear element may have also diverged which would explain the low degree of amino acid similarity between Red1 and Rec10.

A P-loop NTPase and a condensin domain were predicted in AtASY3. A condensin domain was also predicted in Red1. Three *Atasy3* T-DNA insertion lines were characterised in *Arabidopsis* (Ferdous et al, 2012). One T-DNA insertion is located in the predicted P-loop NTPase and the two other T-DNA insertions are predicted to affect the integrity of the putative condensin domain. Condensins are involved in various biological processes such as gene expression and DNA damage repair. However, Ferdous *et al.* (2012) did not report a meiotic defect that could suggest the presence of a condensin activity for AtASY3, such as an increase in SC length (Mets and Meyer, 2009). In addition, there is no study reporting a condensin activity for Red1 or other AtASY3 functional orthologues. Kim *et al.* (2010) recently showed that sister chromatids were prematurely separated in a *red1/rec8* double mutant. In addition, the separation of the sister chromatids occurred earlier in *red1/rec8* double mutant compared to *rec8* single mutant. The authors concluded that Red1 is involved in sister chromatid association. However, the sole absence of Red1 did not affect the cohesion between sister chromatids, presumably because of the presence of the cohesin Rec8. A similar defect in sister chromatid cohesion was previously observed in *red1/mek1* double mutant (Bailis & Roeder, 1998). Two additional studies suggest that SYCP3, a coiled-coil axis protein, favours the association of homologous centromeres and their subsequent bi-orientation at metaphase I in mice (Bisig et al, 2012; Qiao et al, 2012). A potential role for AtASY3 in sister chromatid association was not fully investigated. However, the analysis of three *Atasy3* T-DNA insertion mutant lines suggested that the absence of AtASY3 did not lead to the premature separation of sister chromatids (Ferdous et al, 2012).

3.8.2. The coiled-coil domain of AtASY3 is important for its function

Yeast two-hybrid analysis and immunoprecipitation study revealed that ASY1 forms a complex with ASY3 in *Brassica oleracea* and in yeast two-hybrid (Ferdous et al, 2012). Shorter versions of AtASY3, corresponding to the different putative domains of the protein, were expressed in yeast cells and their potential interaction with AtASY1 were assessed. Yeast two-hybrid analysis and immunoprecipitation studies using anti-AtASY1 antibody-coupled beads on yeast crude extract showed that the coiled-coil domain of AtASY3 was the only domain required for interaction with AtASY1. Additionally, AtASY3 formed a homo-dimer. The homo-dimerisation of AtASY3 was dependent on its putative coiled-coil domain.

Wang *et al.* (2011) reported the identification of a new *Oryza sativa* chromosome axis protein, OsPAIR3, the functional orthologue of AtASY3. Two *Ospair3* mutant lines were characterised and the authors showed that the two lines did not express the putative coiled-coil domain of the protein. Both mutant lines presented meiotic defects such as asynapsis, reduction of inter-homologue COs and improper localisation of OsPAIR2, the functional orthologue of AtASY1, onto the chromatin (Wang et al, 2011). Interestingly, the analysis of three *Atasy3* T-DNA insertion mutant lines, with the T-DNA inserted upstream the nucleotide sequence coding for the coiled-coil domain, showed a reduction in inter-homologue CO formation, a defect in SC formation and an abnormal localisation of AtASY1. Immunocytochemistry analysis indicated that AtASY3 is a structural component of the chromosome axis and that its role in inter-homologue CO formation is epistatic with AtASY1 function. Formation of the complex AtASY1-AtASY3 is dependent on the

putative coiled-coil domain of AtASY3 (Ferdous et al, 2012). In budding yeast, several studies showed that the predicted coiled-coil domain of Red1 is important for homo-dimerisation, and interaction with ZIP1. The interaction between Red1 and Zip1 may not be direct and may be dependent on the sumoylation of Red1 (Eichinger & Jentsch, 2010; Woltering et al, 2000). Coiled-coil domain is the only predicted secondary structure among most functional orthologues of AtASY3 and its localisation towards the C-terminus of the protein is evolutionary conserved.

3.8.3. Biological function of the complex AtASY1-AtASY3

AtASY1 and AtASY3 share functional similarities with Hop1 and Red1 (Ferdous et al, 2012; Sanchez-Moran et al, 2007a). Hop1 and Red1 form an inter-homologue recombination complex and associate with Mek1 (Niu et al, 2005; Wan et al, 2004). The complex activates Mek1 kinase activity which in turn phosphorylates Rad54. This prevents the interaction between Rad51 and its co-factor Rad54. The recombinase activity of Rad51 is then inhibited and inter-sister recombination occurs at low level (Niu et al, 2009). In addition, Red1 and Mek1 counteract the inter-sister bias established by the cohesin Rec8 (Hong et al, 2013; Kim et al, 2010). It is however unclear whether the function of Red1 occurs only when the protein is in a complex with Hop1. Furthermore, Hop1 and Red1 can self-dimerise (Woltering et al, 2000). It is possible that these proteins need to form a tetrameric structure to form a functional inter-homologue recombination complex.

Yeast two-hybrid analysis and immunoprecipitation studies from *Brassica oleracea* crude extract showed that ASY1 and ASY3 form a complex. In addition, AtASY1 localisation

along the chromosome axis was dependent on AtASY3. In the absence of AtASY3, AtASY1 localised as punctuate foci on the chromatin and inter-homologue CO formation was reduced. Sanchez-Moran *et al.* (2007) showed that AtASY1 was required to maintain AtDMC1 on the chromatin. AtDMC1 was more rapidly depleted from the chromatin in *Atasy1*. In addition, the turnover of AtDMC1 was similar between *Atasy1* and *Atasy3* mutants (Ferdous et al, 2012; Sanchez-Moran et al, 2007a). This indicates that AtASY1 was unable to maintain AtDMC1 association with the chromatin in *Atasy3*. It is possible that AtASY1 maintains the association of AtDMC1 onto the chromatin, only when it is in a complex with AtASY3. A similar observation was reported by Blat *et al.* (2002). The authors showed that the localisation of Red1 onto R-band isochores was required to recruit Dmc1 on these chromosomal regions (Blat et al, 2002).

AtASY1 punctuate foci were found associated with γH2AX foci in *Atasy3*. However, AtASY1 was unable to maintain wild-type level of inter-homologue COs. However, the number of inter-homologue COs was higher in *Atasy3* compared to *Atasy1*. The similarity of function between AtASY1/AtASY3 and Hop1/Red1 and the interaction between AtASY1 and AtASY3 is in favour of a model where AtASY1 forms a complex with AtASY3 to mediate inter-homologue CO formation. In the absence of AtASY3, AtASY1 can still associate at the site of DSBs but its efficiency to promote inter-homologue recombination is greatly reduced. This implies that AtASY3 is not essential to repair at least some DSBs towards the formation of AtASY1-dependent inter-homologue COs. Similarly, inter-homologue recombination was observed at low level in *red1* mutant and the dependence of these inter-homologue recombination events was not investigated (Hong et al, 2013; Kim et al, 2010). It is possible that the CO-designated sites are under the

control of additional factors mediating the repair of some DSBs towards inter-homologue recombination in the absence of AtASY3/Red1. Such factors can be the local depletion of cohesin and/or specific chromatin features. Lastly, Hop1 and Red1 form a complex with Mek1 to bias DSB repair towards inter-homologue recombination (Niu et al, 2005; Wan et al, 2004). It has been so far not possible to identify a kinase with an activity similar to Mek1 in organisms other than in fungi (Hollingsworth & Ponte, 1997; Latypov et al, 2010). It is possible that the amino acid sequence of Mek1 has considerably diverged during evolution and thus making the identification of its orthologue in plants and mammals challenging or that Mek1 is not present in the genome of higher order eukaryotes.

Chapter 4

AtPRD3 interacts with components of the chromosome axes and promotes meiotic DSB formation

4.1. Introduction

Meiotic recombination initiates with the formation of DSBs by the topoisomerase-like transesterification activity of SPO11. *Arabidopsis thaliana* genome contains three AtSPO11 paralogues, with only AtSPO11-1 and AtSPO11-2 involved in meiosis (Grelon et al, 2001; Hartung et al, 2007). Spo11 required the presence of 10 accessory proteins to be functionally active at the pre-DSB sites in budding yeast. ChIPchip and immunocytochemistry studies revealed that these proteins form sub-complexes that are spatially distinct (Arora et al, 2004; Kee et al, 2004; Li et al, 2006; Maleki et al, 2007; Panizza et al, 2011). The function of these Spo11 accessory proteins is unclear. The amino-acid sequence of these proteins is poorly conserved between organisms and the proteins lack any functional domains (Kumar et al, 2010). It is thought that these proteins recognise genomic regions, or DSB hotspots, that are pre-determined to undergo DSBs. The determination of a site to become a DSB hotspot occurs at multiple layers. The nucleotide sequence is an important factor for most DSB hotspots in mice (Baudat et al, 2010; Smagulova et al, 2011). However, budding yeast DSB hotspots are not bias towards a specific nucleotide sequence. Moreover, nucleosome positioning, gene expression level, condensation state of the chromatin and cis-trans activators (which could be protein-DNA or locus-locus interaction) are among other factors that determine a site to be hot for DSB formation (Grey et al, 2009; Parvanov et al, 2009).

The chromosome axes have an important role for the formation and the distribution of the DSBs in yeast (Fowler et al, 2013; Panizza et al, 2011). ChIPchip analysis showed that the localisation of some Spo11-accessory proteins is dependent on components of the

chromosome axes. For instance, Rec114 localisation is dependent on Hop1 and Rec8 while Mer2 localisation is dependent on Red1 in budding yeast. Interestingly, Mer2 and Rec114 associate with the axis sites rather than the DSB sites (Panizza et al, 2011). This led the authors to postulate that Rec114 and Mer2 interact with other Spo11-accessory proteins that are localised on the chromatin loops and tether the chromatin loops to the chromosome axes (Panizza et al, 2011). This model is consistent with two recent studies where Spp1 was characterised as a member of the histone H3K4 methyltransferase Set1 complex (Acquaviva et al, 2013; Sommermeyer et al, 2013b). Both studies showed that Spp1 recognise the loci marked with H3K4 methylation. Some of these loci are then tethered to the chromosome axes where DSBs occur.

The lack of sequence conservation at the amino acid level of Spo11-accessory proteins precludes the identification of proteins with similar functions in *Arabidopsis thaliana*. However, screens for reduced fertility mutant lines identified four proteins with a role in DSB formation; AtPRD1, AtPRD2, AtPRD3 and AtDFO (De Muyt et al, 2009; De Muyt et al, 2007; Zhang et al, 2012). Among them, only AtPRD1 has been further studied and the authors proposed that AtPRD1 physically interacts with AtSPO11-1 but not AtSPO11-2 in a yeast two-hybrid assay (De Muyt et al, 2007).

AtPRD3 was first identified in a screen for asynaptic mutant lines and the authors proposed that AtPRD3 is a novel AtSPO11 accessory protein sharing homologies with the homologous pairing aberration in rice meiosis 1 OsPAIR1 (De Muyt et al, 2009; Nonomura et al, 2004). Both mutant lines exhibit asynapsis and an absence of chiasma. Interestingly, AtPRD3 was immunoprecipitated from *Brassica oleracea* crude extract

using an anti-AtASY1 antibody (Osman and Franklin, unpublished). Immunocytochemistry study in conjunction with a BrdU-pulse chase labeling of pre-meiotic S-phase nuclei revealed that the timing of AtSPO11 localisation on the chromatin is concomitant with the formation of the nascent chromosome axes (Sanchez-Moran *et al.*, 2007). In addition, AtASY3, a component of the chromosome axes which shares some functional similarities with the budding yeast Red1 is required for the formation of meiotic DSBs (Ferdous et al, 2012). However, the interplay between chromosome axes and AtSPO11-accessory proteins has not been studied in plants. Thus, to further investigate the role of the chromosome axes in DSB formation, an anti-AtPRD3 antibody was generated to analyse the dynamics of AtPRD3. AtPRD3 associated with AtASY1 foci in G2. The absence of DSB in *Atprd3* can result from a defect in AtSPO11 association with the chromatin or a defect in the tethering of the chromatin loops with the axes. Immunocytochemistry studies revealed that AtPRD3 and AtSPO11-1 were mutually independent for their localisation. In addition, AtPRD3 was found interacting with AtASY1 and AtASY3 in a yeast two-hybrid assay. This suggests that AtPRD3 may be associated with the axes and have a role in the tethering of the chromatin loops with the axes. Lastly, the presence of a negative feedback loop dependent on the kinase activity of AtATM and AtATR and inhibiting the formation of DSBs was identified in *Arabidopsis* meiosis.

4.2. Reduced fertility and asynapsis in *Atprd3* T-DNA insertion mutant line

A T-DNA insertion mutant line (GABI_677D06) was obtained from NASC. The insertion site of the T-DNA was mapped and it is located in the 4th intron within *AtPRD3* gene (West, personal communication). The molecular characterisation of the mutant line confirmed that plants homozygous for the insertion did not express the full length mRNA of *AtPRD3*(West, personal communication). The *Atprd3* T-DNA insertion mutant line showed normal vegetative growth but fertility was greatly reduced compared to wild-type plants (Figure 4.1A-C). The reduced fertility observed in *Atprd3* is consistent with the analysis of *Atprd3* mutant by De Muyt *et al.* (2009) and the role of AtPRD3 during meiosis. To analyse the meiotic stages, DAPI-stained chromosome spread preparations of wild-type and *Atprd3* PMCs were examined by fluorescence microscopy. Wild-type meiotic stages were previously described in Introduction (Figure 1.3). Briefly, chromosomes appeared decondense at leptotene (Figure 4.2A). During mid-prophase I, homologous chromosomes pair, recombine and synapse (Figure 4.2B). Following this, the chromosomes progressively condense leading to the formation of five bivalents, connected at the CO sites, at metaphase I (Figure 4.2C,D). The resolution of the COs is followed by the segregation of the homologous chromosomes towards the opposite poles of the cells (Figure 4.2E). During meiosis II, a second segregation of chromosomes occurs resulting in the formation of four haploid gametes at tetrad (Figure 4.2F). Cytological analysis revealed normal condensation of the chromosomes at G2/ leptotene stages in *Atprd3* (Figure 4.2G). However, chromosomes failed to synapse at mid-prophase I and 10 univalent chromosomes were observed at metaphase I (mean = 10 +/- 0, n=50) (Figure 4.2H-J). The

absence of physical connection between homologous chromosomes led to the mis-segregation of chromosomes in anaphase I and anaphase II (Figure 4.2K,L). Lagging chromosomes were frequently observed from anaphase I onward and resulted from the failure to connect the chromosomes to the meiotic spindle apparatus (Figure 4.2K,L). This is a common feature of T-DNA mutant lines defective in homologous recombination and CO formation (Ferdous et al, 2012). Additionally, connections between univalent chromosomes were prevalent in *Atprd3* (Figure 4.2N). The chromosomes involved in these connections were not identified. Chromosomal connections can be due to unresolved interlocks, chromatin stickiness or arise through recombination (Knoll et al, 2012). However, no evidence of chromosome fragmentation was detected in *Atprd3*. In addition, chromosomal connections were also observed in wild-type and *Atspo11-1-4* meiocytes (Figure 4.2M,O). This suggests that the chromosomal connections observed in both mutant lines may be a cytological representation of chromatin stickiness. Chromosome stickiness is apparent at diakinesis of wild-type PMCs and occurs at the rDNA heterochromatin regions between homologous chromosomes. A similar observation was reported in *pair1* mutant, the functional homologue of AtPRD3 in rice (Nonomura et al, 2004). The proportion of chromosome connections was analysed in wild-type, *Atprd3* and *Atspo11-1-4* metaphase I nuclei. A frequency of 0.12 chromosomal connection per nucleus was observed in wild-type (n=50). However, the frequency of chromosomal connection per nucleus appeared higher in *Atprd3* (0.30, n=50) and *Atspo11-1-4* (0.24, n=50) compared to wild-type metaphase I nuclei. A complementation test, in which a 4kb of wild-type *AtPRD3* construct including the promoter region and the coding region (chromosome I 248371-252379) cloned in the binary vector pCB1300 and incorporated in *Atprd3* genome,

was able to restore normal fertility (West, personal communication). This confirms that the meiotic defect observed in GABI_677D06 line is solely due to a mutation in *AtPRD3* gene.

Figure 4.1. *Atprd3* **mutant phenotype**

Atprd3 T-DNA insertion line present normal vegetative growth (A) compared to wild-type plants (B). However, *Atprd3* plants have shorter silique length which indicates a reduction in fertility (C).
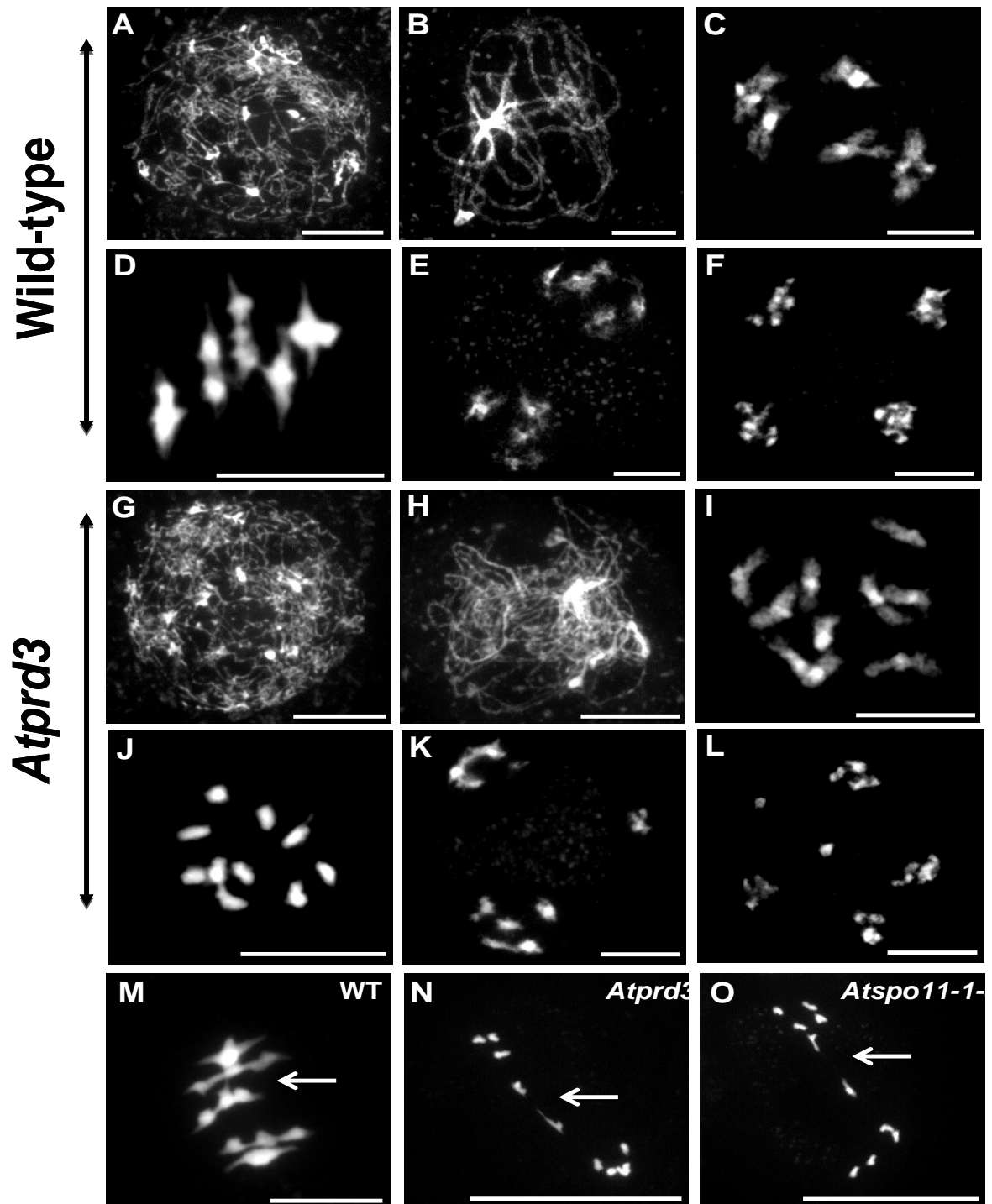
Figure 4.2. Meiotic stages from *Atprd3*, *Atspo11-1-4* and wild-type PMCs.
DAPI-stained (blue) chromosome spread of wild-type (A-F) and *Atprd3* (G-L) PMCs.
Leptotene (A,G), mid-prophase I (B,H), diakinesis (C,I), metaphase I (D,J), dyad (E,K)
and tetrad (F,L). Chromosomal connections, represented by a white arrow, were observed
in wild-type (M), *Atprd3* (N) and *Atspo11-1-4* (O) metaphase I nuclei. Scale bar = 10 μM.

4.3. Meiotic chromosome axes and cohesin are established in *Atprd3* mutant

Cytological analysis of *Atprd3* PMCs suggests that AtPRD3 is essential for inter-homologue CO formation and synapsis (Figure 4.2H,I). The meiotic defects may result from a defect in the formation of the chromosome axes. Nonomura *et al.* (2004) showed that OsPAIR1 contains a putative coiled-coil domain. The authors suggested that OsPAIR1 could be a new component of the chromosome axes. To analyse the formation of the chromosome axes, the localisation of AtASY1 and AtASY3 was studied by immunocytochemistry on chromosome spread preparation of *Atprd3* and wild-type PMCs using anti-AtASY1 and anti-AtASY3 antibodies. AtASY1 is an axis-associated protein and AtASY3 is an axis component (Armstrong et al, 2002; Ferdous et al, 2012). In wild-type PMCs, AtASY1 signal formed numerous punctuate foci in early G2. Throughout G2, AtASY1 signal progressively elongated to form short stretches that eventually extended along the chromosomes by leptotene (Figure 4.3D). AtASY3 signal was fainter than AtASY1 signal in G2 and early leptotene. However, AtASY3 formed a linear signal during early prophase I in wild-type PMCs (Figure 4.3A). Dual immunolocalisation of AtASY1 and AtASY3 revealed that the two signals co-localised (Figure 4.3G). In *Atprd3* PMCs, AtASY1 and AtASY3 signals were indistinguishable from wild-type PMCs. The two signals were co-localising during early prophase I (Figure 4.3J,M,P). This suggests that the chromosome axes are formed in *Atprd3*.

Additionally, the deposition of the cohesin subunit AtSMC3 and the α-kleisin AtSYN1 were analysed. Dual immunolocalisation using anti-AtASY1 antibody and anti-AtSMC3 or anti-AtSYN1 antibodies on chromosome spread preparation of *Atprd3* and wild-type

PMCs was carried out. In wild-type PMCs, AtSYN1 and AtSMC3 formed numerous foci associated with the chromatin in G2. As the formation of the chromosome axes progressed, AtSMC3 and AtSYN1 formed a more continuous signal that co-localised with AtASY1 signal (Figure 4.3B,C,E,F,H,I). In *Atprd3* PMCs, both AtSMC3 and AtSYN1 were detected as linear signals associated with AtASY1 signal (Figure 4.3K,L,N,O,Q,R). The proper localisation of the four components of the chromosome axes suggests that AtPRD3 is not required for axis formation. In addition, AtSMC3 and AtSYN1, two cohesin subunits, were found associated with the axes which reveal that the global cohesion is established in *Atprd3*.
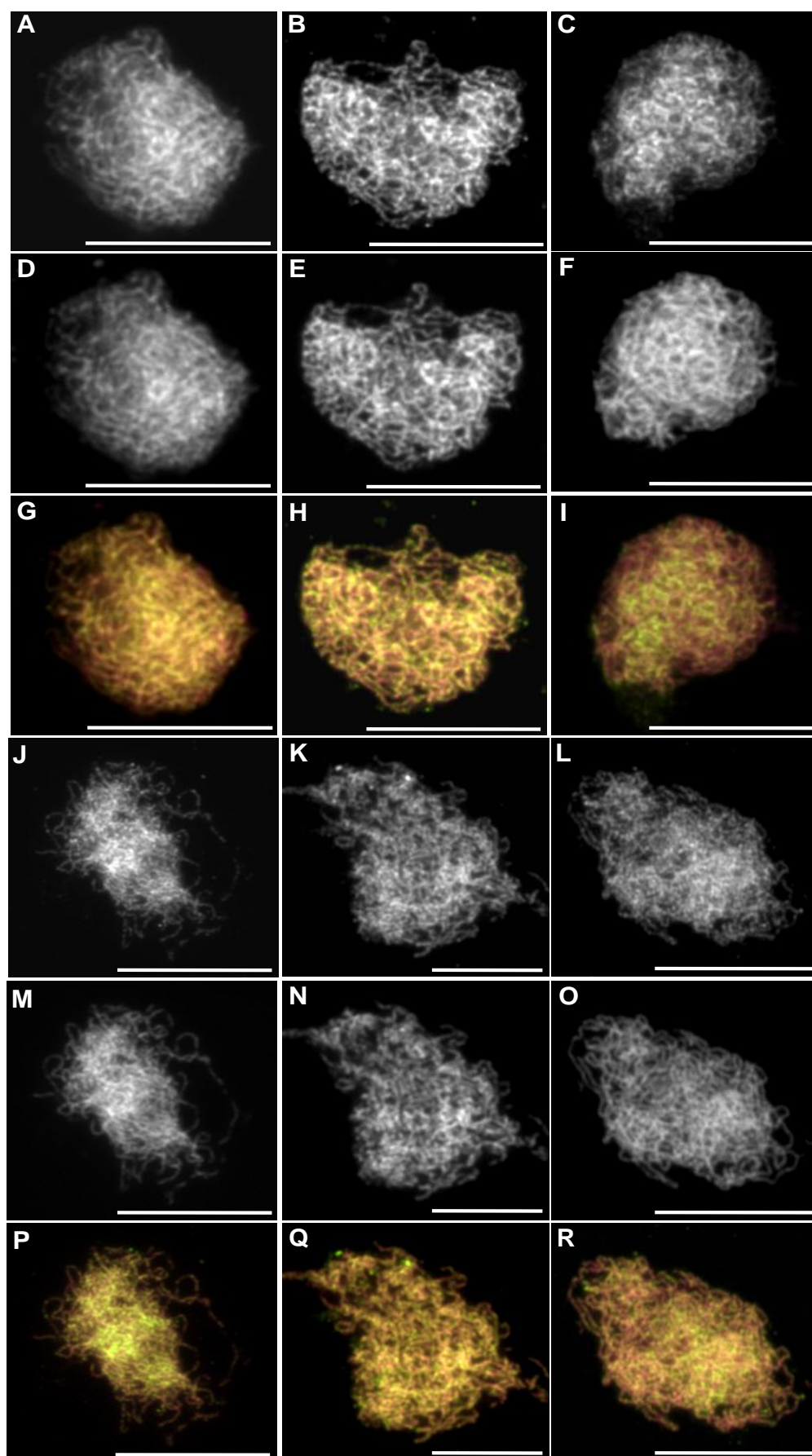
Figure 4.3. AtPRD3 is not required for chromosome axis formation and establishment of the cohesin complex.

(A-F,J-O) Immunolocalisation of AtASY1 (D-F,M-O), AtASY3 (A,J), AtSMC3 (B,K) and AtSYN1 (C,L) on chromosome spread preparations of wild-type (A-F) and *Atprd3* (J-O) PMCs. (G-I,P-R) Merge images of AtASY1 (G-I,P-R; green) and AtASY3 (G,P; magenta) or AtSMC3 (H,Q; magenta) or AtSYN1 (I,R; magenta) on chromosome spread preparations of wild-type (G-I) and *Atprd3* (P-R) PMCs. Scale bar = 10 μM.

4.4. Meiotic DSBs are not formed in *Atprd3* mutant

Since it is not possible to use a physical assay to accurately quantify the level of meiotic DSBs in *Arabidopsis* meiosis, several studies have previously inferred that the number of early recombination nodules can be used to indirectly estimate the number of DSBs formed per nucleus. Following DSB formation, the histone H2A variant is phosphorylated at serine 139. Phosphorylation of H2A or γH2AX, can be monitored by immunolocalisation using an anti-γH2AX antibody on chromosome spread preparation of PMCs. In addition, AtRAD51 and AtDMC1 are two early recombination proteins involved in the early steps of the homologous recombination pathway. Ferdous *et al.* (2012) analysed the number of DSBs per nucleus in wild-type and mutant lines by combining the immunocytochemistry analysis of these three proteins.

Similarly, in this study, immunolocalisation on chromosome spread preparation of *Atprd3, Atspo11-1-4* and wild-type PMCs using an anti-γH2AX antibody was carried out to estimate the number of meiotic DSBs formed per nucleus. In addition, an anti-AtASY1

antibody was used to mark the chromosome axes, and discriminate between real γH2AX foci and background noise. Previous analysis of metaphase I from *Atspo11-1-4* PMCs showed an absence of bivalent. This led to the conclusion that the formation of DSBs was abolished in this mutant. The phosphorylated form of the histone variant H2A was not detected in *Atspo11-1-4* PMCs (Figure 4.4C,F). This confirmed that *Atspo11-1-4* is likely a null mutant that does not generate DSBs and that phosphorylation of H2A can be efficiently used to estimate the number of DSBs formed per nucleus during meiosis. H2A becomes phosphorylated from early leptotene and can be visualised as numerous foci. As prophase I progresses, the phosphorylation of H2A seems to spread along the chromosomes and the γH2AX signal forms a more continuous signal. Therefore, the estimation of the number of γH2AX foci was determined at early leptotene. In wild-type nuclei, γH2AX signal formed numerous foci that were associated with the chromosome axes (Figure 4.4A,D). In contrast, no γH2AX signal above the background noise was detected in *Atprd3* PMCs (Figure 4.4B,E). This observation suggests that meiotic DSBs are not formed or that the phosphorylation of H2AX is defective in *Atprd3*.

As a separate study to validate these data, the localisation of AtDMC1 on the chromatin was investigated. Immunocytochemistry on chromosome spread preparation using anti-AtDMC1 and anti-AtASY1 antibodies was carried out on *Atprd3, Atspo11-1-4* and wild-type PMCs. In wild-type PMCs, AtDMC1 signal was detected as numerous chromatin-associated foci at early leptotene. These foci were associated with the chromosome axes and the number of AtDMC1 progressively decreased during mid-prophase I (Figure 4.4G,J). However, AtDMC1 signal was not observed in *Atprd3* and *Atspo11-1-4* PMCs (Figure 4.4H,I,K,L).

During meiosis, the formation of meiotic DSBs activates the kinase activity of AtATM/AtATR. These kinases phosphorylate proteins involved in the DSB repair pathway. Therefore, proteins phosphorylated by AtATM/AtATR should remain in an non-phosphorylated form when meiotic DSBs are not formed. Anti-p[S/T]Q and anti-AtASY1 antibodies were used for immunocytochemistry analysis of *Atprd3, Atspo11-1-4* and wild-type PMCs. Anti-p[S/T]Q antibody specifically recognised proteins phosphorylated at a SQ or TQ site. These phospho-sites are preferentially phosphorylated by AtATM/AtATR. In wild-type PMCs, a p[S/T]Q signal was observed from early leptotene (Figure 4.5A,D). The signal formed discontinuous stretches and foci. However, p[S/T]Q signal was hardly detectable in *Atspo11-1-4* (Figure 4.5C,F). A very faint signal forming foci was detected in the mutant line. In addition, a similar abnormal p[S/T]Q signal was detected in *Atprd3* PMCs (Figure 4.5B,E). Overall, immunocytochemistry study suggests that meiotic DSBs are not formed in *Atprd3* mutant.

An alternative method to analyse the presence of DSBs in PMCs involves generating a double mutant with *Atrad51* or *Atmre11* to abrogate the homologous recombination pathway. Meiotic DSBs formed and not repaired by the homologous recombination pathway can be visualised by the presence of entangled chromosomes at metaphase I and the presence of chromosome fragmentation from anaphase I onward. AtRAD51 is a recombinase involved in DSB repair. Absence of AtRAD51 results in the accumulation of unrepaired DSBs at metaphase I and the presence of chromosome fragmentation at anaphase I (Figure 4.6C). AtMRE11 acts upstream AtRAD51 in the homologous recombination pathway. AtMRE11 is required for the initial resection of the meiotic DSB

ends. In *Atmre11,* AtSPO11 presumably remains covalently attached with the DSB ends, thus preventing the activation of the DNA repair machinery. Therefore, DSBs are unrepaired and chromosome fragmentation is observed at anaphase I. De Muyt *et al.* (2009) previously reported the absence of chromosome fragmentation in *Atprd3/Atrad51* and *Atprd3/Atmre11* double mutants. Thus, the authors proposed that AtPRD3 was required for DSB formation. *Atprd3/Atrad51* and *Atspo11-1-4/Atrad51* double mutants were generated and the meiotic stages were analysed by DAPI-stained chromosome spread preparation. In *Atspo11-1-4* PMCs, meiotic DSBs were not formed and homologous chromosome failed to synapse and recombine. Ten univalent chromosomes were observed at metaphase I instead of five bivalents observed in wild-type PMCs (Figure 4.6A,B). In *Atspo11-1-4/Atrad51* double mutant, the absence of DSB prevented the accumulation of unrepaired DSBs and therefore 10 univalent chromosomes were observed at metaphase I (Figure 4.6D). In *Atprd3/Atrad51* double mutant, the formation of 10 univalent chromosomes was similarly observed (Figure 4.6E,F). The analysis of *Atprd3/Atmre11* double mutant was not attempted. Overall, immunocytochemistry studies of the early recombination proteins in combination with the analysis of *Atprd3/Atrad51* double mutant suggest that AtPRD3 is essential to promote AtSPO11-1-dependent DSB formation.
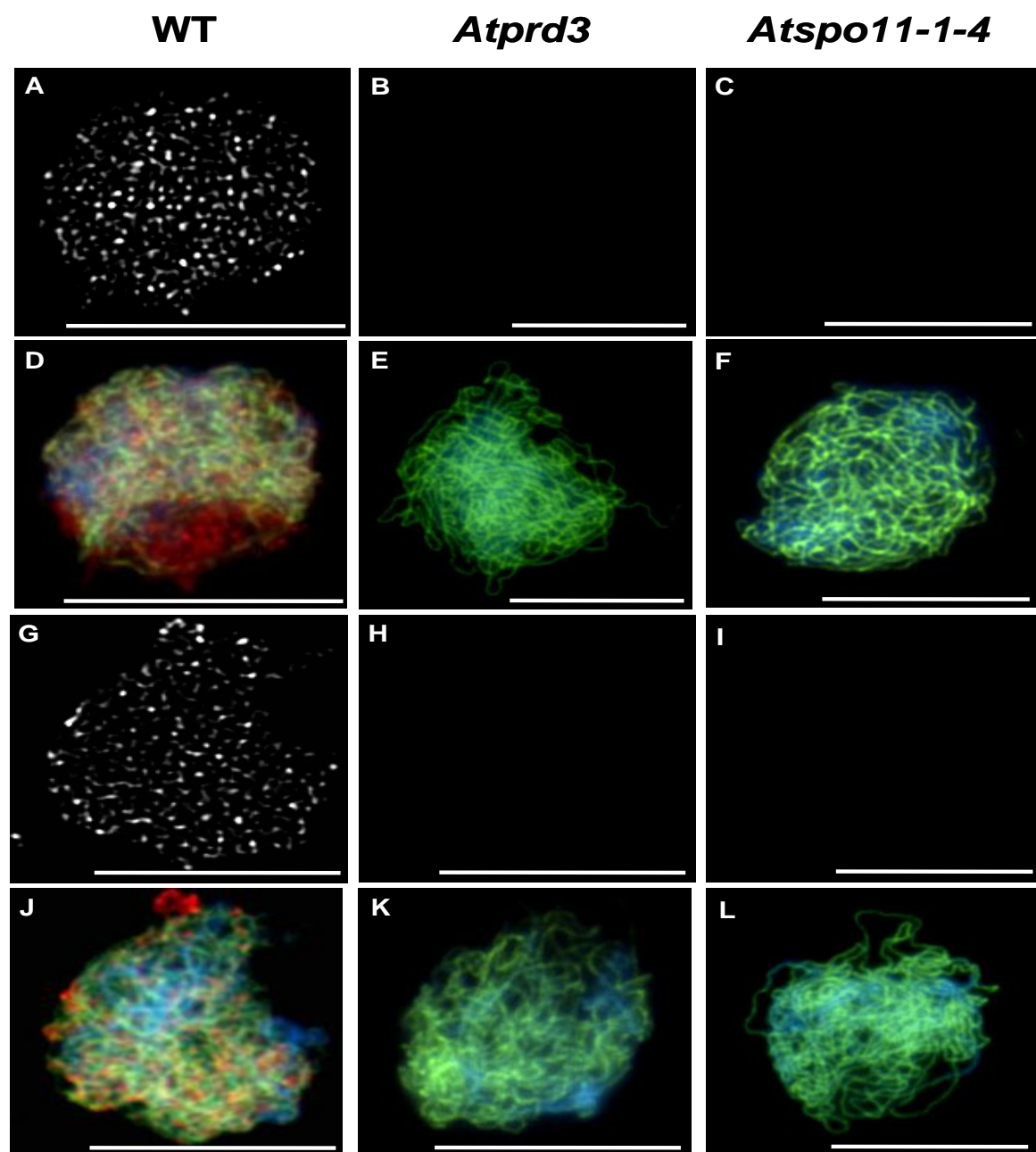
Figure 4.4. Dual immunolocalisation of AtASY1 with recombination proteins in wild-type, *Atprd3* and *Atspo11-1-4* PMCs

Immunolocalisation of γH2AX (A-C) and AtDMC1 (G-I) in wild-type (A,G), *Atprd3* (B,H) and *Atspo11-1-4* (C,I). (D-F). Merge images of AtASY1 (green) and γH2AX (red) in wild-type (D), *Atprd3* (E) and *Atspo11-1-4* (F). (J-L) Merge images of AtASY1 (green) and AtDMC1 (red) in wild-type (J), *Atprd3* (K) and *Atspo11-1-4* (L). Nuclei were counterstained with DAPI (blue). Scale bar = 10 μM.

WT   *Atprd3*   *Atspo11-1-4*
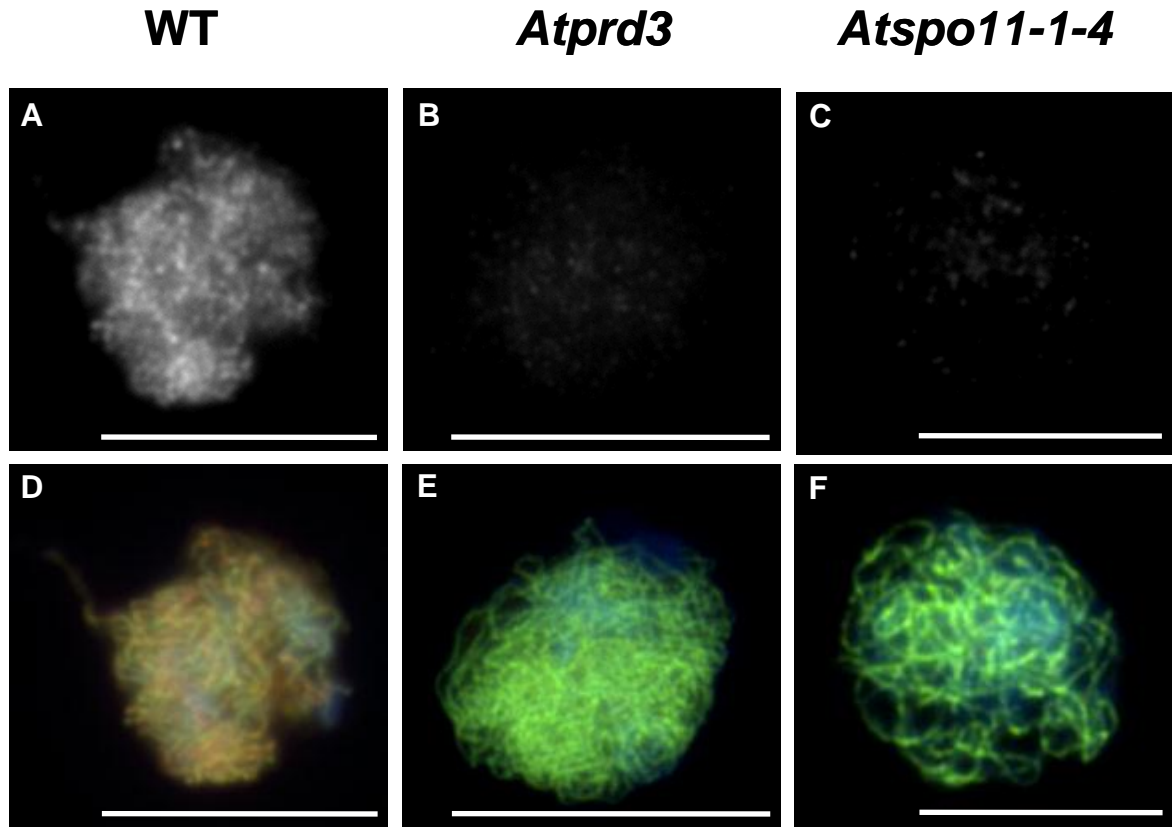
Figure 4.5. Dual immunolocalisation of AtASY1 and p[S/T]Q in wild-type, *Atprd3* **and**
Atspo11-1-4 **PMCs.**

Immunolocalisation of p[S/T]Q (A-C) in wild-type (A), *Atprd3* (B) and *Atspo11-1-4* (C).
(D-F). Merge images of AtASY1 (green) and p[S/T]Q (red) in wild-type (D), *Atprd3* (E)
and *Atspo11-1-4* (F). Nuclei were counterstained with DAPI (blue). Scale bar = 10 μM.
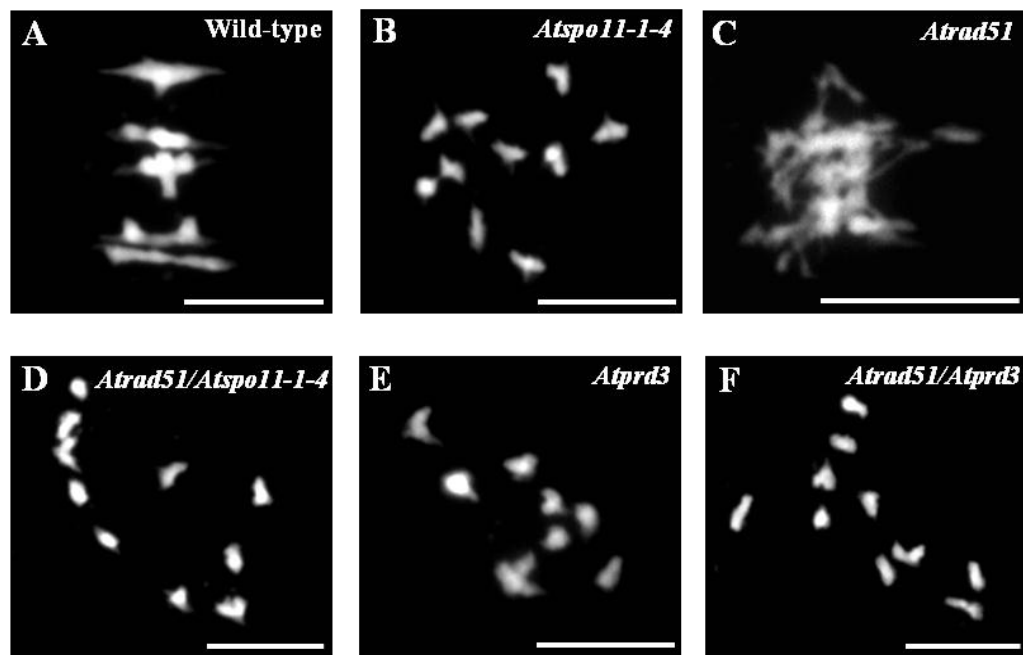
Figure 4.6. Metaphase I from wild-type and mutants PMCs.

DAPI-stained (blue) chromosome spread of wild-type (A), *Atspo11-1-4* (B), *Atrad51* (C), *Atrad51/Atspo11-1-4* (D), *Atprd3* (E) and *Atrad51/Atprd3* (F) metaphase I nuclei.

Scale bar = 10 μM.

4.5. Polymerization of AtZYP1 is disrupted in *Atprd3* mutant

Since DAPI-stained chromosome spread preparation of *Atprd3* PMCs showed an absence of homologous chromosome pairing at mid-prophase I, the formation of the SC was monitored during prophase I. Immunolocalisation of the SC transverse filament AtZYP1 using an anti-AtZYP1 antibody on chromosome spread preparations of *Atprd3* and wild-type PMCs was carried out. In wild-type PMCs, AtZYP1 nucleated at discrete sites (SISs) during leptotene/zygotene transition. SISs are sites located along the chromosome axes where synapsis initiates. The polymerisation of AtZYP1 emanating outwards from these SISs was observed at zygotene (Figure 4.7A). The nucleation and polymerisation of AtZYP1 is asynchronous during meiosis. It is therefore not possible to accurately determine the number of SISs in *Arabidopsis*. By pachytene, the polymerisation of AtZYP1 was complete and AtZYP1 formed a continuous signal (Figure 4.7D). In *Atprd3*, AtZYP1 failed to polymerise. AtZYP1 signal was not consistently observed in each nucleus analysed. When AtZYP1 signal was detected, AtZYP1 formed foci and occasionally short stretches (Figure 4.7B,E). A previous study revealed that AtZYP1 is not detected in *Atspo11-1*(Higgins et al, 2005). To confirm this result, immunolocalisation on chromosome spread preparation of *Atspo11-1-4* PMCs using an anti-AtZYP1 antibody was carried out. AtZYP1 signal was rarely found associated with the chromatin (Figure 4.7C,F).
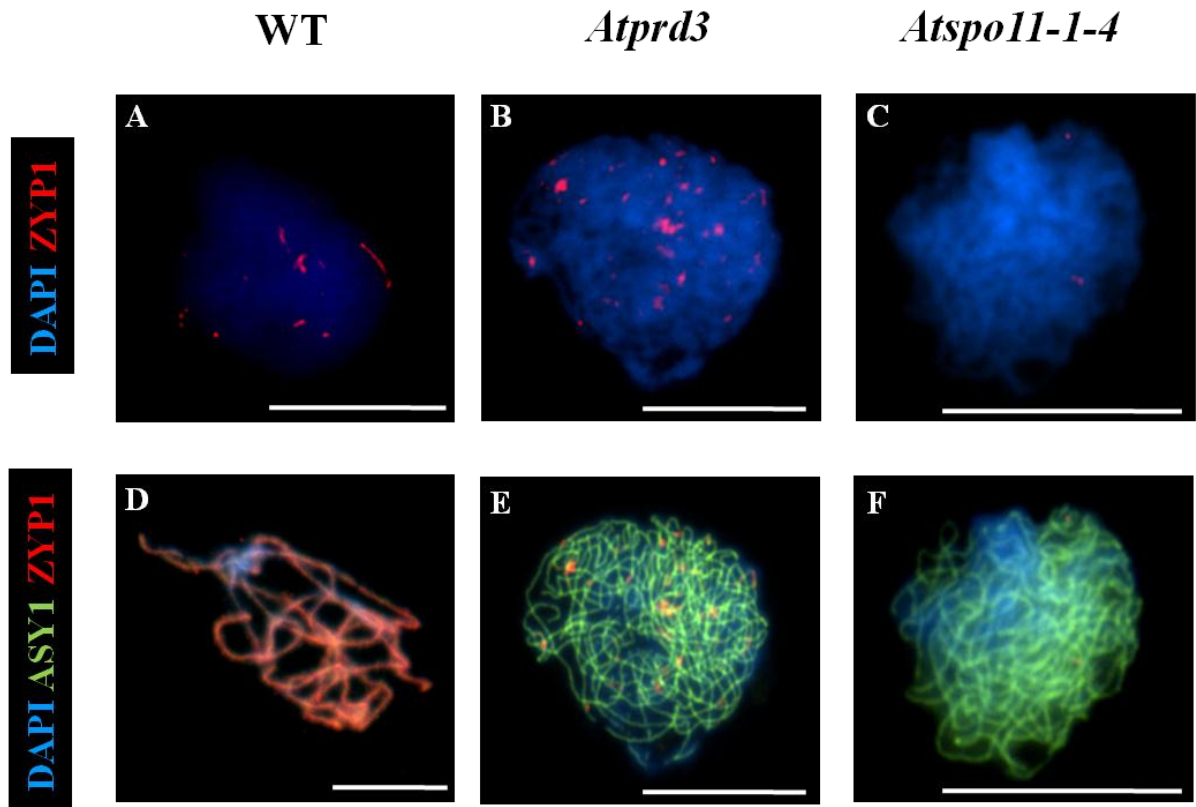
Figure 4.7. Synapsis is defective in *Atprd3*.

Immunolocalisation on chromosome spread preparation of wild-type (A-D), *Atprd3* (B,E) and *Atspo11-1-4* (C,F) PMCs using anti-AtZYP1 (red) and anti-AtASY1 (green) antibodies. (A-C) Immunolocalisation of AtZYP1. (D-F) Dual immunolocalisation of AtZYP1 and AtASY1. Nuclei were counterstained with DAPI (blue). Scale bar = 10 μM.

4.6. Meiotic duration is normal in *Atprd3* mutant

Previous studies suggested the presence of a surveillance mechanism coordinating the progression of prophase I with the repair of meiotic DSBs in *Arabidopsis* (Higgins et al, 2005; Jackson et al, 2006). In *Atprd3*, meiotic DSBs are not formed. To determine the meiotic duration in *Atprd3* mutant, a BrdU pulse-chase labeling of nuclear DNA from pre-meiotic S-phase nuclei, followed by sampling and BrdU detection at various time points, was carried out in wild-type and *Atprd3* PMCs. In wild-type, the duration of meiosis from S-phase to tetrad is between 33h and 36h. Inflorescence from wild-type and *Atprd3* plants were fixed at 0h, 5h, 10h, 24h and 35h post-BrdU pulse-chase labeling. In wild-type PMCs, interphase nuclei were labelled with BrdU at 0h confirming the incorporation of BrdU during the pre-meiotic DNA replication (Table 4.1 and Figure 4.9A). The first appearance of BrdU-labelled leptotene and zygotene occurred at 5h and 10h post-BrdU pulse-chase labelling, respectively (Figure 4.9C,E). Pachytene nuclei were BrdU-labelled at 24h and tetrad at 35h post-BrdU pulse, respectively (Figure 4.9G,I). In *Atprd3*, homologous chromosomes failed to synapse. Therefore, zygotene and pachytene stages were not observed. However, the progression of meiosis and the chromatin cycles of expansion and contraction occurred in *Atprd3*. Therefore, a stage with similar chromatin compaction to zygotene and pachytene were visualised and called zygotene-like and pachytene-like stages in *Atprd3* mutant. In *Atprd3,* the progression of meiosis was similar to wild-type with a duration from S phase to tetrad estimated at 35h (Figure 4.8). Interphase nuclei were labelled at 0h, leptotene at 5h, zygotene-like at 10h, pachytene-like at 24h and tetrad at 35h post-BrdU pulse (Table 4.1. and Figure 4.9B,D,F,H,J).

	Int NL	Int L	Lep NL	Lep L	Zyg/Pac NL	Zyg/Pac L	Dip/MI NL	Dip/MI L	MII/Tet NL	MII/Tet L
Wild-type T=0	17	27 (61%)	10	0 (0%)	13	0 (0%)	ND	ND	ND	ND
Wild-type T=5	16	34 (68%)	5	4 (44%)	0	31 (0%)	ND	ND	ND	ND
Wild-type T=10	1	17 (95%)	1	9 (90%)	55	4 (7%)	ND	ND	ND	ND
Wild-type T=24	ND	ND	0	15 (100%)	6	50 (89%)	14	0 (0%)	ND	ND
Wild-type T=35	ND	ND	ND	ND	ND	ND	ND	ND	8	12 (60%)
Atprd3 **T=0**	19	24 (56%)	10	0 (0%)	16 (100%)	0	ND	ND	ND	ND
Atprd3 **T=5**	15	40 (73%)	7	8 (53%)	69	0 (0%)	ND	ND	ND	ND
Atprd3 **T=10**	3	24 (89%)	0	10 (100%)	53	2 (4%)	ND	ND	ND	ND
Atprd3 **T=24**	ND	ND	0	14 (100%)	21	62 (75%)	18	0 (0%)	ND	ND
Atprd3 **T=35**	ND	ND	ND	ND	ND	ND	ND	ND	14	6 (30%)

Table 4.1. Proportion of BrdU-labelled nuclei for wild-type and *Atprd3* PMCs

Non BrdU-labelled (NL) and BrdU-labelled (L) nuclei were scored and the proportion of labelled nuclei is shown in bracket in the table. Some meiotic stages have short duration and meiosis was divided into 5 categories: interphase (Int), leptotene (Lep), zygotene/pachytene (Zyg/Pac), diplotene to metaphase I (Dip/MI), metaphase II to tetrad (MII/Tet). ND: non determined.

Figure 4.8. Meiotic duration is normal in *Atprd3*

Schematic representation of the duration of meiosis from S-phase to tetrad in wild-type and *Atprd3* PMCs.

Figure 4.9. Meiotic time course for wild-type and *Atprd3* nuclei

Nuclei were BrdU pulse-chase labelled in S-phase and inflorescences from wild-type (A,C,E,G,I) and *Atprd3* (B,D,F,H,J) were taken for analysis at 0h (A,B), 5h (C,D), 10h (E,F), 24h (G,H) and 35h (I,J) post-BrdU pulse-chase. The detection of BrdU-labelled nuclei was carried out with an anti-BrdU antibody (green). Nuclei were counterstained with DAPI (blue). Scale bar = 10 μM.

4.7. AtPRD3 is not required for AtSPO11-1 association with the chromatin

4.7.1. Anti-AtPRD3 antibody is specific to AtPRD3

To study the localisation of AtPRD3 in *Arabidopsis* PMCs, an anti-AtPRD3 antibody was raised against the C-terminus part of the protein. The specificity of the antibody was tested against *E.coli* recombinant protein (provided by Steve Price) on a SDS-page gel. AtPRD3 recombinant protein was fused with a His-tag and had an expected molecular weight of 29 kDa. 8 μg and 5 μg of His-tagged AtPRD3 recombinant protein were loaded into 6 wells onto a SDS-page then transferred to a nitrocellulose membrane. The membrane was cut into 3 parts. One membrane was blotted with an anti-His tag antibody while the two other membranes were blotted with the pre-immune and the anti-AtPRD3 antibody. A strong signal was detected at a molecular weight slightly below 35 kDa with anti-His tag and anti-AtPRD3 antibodies (Figure 4.10A,C). The signal likely represents AtPRD3 recombinant protein as the signal was not observed when the membrane was blotted with the pre-immune (Figure 4.11B). This indicates that anti-AtPRD3 antibody is specific to AtPRD3 recombinant protein.
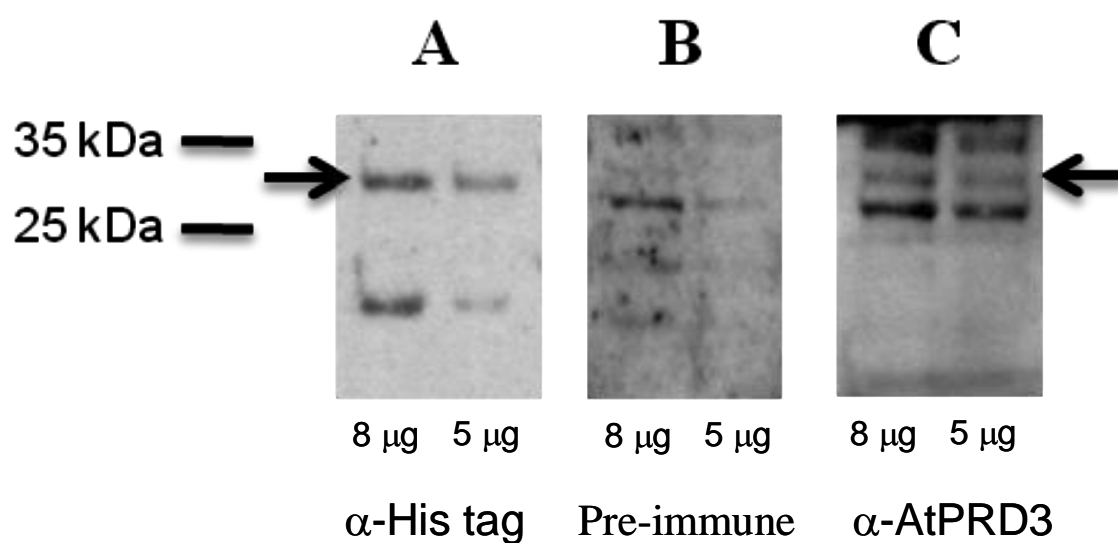
Figure 4.10. Anti-AtPRD3 antibody is specific to AtPRD3 recombinant protein

8 µg and 5 µg of His-tagged AtPRD3 recombinant protein was loaded onto a SDS-page. The protein was transferred to a nitrocellulose membrane and was detected with anti-His tag (A) and anti-AtPRD3 (C) antibodies. As a control, the membrane was blotted with the pre-immune (B). The expected molecular weight of His-tagged AtPRD3 is 29 kDa. The black arrows represent His-tagged AtPRD3.

4.7.2. AtPRD3 associates with the hyper-abundant domains of AtASY1

Sanchez-Moran *et al.* (2007) described the chronology of chromosome axis formation and recombination events during *Arabidopsis* meiosis. The authors showed that AtSPO11-1 briefly associates with the chromatin and this was temporally correlated with the initiation of the polymerisation of AtASY1. The polymerisation of AtASY1 and other axis components occur when short stretches of chromosome threads are detected on DAPI-stained chromosome spreads of *Arabidopsis* PMCs. It is thought that this is a cytological representation of the formation of the meiotic chromosome axes. To investigate the localisation of AtPRD3 in *Arabidopsis* PMCs, dual immunolocalisation using anti-AtPRD3 and anti-AtASY1 antibodies was carried out. AtPRD3 formed numerous foci (51.6, n=5) associated with the chromatin at G2. The localisation of AtASY1 occurred prior to the localisation of AtPRD3. In addition, AtPRD3 was found associated with the chromatin when AtASY1 signal formed numerous foci and short stretches. The majority of AtPRD3 foci were found associated with AtASY1 foci or AtASY1 hyper-abundant domains present on the short stretches of AtASY1 (Figure 4.11A). AtPRD3 remained briefly associated with the chromatin but was no longer detected when AtASY1 polymerised further. No signal was detected in the *Atprd3* mutant confirming the specificity of the anti-AtPRD3 antibody (Figure 4.11C).

4.7.3. AtPRD3 and AtSPO11-1 are mutually independent for localisation

The defect in DSB formation observed in *Atprd3* can result from a defect in the localisation of AtSPO11-1 with the chromatin or a defect in the tethering of the chromatin

loops to the chromosome axes. Dual immunolocalisation using anti-AtASY1 and anti-AtSPO11-1 antibodies from wild-type PMCs revealed that AtSPO11-1 localisation is temporally similar to AtPRD3 localisation. AtSPO11-1 formed numerous foci (79.2 foci, n=5) associated with the chromatin when AtASY1 formed foci and short stretches. Similarly, AtSPO11-1 was not detected when AtASY1 stretches elongated further. The majority of AtSPO11-1 foci were associated with AtASY1 foci and AtASY1 hyper-abundant domains present on the short stretches of AtASY1 (Figure 4.11B). The association between AtSPO11-1/AtPRD3 and AtASY1 foci supports the model where the chromosome axes have an important role in the determination of the sites of future DSBs. In *Atprd3* mutant, the localisation of AtSPO11-1 was indistinguishable from wild-type PMCs. An average of 80.2 AtSPO11-1 foci (n=5) were detected and the majority of AtSPO11-1 foci were associated with AtASY1 foci/hyper-abundant domains (Figure 4.11D). In addition, the localisation of AtPRD3 on the chromatin was independent on AtSPO11-1. In *Atspo11-1* PMCs, an average of 53.8 AtPRD3 foci (n=5) were observed and the majority of AtPRD3 foci were associated with AtASY1 foci/hyper-abundant domains (Figure 4.11E). Overall, this indicates that AtPRD3 and AtSPO11-1 are mutually independent for their localisation.
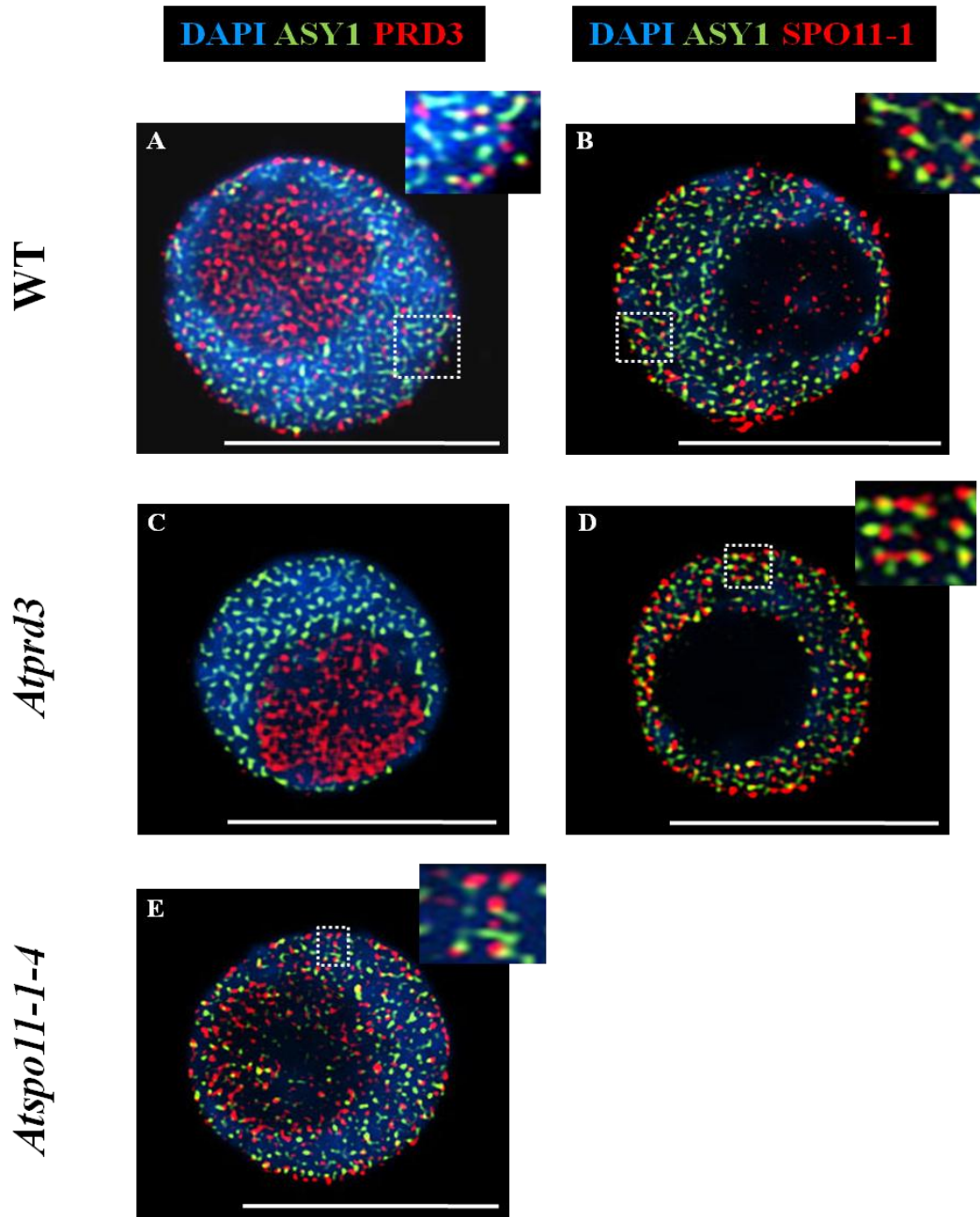
Figure 4.11. AtPRD3 and AtSPO11-1 are mutually independent for their localisation (A,C,E) Dual immunolocalisation of AtASY1 (green) and AtPRD3 (red) on DAPI-stained (blue) chromosome spread preparation of wild-type (A), *Atprd3* (C) and *Atspo11-1-4* (E). (B,D) Dual immunolocalisation of AtASY1 (green) and AtSPO11-1 (red) on DAPI-stained (blue) chromosome spread preparation of wild-type (B) and *Atprd3* (D). Scale bar = 10 μM.

4.8. AtPRD3 forms a homo-dimer and interacts with the chromosome axis components AtASY1 and AtASY3 in a yeast two-hybrid assay

4.8.1. AtPRD3 interacts with AtASY1 in a yeast two-hybrid assay

Immunoprecipitation study using an anti-AtASY1 antibdody on *Brassica oleracea* crude extract revealed that a protein sharing high sequence homology with AtPRD3 was found in the eluate (Osman and Franklin, unpublished). Two recent studies suggest that the number of DSBs is not significantly affected in *Atasy1* (Ferdous et al, 2012; Sanchez-Moran et al, 2007a). However, the number of γH2AX foci was found slightly decreased in *Atasy1*. This indicates that AtASY1 may have a role in DSB formation. To test the interaction between AtASY1 and AtPRD3, the full length coding sequence of *AtASY1* and *AtPRD3* were fused with the activating (-AD) and binding domains (-BD) of GAL4 using the primer sets: pGAD-ASY1F- pGAD-ASY1R, pGBK-ASY1F- pGBK-ASY1R, pGAD-PRD3F- pGAD-PRD3R and pGBK-PRD3F- pGBK-PRD3R. Y2H Gold yeast cells were then co-transformed with AtASY1-AD/AtPRD3-BD and AtPRD3-AD/AtASY1-BD. As negative controls, yeast cells were co-transformed with AtASY1 or AtPRD3 in combination with the complementary empty vector. The interaction between the two proteins was analysed in the GAL4 yeast two-hybrid system as mentioned above.

After 4-5 days of incubation, growth of yeast co-transformed with AtPRD3-AD/AtASY1-BD and AtPRD3-AD/empty vector was observed on the less stringent media SD –LTH but not on the more stringent media SD –LTHA (Figure 4.12). All other negative controls and yeast co-transformed with AtASY1-AD/AtPRD3-BD were unable to growth in the absence

of histidine in the media. To assess the level of activation of *HIS* gene in cells transformed with AtPRD3-AD/AtASY1-BD compared to cells transformed with AtPRD3-AD/empty vector, a serial drop dilution of growing cell culture was carried out. Cell cultures of similar optical density were diluted in serial series. 3 µl of each culture (with no dilution, 1/10 and 1/100 dilution) was dropped on SD –LT, SD –LTH and SD –LTHA. Five independent cultures were prepared for each vector combination. All cultures present a similar growth pattern on SD –LT confirming the similar cell density and growth rate between the different cultures. Weak growth of cells expressing AtPRD3-AD/AtASY1-BD was observed after 1.5 day of incubation on SD -LTH. However, no growth was observed for cells expressing AtPRD3-AD/empty vector on SD -LTH. After 2 days of incubation, growth of AtPRD3-AD/AtASY1-BD cells was more apparent at no dilution and weak growth was observed at 1/10 dilution on SD -LTH. This was consistently observed for all five independent cultures. In contrast, weak growth of cells expressing AtPRD3-AD/empty vector was observed at no dilution only on SD –LTH (Figure 4.12). The five independent cultures revealed a similar growth pattern. By prolonging the incubation time to 2.5 days, growth of AtPRD3-AD/empty cell was detected at 1/10 dilution. This indicates that *HIS* gene expression is elevated in the presence of AtPRD3-AD and AtASY1-BD. The activation of *HIS* gene expression in cells expressing AtPRD3-AD can be explained by the DNA binding properties of AtPRD3. The faster growth rate of cells expressing AtPRD3-AD and AtASY1-BD compared to the negative control suggests that AtPRD3 interacts with AtASY1 in a yeast two-hybrid assay.
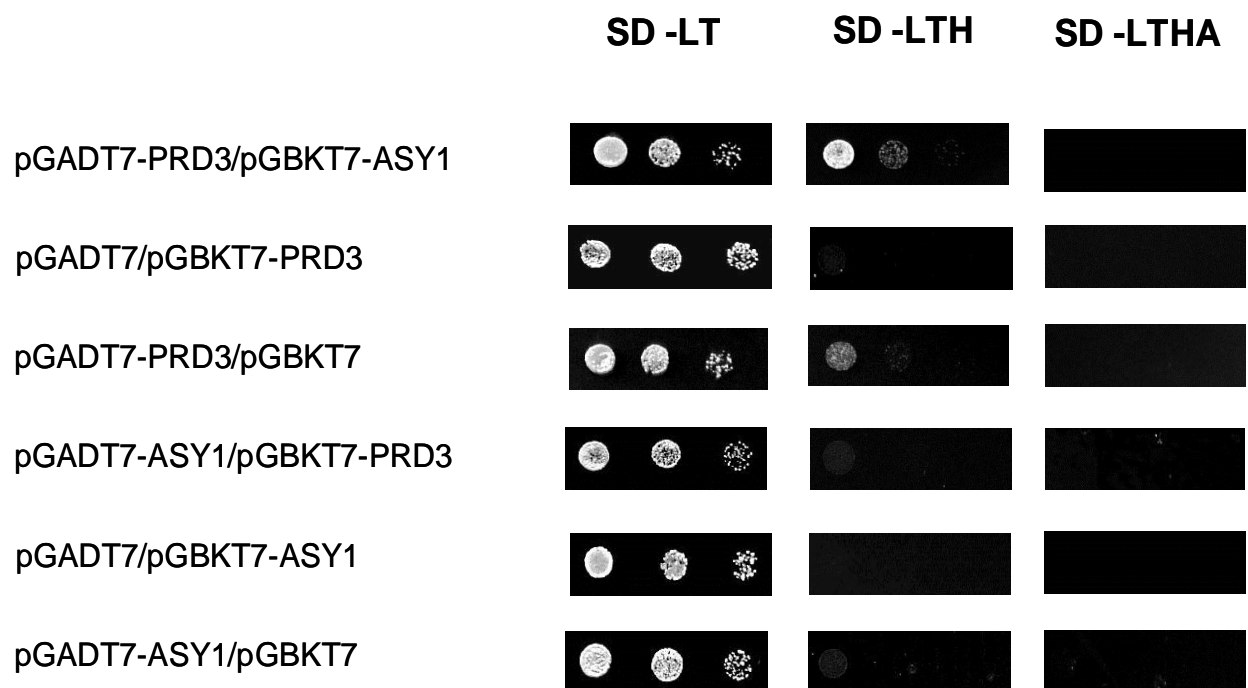
Figure 4.12. AtPRD3 interacts with AtASY1 in a yeast two-hybrid assay.

Full length coding sequence of *AtPRD3* and *AtASY1* were fused with GAL4 activating domain (into pGADT7 vector) and GAL4 binding domain (into pGBKT7 vector). *S. cerevisiae* Y2H Gold cells were co-transformed with a combination of pGADT7/pGBKT7 vectors. Co-transformed yeast cells were screened on the restrictive media SD –LT. Growth of yeast cells expressing AtPRD3-AD and AtASY1-BD was observed on the less stringent media SD -LTH but not on the more stringent media SD -LTHA. In addition, yeast cells expressing AtASY1-AD and AtPRD3-BD were unable to grow on the restrictive media SD -LTH and SD –LTHA. Yeast cells co-transformed with pGADT7-AtPRD3/pGBKT7 empty vector were also able to grow on the less stringent media SD –LTH but at a slower growth rate compared to cells co-transformed with pGADT7-AtPRD3/pGBKT7-AtASY1. All other negative controls did not show yeast growth on the restrictive media SD –LTH and SD –LTHA. This indicates that AtPRD3 weakly interacts with AtASY1 in a yeast two-hybrid assay. The strength of interaction between the two proteins was assessed by serial drop dilutions of mid-exponential-phase cell cultures. 3µl of undiluted, 1/10 and 1/100 diluted cultures were spotted on the selective agar media and incubated at 30°C for 2 days.

169

4.8.2. AtPRD3 interacts with AtASY3 in a yeast two-hybrid assay

To further investigate the potential interaction between AtPRD3 and components of the chromosome axes, the interaction between AtASY3 and AtPRD3 was tested. Similar to the previous yeast two-hybrid experiments, *AtASY3* and *AtPRD3* full length coding sequences were fused with the activating and binding domain of GAL4. Y2H Gold cells were co-transformed with AtASY3-AD/AtPRD3-BD and the reciprocal vector combination. As negative controls, yeast cells were co-transformed with one empty vector and the complementary vector expressing either AtASY3 or AtPRD3.

After 5 days of incubation, only cells expressing AtPRD3-AD/AtASY3-BD were able to grow on the more stringent media SD –LTHA (Figure 4.13). The growth rate of AtPRD3-AD/AtASY3-BD cells was slower on SD –LTHA than on SD –LTH. As previously reported, cells expressing AtPRD3-AD/empty vector were able to grow on the less stringent media SD –LTH. The other vector combinations were unable to activate the expression of the reporter genes in yeast cells. This observation suggests that AtPRD3 physically interacts with AtASY3 in a yeast two-hybrid assay. The absence of interaction between AtASY3-AD/AtPRD3-BD is similar to the absence of interaction between AtASY1-AD/AtPRD3-BD. The fusion of GAL4 binding domain with AtPRD3 could alter the structure of the protein which renders the interaction between AtASY1/AtASY3 and AtPRD3 impossible.
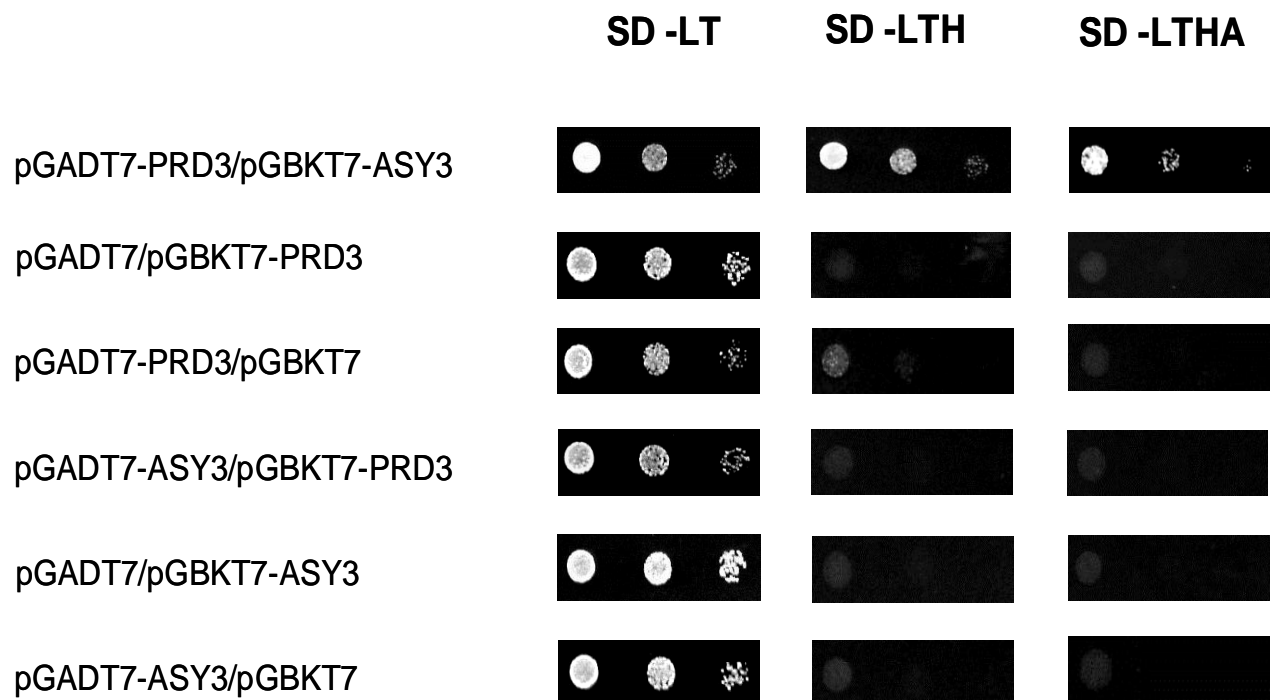
Figure 4.13. AtPRD3 interacts with AtASY3 in a yeast two-hybrid assay.

Full length coding sequence of AtPRD3 and AtASY3 were fused with GAL4 activating domain (into pGADT7 vector) and GAL4 binding domain (into pGBKT7 vector). *S. cerevisiae* Y2H Gold cells were co-transformed with a combination of pGADT7/pGBKT7 vectors. Co-transformed yeast cells were screened on the restrictive media SD –LT. Growth of yeast cells expressing AtPRD3-AD and AtASY3-BD was observed on SD -LTH and SD –LTHA. However, yeast cells expressing AtASY3-AD and AtPRD3-BD were unable to grow on the restrictive media SD -LTH and SD –LTHA. In addition, yeast cells co-transformed with pGADT7-AtPRD3/pGBKT7 empty vector were also able to grow on the less stringent media SD –LTH but not on the more stringent media SD -LTHA. All other negative controls did not show yeast growth on the restrictive media SD –LTH and SD –LTHA. This indicates that AtPRD3 interacts with AtASY3 in a yeast two-hybrid assay. The strength of interaction between the two proteins was assessed by serial drop dilutions of mid-exponential-phase cell cultures. 3μl of undiluted, 1/10 and 1/100 diluted cultures were spotted on the selective agar media and incubated at 30°C for 2.5 days.

171

4.8.3. AtPRD3 forms a homo-dimer in a yeast two-hybrid assay

Finally, the capacity of AtPRD3 to form a homo-dimer was studied. The full length coding sequence of *AtPRD3* was fused with the activating and binding domain of GAL4. Y2H gold cells were co-transformed with AtPRD3-AD/AtPRD3-BD, AtPRD3-AD/empty vector or AtPRD3-BD/empty vector. After 4 days of incubation, growth of cells expressing AtPRD3-AD/AtPRD3-BD was observed on the more stringent media SD –LTHA (Figure 4.14). A weak growth of AtPRD3-AD/empty vector was observed on the less stringent media SD –LTH. This observation shows that AtPRD3 forms a homo-dimer in a yeast two-hybrid assay. The growth rate of cells co-transformed with AtPRD3-AD/AtPRD3-BD was faster than the growth rate of cells co-transformed with AtPRD3-AD/AtASY3-BD. This indicates a difference in the strength of protein-protein interaction between the two complexes in yeast cells.
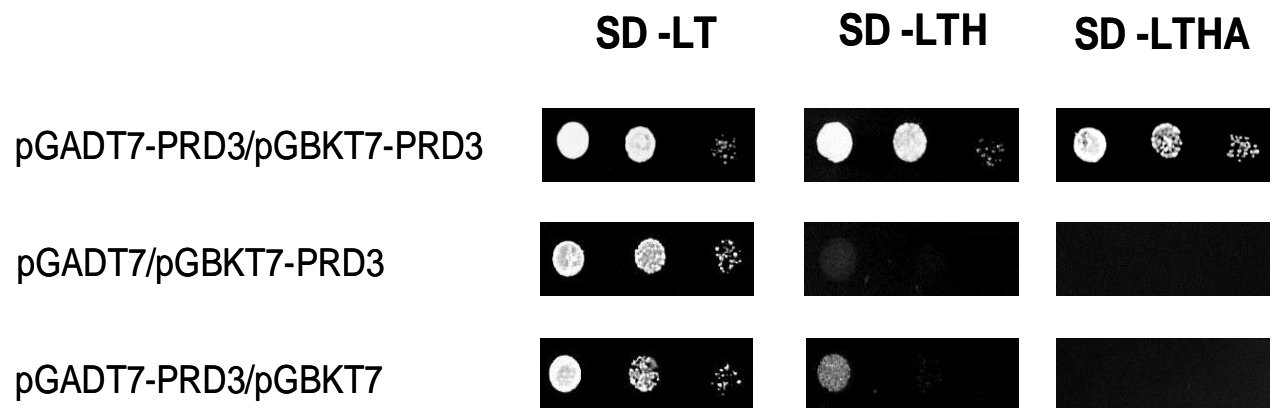
Figure 4.14. AtPRD3 forms a homo-dimer in a yeast two-hybrid assay.

Full length coding sequence of AtPRD3 was fused with GAL4 activating domain (into pGADT7 vector) and GAL4 binding domain (into pGBKT7 vector). *S. cerevisiae* Y2H Gold cells were co-transformed with a combination of pGADT7/pGBKT7 vectors. Co-transformed yeast cells were screened on the restrictive media SD –LT. Growth of yeast cells expressing AtPRD3-AD and AtPRD3-BD was observed on the restrictive media SD -LTH and SD -LTHA. Yeast cells co-transformed with pGADT7-AtPRD3/pGBKT7 empty vector were able to grow on the less stringent media SD –LTH but not on the more stringent media SD -LTHA. However, the cells co-transformed with pGADT7 empty vector/pGBKT7-AtPRD3 were unable to grow on both restrictive media SD –LTH and SD –LTHA. This suggests that AtPRD3 forms a homo-dimer in a yeast two-hybrid assay. The strength of interaction between the two proteins was assessed by serial drop dilutions of mid-exponential-phase cell cultures. 3µl of undiluted, 1/10 and 1/100 diluted cultures were spotted on the selective agar media and incubated at 30°C for 2 days.

4.9. AtATM/AtATR negatively regulate the formation of AtSPO11-dependent DSBs

The number of meiotic DSBs formed per nucleus is regulated by the kinase activity of ATM/ATR in mammals, yeasts and flies (Carballo et al, 2013; Joyce et al, 2011; Lange et al, 2011; Zhang et al, 2011). Ferdous *et al.* (2012) inferred that the number of AtDMC1, AtRAD51 and γH2AX foci found associated with the chromatin at the onset of leptotene were marking the sites of DSB in *Arabidopsis*. AtRAD51 is a recombinase protein thought to be involved in the formation of DSBs during both mitosis and meiosis. AtDMC1 is a meiotic specific recombinase and its loading on the chromatin is dependent on both AtASY1 and AtATR while the phosphorylation of the histone variant H2A is dependent on AtATM/AtATR kinase activity (Kurzbauer et al, 2012; Sanchez-Moran et al, 2007a). Only the recruitment of AtRAD51 at the sites of DSB appears to be independent on axes components and AtATR. Thus, to determine if AtATM/AtATR are involved in the formation of DSBs, an immunocytochemistry study was carried out on chromosome spread preparations of wild-type and the *Atatm/Atatr* double mutant using an anti-AtRAD51 antibody. In wild-type PMCs, the mean number of AtRAD51 foci was 166.7 at early prophase I. In contrast, the mean number of AtRAD51 foci was 229.3 in *Atatm/Atatr* double mutant, representing an increase of AtRAD51 foci by 27 % the wild-type level (Figure 4.15A-F). This suggests that AtATM and/or AtATR negatively regulate(s) the formation of DSBs.

The most effective approach to control the formation of DSBs would consist at regulating the stability of the pre-DSB machinery on the chromatin. In *Arabidopsis,* two SPO11

paralogues, AtSPO11-1 and AtSPO11-2 have been characterised. Four additional proteins have been described as essential for the formation of DSBs (De Muyt et al, 2009; De Muyt et al, 2007; Grelon et al, 2001; Hartung et al, 2007; Stacey et al, 2006; Zhang et al, 2012). ATM/ATR specifically phosphorylates its target proteins at [S/T]Q sites. To identify potential targets of AtATM/AtATR kinase activity, all six proteins were screened for [S/T]Q sites. Only two proteins, AtPRD1 and AtPRD3 have a high number of [S/T]Q sites. AtPRD1 has 10 [S/T]Q and AtPRD3 has 11 [S/T]Q sites (Figure 4.15G). In comparison, the average number of [S/T]Q sites per protein is 2.91 in *Arabidopsis* proteome. Interestingly, AtPRD3 has a high ratio [S/T]Q sites:amino-acid length and has a SCD containing 10 [S/T]Q sites at the N-terminus part of the protein (Figure 4.15H). Further analysis is required to determine whether AtPRD3 is phosphorylated during meiosis.
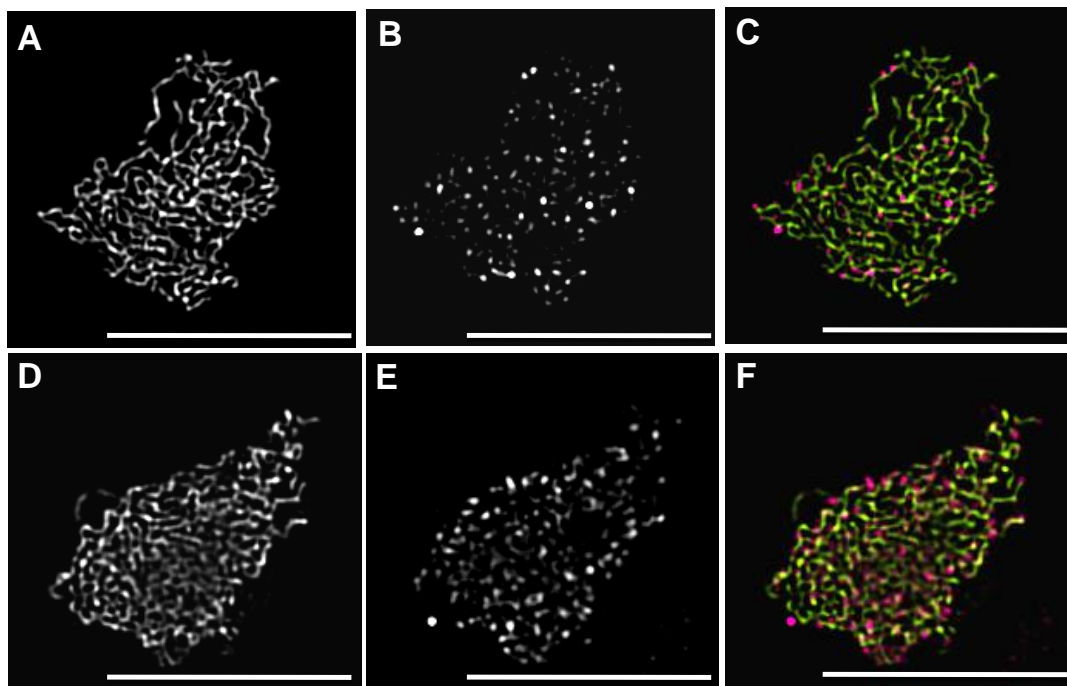
MKMNINKACDLKSISVFPPNLRRSAEPQASQQLRSQQSQQSFSQGPSSSQRGCGGFSQMTQSSIDELLINDQRFSSQERDLSLKKVSSCLPPINHKREDSQLVASRSSSGLSRRWSSASIGESKSQISEELEQRFGMMETSLSRFGMMLDSIQSDIMQANRGTKEVFLETERIQQKLTLQDTSLQQLRKEQADSKASLDGGVKFILEEFSKDPNQEKLQKILQMLTTIPEQVETALQKIQREICHTFTREIQVLASLRTPEPRVRVPTAPQVKAKENLPEQRGQAAKVLTSLKMPEPRVQVPAAPQAKENFPEQRGPVAKSNSFCNTTLKTKQPQFPRNPNDASARAVKPYLSPKIQVGCWKTVKPEKSNFKKRATRKPVKSESTRTQFEQCSVVIDSDEEDIDGGFSCLINENTRGTNFEWDAEKETERILRTARRTKRKFGNPIIIN

Figure 4.15. AtATM/AtATR negatively regulate the formation of meiotic DSBs
(A,B,D,E) Immunolocalisation of AtASY1 (A,D) and AtRAD51 (B,E) on wild-type (A,B) and *Atatm/Atatr* (D,E) PMCs. (C,F) Merge image of AtASY1 (green) and AtRAD51 (magenta) on wild-type (C) and *Atatm/Atatr* (F) PMCs. Scale bar = 10 μm. (G) Table representing the number of [S/T]Q sites for each protein involved in the formation of DSBs. (H) Amino-acid sequence of AtPRD3. SQ sites are represented in red and TQ sites are represented in blue.

4.10. Discussion

4.10.1. AtPRD3 is essential for the formation of meiotic DSBs

The regulation of meiotic DSB formation has been extensively studied in budding and fission yeast. Several components of the pre-DSB complex have been characterised. The association of this complex with the chromatin is spatially and temporally regulated by the replication of DNA during premeiotic S-phase (Borde et al, 2000; Murakami & Nurse, 2001), the chromatin status (Acquaviva et al, 2013; Sommermeyer et al, 2013), the chromosome axes and the formation of DSBs (Carballo et al, 2013; Zhang et al, 2011). Some of these characteristics have also been described in mammals (Kumar et al, 2010) and nematodes (Rosu et al, 2013; Stamper et al, 2013). In contrast, only 6 proteins have been characterised as directly involved in the formation of DSBs in *Arabidopsis* (De Muyt et al, 2009; De Muyt et al, 2007; Grelon et al, 2001; Hartung et al, 2007; Stacey et al, 2006; Zhang et al, 2012). The lack of domain and sequence similarity complicates the

functional analyses of these proteins. AtPRD3 was identified in a screen for asynaptic mutants (De Muyt et al, 2009). AtPRD3 doesn't share sequence/domain similarity with other known meiotic proteins and is essential for the formation of meiotic DSBs. This is suggested by the absence of phosphorylation of H2AX variant and the absence of localisation of AtDMC1 with the chromatin in *Atprd3* mutant. In addition, the lack of AtPRD3 rescues the chromosome fragmentation phenotype detected in *Atrad51* mutant. A similar observation was observed in *Atspo11/Atrad51* double mutant supporting a role for AtPRD3 in the formation of DSBs. However, the function of AtPRD3 is unknown. Recently, Vrielynck and Grelon (personal communication) established a network of protein interactions between pre-DSB proteins, using a yeast two hybrid system.AtPRD3 was found interacting with AtMRE11 but not with any of the proteins essential for the formation of DSBs. In budding yeast, Mre11 is required for wild-type level of DSBs (Johzuka & Ogawa, 1995). However, the formation of DSBs is proficient in *Arabidopsis Atmre11* mutant (Uanschou et al, 2007).

4.10.2. AtPRD3 interacts with the chromosome axes and is not required for the localisation of AtSPO11-1 on the chromatin

At least two models can explain the role of AtPRD3 in the formation of DSBs. AtPRD3 could form a complex with AtSPO11-1/2 and promote/stabilise their association at the pre-determined sites of future DSBs. Alternatively, AtPRD3 could be associated with the chromosome axes and promote the tethering of the chromatin loops to the chromosome axes and/or activate the topoisomerase-like transesterification activity of AtSPO11-1/2

when the chromatin loops are tethered with the axes (Acquaviva et al, 2013; Panizza et al, 2011; Sommermeyer et al, 2013).

The localisation of Spo11 on the chromatin has been investigated in budding yeast. The localisation of Spo11 at the *his4LEU2* hotspot was severely disrupted in *rec102, rec104* and *rec114* mutants (Prieler et al, 2005). In addition, the association of Spo11 with the chromatin is dependent on the phosphorylation status of Rec114. Carballo *et al.* (2013) showed that Rec114 is phosphorylated by Tel1 and/or Mec1 following formation of DSBs. A phosphomimic version of Rec114 (*rec114 -8D*) reduced the number of DSBs and reduce the binding of Spo11 on the chromatin. These two independent studies suggest that both the presence of Rec114 protein on the axes and its phosphorylation status are important to regulate the localisation of Spo11 at the sites of future DSBs. AtPRD3 present limited sequence homology with Rec114. However, AtPRD3 is enriched in [S/T]Q sites and is a potential target of AtATM/AtATR (see below). Interestingly, AtPRD3 and AtSPO11-1 are mutually independent for their localisation. Moreover, AtPRD3 was found interacting with the two chromosome axes components AtASY1 and AtASY3 in a yeast two-hybrid assay and AtPRD3 was pulled down from a Brassica crude extract using an anti-ASY1 antibody. This suggests that AtPRD3 may associate with the underlying chromosome axes and either tether the chromatin loops to the axes at pre-determined sites or activate the topoisomerase-like transesterification activity of AtSPO11-1/2 when the chromatin loops are tethered with the axes. Interestingly, preliminary analysis of APRD3 localisation in chromosome axis mutants showed that AtASY1 is required for proper localisation of AtPRD3 on the chromatin (data not shown). Similarly, chromosome axes components were found important for the distribution of DSBs by regulating the localisation and

distribution of Rec114 and Rec27 along the axes in budding yeast and fission yeast, respectively (Fowler et al, 2013; Panizza et al, 2011).

Recently, Yant *et al.* (2013) identified 44 genes that present a strong ploidy specific differentiation between natural diploid and tetraploid *Arabidopsis arenosa*. Genes coding for chromosome axes components and for AtPRD3 were among these 44 genes. The parallel evolutionary differentiation of chromosome axes genes and *AtPRD3* further supports the coordinate role of AtPRD3 and the axes in the formation of meiotic DSBs (Yant et al, 2013).

4.10.3. The nucleation of AtZYP1 is dependent on the formation of DSBs

The SC nucleates at discrete sites on the chromatin. Several factors determine the sites of SC nucleation. It is thought that the SC nucleates at the CO-designated sites. In *Arabidopsis*, the number of AtZYP1 foci is higher than the number of AtMLH1 foci which are thought to represent the sites of COs of class I. An average of 10 COs is formed per nucleus in *Arabidopsis.* The presence of additional SISs may be required to ensure proper SC polymerisation along the chromosomes. In budding yeast, Zip1 localises at the CO-designated sites and at the centromeres (see below) (Tsubouchi et al, 2008). AtZYP1 is a structural component of the SC transverse filament and has a tendency to aggregate and form polycomplexes in the absence of early recombination events. In *Atprd3* mutant, meiotic DSBs are not formed, thus preventing the initiation of homologous recombination. AtZYP1 was found associated with the chromatin forming foci in most of the nuclei analysed and occasionally forming short stretches. Voelkel-Meiman *et al.* (2012) reported

that Zip1 has a low turnover when the protein was integrated in the SC (Voelkel-Meiman et al, 2012). In mutant lines defective for homologous recombination, the newly synthesise Zip1/AtZYP1 protein may aggregate at the pre-existing chromatin-associated Zip1/AtZYP1 foci forming abnormal thick structures as the SC fails to further elongate. Interestingly, AtZYP1 was found localised on the chromatin at a lower frequency in *Atspo11-1-4* mutant compared to *Atprd3* mutant. The difference in AtZYP1 localisation cannot be explained by the presence of rare DSBs in *Atprd3* mutant as no chromosome fragmentation was observed in *Atprd3/Atrad51* and *Atprd3/Atmre11* double mutants (De Muyt et al, 2009). In budding yeast, Spo11 has a role during pre-meiotic S-phase. The duration of the pre-meiotic S-phase was reduced by 25 % in *spo11* mutant. In addition, the absence of SC nucleation was partially dependent on the role of Spo11 during DNA replication. In *spo11/spo22* double mutant, where DNA replication was prevented, the SC length was restored to 55 % the wild-type level in *Coprinus cinereus* (Merino et al, 2000). The difference observed in AtZYP1 localisation between *Atprd3* and *Atspo11-1-4* mutants could account for an additional role of AtSPO11-1 during pre-meiotic S-phase. Alternatively, the nucleation of AtZYP1 could be tightly regulated by several factors. In mice, SC forms short stretches in *spo11* mutant. The partial polymerisation of the SC is thought to occur between non-homologous chromosomes. In *hormad1/spo11* double mutant, the nucleation of SYCP1 was reduced compared to *spo11* single mutant (Daniel et al, 2011). This indicates that HORMAD1 is needed for SC nucleation independently of recombination events. Similarly, the nucleation and initial elongation of AtZYP1 may be regulated by several factors in *Arabidopsis*.

4.10.4. Achiasmate chromosomes exhibit an increase in chromosomal connections

The presence of inter-chromosomal connections during *Arabidopsis* meiosis was reported by Knoll *et al.* (2012). Although no bivalent was observed in *Atspo11-1-4* and *Atprd3* mutant, ultrafine DNA bridges were observed at higher frequency in these mutants compared to wild-type nuclei. The nature of these bridges is unknown. The presence of ultrafine DNA bridges was recently identified in mitotic human cells (Baumann et al, 2007; Chan et al, 2007). These connections between chromosomes did not contain histones and were associated with the SNF2/SWI family member PICH, RPA and FANCM helicases. The presence of these connections is thought to arise during DNA replication and occur at the centromeric/telomeric regions or at genomic regions where DNA replication occur with difficulties. A similar type of bridges may occur during pre-meiotic S-phase between regions that are late replicating or fail to properly replicate (Mankouri et al, 2013). This is supported by the increase in inter-chromosomal connections reported during meiotic metaphase I in *Atfancm* mutant (Knoll et al, 2012). The frequency of bridges was increased by a factor of 2 when chromosomes failed to form bivalent. The connections were mostly established between non homologous chromosomes. The defect in the obligate CO does not restrict the mobility of univalent chromosomes and thus resulted in an increase in the formation/persistence of bridges. Although the bridges occurred between non homologous chromosomes, they may have a role in the segregation of chromosomes at anaphase I. Ultrafine DNA bridges were found elongated and the connected chromosomes were segregating towards opposite poles during metaphase I/anaphase I transition. In mice (Bisig et al, 2012; Qiao et al, 2012) and yeast (Newnham et al, 2010), a backup mechanism exists increasing the frequency of disjunction of achiasmate

chromosomes. The nature of this mechanism is unknown. However, Spo11 and components of the SC were suggested to be involved in this process. A similar mechanism limiting the non-disjunction of achiasmate chromosomes was suggested in *Arabidopsis* (Pradillo et al, 2007). It is possible that the presence of ultrafine DNA bridges observed in metaphase I favours the segregation of the connected chromosomes toward opposite poles of the cells, thus limiting the frequency of non-disjunction of achiasmate chromosomes in *Arabidopsis*.

4.10.5. AtATM is involved in a negative feedback loop to limit the number of DSBs

In yeasts, mammals and flies, the number of DSBs formed in each nucleus is tightly regulated. Following the formation of DSBs, the kinase activities of ATM/Tel1 and ATR/Mec1 are activated resulting in the establishment of a negative feedback loop inhibiting the formation of additional DSBs (Joyce et al, 2011; Lange et al, 2011; Zhang et al, 2011). The mechanism responsible for the inhibition of DSBs is largely unknown. However, the axis-associated protein Rec114 is essential for the formation of DSBs. In addition, Rec114 becomes phosphorylated by Mec1/Tel in response to the formation of DSBs (Carballo et al, 2013). The phosphorylation of Rec114 results in the inhibition of the formation of additional DSBs. Several aspects of this negative feedback loop remain to be determined. For instance, how many DSBs are required to activate the negative feedback loop? How would the cell sense the number of DSBs? It is possible that this feedback loop relies on a balance between phosphorylation and dephosphorylation status. Similarly to the maintenance of Rec8 at the centromeric regions, Rec114 may be maintained in a dephosphorylated form by a phosphatase. Following DSB formation, the phosphatase

activity may be reduced while the kinase activity of Mec1/Tel1 is activated. In addition, ATM is auto-phosphorylated in response to the formation of DSBs. The number of DSBs formed in the cell could be indirectly sense by the level of phosphorylated ATM protein. This would in turn change the balance in the phosphorylation status of Rec114 and probably of other proteins.

In *Arabidopsis*, a similar negative feedback loop was described in this chapter. The number of AtRAD51 foci was increased by 27 % the wild-type level in *Atatm/Atatr* double mutant. This suggests that AtATM and/or AtATR are regulating the formation of DSBs similarly to their functional counterpart in mammals and yeasts. The inhibitory function of AtATM/AtATR for the formation of DSBs can be directed towards the components of the chromosomes axes and/or the components of the pre-DSB machinery. AtASY1 is an axis-associated protein interacting with AtPRD3 and regulating its distribution on the chromatin. AtASY1 has several [S/T]Q sites and most of these sites were found phosphorylated in Brassica extracts. In addition, AtASY1 is phosphorylated at the residue threonine 295 in response to the formation of DSBs. The phosphorylation at this residue is dependent on AtATM/AtATR (see Chapter 5). The phosphorylation of AtASY1 could disfavour the interaction between AtASY1 and AtPRD3. Two AtSPO11-accessory proteins, AtPRD1 and AtPRD3, are enriched in [S/T]Q sites. The phosphorylation status and the biological significance of the phosphorylation of these two proteins remain to be investigated. However, a direct role of AtATM/AtATR towards AtSPO11-accessory proteins is an attractive model and would potentially provide an effective means to inhibit the formation of additional DSBs.

Chapter 5

Coordination between DSB repair and remodelling

of the chromosome axes during mid-prophase I

5.1. Introduction

Meiotic recombination initiates with the formation of DSBs catalysed by the topoisomerase-like endonuclease SPO11. The formation of DSBs activates the kinase activity of ATM/Tel1 and ATR/Mec1 which phosphorylate proteins involved in the homologous recombination pathway. The DSB ends are resected by the complex MRE11-RAD50-NBS1/XRS2 in conjunction with COM1/SAE2 to generate 3' single-stranded DNA tails. One of the two 3' single-stranded DNA tail is coated by the recombinases RAD51 and DMC1 to form a pre-synaptic nucleofilament that will invade the homologous chromosome. The second 3' single-stranded DNA tail, on the opposite side of the DSB site, is thought to be quiescent until a later stage where it will be involved in the second end capture and formation of a dHJ that will be resolved to form a CO (Osman et al, 2011). Homologous recombination occurs in the context of the meiotic chromosome axes. Immunocytochemistry analysis of GFP-tagged recombination proteins from *Sordaria macrospora* revealed that early recombination proteins localise on the chromosome axes (Storlazzi et al, 2010). At the onset of leptotene, the homologous axes are separated by a distance of 400 nm. During mid-prophase I, GFP-tagged RAD51 foci are redistributed and exhibit a "between-axis" configuration. This is accompanied by a reduction of the separation between homologous axes to 200 nm (Storlazzi et al, 2010). The connection between homologous axes is important for the pairing of homologous chromosomes and the formation of COs in budding yeasts, mammals and plants. In *Arabidopsis,* the formation of D-loops rather that the formation of COs is essential for the establishment of the SC. This is supported by the cytological analysis of *Atmsh5* (Higgins et al, 2008b) and *Atmlh3* mutants (Jackson et al, 2006). The formation of the SC is accompanied by the

remodelling of the chromosome axes. Pch2 and TRIP13 are AAA-ATPase family members involved in the remodelling of the chromosome axes on the synaptic regions in budding yeasts and mice, respectively (Borner et al, 2008; Joshi et al, 2009; Roig et al, 2010; Wojtasz et al, 2009). In both mutants, Hop1 and HORMAD1/HORMAD2 persist on the synaptic regions suggesting that Pch2/TRIP13 have a role in dissociating Hop1/ HORMAD1/HORMAD2 from the nascent SC (Borner et al, 2008; Joshi et al, 2009; Roig et al, 2010; Wojtasz et al, 2009). Recently, Chen *et al.* (2014) showed that Pch2 interacts with Hop1 and its ATP hydrolysis activity is required for depleting Hop1 from the chromosome axes. Interestingly, Pch2 can assemble and disassemble Hop1 on DNA molecules *in-vitro* indicating that the role of Pch2 in chromosome axis morphogenesis is certainly more complex and may not be restricted only to the synaptic regions during mid-prophase I. Additional evidence suggests that Pch2/TRIP13 acts at an early stage in the homologous recombination pathway. Roig *et al.* (2010) showed that DSBs are inefficiently repaired and that DMC1 foci persist in mid-prophase I nuclei of *trip13* mutant. The progression of CO and NCO recombination is delayed in budding yeast *pch2* mutant (Borner et al, 2008). In addition, Ho and Burgess (2011) showed that Pch2 and Tel1 function in the same pathway to phosphorylate Hop1 after DSB resection. Lastly, two recent studies suggest that Pch2/Crc1 have a role in the formation of DSBs in budding yeast and rice (Farmer et al, 2012; Miao et al, 2013).

The biological significance of Hop1 phosphorylation has been extensively studied in budding yeast. Carballo *et al.* (2008) showed that Hop1 is phosphorylated by Mec1/Tel1 in response to the formation of DSBs. The authors suggested that the phosphorylation of Hop1 at residue T318 is important to recruit Mek1 at the DSB sites and promote inter-

187

homologue recombination. The role of Hop1 T318 phosphorylation in inter-homologue recombination and checkpoint pathway was further supported by the recent work of Chuang *et al.* (2012). A HORMA-containing domain protein sharing functional and limited structural similarities with Hop1 and HORMAD1/HORMAD2 was characterised as AtASY1 in *Arabidopsis* (Caryl et al, 2000; Sanchez-Moran et al, 2007a). During early prophase I, AtASY1 localises along the underlying chromosome axes and presents a domainal organisation forming numerous alternate domains of hyper and lower abundance (Ferdous et al, 2012). The hyper-abundant domains of AtASY1 are associated with the early recombination proteins. AtASY1 localisation is partially dependent on AtASY3 as suggested by the analysis of *Atasy3* T-DNA mutant lines (Ferdous et al, 2012). The authors proposed that the chromatin-associated AtASY1 foci detected in *Atasy3* mutant are proficient in mediating inter-homologue CO formation. In plants, the chromosome axes are remodelled on the synaptic regions, similarly to yeasts and mammals. Recently, a protein sharing amino-acid sequence similarities with Pch2 was identified in *Arabidopsis*. Immunocytochemistry studies revealed that AtPCH2 is essential to remove AtASY1 from the synaptic regions and for the elongation of the SC (Nuntasoontorn and Franklin, unpublished). In addition, an antibody was produced against a peptide of AtPCH2. Immunolocalisation using this anti-AtPCH2 antibody showed that AtPCH2 polymerises along the SC during mid-prophase I and that the polymerisation of AtPCH2 occurs concomitantly with the formation of the SC.

To gain additional information on the function of AtASY1 in mediating inter-homologue CO formation, immunoprecipitation of BoASY1 from *Brassica oleracea* meiocytes followed by mass-sprectrometry was undertaken to identify new BoASY1 interacting

proteins and post-translational modifications of the protein. A protein sharing high sequence homology with Pch2 was pulled-down using and anti-ASY1 antibody. In addition, several phospho-modified peptides of BoASY1 were detected. The majority of the phospho-modified peptides were phosphorylated at [S/T]Q sites. Interestingly, the residue T294 (threonine 295 in *Arabidopsis thaliana*), which is evolutionary conserved with Hop1 T318 in budding yeast, was found to be phosphorylated (Osman and Franklin, unpublished). To further analyse the biological significance of ASY1 phosphorylation, a single point mutation was introduced in the coding sequence of AtASY1 to substitute the residue threonine at the position 295 to an alanine. This substitution mimics the non-phosphorylated form of AtASY1 T295. The mutated version of AtASY1 coding sequence was used to transform *Atasy1* plant segregating for a T-DNA insertion in *AtASY1* locus. Four transgenic plants homozygous for the T-DNA and expressing AtASY1 T295A were generated (*Atasy1::AtASY1-TA*). Immunocytochemistry analysis suggested that AtASY1 localisation was abnormal in *Atasy1::AtASY1-TA* PMCs. In the absence of phosphorylation at residue T295, AtASY1 failed to correctly associate with the chromosome axes and AtASY1 signal was found mostly adjacent rather than co-localising with AtSMC3 signal at early prophase I. In addition, AtASY1 signal was found more diffuse, foci and the signal intensity was weaker as in wild-type. The abnormal localisation of AtASY1 along the chromosome axes resulted in a defect in the formation of inter-homologue COs and SC formation. An antibody against the phosphorylated form of AtASY1 at residue T295 was produced (AtASY1 T295p) and immunolocalisation studies showed that AtASY1 was phosphorylated at this residue from late G2. At the onset of leptotene, AtASY1 T295p signal formed a continuous signal along the chromosome axes and overlapped with AtASY1 signal. The phosphorylation of AtASY1 T295 was dependent on the formation of

189

meiotic DSBs and on the kinase activity of AtATM and AtTR. In addition, AtASY3 and AtPCH2, but not AtSYN1, were important for the proper phosphorylation of AtASY1 T295. The basal level of AtASY1 T295 phosphorylation observed in *Atspo11-1* could be essential to maintain AtASY1 associated with the chromosome axes in the absence of DSB formation.

5.2. Remodelling of the chromosome axes during prophase I

The chromosome axis is a dynamic structure that needs to be remodelled co-ordinately with the progression of DSB repair to ensure CO formation and CO interference. AtASY1 is an axis-associated protein and the localisation of AtASY1 along the underlying chromosome axes is regulated throughout prophase I. AtASY1 was detected in late S-phase/early G2 and formed chromatin-associated foci (Figure 5.1A). At the onset of leptotene, AtASY1 formed a continuous signal along the axes (Figure 5.1B). AtASY1 was organised in domains of hyper and lower abundance. A similar domainal organisation was observed for the cohesin subunits AtSMC3 and AtSYN1 and for the structural axis component AtASY3. Dual immunolocalisation using anti-AtSMC3 and anti-AtASY1 antibodies showed that the majority of the hyper-abundant domains of AtASY1 co-localise with the hyper-abundant domains of AtSMC3 (Figure 5.1. Figure 5.1G-I). During SC formation, AtASY1 assumed a differential localisation. AtASY1 formed a continuous signal overlapping with the SC. However, the signal intensity was weaker on the synaptic regions than on the unsynapsed regions (Figure 5.1C-E). At pachytene, when the elongation of the SC is completed, the AtASY1 signal was faint and foci. In addition, AtASY1 signal was found mostly on the sides of the SC which suggests that AtASY1 was

redistributed towards the chromatin loops (Figure 5.1F). Interestingly, AtSMC3 signal appeared to be brighter on the synaptic regions compared to the unsynapsed regions. A similar pattern of localisation was observed for AtSYN1 and AtASY3, although the difference of signal intensity between synaptic and unsynapsed regions was less apparent for AtASY3 (data not shown). This could simply reflect a difference in binding capacity of the antibodies rather than a real biological difference. The elongation of the SC is not continuous. During zygotene, chromosomes are often found entangled with synapsing regions, forming interlocks (Figure 5.1E arrowhead). The interlocks need to be resolved by the action of topoisomerases before the SC can further elongate.
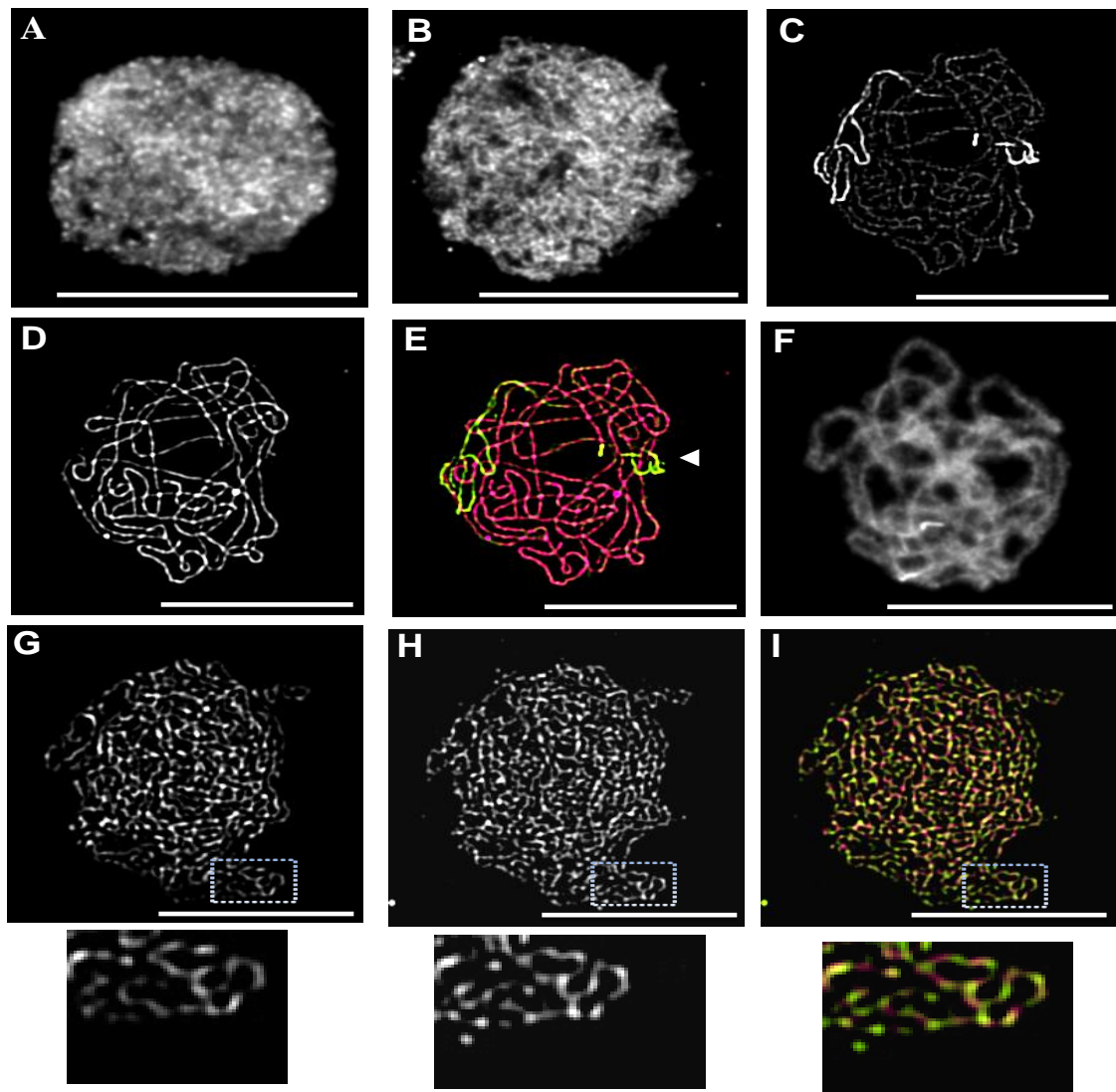
Figure 5.1. AtASY1 localisation is remodelled during meiotic prophase I in wild-type *Arabidopsis*.

(A-C) Immunolocalisation of AtASY1 (white) on chromosome spread preparation of wild-type PMCs. (A) G2, (B) leptotene, (C) zygotene. (D-E) Dual immunolocalisation of AtASY1 (green) and AtZYP1 (white/magenta) of a mid-prophase I nucleus from wild-type PMCs. (F) Immunolocalisation of AtASY1 (white) on DAPI-stained (blue) chromosome spread preparation of pachytene wild-type PMCs. (G-I) Dual immunolocalisation of AtASY1 (G, white) and AtSMC3 (H, white) of an early-prophase I nucleus from wild-type PMCs. (I) Merge image AtASY1 (magenta) and AtSMC3 (green). Both proteins are organised in domain of hyper and lower abundance along the underlying chromosome axes. Arrowhead indicates an interlock. Scale bar = 10 μM.

192

The factors involved in chromosome axes morphogenesis were investigated. Several studies indicate that the formation of the chromosome axes occurs independently on the formation of DSBs (Ferdous et al, 2012; Kim et al, 2010). Immunolocalisation study using an anti-AtASY1 antibody was carried out on chromosome spread preparation of *Atspo11-1* PMCs. To detect subtle changes in AtASY1 localisation, the anti-AtASY1 antibody was diluted to 1:20 000. AtASY1 signal formed a continuous signal at early prophase I and there was not apparent difference in the domainal organisation of AtASY1 between wild-type and *Atspo11-1* PMCs (Figure 5.2A). In contrast, AtASY1 localisation was disrupted in *Atasy3* mutant as previously reported (Ferdous et al, 2012). AtASY1 failed to form a continuous signal along the axes in *Atasy3* PMCs. Instead, AtASY1 formed punctuate chromatin-associated foci (Figure 5.2B). However, the chromosome axes were formed as suggested by the continuous signal of AtSMC3 detected in *Atasy3* PMCs and by electron-microscopy analysis of silver-stained chromosomes (Figure 5.2C). This suggests that AtASY3 is essential to associate AtASY1 with the chromosome axes but is not essential for the formation of the axes (Ferdous et al, 2012). Lastly, AtSYN1 is a α-kleisin and is thought to be a component of the cohesin ring complex. Sister chromatid cohesion is established at the time of DNA replication during the pre-meiotic S-phase. AtSYN1 shares functional similarities with Rec8 in budding yeast. Several studies suggest that Rec8 is required for axis formation (Panizza et al, 2011). In *Arabidopsis thaliana*, AtSYN1 was localised on the chromosome axes from G2 and the loading of the axis component AtASY3 on the chromatin was altered in *Atsyn1* T-DNA insertion line (Ferdous et al, 2012). Therefore, the localisation of AtASY1 was investigated in *Atsyn1* mutant. During mid-prophase I, AtASY1 signal formed foci and long stretches lacking the domainal organisation of alternative high- and low-abundant domains. AtASY1 signal was

consistently observed with an abnormally thick and distorted appearance. This could represent an accumulation of AtASY1, at regions where the axial element was formed. However, AtASY1 failed to properly organise on the residual axes in the absence of AtSYN1. AtASY1 signal was found co-localising with AtSMC3 and AtASY3 signal (Figure 5.2D-F). The presence of aggregate components of the chromosome axes was previously reported in *rad21l/rec8* double mutant in mice (Llano et al, 2012).
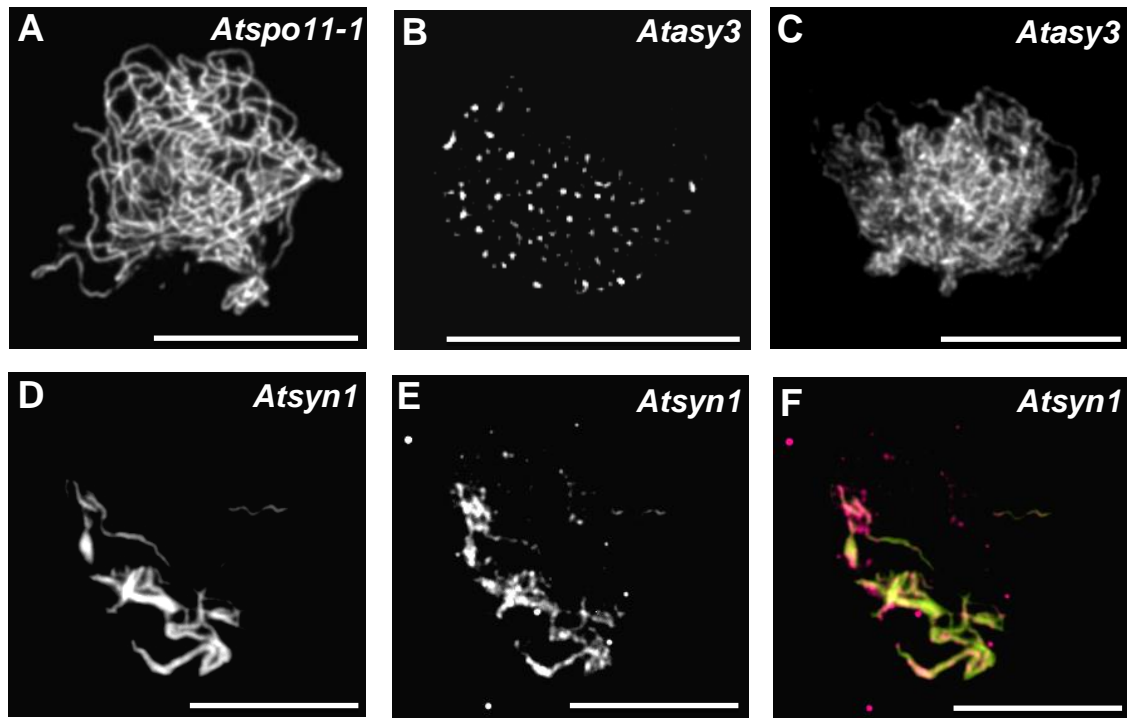
Figure 5.2. Immunolocalisation of chromosome axis proteins on *Atspo11-1* and chromosome axis mutants in *Arabidopsis*.

Immunolocalisation of AtASY1 (A,B,D; white) and AtSMC3 (C,E; white) on chromosome spread preparation of *Atspo11-1-4* (A), *Atasy3* (B-C) and *Atsyn1* (D-F) PMCs. (F) Merge image of AtASY1 (green) and AtSMC3 (magenta) localisation in *Atsyn1*. Scale bar = 10 μM.

5.3. AtPCH2 is involved in the remodelling of the chromosome axes on the synaptic regions

The initial characterisation of the orthologue of Pch2 in *Arabidopsis* was carried out by a former PhD student in the laboratory (Komsun Nuntasoontorn). AtPCH2 is involved in the partial depletion of AtASY1 from the synaptic region. In addition, the SC nucleated and started to elongate but failed to fully polymerise in *Atcph2* mutant. Interestingly, AtASY1 signal was found brighter on the synaptic regions compared to the unsynapsed regions (Nuntasoontorn and Franklin, unpublished). This differential signal intensity of AtASY1 is reminiscent to the differential signal intensity of the cohesin subunits and AtASY3 between synaptic and unsynapsed regions (described above). The biological significance of the difference in signal intensity is unknown. It is possible that the difference in signal intensity is a cytological representation of the close juxtaposition of the two homologue axes. However, it can not be excluded that the difference in the signal intensity resulted from a slower turnover or higher recruitment of proteins.

An antibody was generated against AtPCH2 protein. Immunolocalisation on chromosome spread preparation using an anti-AtPCH2 antibody showed numerous chromatin-associated foci from late S-phase to early zygotene in wild-type PMCs (Figure 5.3A-B). During mid-prophase I, AtPCH2 formed a brighter and more continuous signal along the SC. AtPCH2 signal was organised in domains of hyper and lower abundance (Figure 5.3C-H). However, immunolocalisation on chromosome spread preparation using the same antibody on all three *Atpch2* T-DNA insertion mutant lines revealed numerous foci associated with the chromatin at G2 and leptotene. The foci were slightly less intense than the foci observed in

wild-type PMCs (Figure 5.3I-K). The significance of the chromatin-associated foci observed in early prophase I of WT and *Atpch2* mutants is unclear. In contrast, no signal was detected on the stretches of SC during mid-prophase I in *Atpch2* mutants (data not shown). This suggests that the signal observed on the SC of wild-type nuclei is specific to AtPCH2 protein.

In *Arabidopsis,* the formation of the SC is dependent on the invasions of the 3' single-stranded DNA tails towards homologous chromosomes. To address the basis for the polymerisation of AtPCH2 during mid-prophase I, dual immunolocalisation using anti-AtPCH2 and anti-AtZYP1 antibodies was carried out on several T-DNA insertion mutant lines. In *Atspo11-1* mutant, DSB were not formed and AtZYP1 was rarely found associated with the chromatin. AtPCH2 formed polycomplexes that were sometimes associated with AtZYP1 foci (Figure 5.4D). In *Atdmc1* mutant, DSBs were formed and repaired using the sister chromatids. AtZYP1 and AtPCH2 signals were co-localising forming foci and short streches (Figure 5.4E-G). In *Atasy1* and *Atasy3* mutants, the formation of the SC was defective. Ferdous *et al.* (2012) reported that the few stretches of AtZYP1 were associated with AtMLH1 foci and were marking the sites of future COs in *Atasy3* mutants. The AtPCH2 signal was found co-localising with AtZYP1 signal in *Atasy1* and *Atasy3* mutants (Figure 5.4H-M). Interestingly, AtZYP1 has a tendency to self-interact and forms polycomplexes when early recombination events are defective. In both *Atasy1* and *Atasy3* mutant lines, AtPCH2 was found associated with AtZYP1 polycomplexes. This suggests that the two proteins can associate in a higher order structure independently of factors involved in the homologous recombination pathway. Lastly, D-loop structures are presumably formed but not stabilised in an *Atmsh5* mutant, leading to a defect in the

formation of inter-homologue COs. It seems likely that the formation of D-loops is sufficient to ensure proper SC formation (Higgins et al, 2008b). AtPCH2 and AtZYP1 formed a continuous signal in *Atmsh5* PMCs (Figure 5.4N-P). Overall, immunolocalisation using both anti-AtZYP1 and anti-AtPCH2 antibodies suggest that the polymerisation of AtPCH2 occurs concomitantly with the polymerisation of the SC.

Recently, Chen *et al.* (2014) suggested that Pch2 was required for the depletion of Hop1 from the SIS before SC nucleates. In *Arabidopsis* the nascent SC was often found co-localising with a bright AtASY1 signal. In contrast, AtASY1 was found partially depleted when the SC was further elongating (Figure 5.5A-C). This suggests that either additional factors are required to deplete AtASY1 from the SC or that there is a surveillance mechanism ensuring that the SC is properly polymerising between homologous chromosomes before remodelling the chromosome axes and further elongation of the SC. In the scenario where AtPCH2 is directly involved in the depletion of AtASY1 from the synaptic regions, AtPCH2 would physically interact/form a complex with AtASY1 and the hyper-abundant domains of AtPCH2 would be co-localising with the hyper-abundant domains of AtASY1 on the nascent SC. Osman and Franklin (unpublished) reported that PCH2 was co-immunoprecipitated using an anti-AtASY1 antibody from Brassica meiocyte extracts. However, yeast two-hybrid analysis has so far failed to detect a direct physical interaction between the two proteins (data not shown). Dual immunolocalisation using anti-AtASY1 and anti-AtPCH2 antibodies showed that the hyper-abundant domains of AtPCH2 mostly co-localise with the hyper-abundant domains of AtASY1 on the synaptic and unsynaptic regions. Hence, this supports the model where AtPCH2 would localise on

the synaptic regions to remodel the chromosome axes by partially depleting AtASY1 (Figure 5.5D-F).
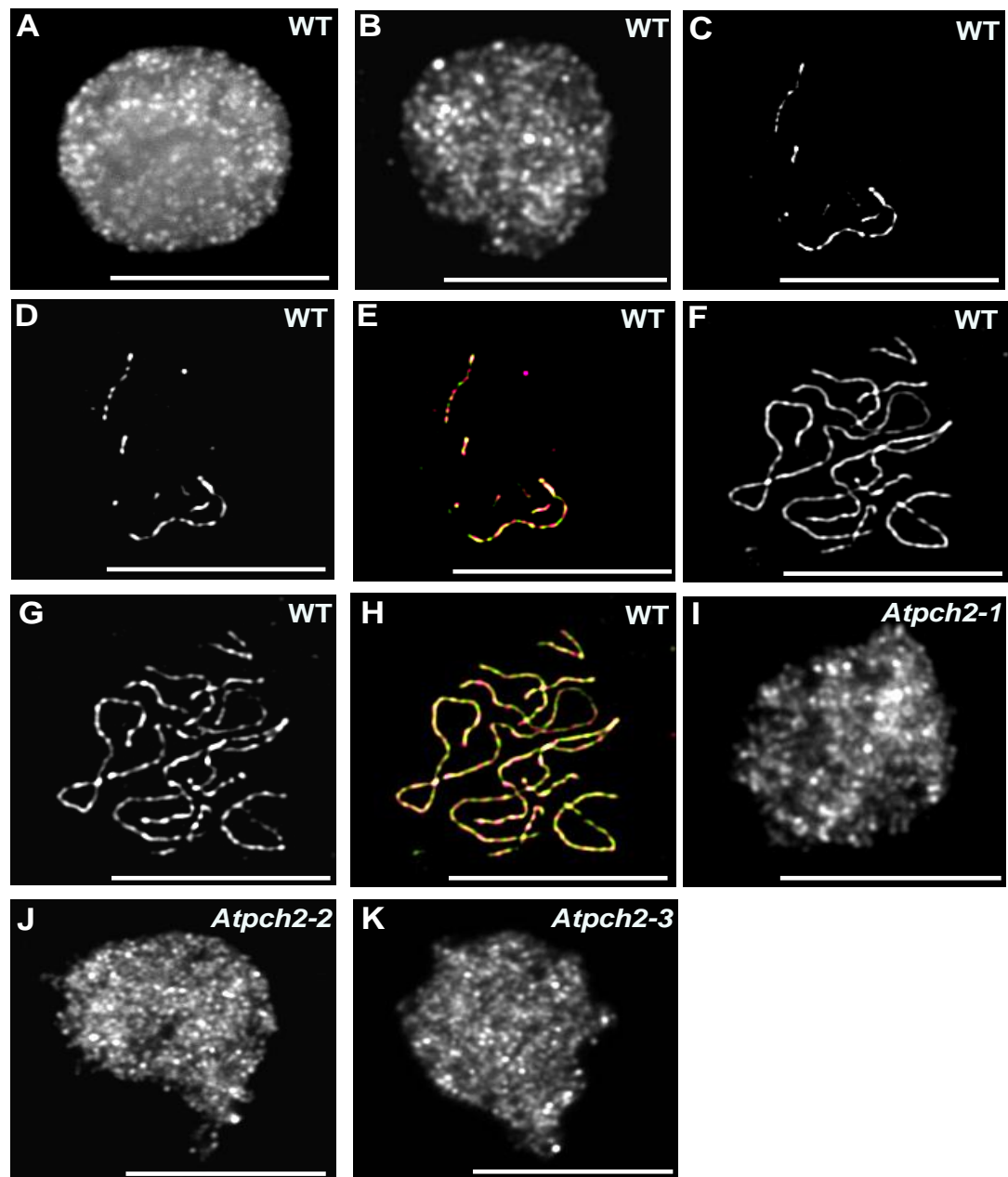
Figure 5.3. Immunolocalisation of AtPCH2.

(A-B) Immunolocalisation of AtPCH2 on chromosome spread preparation of wild-type PMCs. (A) G2, (B) leptotene. (C-H) Dual immunolocalisation of AtPCH2 (D,E,G,H) and AtZYP1 (C,E,F,H) on chromosome spread preparation of wild-type PMCs. (C-E) zygotene, (F-H) pachytene. (E,H) Merge image of AtZYP1 (green) and AtPCH2 (magenta). (I-K) Immunolocalisation of AtPCH2 on chromosome spread preparation of *Atpch2* mutant PMCs. Scale bar = 10 μM.
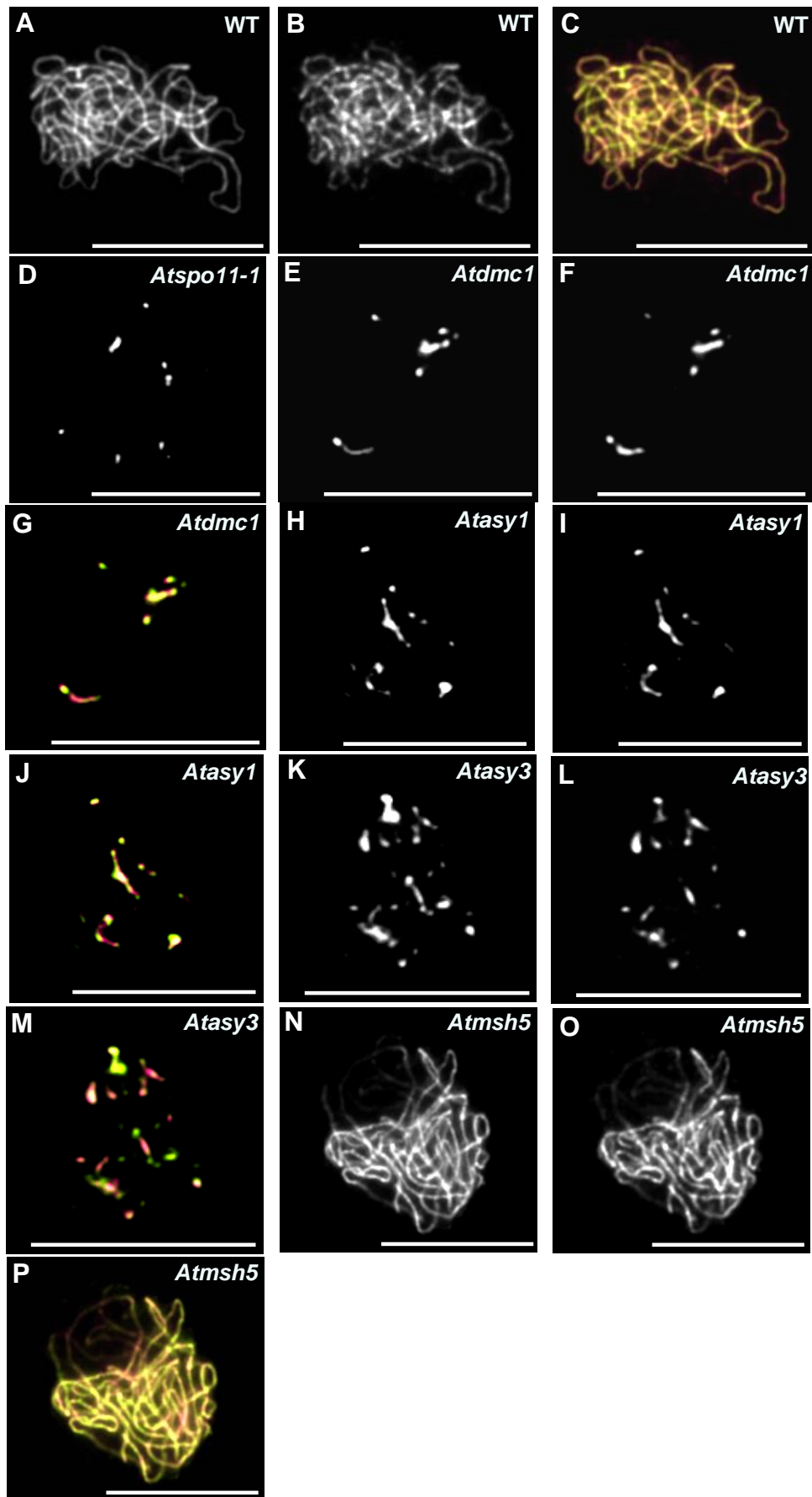
Figure 5.4. Immunolocalisation of AtPCH2 in various mutants defective for homologous recombination.

Immunolocalisation of AtZYP1 (A,C,E,G,H,J,K,M,N,P) and AtPCH2 (B,C,D,F,G,I,J,L,M,O,P) on chromosome spread preparation of wild-type (A-C), *Atspo11-1-4* (D), *Atdmc1* (E-G), *Atasy1* (H-J), *Atasy3* (K-M) and *Atmsh5* (N-P) of mid-prophase I nuclei. (C,G,J,M,P) Merge images of AtZYP1 (green) and AtPCH2 (magenta). Scale bar = 10 μM.
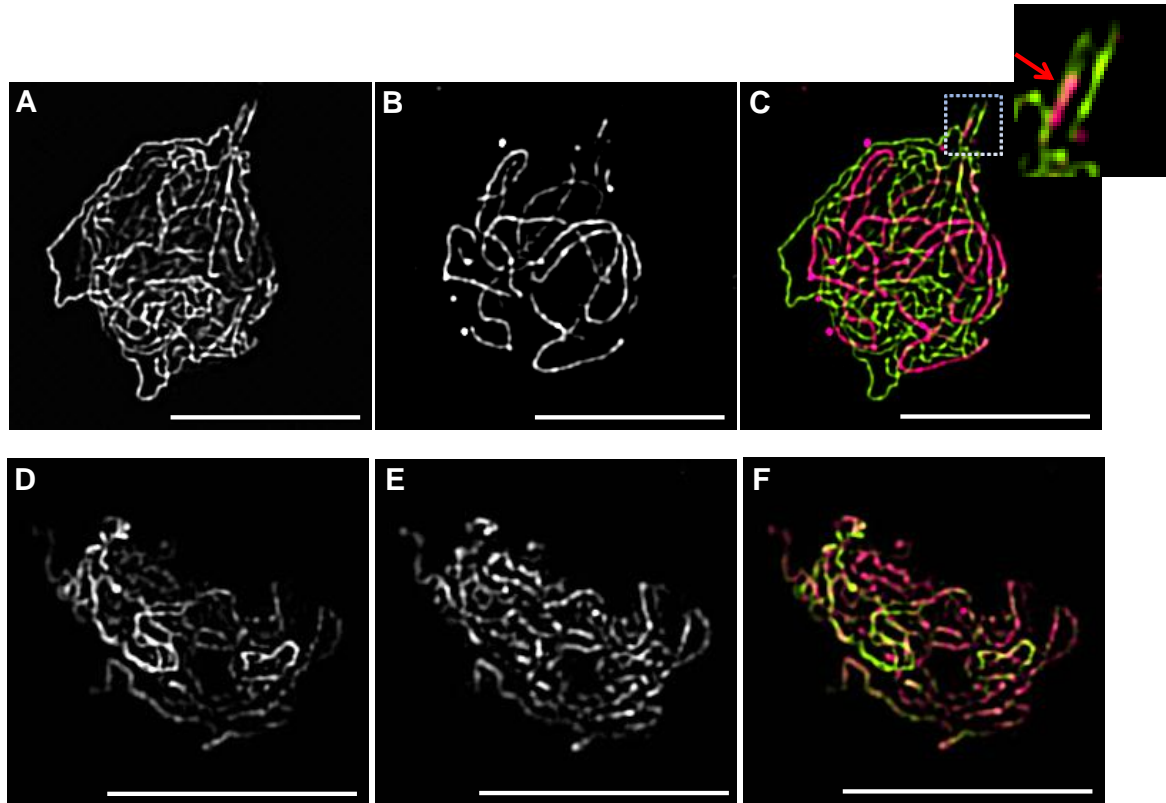
Figure 5.5. AtASY1 is progressively depleted from the synaptic regions at mid-prophase I.

(A-C) Dual immunolocalisation of AtASY1 (A,C green) and AtZYP1 (B,D, magenta) on chromosome spread preparation of a mid-prophase I wild-type nucleus. The red arrow shows AtASY1 signal persisting on the nascent short stretch of AtZYP1. (D-F) Dual immunolocalisation of AtASY1 (D,F, green) and AtPCH2 (E,F, magenta) on chromosome spread preparation of a mid-prophase I wild-type nucleus. Scale bar = 10 μM.

5.4. ASY1 is phosphorylated at several sites

Recent studies indicate that Pch2 regulates the phosphorylation status of Hop1 in budding yeast (Ho & Burgess, 2011; Lo et al, 2014). Pch2 is an evolutionary conserved protein and it is likely that AtPCH2 also modulates the phosphorylation status of AtASY1. Therefore, AtASY1 protein was analysed to determine whether AtASY1 is a phospho-modified protein. Immunoprecipitation using an anti-AtASY1 antibody on *Brassica oleracea* meiocyte extracts followed by mass spectrometry analysis revealed that BoASY1 was phosphorylated at several residues. 11 phospho-modified peptides were detected. Among them, some peptides had multiple phosphorylated residues. 5 phospho-modified [S/T]Q sites were identified, among them the residue T294 (Osman and Franklin, unpublished). The residue T294 is conserved and corresponds to residue threonine 295 in *Arabidopsis* and Hop1 T318 in budding yeast (Figure 5.6A). Carballo et al (2008) showed that Hop1 T318 phosphorylation is required for inter-homologue recombination.

To further investigate the degree of AtASY1 phosphorylation, a two dimensional gel electrophoresis was carried out on wild-type and *Atasy1 Arabidopsis* crude extract. An anti-AtASY1 antibody was used to detect the protein. However, no signal was detected. When the proteins from *Arabidopsis* crude extract were separated by their molecular weight only, AtASY1 was detected by western blot. *Arabidopsis* crude extract is relatively poor in meiotic proteins which renders biochemical study challenging. To overcome this limitation, *Brassica oleracea,* a close relative species to *Arabidopsis*, was chosen for biochemical analysis. Anthers with meiocytes at early prophase I were selected and proteins were extracted as described in Materials and Methods. Proteins were then

separated by their isoelectric point and by their molecular weight using a two dimensional gel electrophoresis. An anti-AtASY1 antibody was used to specifically visualise AtASY1 protein. Several dots were observed on two horizontal lanes (Figure 5.6B). The lane with the higher molecular weight corresponded to a molecular weight of 70 kDa (similar to the estimated molecular weight of ASY1) while the second lane corresponded to a molecular weight of 50 kDa. Between 9 and 11 spots were observed on the slow migrating lane of spots. The spots were brighter close to pH 5.6, with the most intense spot found at the extreme left side of the gel. BoASY1 has a predictive isoelectric point of 5.28. The brightest signal close to pH 5.6 likely corresponds to the non-phosphorylated form of AtASY1. In addition, the presence of several spots on the second dimensional gel suggests that BoASY1 was phosphorylated at multiple sites and was present in multiple phosphorylation states. On a one dimensional gel electrophoresis, ASY1 was detected at the predicted molecular weight of 70 kDa and at a lower molecular weight (55 kDa) from *Arabidopsis* and *Brassica oleracea* crude extracts (Figure 5.6C). This observation was consistently observed from different samples and the ratio between the two forms was variable. The fast migration band may represent a degradation product of the protein, although this has not been formally demonstrated. However, the two forms of ASY1 that were detected by one dimensional gel electrophoresis are consistent with the two lanes of spots observed on the two dimensional gel electrophoresis. Interestingly, the fast migrating lane of spots has the spots at a similar position on the horizontal axis as the slow migrating lane of spots. This suggests that the truncated AtASY1 protein was present in a similar phosphorylation status as the full length BoASY1 protein (Figure 5.6B). However, it was not possible to confirm that the signal detected by the anti-AtASY1 antibody was BoASY1 because of the lack of a *Boasy1* mutant.
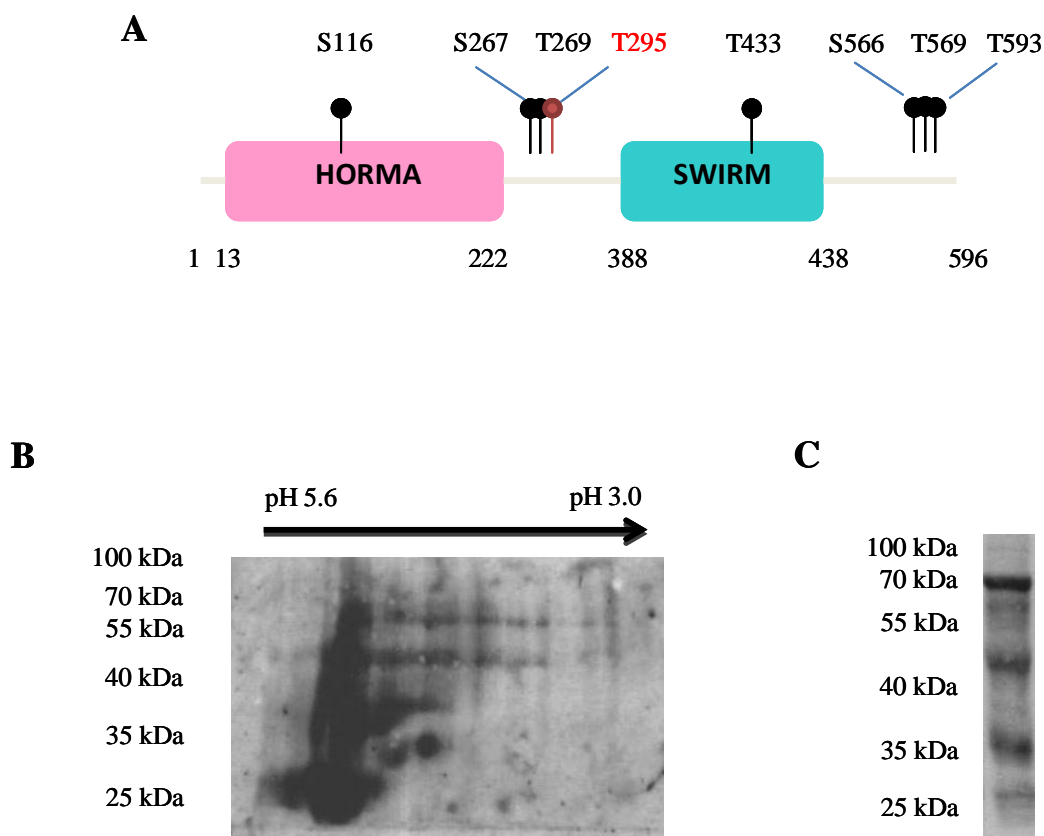
Figure 5.6. BoASY1 is phosphorylated at multiple sites

(A) Schematic representation of AtASY1 with the 8 [S/T]Q sites. The phospho-site that has been mutated and corresponding to residue threonine 295 is represented in red.

(B) 2 dimensional gel electrophoresis using an anti-AtASY1 antibody on *Brassica oleracea* crude extract.

(C) One dimensional gel electrophoresis using an anti-AtASY1 antibody on *Brassica oleracea* crude extract.

5.5. AtASY1-T295A mutation leads to reduced fertility and a reduced number of inter-homologue COs in *Arabidopsis*

To investigate the biological significance of AtASY1 T295 phosphorylation, a single point mutation was introduced in the coding sequence of *AtASY1* to substitute the codon ACA by GCA at position 883. This mutation in the nucleotide sequence generates a substitution of the residue threonine by an alanine at the position 295 of AtASY1 (referred as *AtASY1-TA*). The substitution of this residue mimics the absence of phosphorylation of the protein at this phospho-site. The mutated coding sequence of *AtASY1* was cloned into the Early Gate vector pEG100 and the expression of the transgene was driven by 35S promoter. This construct was used to transform plants heterozygous for the T-DNA insertion in *AtASY1* (this work was done by Eduardo Corredor). Four transgenic plants homozygous for the T-DNA insertion in *AtASY1* and expressing *AtASY1-TA* were identified (this work was done by Adriana Machlicova). The molecular characterisation of all four lines confirmed the presence of the mutation T295A at the TQ site within AtASY1 (this work was done by Maheen Ferdous).

All four independent transgenic plants were genotyped. DNA from wild-type and *Atasy1* plants was extracted and used as control. All four transgenic plants were homozygous for the T-DNA insertion in *AtASY1* (Figure 5.7A,B) and had the transgene *AtASY1-TA* (Figure 5.7C). These plants will be referred as *Atasy1::AtASY1-TA 1, Atasy1::AtASY1-TA 2, Atasy1::AtASY1-TA 3* and *Atasy1::AtASY1-TA 4. Atasy1::AtASY1-TA 1-4* plants showed normal vegetative growth but fertility was greatly reduced compared to wild-type plants (Figure 5.8A-E,G-K). The fertility was analysed by measuring the length of the siliques

and scoring the number of seeds per silique. *Atasy1* plant was used as a control. Analysis of fertility revealed that the fertility of *Atasy1::AtASY1-TA 1-4* was drastically reduced at a level similar to *Atasy1* fertility (Figure 5.8B-L and Figure 5.9A,B). The reduced fertility observed in *Atasy1::AtASY1-TA 1-4* suggests that meiosis may be affected as in *Atasy1*. To confirm this, DAPI-stained chromosome spread preparations from wild-type, *Atasy1::AtASY1-TA 1-4* and *Atasy1* PMCs were examined by fluorescence microscopy. In wild-type PMCs, chromosomes began to undergo a gradual condensation of the pericentromeric heterochromatin at leptotene (Figure 5.10A). At the onset of zygotene, the chromosomes were more condensed and pairing between homologous chromosomes was apparent. At pachytene, homologous chromosomes were fully synapsed and chromosomes were shorter and tightly associated (Figure 5.10D). Homologous recombination resulted in the formation of inter-homologue COs and the formation of five bivalents at diakinesis and metaphase I (Figure 5.10G). The segregation of chromosomes towards opposite poles of the cells at anaphase I and anaphase II resulted in the formation of four haploid gametes at tetrad (Figure 5.10J,M). In *Atasy1::AtASY1-TA1-4*, chromosome behaviour was apparently similar to wild-type in G2 and through early prophase I (Figure 5.10B and Figure 5.11A-C). However, no pachytene stage was observed and the chromosomes failed to synapse during mid-prophase I (Figure 5.10E and Figure 5.11D-F). By metaphase I, the presence of univalent chromosomes was apparent suggesting that a proportion of the chromosomes failed to form the obligate CO with their homologue (Figure 5.10H and Figure 5.11G-I). The absence of chiasma on some chromosomes led to their mis-segregation at anaphase I and resulted in the formation of aneuploid polyads (Figure 5.10K,N and Figure 5.11J-O). DAPI-stained chromosome spread preparation of *Atasy1* PMCs showed that homologous chromosomes failed to pair, recombine and synapse during prophase I (Figure 5.10C,F,I).

In addition, mis-segregation of chromosomes and aneuploid gametes at tetrad were observed (Figure 5.10L,O). The meiotic defect of *Atasy1* reported in this study and previously described by Caryl *et al.* (2000) were indistinguishable to the meiotic defected observed in *Atasy1::AtASY1-TA1-4* (Figure 5.10 and Figure 5.11).

Since the four *Atasy1::AtASY1-TA* lines exhibited the same cytological phenotype, *Atasy1::AtASY1-TA-1* plant was used for further analysis. The presence of univalents at metaphase I of *Atasy1::AtASY1-TA* PMCs suggests that not all homologous chromosomes formed the obligate CO. To quantify the number of COs formed per nucleus, a survey of 50 meiocytes at metaphase I was carried out in wild-type and *Atasy1::AtASY1-TA-1* to determine the mean number of chiasma, which is the cytological representation of a CO, per nucleus. In wild-type PMCs, the number of chiasma ranged between 8 and 12 per nuclei with a mean chiasma frequency of 9.81 (Figure 5.12A). In contrast, the mean chiasma frequency was significantly reduced in *Atasy1::AtASY1-TA-1*. The number of chiasmata was variable between nuclei, ranging between 0 and 5 chiasmata, with an overall mean chiasma frequency of 2.36 (Figure 5.12B). Since the meiotic defects observed on DAPI-stained chromosome spread preparation of *Atasy1* and *Atasy1::AtASY1-TA-1* PMCs were indistinguishable, the mean chiasma frequency was compared between the two mutant lines. In *Atasy1*, the number of chiasmata was found to be between 0 and 5 with an overall mean chiasma frequency of 2.22 per nucleus (Figure 5.12C). The overall mean chiasma frequency was not significantly different between the two mutant lines (n=50; P=0.642) suggesting that the phosphorylation of AtASY1 at residue threonine 295 is essential for the function of the protein in inter-homologue CO formation.
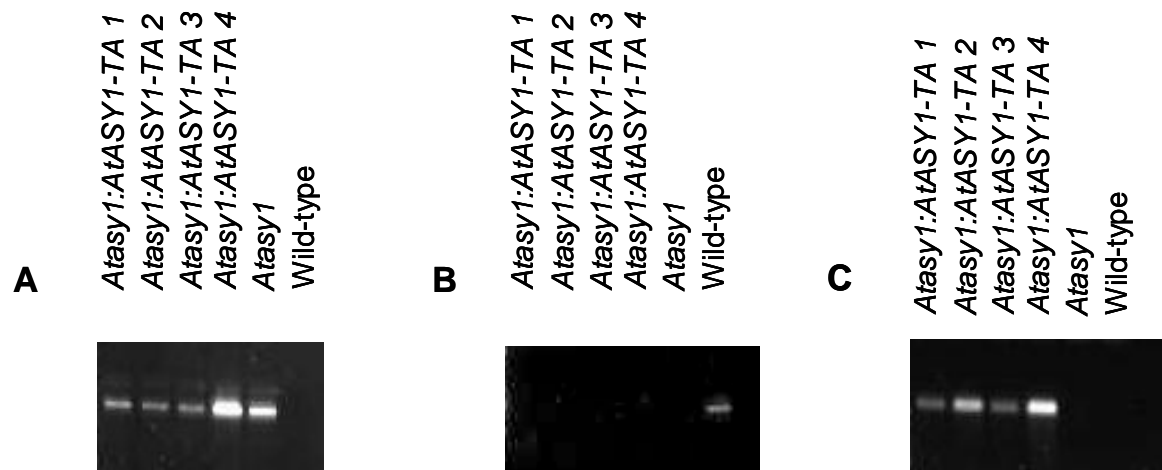
Figure 5.7. Genotyping of *Atasy1:AtASY1-TA* transgenic plants

(A) Amplification of the region located between the T-DNA insertion and *AtASY1* genomic locus

(B) Amplification of the wild-type *AtASY1* genomic locus

(C) Amplification of *AtASY1-TA* transgene

Extracted DNA from wild-type and *Atasy1* plants were used as controls
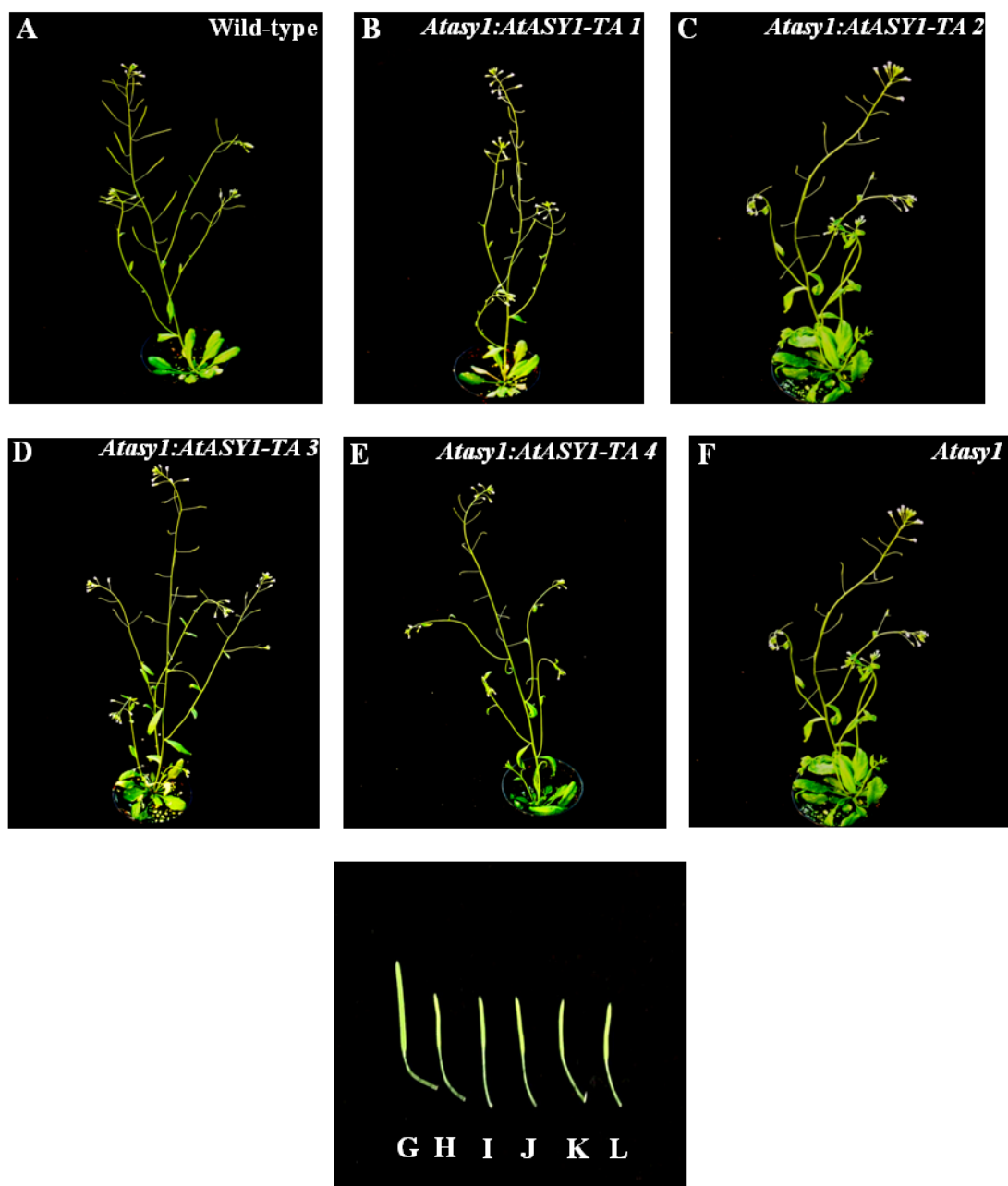
Figure 5.8. *Atasy1:AtASY1-TA* mutant phenotype

Atasy1:AtASY1-TA 1 (B,H), *Atasy1:AtASY1-TA 2* (C,I), *Atasy1:AtASY1-TA 3* (D,J) and *Atasy1 :AtASY1-TA 4* (E,K) had normal vegetative growth but fertility was reduced. Wild-type (A,G) and *Atasy1* (F,L) plants were used for comparison .

A

B
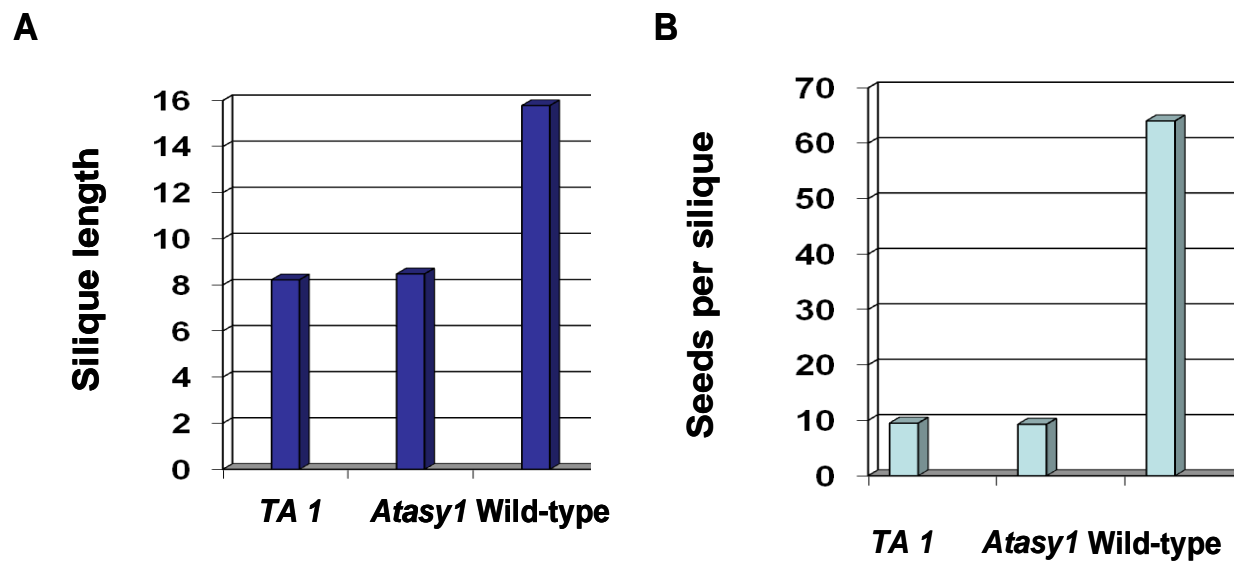
Figure 5.9. Reduced fertility in *Atasy1:AtASY1-TA 1* and *Atasy1* plants

The silique length (A) and the number of seeds per silique (B) were similarly reduced in *Atasy1* and *Atasy1:AtASY1-TA 1* (*TA 1*) plants compared to wild-type plants.
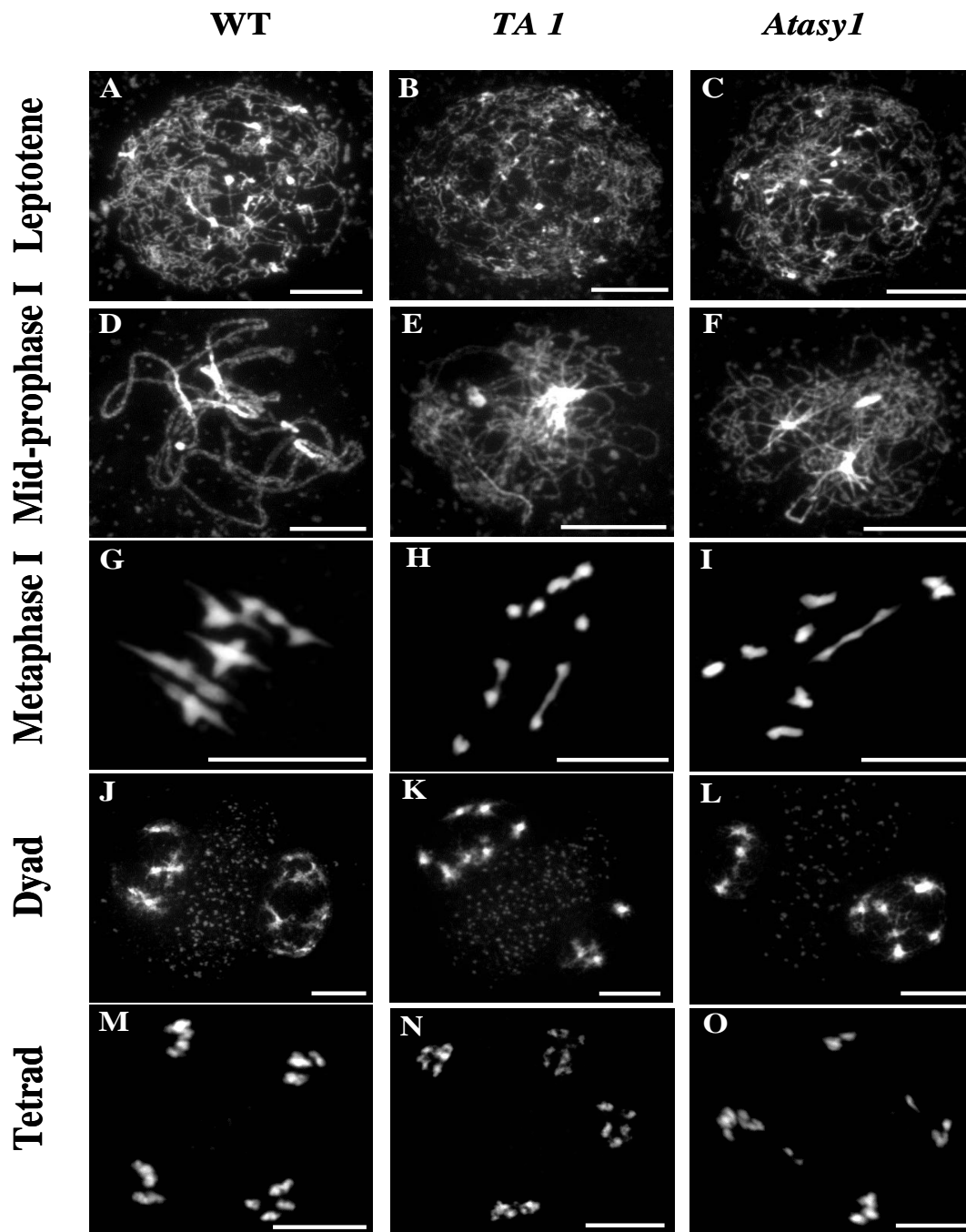
Figure 5.10. Meiotic stages from wild-type, *Atasy1 :AtASY1-TA 1* **and** *Atasy1* **PMCs**

DAPI-stained chromosome spread of wild-type (A,D,G,J,M), *Atasy1 :AtASY1-TA 1* (*TA 1*) (B,E,H,K,N) and *Atasy1* (C,F,I,L,O) PMCs. Leptotene (A,B,C), mid-prophase I (D,E,F), metaphase I (G,H,I), dyad (J,K,L) and tetrad (M,N,O). Nuclei were counterstained with DAPI (blue). Scale bar = 10 μM.
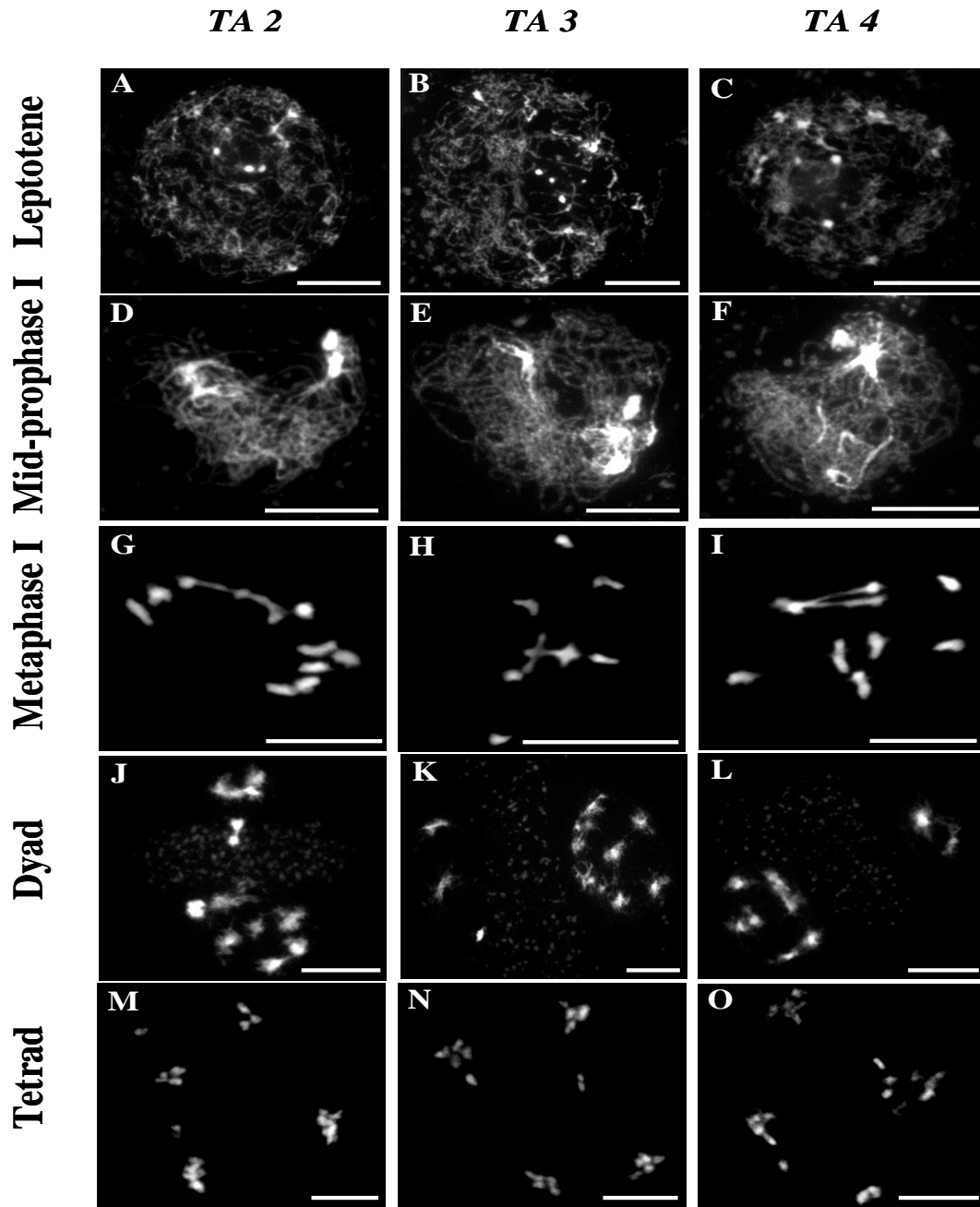
Figure 5.11. Meiotic stages from *Atasy1 :AtASY1-TA 2*, *Atasy1 :AtASY1-TA 3* and *Atasy1 :AtASY1 TA-4* PMCs

DAPI-stained chromosome spread of *Atasy1 :AtASY1 TA-2* (*TA 2*) (A,D,G,J,M), *Atasy1 :AtASY1-TA 3* (*TA 3*) (B,E,H,K,N) and *Atasy1 :AtASY1 TA-4* (*TA 4*) (C,F,I,L,O) PMCs. Leptotene (A,B,C), mid-prophase I (D,E,F), metaphase I (G,H,I), dyad (J,K,L) and tetrad (M,N,O). Nuclei were counterstained with DAPI (blue). Scale bar = 10 μM.
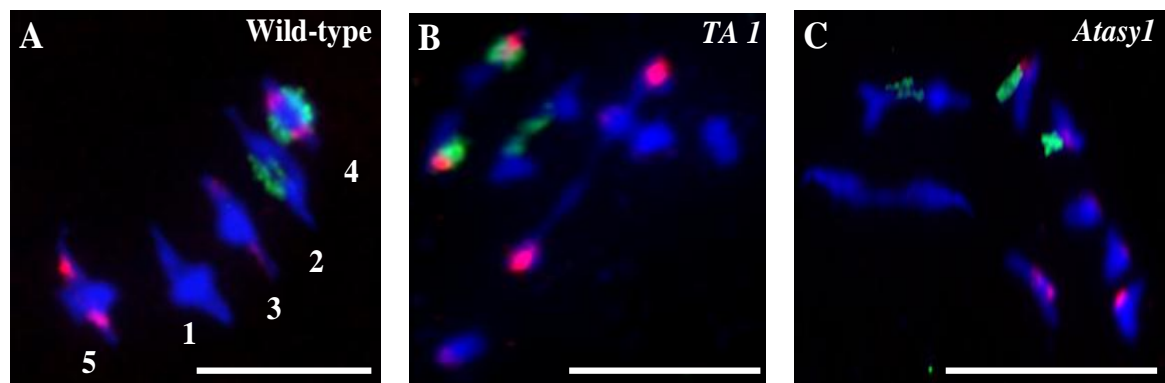
Figure 5.12. Inter-homologue CO formation is reduced in *Atasy1 :AtASY1-TA 1*

DAPI-stained chromosome spread of wild-type (A), *Atasy1 :AtASY1-TA 1* (*TA 1*) (B) and *Atasy1* (C) PMCs. Metaphase I were labelled with 45S (green) and 5S (red) ribosomal DNA. The five bivalents were identified with the fluorescent probes and annotated on (A). Nuclei were counterstained with DAPI (blue). Scale bar = 10 μM.

5.6. Synapsis is defective in *Atasy1::AtASY1-TA*

Since DAPI-stained chromosome spread preparation of *Atasy1::AtASY1-TA1-4* PMCs showed that the chromosomes failed to synapse, the formation of the SC was investigated. AtZYP1a and AtZYP1b are two closely related proteins forming the SC transverse filament in *Arabidopsis* (Higgins et al, 2005). AtZYP1a and AtZYP1b can be detected on the synaptic regions of chromosome spread preparation of wild-type PMCs by using an anti-AtZYP1 antibody that recognises AtZYP1a and AtZYP1b. In wild-type PMCs, AtZYP1 was first detected at zygotene. AtZYP1 signal formed foci and short stretches as mentioned in Chapter 4. At pachytene, when the homologous chromosomes were fully synapsed, AtZYP1 formed a continuous signal (Figure 5.13A). In *Atasy1::AtASY1-TA-1*, AtZYP1 formed foci and short stretched but failed to form a continuous signal at mid-prophase I (Figure 5.13B). Some foci were found thicker in appearance and could represent polycomplexes of AtZYP1. Cytological analysis of AtZYP1 revealed a similar polymerisation defect for the three other transgenic lines *Atasy1::AtASY1-TA 2-4* (Figure 5.13C-E). The presence and the length of AtZYP1 stretches were variable between nuclei. The variation in AtZYP1 polymerisation likely correlated with the variation in the number of residual COs formed in *Atasy1::AtASY1-TA 1-4*. The defect in SC formation observed in *Atasy1::AtASY1-TA* is consistent with the defect in chromosome pairing observed on DAPI-stained chromosome spread preparation of *Atasy1::AtASY1-TA 1-4* PMCs. SC formation was also analysed in *Atasy1*. Similarly to *Atasy1::AtASY1-TA 1-4* PMCs, AtZYP1 failed to fully polymerise and AtZYP1 signal formed foci and short stretches of variable length (Figure 5.13F).
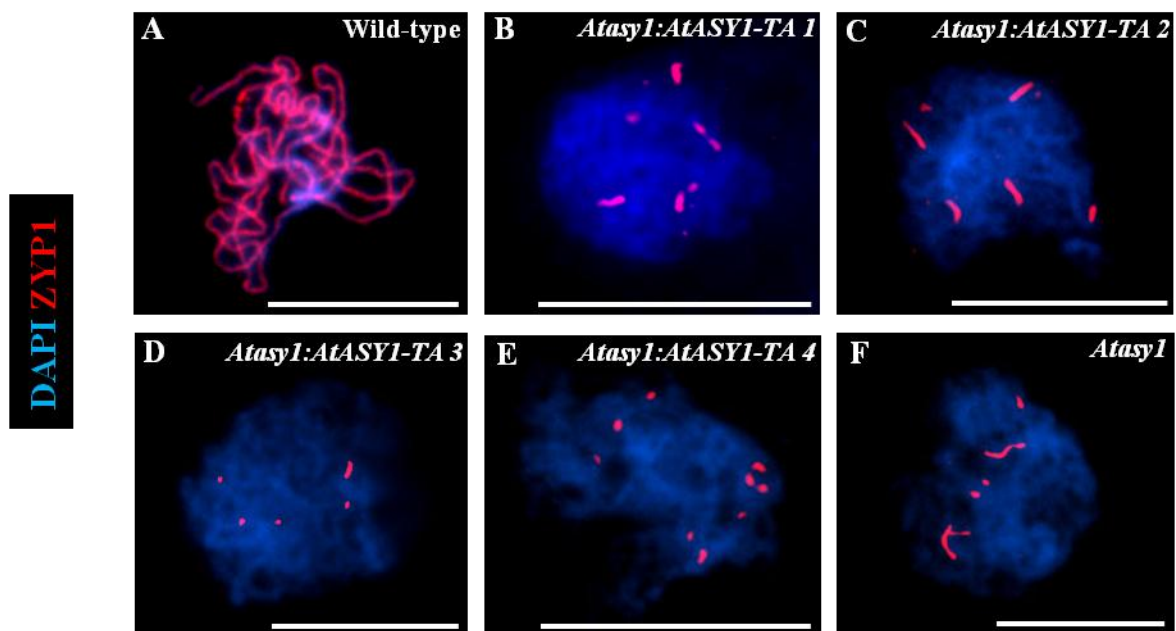
Figure 5.13. AtZYP1 polymerisation is defective in *Atasy1:AtASY1-TA*

Immunolocalisation of AtZYP1 at mid-prophase I of wild-type (A), *Atasy1:AtASY1-TA 1* (B), *Atasy1:AtASY1-TA 2* (C), *Atasy1:AtASY1-TA 3* (D), *Atasy1:AtASY1-TA 4* (E) and *Atasy1* (F) nuclei. Nuclei were counterstained with DAPI (blue). Scale bar = 10 μM.

5.7. AtASY1-TA fails to correctly associate with the chromosome axes

In *Atasy1::AtASY1-TA* PMCs, the majority of the chromosomes failed to form the obligate CO resulting in the presence of univalent at metaphase I and non-disjunction of chromosomes at anaphase I. A similar defect in homologous recombination was reported for *hop1* and *hop1 T318A* mutant (Carballo et al, 2008). To address the basis for the reduction in inter-homologue CO formation, the localisation of AtASY1 was studied by immunocytochemistry analysis on chromosome spread preparation of wild-type and *Atasy1::AtASY1-TA 1* PMCs using an anti-AtASY1 antibody. In wild-type PMCs, AtASY1 formed numerous chromatin-associated foci during early G2. AtASY1 signal progressively elongated during late G2 to form a continuous signal associated with the underlying chromosome axes by leptotene (Figure 5.14A,B). The distribution of AtASY1 was not evenly distributed along the chromosome axes and AtASY1 was organised in domains of hyper and lower abundance.

In *Atasy1:AtASY1-TA 1* PMCs, AtASY1 signal formed numerous chromatin-associated foci at G2. The localisation of AtASY1 was indistinguishable from wild-type. However, AtASY1 appeared more diffuse and less continuous at the onset of leptotene in *Atasy1:AtASY1-TA 1* PMCs (Figure 5.14C,D). Dual immunolocalisation of AtASY1 and AtSMC3 showed that AtASY1 signal was mostly not overlapping with AtSMC3 signal. AtASY1 signal was found rather adjacent to AtSMC3 signal. A similar abnormal localisation of AtASY1 was observed for *Atasy1:AtASY1-TA 2* and *Atasy1:AtASY1-TA -3* PMCs (Figure 5.14E,F),. However, the signal was not diffuse for these 2 lines. The diffuseness observed in *Atasy1:AtASY1-TA 1* could result from a difference in gene

expression between the mutant lines. No AtASY1 signal was detected in *Atasy1:AtASY1-TA 4* (Figure 5.14G). After a few generations of growth, the transgene can become silence which could explain the absence of AtASY1 detection in *Atasy1:AtASY1-TA 4*. As a negative control, immunolocalisation using an anti-AtASY1 antibody confirmed that no signal was observed in *Atasy1* mutant (Figure 5.14H). The abnormal localisation of AtASY1 with the substitution T295A results in the defect in inter-homologue CO formation observed on DAPI-stained chromosome spread preparation of PMCs.
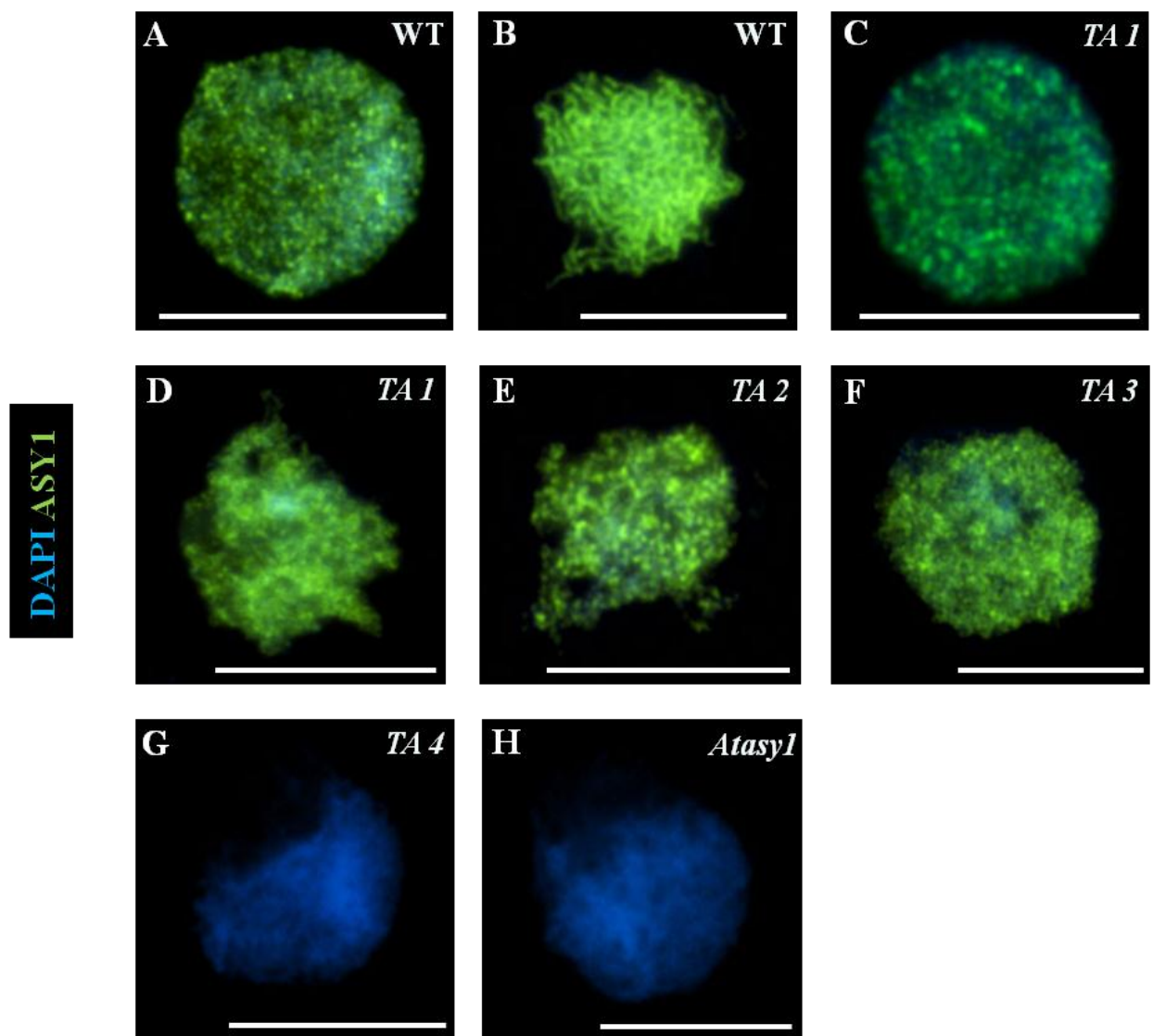
Figure 5.14. Dual immunolocalisation of AtASY1 and AtSMC3

Immunolocalisation of AtASY1 (green) of G2 nuclei from wild-type (A) and *Atasy1:AtASY1-TA 1* (C). Immunolocalisation of AtASY1 (green) of mid-prophase I nuclei from wild-type (B), *Atasy1:AtASY1-TA 1* (D), *Atasy1:AtASY1-TA 2* (E), *Atasy1:AtASY1-TA 3* (F), *Atasy1:AtASY1-TA 4* (H) and *Atasy1* (H). Nuclei were counterstained with DAPI (blue). Scale bar = 10 μM.

5.8. AtASY1 T295 is phosphorylated along the chromosome axes during early prophase I

To investigate the spatio-temporal localisation of AtASY1 T295 phosphorylation, an antibody raised against AtASY1 T295 phosphorylation (AtASY1 T295p) was generated. Dual immunolocalisation of AtASY1 T295p and AtASY1 was carried out on chromosome spread preparation of *Brassica oleracea* and *Arabidopsis thaliana* PMCs. AtASY1 T295p signal had a similar localisation pattern between the two organisms. In the transition from S-phase/G2, ASY1 formed numerous faint foci that were associated with the chromatin (Figure 5.15A). However, no ASY1 T295p signal was detected at this stage (Figure 5.15B). At mid-G2, when ASY1 signal formed short stretches and numerous foci, ASY1 T295p formed numerous foci (Figure 5.15C-D). The number of ASY1 foci outnumbered the number of ASY1 T295p foci. At the onset of leptotene, ASY1 and ASY1 T295p formed an overlapping continuous signal (Figure 5.15E-G). At mid-prophase I, ASY1 T295p signal was faint and punctuate on the synaptic regions in Brassica. The ASY1 T295p signal was not always differentiable from the background noise (data not shown). In *Arabidopsis*, AtASY1 T295p signal had a similar pattern as ASY1 T295p signal described in Brassica (Figure 5.15H). At zygotene, AtASY1 T295p signal was faint but continuous on the synaptic regions in *Arabidopsis* (Figure 5.15I). It was found that AtASY1 T295p signal was affected when an anti-AtASY1 T295p antibody was used with an anti-AtASY1 antibody during the immunocytochemistry procedure on *Arabidopsis* PMCs. Therefore, an anti-AtSMC3 antibody was used in conjunction with an anti-AtASY1 T295p antibody for all subsequent experiments. The specificity of the anti-AtASY1 T295p antibody was tested

by immunolocalisation on *Atasy1:AtASY1-TA 1*. No signal was detected confirming the specificity of the antibody (Figure 5.15J).
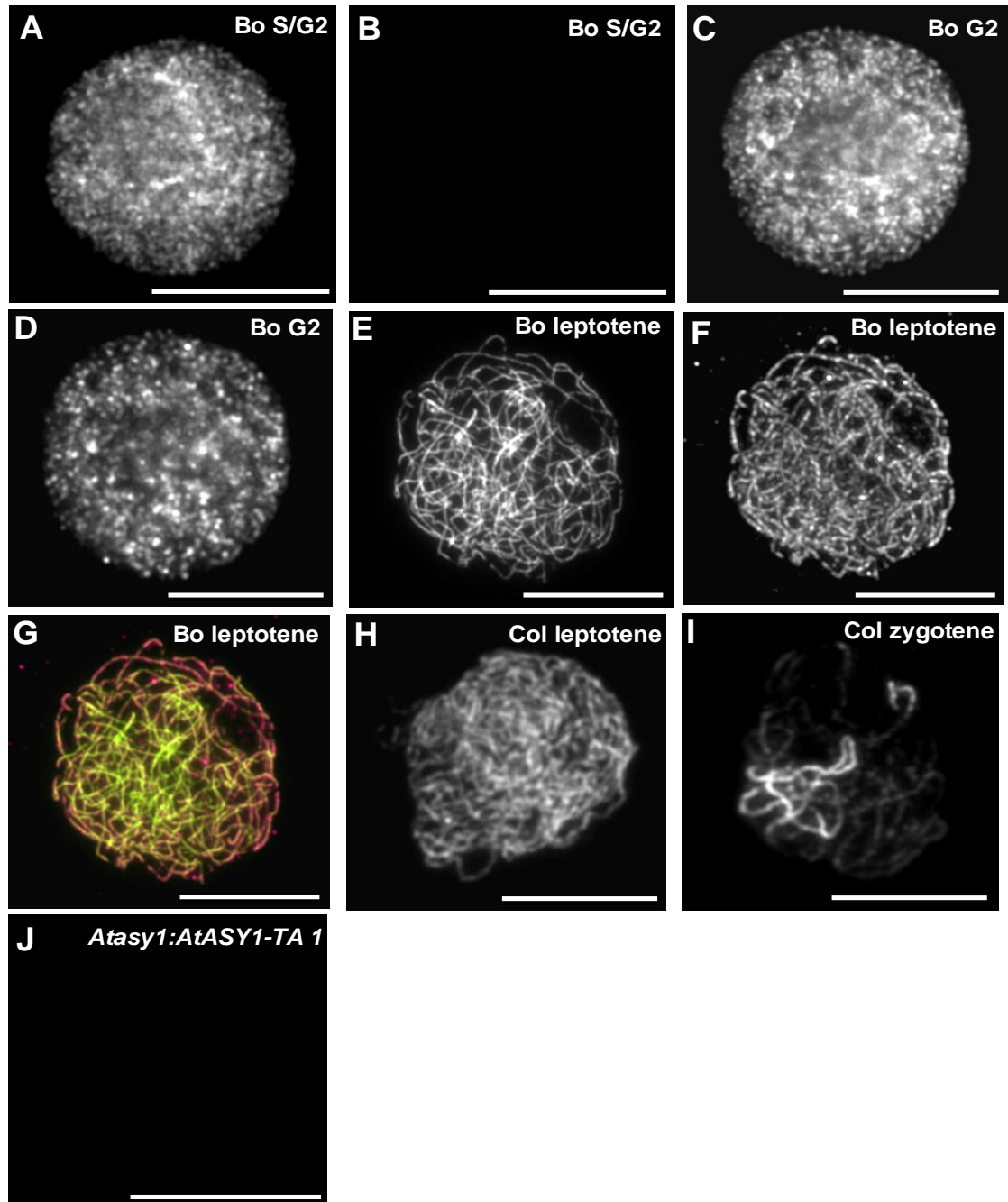
Figure 5.15. ASY1 T294/T295 is phosphorylated from mid-G2 onwards in *Brassica oleracea* and *Arabidopsis*.

Immunolocalisation of AtASY1 (A,C,E,G) and AtASY1 T294/T295 (B,D,F-J) in *Brassica oleracea* (A-G), wild-type *Arabidopsis* (H,I) and *Atasy1:AtASY1-TA1* (J) PMCs. (A-B) late S-phase/early G2, (C-D) G2, (E-H,J) leptotene, (I) zygotene, (J) leptotene. (G) Merge image of ASY1 (green) and AtASY1 T294 (magenta). Scale bar = 10 μM.

5.9. AtASY1 T295 is phosphorylated in response to the formation of DSBs in a pathway dependent on AtATM/AtATR.

The phosphorylation of Hop1 and HORMAD1/HORMAD2 is dependent on the formation of DSBs (Carballo et al, 2008; Fukuda et al, 2012). Immunolocalisation of AtASY1 T295p was carried out in *Atspo11-1* mutant. In this mutant, the formation of DSBs was abolished. The signal intensity of AtASY1 T295p was significantly reduced in *Atspo11-1* compared to wild-type PMCs. To quantify the degree of AtASY1 T295 phosphorylation, images were captured as Z-stacks of 10 sections of 0.1 μm each. The maximum intensity projection of AtASY1 T295p for each nucleus was generated and the signal intensity was calculated using imageJ. The mean maximum intensity projection of AtASY1 T295p from 15 wild-type nuclei was normalised to 1. Using this approach, the degree of AtASY1 T295 phosphorylation was estimated to be reduced to 40.3 % the wild-type level in *Atspo11-1* PMCs (n=15, P=3.10^{-7}) (Figure 5.16A,B,F). In yeast, Hop1 T318 is phosphorylated by Mec1/Tel1 in response to the formation of DSBs. To analyse the role of AtATM/AtATR in the phosphorylation of AtASY1 T295, immunolocalisation of AtASY1 T295p was carried out in *AtatmAtatr* double mutant. Using the same approach as previously described, the degree of AtASY1 T295 phosphorylation was found to be reduced to 31.4 % the wild-type level in *Atatm/Atatr* double mutant (n=15, P=5.10^{-6}) (Figure 5.16A,C,F). In contrast, the signal intensity of AtASY1 T295 phosphorylation was not significantly reduced in *Atatm* mutant (n=15, P=0.26) and *Atatr* mutant (n=15, P=0.52) (Figure 5.16A,D,E,F). Although the signal intensity of AtASY1 T295p was reduced in both *Atspo11-1* and *Atatm/Atatr* double mutant, AtASY1 T295p formed a continuous signal along the underlying axes as

observed when the exposure time for capturing the images was increased (Figure 5.17A,B,C,D,E).
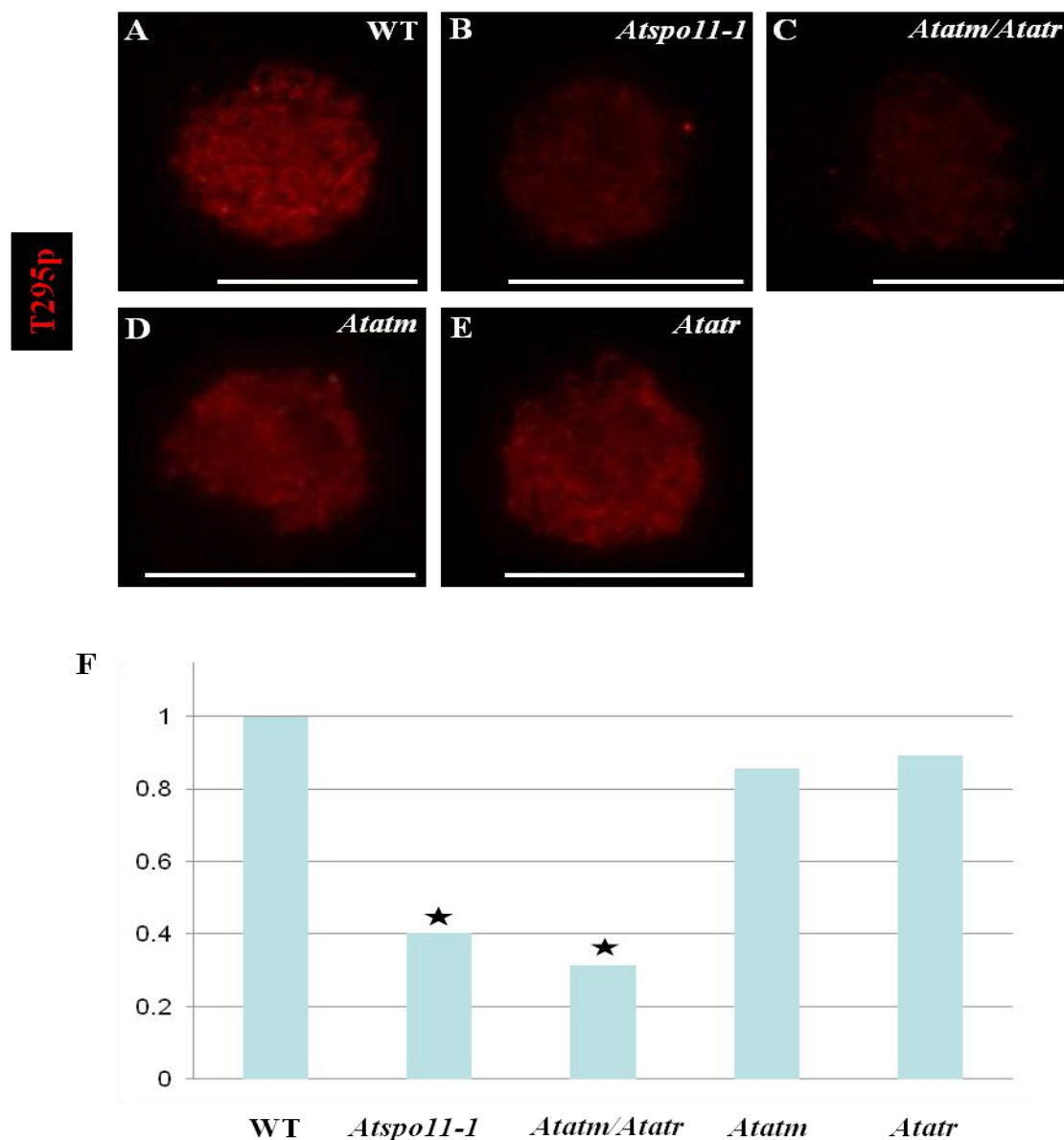
Figure 5.16. AtASY1 T295 is phosphorylated in response to the formation of DSBs in a pathway dependent on AtATM/AtATR.

Maximum intensity projection of AtASY1 T295p of chromosome spread preparation on wild-type (A), *Atspo11-1-4* (B), *Atatm/Atatr* (C), *Atatm* (D) and *Atatr* (E) PMCs. Scale bar = 10 μM. (F) Quantification of the AtASY1 T295p signal intensity. The mean AtASY1 T295p signal intensity of wild-type nuclei was normalised to 1. The mean signal intensity was calculated by analysing 15 early prophase I nuclei for each line. The black stars represent a statistical difference in the mean signal intensity between wild-type and mutants (ANOVA test).
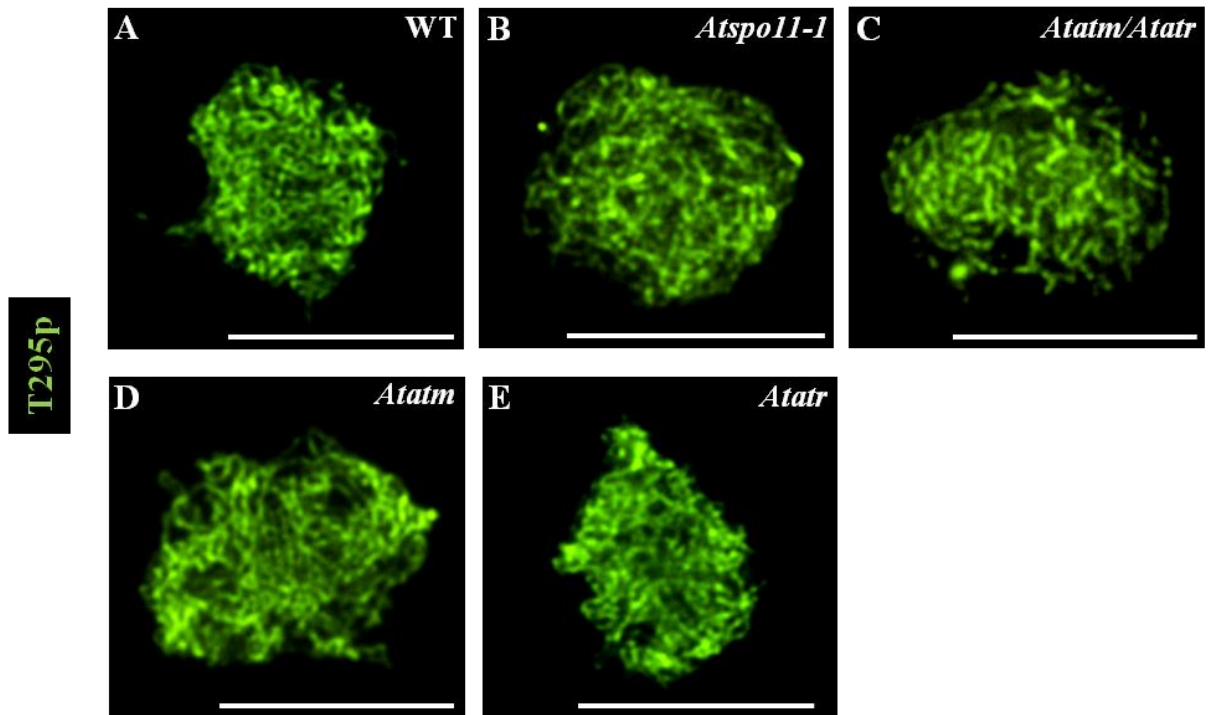
Figure 5.17. AtASY1 T295 is phosphorylated along the chromosome axes in the absence of meiotic DSBs and AtATM/AtATR.

Immunolocalisation of AtASY1 T295p (green) of chromosome spread preparation on wild-type (A), *Atspo11-1-4* (B), *Atatm/Atatr* (C), *Atatm* (D) and *Atatr* (E) early prophase I nuclei. Scale bar = 10 μM.

5.10. AtASY3 and AtPCH2 are required for AtASY1-T295 phosphorylation

Ferdous *et al.* (2012) showed that AtASY3 was essential for the proper localisation of AtASY1 along the axes. In the absence of AtASY3, AtASY1 formed punctuate chromatin-associated foci. The mean chiasma frequency was higher in *Atasy3* compared to *Atasy1* PMCs. The difference in the number of COs was dependent on AtASY1. This indicates that AtASY1 associated with the chromatin was competent for mediating inter-homologue COs in the absence of AtASY3 (Ferdous et al, 2012). To investigate if AtASY1 foci observed in *Atasy3* mutant were phosphorylated at residue T295, immunocytochemistry analysis on chromosome spread preparation was carried out with an anti-AtASY1 T295p antibody. Punctuate AtASY1 T295p foci overlapping with AtASY1 foci were detected during mid-prophase I of *Atasy3* PMCs (Figure 5.18A-D). The number of AtASY1 T295 phosphorylation was significantly lower than the number of AtASY1 and only 48.7 % of AtASY1 foci (n=10) were co-localising with AtASY1 T295p foci.

In budding yeast, Pch2 and Tel1 function in the same pathway to phosphorylate Hop1 (Ho & Burgess, 2011). To address the potential role of AtPCH2 in the phosphorylation of AtASY1 T295, dual immunolocalisation of AtSMC3 and AtASY1 T295p was carried out on wild-type and *Atpch2* PMCs. AtASY1 T295p signal was aberrant, forming numerous foci and faint stretches in *Atpch2* mutant (Figure 5.18E-G). In this study, a mean of 144.8 AtASY1 T295p foci (n=10) was observed. The majority of AtASY1 T295p foci were found associated with AtDMC1 foci (84.6 %, n=5). At mid-prophase I, AtASY1 T295

phosphorylation signal formed a brighter and more continuous signal on the SC in *Atpch2* mutant (Figure 5.18H-J).

AtSYN1 is a component of the cohesin ring complex and is involved in the formation of the chromosome axes. The phosphorylation of AtASY1 T295 was investigated in *Atsyn1* mutant. AtASY1 was found to be phosphorylated at the residue T295 during prophase I of *Atsyn1* PMCs (Figure 5.18K-M).
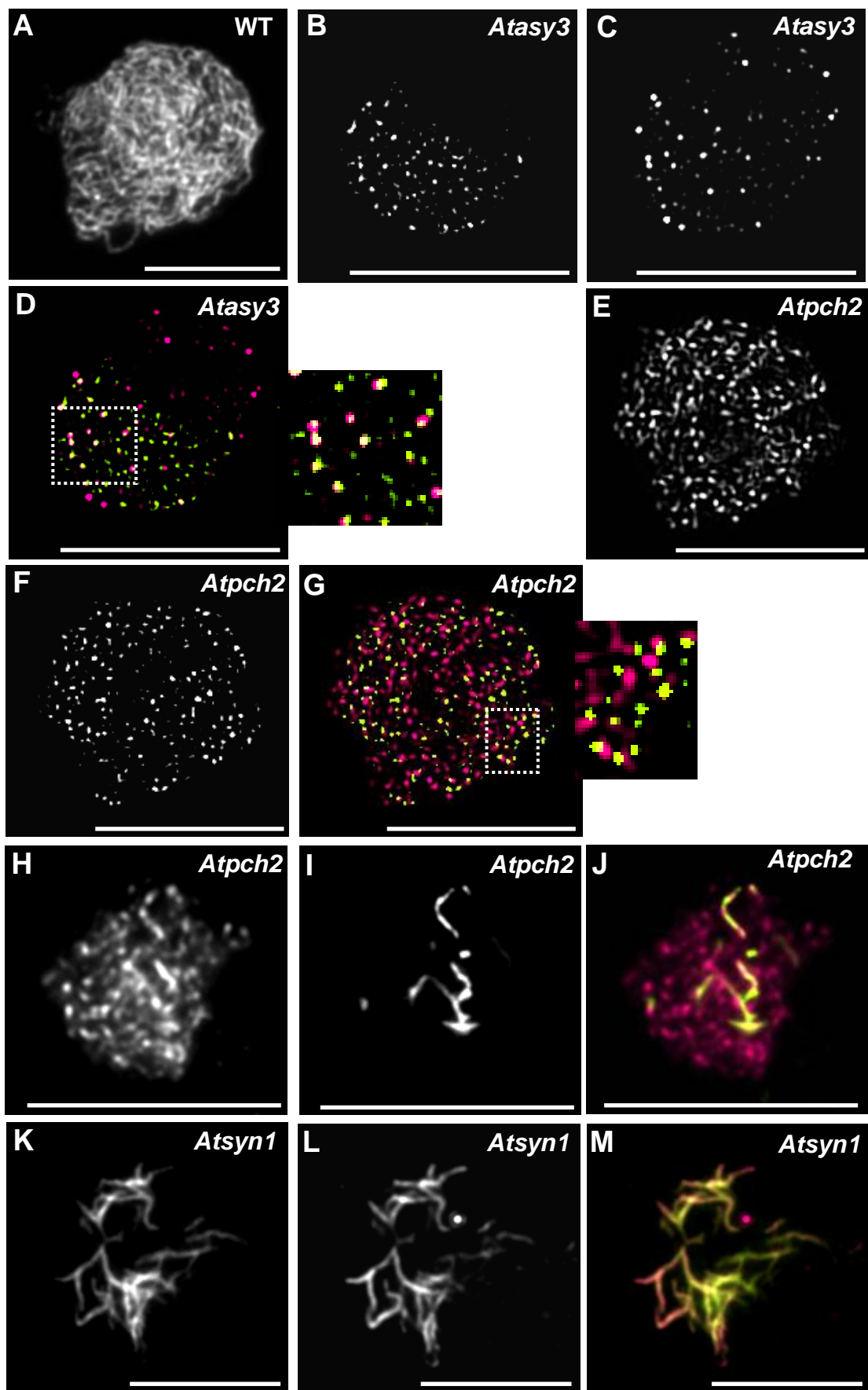
Figure 5.18. Phosphorylation of AtASY1 T295 is dependent on AtASY3 and AtPCH2
(A-C) Immunolocalisation of AtASY1 (B) and AtASY1 T295p (A,C) of chromosome spread preparation on wild-type (A) and *Atasy3* (B-C). (D) Merge image of AtASY1 (green) and AtASY1 T295p (magenta) immunolocalisation in *Atasy3*. (E,F) Immunolocalisation of AtASY1 T295p (E) and AtDMC1 (F) in *Atpch2*. (G) Merge image of AtDMC1 (green) and AtASY1 T295p (magenta) immunolocalisation in *Atpch2*. (H,I) Immunolocalisation of AtASY1 T295p (H) and AtZYP1 (I) in *Atpch2*. (J) Merge image of AtZYP1 (green) and AtASY1 T295p (magenta) immunolocalisation in *Atpch2*. (K,L) Immunolocalisation of AtASY1 (K) and AtASY1 T295p (L) in *Atsyn1*. (M) Merge image of AtASY1 (green) and AtASY1 T295p (magenta) immunolocalisation in *Atsyn1*. Scale bar = 10 μM.

5.11. Discussion

5.11.1. Remodelling of the chromosome axes during during prophase I

During meiosis, DSBs are repaired by homologous recombination using the homologous chromosomes as template. In budding yeast, the chromosome axes are essential to promote the homologue bias and counteract the sister bias established by the cohesin subunit Rec8 (Hong et al, 2013; Kim et al, 2010). Several lines of evidence suggest that the formation of the chromosome axes initiates before the formation of DSBs (Kim et al, 2010; Sanchez-Moran et al, 2007a). In addition, the formation of DSBs and their subsequent repair occurs in the context of the axes. However, the chromosome axes are not static and are remodelled during prophase I according to the chromatin and DNA damage status. Hence, chromosome axis morphogenesis and DSB repair are two co-ordinated processes.

The chromosome axes can be visualised cytologically by immunocytochemistry study of axis components. In *Arabidopsis,* four cohesin subunits have been characterised and were found localising with the underlying chromosome axes (Chelysheva et al, 2005; Lam et al, 2005). In addition, the structural axis component AtASY3 and the axis-associated protein AtASY1 form a complex to mediate inter-homologue CO formation. The formation of the chromosome axes initiates at early G2 as suggested by the progressive polymerisation of all 6 axis components and by the presence of short stretches of chromosome thread on DAPI-stained chromosome spreading of *Arabidopsis* PMCs (Ferdous et al, 2012). Storlazzi *et al.* (2008) showed that the early recombination events occurred between the two homologue axes. The authors also reported that the sites of DSB were locally depleted in

cohesin (Storlazzi et al, 2008). During early prophase I, the chromatin undergoes cycles of expansion and contraction (Higgins et al, 2012; Kleckner et al, 2004). The expanding chromatin generates compression stress against the underlying chromosome axes which are thought to be essential to designate a subset of DSB sites to become CO sites and to spread CO interference along the chromosomes. The resolution of the chromosome axis structure using conventional widefield epifluorescence microscopy is insufficient to study the local remodelling of the axes at the site of DSBs during early prophase I in *Arabidopsis*. However, the chromosome axes were found remodelled on the synaptic regions. In wild-type PMCs, AtASY1 signal intensity was significantly weaker on the synaptic regions. This observation was inversely correlated with the increase in the signal intensity of AtASY3 and the cohesin subunits. The partial depletion of the functional orthologues of AtASY1 during mid-prophase I has been extensively described in budding yeast (Joshi et al, 2009; Zanders & Alani, 2009), mice (Roig et al, 2010) and nematodes (Martinez-Perez et al, 2008). The increase in the signal intensity of cohesin subunits and AtASY3 is unclear. The formation of the SC is asynchronous in *Arabidopsis*. A CO-designated site matures to form an intermediate joint molecule and the SC elongates outwards from this site. Several AtRAD51 foci are localising along the nascent SC suggesting that the non CO-designated DSB sites are not yet repaired at the time the SC nucleates. It is possible that the accumulation of cohesin and the depletion of AtASY1 direct the repair of the non CO-designated DSB sites towards the sister chromatids. The increase in cohesin could also be important for the second end capture and the formation of dHJs. The concomitant increase in the signal intensity of AtASY3 may not interfere with the inter-sister bias imposed by the cohesin. The role of AtASY3 in inter-homologue CO formation may be indirect and reside in the proper association of AtASY1 with the axes. Alternatively, the

233

increase in the signal intensity of AtASY3 and cohesin subunits may simply be a cytological representation of the close juxtaposition of the two homologous axes.

5.11.2. AtPCH2 is essential for the re-distribution of AtASY1 on the synaptic regions

Pch2 protein has an AAA ATPase activity *in-vitro* and its function during meiosis is conserved between plants (Miao et al, 2013), mammals (Roig et al, 2010) and budding yeast (Joshi et al, 2009; Zanders & Alani, 2009). Pch2 physically interacts with Hop1 *in-vitro* and can promote both the assembly and the disassembly of Hop1 on DNA molecules (Chen et al, 2014). The formation of the SC is defective in *Atpch2/trip13* mutants in *Arabidopsis* and mice (Joshi et al, 2009; Roig et al, 2010). However, the defect in SC elongation does not result from the persistence of AtASY1/HORMAD1 on the SC but from a defect in DSB repair and CO formation as suggested by the analysis of a hypomorphic *trip13* mutant (Li & Schimenti, 2007). A more severe *trip13* mutant presents a defect in the localisation of recombination proteins as described in the hypomorphic *trip13* mutant but also a defect in SC formation (Roig et al, 2010). Interestingly, *S. pombe* lacks both a Pch2 orthologue in its genome and a SC. It is possible that TRIP13 and AtPCH2 have a role in SC formation independently of their role in early recombination steps. AtPCH2 was found localising with AtZYP1 polycomplexes in T-DNA mutant lines defective for homologous recombination. This indicates that AtPCH2 can certainly associates with AtZYP1 independently of additional factors in the homologous recombination pathways. Moreover, CRC1, the orthologue of Pch2 in rice, was found interacting with ZEP1, a component of the SC transverse filament (Miao et al, 2013).

Recently, Chen *et al.*, 2014 showed that the ATP hydrolysis activity of Pch2 was essential to dissociate Hop1 from DNA molecules. AtPCH2 could have a dual role in associating AtASY1 with the underlying axes during early prophase I and disassembling AtASY1 on the synaptic regions at mid-prophase I. This is in accord with the localisation defect of AtASY1 observed in *Atpch2* mutant using 3D structure illumination microscopy (Nuntasoontorn and Franklin, unpublished). In addition, an improper association of AtASY1 with the chromosome axes and specifically with AtASY3 can explain the defect in AtASY1-T295 phosphorylation along the axes. Dual immunolocalisation of AtASY1 and AtPCH2 revealed that AtPCH2 forms domains of high and low abundance on the SC and that the hyper-abundant domains of AtPCH2 mostly co-localised with the hyper-abundant domains of AtASY1. Interestingly, AtASY1 was not depleted on the short stretches of AtZYP1. This suggests that the antagonistic localisation of AtASY1 and AtZYP1 is temporally regulated and the partial depletion of AtASY1 from the synaptic regions occurs after the SC had formed short stretches. Zickler and Kleckner (1999) proposed that the formation of the SC occurs in two waves. The SC first nucleates at the SISs and starts to elongate. A mechanical stress is then imposed on the nascent SC and the improperly localised SC is depolymerised. A second wave of SC formation occurs where the SC can no longer nucleate *de-novo*. SC will elongate from the remaining SC stretches under less stringent conditions to ensure maximum synapsis (Zickler & Kleckner, 1999). In this scenario, it is most straightforward to speculate that the partial depletion of AtASY1 from the synaptic regions initiates after the first wave of SC formation had occurred.

The disassembly of AtASY1 from the synaptic regions is coupled with the DNA damage status. In *Arabidopsis,* the number of SISs outnumbers the number of COs. The SC

elongates along chromosomal regions where the non CO-designated DSBs are undergoing repair using the sister chromatids as the template. It is important that the inter-homologue bias is removed, after a CO-designated site has been implemented to mature into an intermediate joint molecule, to favour the repair of the DSBs surrounding the CO-designated site towards the sister chromatids. In the absence of AtPCH2, AtASY1 T295 is phosphorylated and presumably active in mediating inter-homologue CO formation. The active form of AtASY1 would maintain AtDMC1 on the synaptic regions. This can explain the persistence of AtDMC1 on the chromatin in mice *trip13* mutant (Roig et al, 2010; Wojtasz et al, 2009). In addition, several lines of evidence suggest that Dmc1 inhibits the recombinase activity of Rad51 (Lao et al, 2013; Uanschou et al, 2013). The persistence of an active form of DMC1 at the DSB sites can result in the persistence of unrepaired DSBs and eventually the formation of additional COs at regions surrounding the initial CO-designated site. This situation can specifically occur if the chromosome axes present additional morphological defects. This model is supported by the delay in the progression of prophase I observed in *Arabidopsis Atpch2* mutant and the delay in the progression of CO and NCO recombination in *pch2* mutant in budding yeast (Borner et al, 2008).

5.11.3. AtPCH2 has an additional role in early prophase I

Immunolocalisation of AtPCH2 from wild-type PMCs revealed numerous chromatin-associated foci from late S-phase/early G2. At the onset of leptotene, AtPCH2 formed more abundant foci that are associated with AtASY1. However, a similar localisation pattern, although slightly weaker, was observed for all three *Atpch2* mutant lines. The signal observed during G2 and leptotene in wild-type PMCs may not be specific to

AtPCH2 and the anti-AtPCH2 antibody may cross-react with other proteins in *Arabidopsis*. In contrast, the signal overlapping with the SC is specific to AtPCH2 protein as it was only detected in wild-type PMCs. The role of Pch2/TRIP13 in the repair of DSBs and CO formation is poorly understood. In mice, the number of DMC1 persists on the chromatin in *trip13* (Roig et al, 2010; Wojtasz et al, 2009). In budding yeast, there is an increase in gene conversion in *Atpch2* and a defect in Hop1 phosphorylation at an early stage of the homologous recombination pathway in both *pch2* single mutant and *pch2/red1* double mutant (Joshi et al, 2009; Lo et al, 2014). In addition, Pch2 acts in the same pathway as Xrs2 and Tel1 to phosphorylate Hop1 at threonine 318 (Ho & Burgess, 2011). The authors showed that Pch2 physically interacts with Xrs2 suggesting that Pch2 may have a role during the resection of DSBs. In addition, Pch2 is involved in the distribution of COs, CO interference and CO homeostasis, although CO interference and CO homeostasis can be uncoupled under certain conditions in *pch2* mutant (Ho & Burgess, 2011; Zanders & Alani, 2009; Zanders et al, 2011). CO designation occurs at/prior to the strand invasion/exchange. It is possible that Pch2 localises at the DSB sites by interacting with Xrs2 and promotes inter-homologue bias by elevating Tel1 kinase activity and subsequent phosphorylation of Hop1. Pch2 has certainly a role in CO designation as suggested by the redistribution of COs in yeast and plants (Joshi et al, 2009; Nuntasoontorn and Franklin, unpublished). The Pch2 function in CO designation could be dependent on Zip3. In yeast, Zip3 is a component of the ZMM complex and is thought to be the earliest marker of COs (Agarwal & Roeder, 2000). Interestingly, Joshi et al, (2009) reported an increase in the number of Zip3 foci in *pch2* mutant compared to wild-type. In this model, Pch2 could act on both CO formation and CO designation. In the absence of Pch2, more DSB sites are designated to form a CO but the absence of Pch2 results in a less efficient formation of

COs. The reduction in the phosphorylation of Hop1 could be responsible for the defect in CO formation. However, the degree of CO formation has not been globally assessed in a yeast *pch2* mutant. In addition budding yeast forms an average of 5 COs per bivalent and a subtle defect in CO formation would not be detected by monitoring sporulation frequency and spore germination. This attractive model could explain both the persistence of DMC1 in *trip13* in mice and the defect in CO formation and AtASY1 phosphorylation in *Arabidopsis* (Roig et al, 2010; Wojtasz et al, 2009).

CO interference is weaker in *pch2/Atpch2* mutant in budding yeast and plants. Zip3 foci and AtMLH1 foci were found more closely distributed in yeast *pch2* mutant and in *Arabidopsis Atpch2* mutant, respectively (Joshi et al, 2009). This indicates that the weaker strength of interference certainly account for a defect at the time CO interference is spreading rather than an indirect consequence of a differential timing of CO formation. If Pch2 has a role in chromosome axis morphogenesis before nucleation of the SC, this could have an impact on the strength of interference. In line of this scenario, the chromosome axis length was found shorter in *trip13* (Roig et al, 2010).

5.11.4. Phosphorylation of AtASY1 T295 is essential to associate AtASY1 with the chromosome axes

AtASY1 functional orthologues are phosphorylated in yeast and mammals during early prophase I. Phosphorylation of Hop1 at residue T318 (conserved residue with AtASY1 T295) is mediated by Mec1/Tel1 in response to the formation of meiotic DSBs. Hop1 T318 phosphorylation is required to recruit Mek1 at the sites of DSBs and for activation of

Mek1 kinase activity. Mek1 will then phosphorylate Rad54 which prevents the formation of a Rad51-Rad54 complex and hence promotes the homologue bias (Niu et al, 2009). In addition, the interaction between Mek1 and Hop1 maintains Hop1 in a phosphorylated form (Chuang et al, 2012). Hop1 is phosphorylated at multiple sites as suggested by the presence of several slow-migration bands observed on an electrophoretic mobility shift assay and by mutational analysis of several [S/T]Q sites of Hop1 (Carballo et al, 2008). Hop1 localisation was not thoroughly studied in these mutants. Hop1 S298A/S311A/T318A can properly associate with the chromatin. However, the localisation of Hop1 in the context of the chromosome axes was not analysed (Carballo et al, 2008). In mice, two HORMA domain-containing proteins have been characterised. HORMAD1 and HORMAD2 were found phosphorylated at multiple sites. HORMAD1 is phosphorylated at the residue serine 375 from early prophase I on the unsynapsed chromosome axes (Fukuda et al, 2012). At mid-prophase I, HORMAD1 S375 is phosphorylated on the XY chromosomes only. The biological significance of HORMAD1 S375 phosphorylation was not investigated. However, the specific localisation of HORMAD1 S375 phosphorylation on the unsynaptic regions and XY chromosomes suggests that it may be associated with the meiotic silencing of unsynapsed chromatin (Fukuda et al, 2012). AtASY1 shows structural and functional similarities with its orthologues. AtASY1 has a HORMA domain located in the N-terminus, localises on the unsynapsed regions, is essential for inter-homologue CO formation and is phosphorylated at multiple sites as suggested by 2-D gel electrophoresis analyses. Moreover, BoASY1 was found phosphorylated at 11 sites, including the residue threonine 294. Mutational analysis revealed that AtASY1 T295 phosphorylation is required to properly associate AtASY1 with the chromosome axes. In *Atasy1::AtASY1 T295A,* AtASY1 signal formed short

stretches that were co-localising with the chromosome axes. However, most of AtASY1 signal was aberrant and was distributed adjacent to the chromosome axes rather than on them. Immunolocalisation of AtASY1 T295p showed that AtASY1 T295 was phosphorylated along the chromosome axes in *Atspo11-1-4* and *Atatm/Atatr* mutants. In addition, the phosphorylation of AtASY1 T295 was concomitant with the formation of the chromosome axes and the formation of a continuous signal of AtASY1. This indicates that the phosphorylation of AtASY1 T295 is required to associate AtASY1 with the chromosome axes. The kinase involved in the phosphorylation of AtASY1 T295 remains to be characterised. The localisation defect of AtASY1 differs between *Atasy1;AtASY1-TA* and *Atasy3* mutants. This suggests that the defect in AtASY1 localisation observed in *Atasy1;AtASY1-TA* is not due to a defect in AtASY1-AtASY3 interaction. The phosphorylation of AtASY1 T295 may be important to structure the protein and modulate the turnover of the protein. Interestingly, the phosphomimic Hop1 T318E does not restore Hop1 function in CO formation (Carballo et al, 2008).

5.11.5. AtASY1 T295 is phosphorylated in response to the formation of DSBs

To address the level of AtASY1 T295 phosphorylation in various mutant lines, immunolocalisation was carried out using an anti-AtASY1 T295p antibody. Images were captures as Z-stacks of 10 sections of 0.1 um each and the maximum intensity projection of AtASY1 T295p signal was quantified for each nucleus. Quantitative comparison of AtASY1 T295p signal intensity between mutant lines revealed that the signal intensity was weaker in *Atspo11-1-4* and *Atatm/Atatr*. Although AtASY1 T295p signal intensity was reduced in *Atatm* and *Atatr* single mutant, the difference in the signal intensity between

each mutant line and wild-type was not statistically different. This indicates that both AtATM and AtATR are involved in the phosphorylation of AtASY1 T295 in response to the formation of DSBs.

In yeast, Hop1 T318 is phosphorylated by Mec1 and Tel1. Carballo *et al.* (2008) suggested that Hop1 was phosphorylated by Mec1/Tel1 in response to the formation of meiotic DSBs. Hop1 phosphorylation was not detected in *spo11* mutant using an eletrophoretic mobility shift assay. In addition, Mec1 was essential for Hop1 phosphorylation while Tel kinase activity was found important for Hop1 phosphorylation only when Mec1 was absent. However, Tel1 could not fully compensate for the absence of Mec1 function in the phosphorylation of Hop1 (Carballo et al, 2008; Chuang et al, 2012). In mice, two independent studies showed that HORMAD1 is phosphorylated in *spo11* mutant (Fukuda et al, 2012; Kogo et al, 2012). HORMAD1 S375 phosphorylation is mostly dependent on the formation of meiotic DSBs. However, an eletrophoretic mobility shift assay suggested that additional residue(s) is/are phosphorylated in the absence of DSB formation (Fukuda et al, 2012). ATM, the orthologue of Tel1, is dispensable for HORMAD1 and HORMAD2 phosphorylation. In contrast, the phosphorylation of HORMAD1 and HORMAD2 was reduced in *atr* mutant, the mice orthologue of Mec1 (Fukuda et al, 2012; Kogo et al, 2012; Royo et al, 2013; Shin et al, 2010).

Although, Hop1 T318 appears evolutionary conserved with AtASY1 T295, significant differences exist. The low resolution of the eletrophoretic mobility shift assay compare to immunocytochemistry analyses could explain the difference in Hop T318/AtASY1 T295 phosphorylation in the context of *mec1/tel1* and *Atatm/Atatr* and *spo11* mutants. The

increase in AtASY1 T295p signal intensity in response to DSB formation can results from an increase in the phosphorylation of AtASY1 T295 and/or a stabilisation of the pre-existing phosphorylation status of AtASY1 T295. In addition, the increase in AtASY1 T295p signal intensity by AtATM/AtATR may be indirect. In budding yeast, the association of Mek1 with Hop1 is sufficient to stabilise Hop1 T318 phosphorylation (Chuang et al, 2012). A similar mechanism may exist in plants where (an) additional factor(s), dependent on the formation of meiotic DSBs and on AtATM/AtATR, would modulate AtASY1 T295 phosphorylation status. This/these factor(s) could be the phosphorylation of AtASY1 at other [S/T]Q sites by AtATM/AtATR in the response of DSBs. This could in turn make the residue T295 more accessible to a kinase or less accessible to a phosphatase. This/these factor(s) could also be a protein or another post-translational modification of AtASY1 that would have a positive effect on AtASY1 T295 phosphorylation.

5.11.6. Phosphorylation of AtASY1 T295 is partially dependent on AtASY3 and AtPCH2

To identify additional factors involved in the phosphorylation of AtASY1 T295, immunolocalisation of AtASY1 T295p was carried out in various chromosome axis mutants. AtASY3 and AtSYN1 are two components of the chromosome axes. Both proteins are essential for the proper localisation and domainal organisation of AtASY1 along the axes. In *Atasy3* mutant, AtASY1 T295 was phosphorylated. However, the number of AtASY1 foci was substantially higher than the number of AtASY1 T295p foci. AtASY1 formed foci of different abundance in *Atasy3* mutants. There was no positive

correlation between the large AtASY1 foci and the presence of AtASY1 T295p foci. AtASY3 forms a complex with AtASY1 in a yeast two-hybrid assay and *in-vivo*. In addition, AtASY3 is required for the correct association of AtASY1 with the axes. It is possible that only a proportion of AtASY1 foci are properly organised on the axes and can therefore become phosphorylated at the residue T295. Electron microscopy analyses of silver stained meiotic prophase I nuclei of *Atasy3* mutant indicates that the chromosome axes present some structural alterations (Ferdous et al, 2012). These defects in axes could affect the tendency for AtASY1 T295 to be phosphorylated. However, AtSYN1 is important for the chromosome axis morphogenesis. AtASY1 can efficiently associate with the aberrant chromosome axes and is proficient in T295 phosphorylation in *Atsyn1*. This suggests that AtASY3 rather than the chromosome axis status is important to promote AtASY1 T295 phosphorylation. Similarly, the phosphorylation of Hop1 and HORMAD1 is defective in *red1* and *sycp3* mutants, the functional orthologues of AtASY3 in budding yeast (Carballo et al, 2008) and mice, respectively (Fukuda et al, 2012).

Pch2 is an AAA-ATPase family member and is important for remodelling Hop1 from the synaptic regions. Recently, Ho and Burgess (2011) showed that Pch2 is involved in the same pathway as Tel1 to phosphorylate Hop1. Interestingly, AtASY1 T295 phosphorylation was abnormal in *Atpch2* mutant from early prophase I. AtASY1 T295 phosphorylation signal was discontinuous and formed bright foci that were mostly associated with AtDMC1 foci. 3D structure illumination microscopy analysis of chromosome spread preparation of *Atpch2* PMCs suggests that AtASY1 localisation is abnormal (Nuntasoontorn and Franklin, unpublished). AtASY1 may fail to properly associate with the axes which will in turn prevent AtASY1 T295 from being

phosphorylated. Interestingly, the signal intensity of AtASY1 T295p foci associated with AtDMC1 foci was similar to wild-type level in *Atpch2*. Additional factors, possibly dependent on the formation of DSBs, ensure that AtASY1 T295 is phosphorylated at the sites of DSBs to promote inter-homologue bias. However, AtASY1 T295 phosphorylation was defective outwards of these sites.

Chapter 6

Discussion

6.1. Introduction

During meiosis and mitosis, the chromatin is organised stochastically in loop arrays. The formation and stabilisation of chromatin loop arrays is dependent on both cohesin and condensin but independent of the presence of a chromosome axis (Naumova et al, 2013; Sofueva et al, 2013; Zickler & Kleckner, 1999). The meiotic chromosome axes differ significantly from the mitotic axes. Components of the meiotic chromosome axes are thought to localise on the chromatin during G2 and promote the formation of meiotic DSBs (Ferdous et al, 2012; Kim et al, 2010). In addition, several evidences suggest that the chromosome axes are required for the repair of SPO11-dependent DSBs using the homologous chromosomes as a template (Blat et al, 2002; Carballo et al, 2008; Daniel et al, 2011; Ferdous et al, 2012; Fowler et al, 2013; Hong et al, 2013; Kim et al, 2010; Mallela et al, 2011; Niu et al, 2005; Prieler et al, 2005; Shin et al, 2010). In contrast, a homologue bias would be detrimental during interphase of mitotic cells. The mis-regulation of meiotic specific gene expression and the presence of meiotic axis proteins during mitosis have been associated with tumours (Hosoya et al, 2012; Ianzini et al, 2009; Kalejs et al, 2006). Moreover, the status of the meiotic axes is thought to have an important role for the designation of future CO sites and the propagation of CO interference along the chromosomes (Kleckner et al, 2004). However, the composition of the chromosome axes, the regulation of its morphology and its function during meiosis are poorly understood in plants.

The aims of this study were to conduct a further investigation into the function of AtASY1 during DSB formation and DSB repair.

6.2. AtASY1 physically interacts with AtASY3 to mediate inter-homologue CO formation

AtASY1 and AtASY3 share structural and functional similarities with Hop1/Red1 and SYCP2-3/HORMAD1-2 in yeast and mice, respectively. In yeast, Hop1 physically interacts with Red1 to activate the kinase activity of Mek1 and promote homologue bias (Niu et al, 2009; Wan et al, 2004). In *Arabidopsis*, AtASY1 was found interacting with AtASY3 in yeast two-hybrid and pull down assays. The functional significance of this interaction is unknown. AtASY1 and AtASY3 localised along the chromosome axes during early prophase I. AtASY1 was not required for AtASY3 localisation. However, the organisation of AtASY1 localisation along the axes is dependent on AtASY3. This suggests that the interaction between AtASY1 and AtASY3 may be essential to recruit/stabilise AtASY1 with the axes. Similarly, Red1 and SYCP3 are epistatic to Hop1 and HORMAD1 for localisation on the chromatin in budding yeast (Smith & Roeder, 1997) and mice (Fukuda et al, 2010; Shin et al, 2010), respectively.

Components of the chromosome axes are required for wild-type level of DSBs. Hop1 and Red1 are essential for the formation of DSBs in yeast (Carballo et al, 2008; Kim et al, 2010; Niu et al, 2005). In mice, a substantial reduction in the level of SPO11-oligonucleotides and chromatin-associated DMC1/RAD51 foci was detected in *hormad1* mutant suggesting that the protein is involved in the formation of DSBs (Daniel et al, 2011; Shin et al, 2010). In *Arabidopsis*, the number of early recombination nodules was decreased in *Atasy3* mutant but not in *Atasy1* mutant (Ferdous et al, 2012). However, AtASY1 was important for the localisation of AtPRD3 on the chromatin and both AtPRD3

and AtSPO11-1 foci were found associated with AtASY1 foci during G2. It is possible that AtASY1 has a role in the distribution of the DSBs along the chromosome axes rather than a global effect on the formation of DSBs. It is unclear if AtASY3 forms a complex with AtASY1 before the formation of DSBs. AtASY1 localisation appeared normal at G2 in *Atasy3* mutant. A similar wild-type localisation pattern of AtASY1 was detected in *Atsyn1* mutant. AtASY1 is an axis-associated protein and may localise both on the chromatin loop and on the axes during G2. This dual localisation of AtASY1 would render the study of its axis localisation during G2 more challenging. It is more straightforward to speculate that AtASY1 associates with the chromatin loops independently of axes components and associates with the axes in a process dependent on AtASY3 prior to formation of DSBs. AtASY1 would be re-localised from an "on chromatin loop" configuration to an "axis-associated" configuration during axis formation as suggested by immunogold localisation of AtASY1 on chromosome spread preparation of *Brassica oleracea* PMCs (Armstrong et al, 2002). The redistribution of AtASY1 localisation may be correlated with the progressive organisation of the chromatin into loop arrays and the formation of the underlying chromosome axes. The association of AtASY1 with the axes prior to DSB formation would modulate the distribution and/or turnover of the pre-DSB machinery and ensure an effective stabilisation of AtDMC1 on these sites after DSBs had occurred.

The presence of a homologue bias has been well documented in budding yeast. Almost half of the DSBs are repaired to form a CO. This results in the formation of an average of 5 COs per bivalent. In contrast, the ratio DSB:CO is considerably lower and estimated at 6-9 and 11 in mice (Cole et al, 2012) and *Arabidopsis*, respectively (Ferdous et al, 2012). In addition, the forkhead kinase Mek1, essential to form the barrier against the sister

chromatid has not been characterised in mammals and plants. In higher eukaryotes, the homologue bias may be less efficient and a more complex and regulated process may operate to ensure that a subset of the DSB sites is CO-designated sites. The complex HEI10/RNF212 may be a key factor in this crucial step and in limiting the number of COs per nucleus in mice (Qiao et al, 2014). The absence of AtASY1 or AtASY3 significantly reduces the number of inter-homologue COs in *Arabidopsis* PMCs. Interestingly, the number of inter-homologue COs is higher in *Atasy3* mutant compared to *Atasy1* mutant and these COs are dependent on AtASY1. AtASY1 and HORMAD1 are essential to associate DMC1 with the chromatin (Sanchez-Moran et al, 2007a; Shin et al, 2013). DMC1 is a recombinase with an activity directed towards the homologous chromosomes. In the absence of DMC1, the DSBs are repaired using the sister chromatids as a template. In budding yeast, Red1 was shown to be required to promote the loading of Dmc1 at R-band isochores (Blat et al, 2002). The localisation of Hop1 is defective in *red1* mutant and the function of Red1 in promoting DMC1 loading may be indirect and dependent on Hop1 function. The role of AtASY3 in inter-homologue CO formation cannot be separated from its structural role in recruiting AtASY1 to the axes. In *Atasy3,* AtASY1 forms foci that associate with AtDMC1 foci, which presumably mark the sites of DSBs. In addition, 48.7 % of AtASY1 foci were found phosphorylated at residue T295 in *Atasy3*. This suggests that AtASY1 is proficient in maintaining AtDMC1 at some DSB sites to mediate inter-homologue CO formation. The function of AtASY3 in CO formation may simply rely in a structural role to properly recruit/maintain AtASY1 on the axes. The observation that some but not all AtASY1 foci were phosphorylated in *Atasy3* may represent a differential in the turnover of AtASY1 protein. Additional factors may also be involved to ensure the association of AtASY1 to the axes in the absence of AtASY3. Such factors could be other

axes proteins or factors specific to the homologous recombination pathway. Chambon and Grelon identified a new coiled-coil protein AtASY4 that localises with the axes. Interestingly, AtASY4 was pull-downed by an anti-AtASY1 antibody from *Brassica oleracea* meiocyte extract (Osman and Franklin, unpublished) and interacts with AtASY3 in a yeast two-hybrid assay. The epistatic relationship between AtASY4 and AtSAY3/AtASY1 remains to be determined.

6.3. The formation of meiotic DSBs occurs in the context of the chromosome axes

The formation of meiotic DSBs is thought to occur in the context of the chromosome axes. The DSB sites are associated with the chromatin loops while some components of the pre-DSB machinery are associated with the axes. In addition, the distribution of Spo11-accessory proteins along the axes is modulated by the components of the underlying chromosome axes in yeast (Fowler et al, 2013; Kee et al, 2004; Panizza et al, 2011). The tethering of the chromatin loops to the chromosome axes implies additional controls over the formation of DSBs. It is thought that only one DSB occurs per chromatin loop. Moreover, the formation of a DSB at a given initiation site inhibits the formation of a DSB at the same genomic region but on the homologous chromosome (Zhang et al, 2011). This control is crucial to ensure proper repair of the DSBs by homologous recombination. The regulation of the association of Spo11-accessory proteins with the axes forms a first layer of control and determines the genomic regions where the meiotic DSBs will form. In addition, the tethering of the chromatin loops to the axes results in the contraction of the loops and hence disfavours the loading of the Spo11-accessory proteins on the loops and inhibits the formation of additional DSBs in the surrounding region. A third control occurs

in response to the formation of DSBs. DSB formation activates the kinase activity of Mec1/Tel1 which inhibits the formation of additional DSBs (Joyce et al, 2011; Lange et al, 2011; Zhang et al, 2011). In yeast, the axis-associated-Spo11-accessory-protein Rec114 is phosphorylated by Mec1/Tel1. The phosphorylation of Rec114 inhibits the formation of DSBs (Carballo et al, 2013). Finally, the depletion of Spo11-accessory-proteins from the synaptic regions as described in yeasts (Carballo et al, 2013) and mammals (Kumar et al, 2010) is another control over the formation of DSBs.

In *Arabidopsis*, four AtSPO11-accessory proteins have been characterised (De Muyt et al, 2009; De Muyt et al, 2007; Zhang et al, 2012). The function of AtPRD3 was further investigated in this study. AtPRD3 is essential for the formation of DSBs as suggested by the absence of early recombination proteins on the chromatin in *Atprd3* mutant. Immunocytochemistry analyses showed that AtPRD3 associated with AtASY1 foci at G2. AtPRD3 and AtSPO11-1 were mutually independent for their localisation suggesting that the two proteins are part of two distinct pre-DSB complexes. AtPRD3 was found interacting with AtASY1 and AtASY3 in a yeast two-hybrid assay and AtPRD3 was pull-downed by an anti-AtASY1 antibody from *Brassica oleracea* meiocyte extract. In addition, genes encoding axis proteins and for *PRD3* underwent a selective differentiation to overcome the increase in ploidy in *Arabidopsis arenosa* tetraploid. This highlights the evolutionary adaption of axes proteins and axis-associated-AtSPO11-accessory proteins to adapt meiosis to cellular challenges such as an increase in ploidy (Yant et al, 2013).

Althought it is not technically feasible to visualise the tethering of the chromatin loops to the axes, AtPRD3 likely associates with the chromosome axes to promote the tethering of

the chromatin loops to the axes and/or activate the topoisomerase-like transesterification activity of AtSPO11-1/2 when the chromatin loops are tethered with the axes.

6.4. AtATM is essential to limit the formation of meiotic DSBs in *Arabidopsis*

The formation of DSBs must be regulated during meiosis. Too few DSBs result in a defect in CO formation while too many DSBs can be deleterious for the cells. ATM/ATR kinases are essential for the repair of meiotic DSBs. Recently, ATM/Tel1 and ATR/Mec1 kinase activities were shown to be involved in a negative feedback loop for DSB formation in mammals (Lange et al, 2011), yeasts (Carballo et al, 2013; Zhang et al, 2011) and flies (Joyce et al, 2011).

Several factors exist to determine the DSB sites and regulate the formation of DSBs. The chromosome axes are required for the formation of DSBs. It has been shown that some components of the chromosome axes recruit components of the pre-DSB complexes (Fowler et al, 2013; Panizza et al, 2011). The axis components determine the distribution of these SPO11-accessory proteins along the axes which will in turn favour the formation of DSBs. However, ATM/Tel1 and ATR/Mec1 does not seem to be involved in the regulation of the association between SPO11-accessory proteins and the axes. This is supported by the persistence of Rec114 on the axes when 8 [S/T]Q sites were replaced by aspartic acids to phosphomimic the phosphorylated form of the protein. In addition, SPO11-accessory proteins persist on the unsynapsed regions until the SC starts to nucleate in yeasts (Carballo et al, 2013) and mammals (Kumar et al, 2010). The formation of the SC rather than the formation of DSBs seems to be a determining factor for the removal of

SPO11-accessory proteins from the chromosome axes. Interestingly, the localisation of AtPCH2 with the axes is concomitant with the nucleation of the SC. AtPCH2 was found interacting with AtPRD3 in a yeast two-hybrid assay. In budding yeast, Pch2 has an AAA ATPase hydrolysis activity. Pch2 interacts with Hop1 in a pathway dependent on ATP and it is thought that Pch2 depletes Hop1 from the synaptic regions (Borner et al, 2008; Chen et al, 2014). Similarly, Pch2 could be involved in the depletion of SPO11-accessory proteins associated with the axes on the synaptic regions. The formation of the SC is coordinated with the progression of the DNA damage status and the homologous recombination pathway. The formation of the SC could be a distinct signal to ATM/ATR kinase activity, to permanently inhibit the formation of DSBs.

In *Arabidopsis,* AtATM/AtATR inhibits the formation of DSBs. The proteins phosphorylated by AtATM/AtATR during meiosis are unknown. However, two AtSPO11-accessory proteins, AtPRD1 and AtPRD3, are enriched in [S/T]Q sites. AtPRD1 was found forming a complex with AtSPO11-1 (De Muyt et al, 2007). In contrast, AtPRD3 interacts with axis components and AtSPO11-1 and AtPRD3 are mutually independent for their localisation. This suggests that AtATM/AtATR could inhibit the formation of DSBs by phosphorylating components of two distinct pre-DSB complexes. An AtPRD1-containing complex is thought to be located on the chromatin loops and is probably involved in the stabilisation of AtSPO11-1 on the chromatin. In contrast, an AtPRD3-containing complex is associated with the underlying chromosome axes and is involved in the tethering of the chromatin loops to the axes or involved in the activation of the topoisomerase-like transesterification activity of AtSPO11-1/2 when the chromatin loops are tethered with the

axes. The inhibition of the two distinct complexes could efficiently inhibit the formation of additional DSBs.

Additional factors could be involved in the temporal formation of DSBs. During meiosis, the chromatin loops undergo cycle of expansion and contraction. The first expansion of the chromatin is thought to occur during G2 at the time of the formation of DSBs. Interestingly, AtSPO11-1 was found localised on the chromatin at G2 but was no longer associated with the chromatin at the onset of leptotene in both wild-type and *Atprd3* nuclei. In *Atprd3* mutant, the formation of meiotic DSBs is defective. Meiosis is a well evolutionary conserved biological process and it is likely that the AtSPO11-accessory proteins associated with the chromosome axes at G2, remain associated with the axes at the onset of leptotene when the DSBs are not formed. In contrast, the pre-DSB complex containing AtSPO11-1 and localising on the chromatin loop may be destabilised when the chromatin is contracting. This would explain the absence of AtSPO11-1 signal in *Atprd3* mutant during early prophase I and would represent an additional layer of control over the temporal formation of DSBs during meiosis.

6.5. AtPCH2 modulates the distribution of AtASY1 during prophase I and mediates SC formation and CO formation

PCH2 is a conserved protein found in yeasts, mammals and plants. PCH2 is required for CO formation, CO interference and SC elongation (Joshi et al, 2009; Miao et al, 2013; Roig et al, 2010; Zanders & Alani, 2009). Pch2 interacts with Hop1 and modulates the association/dissociation of Hop1 with DNA molecules *in-vitro* (Chen et al, 2014).

Hop1/HORMAD1 was found depleted from the synaptic regions in wild-type budding yeast and mice. In contrast, Hop1/HORMAD1 persisted on the synaptic regions in *pch2/trip13* mutants supporting a role for Pch2 in regulating the association of Hop1/HORMAD1 with DNA molecules (Borner et al, 2008; Roig et al, 2010; Wojtasz et al, 2009). The role of Pch2 in remodelling the axes is dependent on its AAA ATPase activity in yeast (Chen et al, 2014).

In plants, immunocytochemistry analysis on chromosome spread preparation using an anti-AtPCH2 antibody showed that AtPCH2 was co-localising with the SC at mid-prophase I. Similarly, CRC1 co-localised with the SC and interacted with the transverse filament ZEP1 in rice (Miao et al, 2013). Moreover, AtPCH2 was found associated with AtZYP1 polycomplexes in *Arabidopsis* asynaptic mutants. This indicates that AtPCH2 and AtZYP1 can aggregate independently of factors involved in the homologous recombination pathway. The localisation of AtPCH2 at the SISs is consistent with a role in CO formation and CO interference. However, recent studies indicate that Pch2 may have a role at an earlier step of the homologous recombination pathway. The number of DSBs was reduced in *pch2* mutant in budding yeast (Farmer et al, 2012) and abolished in *crc1* mutant in rice (Miao et al, 2013). In addition, the phosphorylation of AtASY1 T295 occurred prior to the nucleation of the SC in *Arabidopsis*. However, AtASY1 T295 was phosphorylated at numerous sites on the chromatin but failed to be phosphorylated along the chromosome axes in *Atpch2* mutant. Ho and Burgess (2011) showed that Pch2 has a role at the DSB end resection step and is involved in the same pathway as Tel1 for the phosphorylation of Hop1 (Ho & Burgess, 2011).

CO interference was found weaker in *pch2/trip13* mutant. The mechanism propagating CO interference along the chromosomes is unknown. The most widely accepted model for explaining the propagation of CO interference is the stress relief model (Kleckner et al, 2004). In this model, the propagation of CO interference is dependent on both the chromatin and the chromosome axes status. Any structural alteration in the chromosome axes may affect the strength of CO interference, although this has not been formally demonstrated. The axis length was shorter in *trip13* mutant and the number of ZIP3 foci, an early marker of CO sites in budding yeast, was significantly increased in *pch2* mutant suggesting that PCH2/TRIP13 may have a role in the structure of the axes and in the designation of the CO sites (Joshi et al, 2009; Roig et al, 2010). This is consistent with a defect in CO formation and CO interference reported in *pch2/trip13* mutants.

In *Atpch2/trip13* mutant, AtASY1 and HORMAD1 persisted on the synaptic regions. Both proteins are required to maintain the association of DMC1 with the chromatin (Sanchez-Moran et al, 2007a; Shin et al, 2013). DMC1 is a meiotic specific recombinase involved in the repair of meiotic DSBs towards the homologous chromosomes. Consistent with this observation, DMC1 persisted on the synaptic regions in *trip13* mutant (Roig et al, 2010; Wojtasz et al, 2009). The weaker strength in CO interference reported in *pch2/trip13* mutant may result from a differential timing of CO formation. A proportion of the CO-designated DSB sites will be repaired to form CO. However, the absence of PCH2/TRIP13 results in the failure to form wild-type level of COs. The persistence of AtASY1/HORMAD1 on the synaptic regions and the close juxtaposition of the two homologue axes may maintain the homologue bias and some DSBs may be repaired and form a CO at a later time than the first wave of CO formation. Alternatively, the increase

of Zip3 foci and the delay in the progression of CO and NCO recombination reported in *pch2* mutant in budding yeast suggests that more DSB are CO-designated (Borner et al, 2008; Joshi et al, 2009). However, the defect in SC formation affects the efficiency of CO implementation thus resulting in an overall reduction of CO formation. On the synapsed regions, the CO implementation is established and mediate CO formation to form COs that are closer together than in wild-type.

6.6. AtASY1 T295 phosphorylation is required to maintain AtASY1 associated with the chromosome axes

AtASY1/Hop1 is a HORMA-containing protein essential for the formation of inter-homologue COs. AtASY1 and its functional and structural counterparts in yeasts and mammals are phosphorylated at multiple sites. In budding yeast, the phosphorylation of Hop1 at [S/T]Q sites is required for the homologue bias (Carballo et al, 2008). In contrast, the biological significance of HORMAD1 phosphorylation is unclear. However, the phosphorylation of HORMAD1 S375 was suggested to be associated with the meiotic silencing of unsynapsed chromatin (Fukuda et al, 2012). Hop1, HORMAD1 and AtASY1 phsophorylation occur in response to the formation of DSBs and are dependent on the kinase activity of ATM/Tel1 and/or ATR/Mec1. However, some divergence exists between the three proteins. Hop1 was not found phosphorylated in *spo11* mutant (Carballo et al, 2008). In contrast, HORMAD1 was phosphorylated at wild-type level in *atm* mutant and a residual level of phosphorylation was detected in *spo11* mutant (Fukuda et al, 2012; Kogo et al, 2012; Royo et al, 2013; Shin et al, 2010). In *Arabidopsis,* a basal level of AtASY1 T295 phosphorylation was observed in *Atspo11-1* mutant. In addition, AtASY1 T295

phosphorylation was significantly reduced in *Atatm/Atatr* double mutant. The role of AtATM and AtATR in AtASY1 T295 phosphorylation may be indirect. In *Atspo11-1,* the phosphorylation of AtASY1 T295 accumulated progressively during prophase I. AtATM/AtATR are activated in response to the formation of DSBs and may target proteins that will promote the phosphorylation of AtASY1 T295. In budding yeast, Hop1 and Red1 form a complex. The phosphorylation of Hop1 by Mec1/Tel1 promotes the recruitment of Mek1 at the DSB sites. The kinase activity of Mek1 is then activated and the protein promotes homologue bias. In addition, the stabilisation of Mek1-Hop1 complex is important to maintain the phosphorylation status of Hop1 T318 (Chuang et al, 2012). A similar mechanism may exist in plants where a protein, dependent on the initiation of homologous recombination, associates with the axes and alters the phosphorylation status of AtASY1. AtASY1 T295 phosphorylation may be in a near equilibrium state between phosphorylation and dephosphorylation/turnover of the protein prior to formation of DSBs. The phosphorylation of the protein would be the prominent state. This would explain the weak progressive accumulation of AtASY1 T295 phosphorylation during prophase I of *Atspo11-1* PMCs. Following DSB formation, AtATM/AtATR activates a factor that alters the near equilibrium state of AtASY1 T295 phosphorylation and increases the level of AtASY1 T295 phosphorylation. The factor could be a protein or the phosphorylation of AtASY1 at another [S/T]Q site.

The phosphorylation of AtASY1 T295 was concomitant with the formation of the chromosome axes. Moreover, AtASY1 T295 was phosphorylated in *Atspo11-1* mutant where the axes were properly formed. In contrast, AtASY1 T295A failed to localise along the axes and formed a diffuse signal on the chromatin. This indicates that the

phosphorylation of AtASY1 T295 is important for the association of AtASY1 with the axes. Interestingly, AtASY3 was not essential for the phosphorylation of AtASY1 T295. AtASY1 T295 was found phosphorylated in *Atasy3* mutant and the number of inter-homologue CO was higher in *Atasy3* mutant compared to *Atasy1* mutant. These additional COs were dependent on AtASY1. This implies that AtASY1 T295 can be phosphorylated in the absence of AtASY3. In addition, the phosphorylation of AtASY1 T295 stabilises the protein on the chromatin. Phosphorylated AtASY1 T295 is proficient in mediating inter-homologue CO formation and likely accounts for the formation of the additional COs observed in *Atasy3* mutant compared to *Atasy3/Atasy1* double mutant.

6.7. Conclusion

This study applied a combination of biochemical assays, cytological procedures and mutational analysis to investigate the interplay between the chromosome axes and the DSB repair by homologous recombination during *Arabidopsis* meiosis. This study showed that the formation of DSBs is temporally correlated with the formation of the chromosome axes. In addition, the chromosome axes have an important role during the formation of DSBs. The axes determine the number of DSBs formed per nuclei and modulate the distribution of the AtSPO11-accesssory protein AtPRD3. The initiation of the homologous recombination results in the remodelling of the chromosome axes with an increase in the phosphorylation level of AtASY1 T295, the nucleation of the SC and the depletion of AtASY1 from the synaptic regions. The proper remodelling of the chromosome axes is essential to ensure wild-type level of inter-homologue COs and CO interference.

To summarise, AtASY1 localises as numerous chromatin-associated foci at G2 (Figure 6.1.a). During the formation of the chromosome axes, AtASY1 associates with the nascent chromosome axes forming domains of hyper and lower abundance. The domainal axis organisation of AtASY1 is dependent on the cohesin subunit AtSYN1 and the recruitment of AtASY1 along the axes is dependent on the structural axis component AtASY3 (Figure 6.1.b). In the absence of DSB formation, AtASY1 T295 becomes progressively phosphorylated from G2/leptotene transition (Figure 6.1.g). The kinase involved in the phosphorylation of AtASY1 T295 remains to be characterised. In contrast, two distinct pre-DSB complexes, containing AtPRD3 or AtSPO11-1, associates with AtASY1 foci in wild-type PMCs. The distribution of AtPRD3 is regulated by AtASY1 but not AtSYN1. As illustrated on the hypothetic model (Figure 6.1.), following the formation of meiotic DSBs, the MRN complex is thought to be recruited at the sites of DSB (Figure 6.1.d) and activates the kinase activity of AtATM/AtATR (Figure 6.1.e). AtATM/AtATR will then inhibit the formation of additional DSBs (Figure 6.1.f). AtPRD1 and AtPRD3 are two AtSPO11-accessory proteins enriched in [S/T]Q sites and are potential targets of AtATM/AtATR. In addition, AtATM/AtATR increases the phosphorylation of AtASY1 T295 (Figure 6.1.g), either directly or indirectly. The phosphorylation of AtASY1 T295 is thought to have a role in promoting the formation of inter-homologue COs (Figure 6.1.h), although this can not be formally tested. The function of AtASY1 in the formation of inter-homologue COs relies at least in part in the maintenance of AtDMC1 at the sites of DSBs to favour CO formation. AtDMC1 recombinase direct the single stranded 3' DNA tails towards the homologous chromosomes resulting in the formation of D-loop structures and the nucleation of the SC. AtPCH2 localisation on the chromatin occurs concomitantly with SC formation. AtPCH2 remodels the axes by partially depleting AtASY1 from the synaptic

regions, promotes inter-homologue CO information and has a role in CO interference (Figure 6.1.j). AtPCH2 was found interacting with AtPRD3 in a yeast two-hybrid assay. Immunocytochemistry analyses on chromosome spread preparations of wild-type PMCs using an anti-AtPCH2 antibody showed numerous chromatin-associated foci of AtPCH2 at G2. AtPCH2 could have a role in the formation of DSBs by regulating AtPRD3 activity (Figure 6.1.c). Additionally, AtPCH2 could deplete AtPRD3 from the synaptic regions in a process similar to the depletion of AtASY1 (Figure 6.1.).
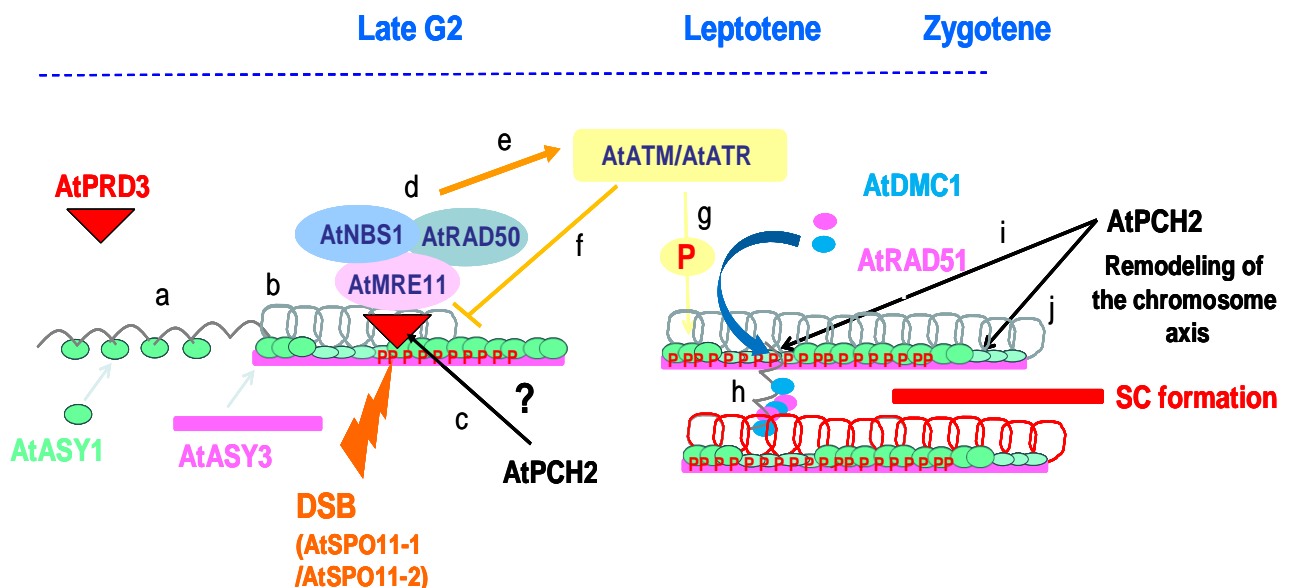
Figure 6.1. A hypothetic model illustrating the interplay between chromosome axis morphogenesis and homologous recombination in *Arabidopsis* meiosis.

At S-phase/early G2, AtASY1 forms punctuate chromatin-associated foci (a). At mid-G2, AtASY1 presents a domainal organisation of hyper- and lower-abundance along the underlying nascent chromosome axes (b). AtSPO11-1-dependend DSBs occurs in the context of the chromosome axes. The direct interaction between AtPCH2 and AtPRD3

suggests that AtPCH2 may have a role in DSB formation (c). The MRN complex is recruited at the DSB sites (d) and activates the kinase activity of AtATM and AtATR (e). AtATM/AtATR are involved in a negative feedback loop inhibiting the formation of DSBs (f). In addition, AtATM/AtATR phosphorylate proteins involved in DSB repair and the homologous recombination pathway. AtASY1 is phosphorylated at residue T295 by AtATM/AtATR (g). The phosphorylation of AtASY1 T295 is required to maintain the protein associated with the axes and to indirectly mediate inter-homologue CO formation (h). AtPCH2 regulates the phosphorylation of AtASY1 T295 (i). In addition, AtPCH2 is an integral component of the SC and remodels the axes by depleting AtASY1 from the axes as the SC elongates (j).

Chapter 7

References

Abdu U, Gonzalez-Reyes A, Ghabrial A, Schupbach T (2003) The Drosophila spn-D gene encodes a RAD51C-like protein that is required exclusively during meiosis. *Genetics* 165: 197-204

Abe K, Osakabe K, Nakayama S, Endo M, Tagiri A, Todoriki S, Ichikawa H, Toki S (2005) *Arabidopsis* RAD51C gene is important for homologous recombination in meiosis and mitosis. *Plant physiology* 139: 896-908

Acquaviva L, Szekvolgyi L, Dichtl B, Dichtl BS, de La Roche Saint Andre C, Nicolas A, Geli V (2013) The COMPASS subunit Spp1 links histone methylation to initiation of meiotic recombination. *Science* 339: 215-218

Adkins NL, Niu H, Sung P, Peterson CL (2013) Nucleosome dynamics regulates DNA processing. *Nature structural & molecular biology* 20: 836-842

Agarwal S, Roeder GS (2000) Zip3 provides a link between recombination enzymes and synaptonemal complex proteins. *Cell* 102: 245-255

Albini SM, Jones GH (1988) Synaptonemal Complex Spreading in Allium-Cepa and Allium-Fistulosum .2. Pachytene Observations - the Sc Karyotype and the Correspondence of Late Recombination Nodules and Chiasmata. *Genome / National Research Council Canada = Genome / Conseil national de recherches Canada* 30: 399-410

Allers T, Lichten M (2001) Intermediates of yeast meiotic recombination contain heteroduplex DNA. *Molecular cell* 8: 225-231

An XJ, Deng ZY, Wang T (2011) OsSpo11-4, a rice homologue of the archaeal TopVIA protein, mediates double-strand DNA cleavage and interacts with OsTopVIB. *PloS one* 6: e20327

Armstrong SJ, Caryl AP, Jones GH, Franklin FC (2002) Asy1, a protein required for meiotic chromosome synapsis, localizes to axis-associated chromatin in Arabidopsis and Brassica. *Journal of cell science* 115: 3645-3655

Armstrong SJ, Franklin FCH, Jones GH (2001) Nucleolus-associated telomere clustering and pairing precede meiotic chromosome synapsis in *Arabidopsis thaliana. Journal of cell science* 114: 4207-4217

Armstrong SJ, Franklin FCH, Jones GH (2003) A meiotic time-course for *Arabidopsis thaliana. Sex Plant Reprod* 16: 141-149

Armstrong SJ, Jones GH (2003) Meiotic cytology and chromosome behaviour in wild-type *Arabidopsis thaliana. Journal of experimental botany* 54: 1-10

Arora C, Kee K, Maleki S, Keeney S (2004) Antiviral protein Ski8 is a direct partner of Spo11 in meiotic DNA break formation, independent of its cytoplasmic role in RNA metabolism. *Molecular cell* 13: 549-559

Bai X, Peirson BN, Dong F, Xue C, Makaroff CA (1999) Isolation and characterization of SYN1, a RAD21-like gene essential for meiosis in *Arabidopsis*. *Plant Cell* 11: 417-430

Bailis JM, Roeder GS (1998) Synaptonemal complex morphogenesis and sister-chromatid cohesion require Mek1-dependent phosphorylation of a meiotic chromosomal protein. *Genes & development* 12: 3551-3563

Baudat F, Buard J, Grey C, Fledel-Alon A, Ober C, Przeworski M, Coop G, de Massy B (2010) PRDM9 is a major determinant of meiotic recombination hotspots in humans and mice. *Science* 327: 836-840

Baudat F, Manova K, Yuen JP, Jasin M, Keeney S (2000) Chromosome synapsis defects and sexually dimorphic meiotic progression in mice lacking Spo11. *Molecular cell* 6: 989-998

Baumann C, Korner R, Hofmann K, Nigg EA (2007) PICH, a centromere-associated SNF2 family ATPase, is regulated by Plk1 and required for the spindle checkpoint. *Cell* 128: 101-114

Bellani MA, Boateng KA, McLeod D, Camerini-Otero RD (2010) The expression profile of the major mouse SPO11 isoforms indicates that SPO11beta introduces double strand breaks and suggests that SPO11alpha has an additional role in prophase in both spermatocytes and oocytes. *Molecular and cellular biology* 30: 4391-4403

Berchowitz LE, Copenhaver GP (2010) Genetic interference: don't stand so close to me. *Current genomics* 11: 91-102

Berchowitz LE, Francis KE, Bey AL, Copenhaver GP (2007) The role of AtMUS81 in interference-insensitive crossovers in *Arabidopsis thaliana*. *PLoS genetics* 3: e132

Bergerat A, de Massy B, Gadelle D, Varoutas PC, Nicolas A, Forterre P (1997) An atypical topoisomerase II from Archaea with implications for meiotic recombination. *Nature* 386: 414-417

Bhaskara V, Dupre A, Lengsfeld B, Hopkins BB, Chan A, Lee JH, Zhang X, Gautier J, Zakian V, Paull TT (2007) Rad50 adenylate kinase activity regulates DNA tethering by Mre11/Rad50 complexes. *Molecular cell* 25: 647-661

Bishop DK (1994) RecA homologs Dmc1 and Rad51 interact to form multiple nuclear complexes prior to meiotic chromosome synapsis. *Cell* 79: 1081-1092

Bishop DK, Park D, Xu L, Kleckner N (1992) DMC1: a meiosis-specific yeast homolog of *E. coli* recA required for recombination, synaptonemal complex formation, and cell cycle progression. *Cell* 69: 439-456

Bisig CG, Guiraldelli MF, Kouznetsova A, Scherthan H, Hoog C, Dawson DS, Pezza RJ (2012) Synaptonemal Complex Components Persist at Centromeres and Are Required for Homologous Centromere Pairing in Mouse Spermatocytes. *PLoS genetics* 8

Blat Y, Kleckner N (1999) Cohesins bind to preferential sites along yeast chromosome III, with differential regulation along arms versus the centric region. *Cell* 98: 249-259

Blat Y, Protacio RU, Hunter N, Kleckner N (2002) Physical and functional interactions among basic chromosome organizational features govern early steps of meiotic chiasma formation. *Cell* 111: 791-802

Bleuyard JY, Gallego ME, Savigny F, White CI (2005) Differing requirements for the *Arabidopsis* Rad51 paralogs in meiosis and DNA repair. *Plant J* 41: 533-545

Bleuyard JY, Gallego ME, White CI (2004) The *atspo11-1* mutation rescues *atxrcc3* meiotic chromosome fragmentation. *Plant Mol Biol* 56: 217-224

Blitzblau HG, Hochwagen A (2013) ATR/Mec1 prevents lethal meiotic recombination initiation on partially replicated chromosomes in budding yeast. *eLife* 2: e00844

Borde V, Goldman AS, Lichten M (2000) Direct coupling between meiotic DNA replication and recombination initiation. *Science* 290: 806-809

Borner GV, Barot A, Kleckner N (2008) Yeast Pch2 promotes domainal axis organization, timely recombination progression, and arrest of defective recombinosomes during meiosis. *Proceedings of the National Academy of Sciences of the United States of America* 105: 3327-3332

Borner GV, Kleckner N, Hunter N (2004) Crossover/noncrossover differentiation, synaptonemal complex formation, and regulatory surveillance at the leptotene/zygotene transition of meiosis. *Cell* 117: 29-45

Bugreev DV, Yu X, Egelman EH, Mazin AV (2007) Novel pro- and anti-recombination activities of the Bloom's syndrome helicase. *Genes & development* 21: 3085-3094

Buonomo SB, Clyne RK, Fuchs J, Loidl J, Uhlmann F, Nasmyth K (2000) Disjunction of homologous chromosomes in meiosis I depends on proteolytic cleavage of the meiotic cohesin Rec8 by separin. *Cell* 103: 387-398

Busygina V, Saro D, Williams G, Leung WK, Say AF, Sehorn MG, Sung P, Tsubouchi H (2012) Novel attributes of Hed1 affect dynamics and activity of the Rad51 presynaptic filament during meiotic recombination. *The Journal of biological chemistry* 287: 1566-1575

Busygina V, Sehorn MG, Shi IY, Tsubouchi H, Roeder GS, Sung P (2008) Hed1 regulates Rad51-mediated recombination via a novel mechanism. *Genes & development* 22: 786-795

Cai X, Dong F, Edelmann RE, Makaroff CA (2003) The *Arabidopsis* SYN1 cohesin protein is required for sister chromatid arm cohesion and homologous chromosome pairing. *Journal of cell science* 116: 2999-3007

Carballo JA, Johnson AL, Sedgwick SG, Cha RS (2008) Phosphorylation of the axial element protein Hop1 by Mec1/Tel1 ensures meiotic interhomolog recombination. *Cell* 132: 758-770

Carballo JA, Panizza S, Serrentino ME, Johnson AL, Geymonat M, Borde V, Klein F, Cha RS (2013) Budding yeast ATM/ATR control meiotic double-strand break (DSB) levels by down-regulating Rec114, an essential component of the DSB-machinery. *PLoS genetics* 9: e1003545

Carpenter AT (1975) Electron microscopy of meiosis in Drosophila melanogaster females: II. The recombination nodule--a recombination-associated structure at pachytene? *Proceedings of the National Academy of Sciences of the United States of America* 72: 3186-3189

Caryl AP, Armstrong SJ, Jones GH, Franklin FC (2000) A homologue of the yeast HOP1 gene is inactivated in the *Arabidopsis* meiotic mutant asy1. *Chromosoma* 109: 62-71

Cavalier-Smith T (2002) Origins of the machinery of recombination and sex. *Heredity* 88: 125-141

Cha RS, Weiner BM, Keeney S, Dekker J, Kleckner N (2000) Progression of meiotic DNA replication is modulated by interchromosomal interaction proteins, negatively by Spo11p and positively by Rec8p. *Genes & development* 14: 493-503

Chai B, Huang J, Cairns BR, Laurent BC (2005) Distinct roles for the RSC and Swi/Snf ATP-dependent chromatin remodelers in DNA double-strand break repair. *Genes & development* 19: 1656-1661

Chan KL, North PS, Hickson ID (2007) BLM is required for faithful chromosome segregation and its localization defines a class of ultrafine anaphase bridges. *The EMBO journal* 26: 3397-3409

Chan YL, Brown MS, Qin D, Handa N, Bishop DK (2014) The 3rd exon of the budding yeast meiotic recombination gene HOP2 is required for calcium-dependent and recombinase Dmc1-specific stimulation of homologous strand assimilation. *The Journal of Biological Chemistry* ahead of print

Chapman JR, Taylor MR, Boulton SJ (2012) Playing the end game: DNA double-strand break repair pathway choice. *Molecular cell* 47: 497-510

Chelysheva L, Diallo S, Vezon D, Gendrot G, Vrielynck N, Belcram K, Rocques N, Marquez-Lema A, Bhatt AM, Horlow C, Mercier R, Mezard C, Grelon M (2005) AtREC8 and AtSCC3 are essential to the monopolar orientation of the kinetochores during meiosis. *Journal of cell science* 118: 4621-4632

Chelysheva L, Vezon D, Belcram K, Gendrot G, Grelon M (2008) The *Arabidopsis* BLAP75/Rmi1 homologue plays crucial roles in meiotic double-strand break repair. *PLoS genetics* 4: e1000309

Chelysheva L, Vezon D, Chambon A, Gendrot G, Pereira L, Lemhemdi A, Vrielynck N, Le Guin S, Novatchkova M, Grelon M (2012) The *Arabidopsis* HEI10 is a new ZMM protein related to Zip3. *PLoS genetics* 8: e1002799

Chen C, Jomaa A, Ortega J, Alani EE (2014) Pch2 is a hexameric ring ATPase that remodels the chromosome axis protein Hop1. *Proceedings of the National Academy of Sciences of the United States of America* 111: E44-53

Chen X, Cui D, Papusha A, Zhang X, Chu CD, Tang J, Chen K, Pan X, Ira G (2012) The Fun30 nucleosome remodeller promotes resection of DNA double-strand break ends. *Nature* 489: 576-580

Cheng CH, Lo YH, Liang SS, Ti SC, Lin FM, Yeh CH, Huang HY, Wang TF (2006) SUMO modifications control assembly of synaptonemal complex and polycomplex in meiosis of *Saccharomyces cerevisiae*. *Genes and Development* 20: 2067-2081

Chin GM, Villeneuve AM (2001) *C. elegans* mre-11 is required for meiotic recombination and DNA repair but is dispensable for the meiotic G(2) DNA damage checkpoint. *Genes & development* 15: 522-534

Chua PR, Roeder GS (1998) Zip2, a meiosis-specific protein required for the initiation of chromosome synapsis. *Cell* 93: 349-359

Chuang CN, Cheng YH, Wang TF (2012) Mek1 stabilizes Hop1-Thr318 phosphorylation to promote interhomolog recombination and checkpoint responses during yeast meiosis. *Nucleic acids research* 40: 11416-11427

Clerici M, Mantiero D, Lucchini G, Longhese MP (2005) The *Saccharomyces cerevisiae* Sae2 protein promotes resection and bridging of double strand break ends. *The Journal of biological chemistry* 280: 38631-38638

Cloud V, Chan YL, Grubb J, Budke B, Bishop DK (2012) Rad51 is an accessory factor for Dmc1-mediated joint molecule formation during meiosis. *Science* 337: 1222-1225

Colaiacovo MP, MacQueen AJ, Martinez-Perez E, McDonald K, Adamo A, La Volpe A, Villeneuve AM (2003) Synaptonemal complex assembly in *C. elegans* is dispensable for loading strand-exchange proteins but critical for proper completion of recombination. *Developmental cell* 5: 463-474

Cole F, Kauppi L, Lange J, Roig I, Wang R, Keeney S, Jasin M (2012) Homeostatic control of recombination is implemented progressively in mouse meiosis. *Nature cell biology* 14: 424-430

Cole F, Keeney S, Jasin M (2010) Evolutionary conservation of meiotic DSB proteins: more than just Spo11. *Genes & development* 24: 1201-1207

Colombo PC, Jones GH (1997) Chiasma interference is blind to centromeres. *Heredity* 79 (Pt 2): 214-227

Costa Y, Speed R, Ollinger R, Alsheimer M, Semple CA, Gautier P, Maratou K, Novak I, Hoog C, Benavente R, Cooke HJ (2005) Two novel proteins recruited by synaptonemal complex protein 1 (SYCP1) are at the centre of meiosis. *Journal of cell science* 118: 2755-2762

Costelloe T, Louge R, Tomimatsu N, Mukherjee B, Martini E, Khadaroo B, Dubois K, Wiegant WW, Thierry A, Burma S, van Attikum H, Llorente B (2012) The yeast Fun30 and human SMARCAD1 chromatin remodellers promote DNA end resection. *Nature* 489: 581-584

Couteau F, Belzile F, Horlow C, Grandjean O, Vezon D, Doutriaux MP (1999) Random chromosome segregation without meiotic arrest in both male and female meiocytes of a dmc1 mutant of *Arabidopsis*. *Plant Cell* 11: 1623-1634

Crismani W, Girard C, Froger N, Pradillo M, Santos JL, Chelysheva L, Copenhaver GP, Horlow C, Mercier R (2012) FANCM limits meiotic crossovers. *Science* 336: 1588-1590

Crismani W, Portemer V, Froger N, Chelysheva L, Horlow C, Vrielynck N, Mercier R (2013) MCM8 is required for a pathway of meiotic double-strand break repair independent of DMC1 in *Arabidopsis thaliana*. *PLoS genetics* 9: e1003165

Da Ines O, Abe K, Goubely C, Gallego ME, White CI (2012) Differing requirements for RAD51 and DMC1 in meiotic pairing of centromeres and chromosome arms in *Arabidopsis thaliana*. *PLoS genetics* 8: e1002636

Da Ines O, Degroote F, Amiard S, Goubely C, Gallego ME, White CI (2013a) Effects of XRCC2 and RAD51B mutations on somatic and meiotic recombination in *Arabidopsis thaliana*. *Plant J* 74: 959-970

Da Ines O, Degroote F, Goubely C, Amiard S, Gallego ME, White CI (2013b) Meiotic Recombination in *Arabidopsis* Is Catalysed by DMC1, with RAD51 Playing a Supporting Role. *PLoS genetics* 9: e1003787

Daniel K, Lange J, Hached K, Fu J, Anastassiadis K, Roig I, Cooke HJ, Stewart AF, Wassmann K, Jasin M, Keeney S, Toth A (2011) Meiotic homologue alignment and its quality surveillance are controlled by mouse HORMAD1. *Nature cell biology* 13: 599-610

Danilowicz C, Peacock-Villada A, Vlassakis J, Facon A, Feinstein E, Kleckner N, Prentiss M (2013) The differential extension in dsDNA bound to Rad51 filaments may play important roles in homology recognition and strand exchange. *Nucleic acids research*

Davis L, Rozalen AE, Moreno S, Smith GR, Martin-Castellanos C (2008) Rec25 and Rec27, novel linear-element components, link cohesin to meiotic DNA breakage and recombination. *Current biology : CB* 18: 849-854

de Boer E, Stam P, Dietrich AJ, Pastink A, Heyting C (2006) Two levels of interference in mouse meiotic recombination. *Proceedings of the National Academy of Sciences of the United States of America* 103: 9607-9612

de Jager M, van Noort J, van Gent DC, Dekker C, Kanaar R, Wyman C (2001) Human Rad50/Mre11 is a flexible complex that can tether DNA ends. *Molecular cell* 8: 1129-1135

De Muyt A, Jessop L, Kolar E, Sourirajan A, Chen J, Dayani Y, Lichten M (2012) BLM helicase ortholog Sgs1 is a central regulator of meiotic recombination intermediate metabolism. *Molecular cell* 46: 43-53

De Muyt A, Pereira L, Vezon D, Chelysheva L, Gendrot G, Chambon A, Laine-Choinard S, Pelletier G, Mercier R, Nogue F, Grelon M (2009) A high throughput genetic screen identifies new early meiotic recombination functions in *Arabidopsis thaliana*. *PLoS genetics* 5: e1000654

De Muyt A, Vezon D, Gendrot G, Gallois JL, Stevens R, Grelon M (2007) AtPRD1 is required for meiotic double strand break formation in *Arabidopsis thaliana*. *The EMBO journal* 26: 4126-4137

Dekker J, Rippe K, Dekker M, Kleckner N (2002) Capturing chromosome conformation. *Science* 295: 1306-1311

Deng Y, Guo X, Ferguson DO, Chang S (2009) Multiple roles for MRE11 at uncapped telomeres. *Nature* 460: 914-918

Dernburg AF, McDonald K, Moulder G, Barstead R, Dresser M, Villeneuve AM (1998) Meiotic recombination in *C. elegans* initiates by a conserved mechanism and is dispensable for homologous chromosome synapsis. *Cell* 94: 387-398

Doutriaux MP, Couteau F, Bergounioux C, White C (1998) Isolation and characterisation of the RAD51 and DMC1 homologs from *Arabidopsis thaliana*. *Molecular & general genetics : MGG* 257: 283-291

Drouaud J, Khademian H, Giraut L, Zanni V, Bellalou S, Henderson IR, Falque M, Mezard C (2013) Contrasted patterns of crossover and non-crossover at *Arabidopsis thaliana* meiotic recombination hotspots. *PLoS genetics* 9: e1003922

Drouaud J, Mercier R, Chelysheva L, Berard A, Falque M, Martin O, Zanni V, Brunel D, Mezard C (2007) Sex-specific crossover distributions and variations in interference level along *Arabidopsis thaliana* chromosome 4. *PLoS genetics* 3: e106

Eichinger CS, Jentsch S (2010) Synaptonemal complex formation and meiotic checkpoint signaling are linked to the lateral element protein Red1. *Proceedings of the National Academy of Sciences of the United States of America* 107: 11370-11375

Estreicher A, Lorenz A, Loidl J (2012) Mug20, a novel protein associated with linear elements in fission yeast meiosis. *Current genetics* 58: 119-127

Evans DH, Li YF, Fox ME, Smith GR (1997) A WD repeat protein, Rec14, essential for meiotic recombination in *Schizosaccharomyces pombe*. *Genetics* 146: 1253-1264

Farah JA, Cromie GA, Smith GR (2009) Ctp1 and Exonuclease 1, alternative nucleases regulated by the MRN complex, are required for efficient meiotic recombination. *Proceedings of the National Academy of Sciences of the United States of America* 106: 9356-9361

Farmer S, Hong EJ, Leung WK, Argunhan B, Terentyev Y, Humphryes N, Toyoizumi H, Tsubouchi H (2012) Budding yeast Pch2, a widely conserved meiotic protein, is involved in the initiation of meiotic recombination. *PloS one* 7: e39724

Ferdous M, Higgins JD, Osman K, Lambing C, Roitinger E, Mechtler K, Armstrong SJ, Perry R, Pradillo M, Cunado N, Franklin FC (2012) Inter-homolog crossing-over and synapsis in *Arabidopsis* meiosis are dependent on the chromosome axis protein AtASY3. *PLoS genetics* 8: e1002507

Ferrari SR, Grubb J, Bishop DK (2009) The Mei5-Sae3 protein complex mediates Dmc1 activity in *Saccharomyces cerevisiae*. *The Journal of biological chemistry* 284: 11766-11770

Foss E, Lande R, Stahl FW, Steinberg CM (1993) Chiasma interference as a function of genetic distance. *Genetics* 133: 681-691

Fowler KR, Gutierrez-Velasco S, Martin-Castellanos C, Smith GR (2013) Protein determinants of meiotic DNA break hot spots. *Molecular cell* 49: 983-996

Franklin FC, Higgins JD, Sanchez-Moran E, Armstrong SJ, Osman KE, Jackson N, Jones GH (2006) Control of meiotic recombination in *Arabidopsis*: role of the MutL and MutS homologues. *Biochemical Society transactions* 34: 542-544

Fukuda T, Daniel K, Wojtasz L, Toth A, Hoog C (2010) A novel mammalian HORMA domain-containing protein, HORMAD1, preferentially associates with unsynapsed meiotic chromosomes. *Experimental cell research* 316: 158-171

Fukuda T, Pratto F, Schimenti JC, Turner JMA, Camerini-Otero RD, Hoog C (2012) Phosphorylation of Chromosome Core Components May Serve as Axis Marks for the Status of Chromosomal Events during Mammalian Meiosis. *PLoS genetics* 8

Fung JC, Rockmill B, Odell M, Roeder GS (2004) Imposition of crossover interference through the nonrandom distribution of synapsis initiation complexes. *Cell* 116: 795-802

Furuse M, Nagase Y, Tsubouchi H, Murakami-Murofushi K, Shibata T, Ohta K (1998) Distinct roles of two separable in vitro activities of yeast Mre11 in mitotic and meiotic recombination. *The EMBO journal* 17: 6412-6425

Garcia-Cruz R, Brieno MA, Roig I, Grossmann M, Velilla E, Pujol A, Cabero L, Pessarrodona A, Barbero JL, Garcia Caldes M (2010a) Dynamics of cohesin proteins REC8, STAG3, SMC1 beta and SMC3 are consistent with a role in sister chromatid cohesion during meiosis in human oocytes. *Hum Reprod* 25: 2316-2327

Garcia-Cruz R, Casanovas A, Brieno-Enriquez M, Robles P, Roig I, Pujol A, Cabero L, Durban M, Garcia Caldes M (2010b) Cytogenetic analyses of human oocytes provide new data on non-disjunction mechanisms and the origin of trisomy 16. *Hum Reprod* 25: 179-191

Garcia V, Phelps SE, Gray S, Neale MJ (2011) Bidirectional resection of DNA double-strand breaks by Mre11 and Exo1. *Nature* 479: 241-244

Gerecke EE, Zolan ME (2000) An mre11 mutant of *Coprinus cinereus* has defects in meiotic chromosome pairing, condensation and synapsis. *Genetics* 154: 1125-1139

Giraut L, Falque M, Drouaud J, Pereira L, Martin OC, Mezard C (2011) Genome-wide crossover distribution in *Arabidopsis thaliana* meiosis reveals sex-specific patterns along chromosomes. *PLoS genetics* 7: e1002354

Gladstone MN, Obeso D, Chuong H, Dawson DS (2009) The synaptonemal complex protein Zip1 promotes bi-orientation of centromeres at meiosis I. *PLoS genetics* 5: e1000771

Glynn EF, Megee PC, Yu HG, Mistrot C, Unal E, Koshland DE, DeRisi JL, Gerton JL (2004) Genome-wide mapping of the cohesin complex in the yeast *Saccharomyces cerevisiae*. *PLoS biology* 2: E259

Goedecke W, Eijpe M, Offenberg HH, van Aalderen M, Heyting C (1999) Mre11 and Ku70 interact in somatic cells, but are differentially expressed in early meiosis. *Nature Genetics* 23: 194-198

Goldfarb T, Lichten M (2010) Frequent and efficient use of the sister chromatid for DNA double-strand break repair during budding yeast meiosis. *PLoS biology* 8: e1000520

Goldstein P (1997) The synaptonemal complexes of the nematode *Caenorhabditis elegans*: gametic response to retinol. *Cytobios* 91: 53-67

Golubovskaya IN, Wang CJ, Timofejeva L, Cande WZ (2011) Maize meiotic mutants with improper or non-homologous synapsis due to problems in pairing or synaptonemal complex formation. *Journal of experimental botany* 62: 1533-1544

Grabarz A, Barascu A, Guirouilh-Barbat J, Lopez BS (2012) Initiation of DNA double strand break repair: signaling and single-stranded resection dictate the choice between homologous recombination, non-homologous end-joining and alternative end-joining. *American journal of cancer research* 2: 249-268

Grelon M, Vezon D, Gendrot G, Pelletier G (2001) AtSPO11-1 is necessary for efficient meiotic recombination in plants. *The EMBO journal* 20: 589-600

Grey C, Baudat F, de Massy B (2009) Genome-wide control of the distribution of meiotic recombination. *PLoS biology* 7: e35

Guiraldelli MF, Eyster C, Wilkerson JL, Dresser ME, Pezza RJ (2013) Mouse HFM1/Mer3 is required for crossover formation and complete synapsis of homologous chromosomes during meiosis. *PLoS genetics* 9: e1003383

Hamer G, Gell K, Kouznetsova A, Novak I, Benavente R, Hoog C (2006) Characterization of a novel meiosis-specific protein within the central element of the synaptonemal complex. *Journal of cell science* 119: 4025-4032

Hartung F, Puchta H (2000) Molecular characterisation of two paralogous SPO11 homologues in *Arabidopsis thaliana*. *Nucleic acids research* 28: 1548-1554

Hartung F, Puchta H (2001) Molecular characterization of homologues of both subunits A (SPO11) and B of the archaebacterial topoisomerase 6 in plants. *Gene* 271: 81-86

Hartung F, Suer S, Knoll A, Wurz-Wildersinn R, Puchta H (2008) Topoisomerase 3alpha and RMI1 suppress somatic crossovers and are essential for resolution of meiotic recombination intermediates in *Arabidopsis thaliana*. *PLoS genetics* 4: e1000285

Hartung F, Wurz-Wildersinn R, Fuchs J, Schubert I, Suer S, Puchta H (2007) The catalytically active tyrosine residues of both SPO11-1 and SPO11-2 are required for meiotic double-strand break induction in *Arabidopsis*. *Plant Cell* 19: 3090-3099

Hawley RS (2011) Solving a meiotic LEGO puzzle: transverse filaments and the assembly of the synaptonemal complex in *Caenorhabditis elegans*. *Genetics* 189: 405-409

Hayase A, Takagi M, Miyazaki T, Oshiumi H, Shinohara M, Shinohara A (2004) A protein complex containing Mei5 and Sae3 promotes the assembly of the meiosis-specific RecA homolog Dmc1. *Cell* 119: 927-940

Henderson KA, Kee K, Maleki S, Santini PA, Keeney S (2006) Cyclin-dependent kinase directly regulates initiation of meiotic recombination. *Cell* 125: 1321-1332

Henderson KA, Keeney S (2004) Tying synaptonemal complex initiation to the formation and programmed repair of DNA double-strand breaks. *Proceedings of the National Academy of Sciences of the United States of America* 101: 4519-4524

Henzel JV, Nabeshima K, Schvarzstein M, Turner BE, Villeneuve AM, Hillers KJ (2011) An asymmetric chromosome pair undergoes synaptic adjustment and crossover redistribution during *Caenorhabditis elegans* meiosis: implications for sex chromosome evolution. *Genetics* 187: 685-699

Heyer WD (2004) Recombination: Holliday junction resolution and crossover formation. *Current biology : CB* 14: R56-58

Higgins JD, Armstrong SJ, Franklin FC, Jones GH (2004) The *Arabidopsis* MutS homolog AtMSH4 functions at an early step in recombination: evidence for two classes of recombination in *Arabidopsis*. *Genes & development* 18: 2557-2570

Higgins JD, Buckling EF, Franklin FC, Jones GH (2008a) Expression and functional analysis of AtMUS81 in *Arabidopsis* meiosis reveals a role in the second pathway of crossing-over. *Plant J* 54: 152-162

Higgins JD, Perry RM, Barakate A, Ramsay L, Waugh R, Halpin C, Armstrong SJ, Franklin FC (2012) Spatiotemporal asymmetry of the meiotic program underlies the predominantly distal distribution of meiotic crossovers in barley. *Plant Cell* 24: 4096-4109

Higgins JD, Sanchez-Moran E, Armstrong SJ, Jones GH, Franklin FC (2005) The *Arabidopsis* synaptonemal complex protein ZYP1 is required for chromosome synapsis and normal fidelity of crossing over. *Genes & development* 19: 2488-2500

Higgins JD, Vignard J, Mercier R, Pugh AG, Franklin FC, Jones GH (2008b) AtMSH5 partners AtMSH4 in the class I meiotic crossover pathway in *Arabidopsis thaliana*, but is not required for synapsis. *Plant J* 55: 28-39

Ho HC, Burgess SM (2011) Pch2 acts through Xrs2 and Tel1/ATM to modulate interhomolog bias and checkpoint function during meiosis. *PLoS genetics* 7: e1002351

Hollingsworth NM, Brill SJ (2004) The Mus81 solution to resolution: generating meiotic crossovers without Holliday junctions. *Genes & development* 18: 117-125

Hollingsworth NM, Ponte L (1997) Genetic interactions between HOP1, RED1 and MEK1 suggest that MEK1 regulates assembly of axial element components during meiosis in the yeast *Saccharomyces cerevisiae*. *Genetics* 147: 33-42

Holloway JK, Booth J, Edelmann W, McGowan CH, Cohen PE (2008) MUS81 generates a subset of MLH1-MLH3-independent crossovers in mammalian meiosis. *PLoS genetics* 4: e1000186

Hong S, Sung Y, Yu M, Lee M, Kleckner N, Kim KP (2013) The logic and mechanism of homologous recombination partner choice. *Molecular cell* 51: 440-453

Honigberg SM, Esposito RE (1994) Reversal of Cell Determination in Yeast Meiosis - Postcommitment Arrest Allows Return to Mitotic Growth. *Proceedings of the National Academy of Sciences of the United States of America* 91: 6559-6563

Hopfner KP, Craig L, Moncalian G, Zinkel RA, Usui T, Owen BA, Karcher A, Henderson B, Bodmer JL, McMurray CT, Carney JP, Petrini JH, Tainer JA (2002) The Rad50 zinc-hook is a structure joining Mre11 complexes in DNA recombination and repair. *Nature* 418: 562-566

Hosoya N, Okajima M, Kinomura A, Fujii Y, Hiyama T, Sun J, Tashiro S, Miyagawa K (2012) Synaptonemal complex protein SYCP3 impairs mitotic recombination by interfering with BRCA2. *EMBO reports* 13: 44-51

Howard-Till RA, Lukaszewicz A, Novatchkova M, Loidl J (2013) A single cohesin complex performs mitotic and meiotic functions in the protist tetrahymena. *PLoS genetics* 9: e1003418

Hulten MA (2011) On the origin of crossover interference: A chromosome oscillatory movement (COM) model. *Molecular cytogenetics* 4: 10

Humphryes N, Leung WK, Argunhan B, Terentyev Y, Dvorackova M, Tsubouchi H (2013) The Ecm11-Gmc2 complex promotes synaptonemal complex formation through assembly of transverse filaments in budding yeast. *PLoS genetics* 9: e1003194

Hunter N, Kleckner N (2001) The single-end invasion: an asymmetric intermediate at the double-strand break to double-holliday junction transition of meiotic recombination. *Cell* 106: 59-70

Ianzini F, Kosmacek EA, Nelson ES, Napoli E, Erenpreisa J, Kalejs M, Mackey MA (2009) Activation of meiosis-specific genes is associated with depolyploidization of human tumor cells following radiation-induced mitotic catastrophe. *Cancer research* 69: 2296-2304

Ishiguro T, Tanaka K, Sakuno T, Watanabe Y (2010) Shugoshin-PP2A counteracts casein-kinase-1-dependent cleavage of Rec8 by separase. *Nature cell biology* 12: 500-506

Jackson N, Sanchez-Moran E, Buckling E, Armstrong SJ, Jones GH, Franklin FC (2006) Reduced meiotic crossovers and delayed prophase I progression in AtMLH3-deficient *Arabidopsis*. *The EMBO journal* 25: 1315-1323

Jessop L, Lichten M (2008) Mus81/Mms4 endonuclease and Sgs1 helicase collaborate to ensure proper recombination intermediate metabolism during meiosis. *Molecular cell* 31: 313-323

Ji J, Tang D, Wang K, Wang M, Che L, Li M, Cheng Z (2012) The role of OsCOM1 in homologous chromosome synapsis and recombination in rice meiosis. *Plant J* 72: 18-30

John B (1990) *Meiosis*, Cambridge England ; New York: Cambridge University Press.

Johzuka K, Ogawa H (1995) Interaction of Mre11 and Rad50: two proteins required for DNA repair and meiosis-specific double-strand break formation in *Saccharomyces cerevisiae*. *Genetics* 139: 1521-1532

Jolivet S, Vezon D, Froger N, Mercier R (2006) Non conservation of the meiotic function of the Ski8/Rec103 homolog in *Arabidopsis*. *Genes to cells : devoted to molecular & cellular mechanisms* 11: 615-622

Jones GH, Franklin FC (2006) Meiotic crossing-over: obligation and interference. *Cell* 126: 246-248

Joshi N, Barot A, Jamison C, Borner GV (2009) Pch2 links chromosome axis remodeling at future crossover sites and crossover distribution during yeast meiosis. *PLoS genetics* 5: e1000557

Joyce EF, Pedersen M, Tiong S, White-Brown SK, Paul A, Campbell SD, McKim KS (2011) Drosophila ATM and ATR have distinct activities in the regulation of meiotic DNA damage and repair. *J Cell Biol* 195: 359-367

Kalejs M, Ivanov A, Plakhins G, Cragg MS, Emzinsh D, Illidge TM, Erenpreisa J (2006) Upregulation of meiosis-specific genes in lymphoma cell lines following genotoxic insult and induction of mitotic catastrophe. *BMC cancer* 6: 6

Kalocsay M, Hiller NJ, Jentsch S (2009) Chromosome-wide Rad51 spreading and SUMO-H2A.Z-dependent chromosome fixation in response to a persistent DNA double-strand break. *Molecular cell* 33: 335-343

Kan FL, Davidson MK, Wahls WP (2011) Meiotic recombination protein Rec12: functional conservation, crossover homeostasis and early crossover/non-crossover decision. *Nucleic acids research* 39: 1460-1472

Kassir Y, Granot D, Simchen G (1988) IME1, a positive regulator gene of meiosis in *S. cerevisiae*. *Cell* 52: 853-862

Kauppi L, Barchi M, Lange J, Baudat F, Jasin M, Keeney S (2013) Numerical constraints and feedback control of double-strand breaks in mouse meiosis. *Genes & development* 27: 873-886

Kaye JA, Melo JA, Cheung SK, Vaze MB, Haber JE, Toczyski DP (2004) DNA breaks promote genomic instability by impeding proper chromosome segregation. *Current biology : CB* 14: 2096-2106

Kee K, Protacio RU, Arora C, Keeney S (2004) Spatial organization and dynamics of the association of Rec102 and Rec104 with meiotic chromosomes. *The EMBO journal* 23: 1815-1824

Keeney S (2008) Spo11 and the Formation of DNA Double-Strand Breaks in Meiosis. *Genome dynamics and stability* 2: 81-123

Keeney S, Giroux CN, Kleckner N (1997) Meiosis-specific DNA double-strand breaks are catalyzed by Spo11, a member of a widely conserved protein family. *Cell* 88: 375-384

Kim KP, Weiner BM, Zhang L, Jordan A, Dekker J, Kleckner N (2010) Sister cohesion and structural axis components mediate homolog bias of meiotic recombination. *Cell* 143: 924-937

King JS, Mortimer RK (1990) A polymerization model of chiasma interference and corresponding computer simulation. *Genetics* 126: 1127-1138

Kleckner N (2006) Chiasma formation: chromatin/axis interplay and the role(s) of the synaptonemal complex. *Chromosoma* 115: 175-194

Kleckner N, Storlazzi A, Zickler D (2003) Coordinate variation in meiotic pachytene SC length and total crossover/chiasma frequency under conditions of constant DNA length. *Trends in genetics : TIG* 19: 623-628

Kleckner N, Zickler D, Jones GH, Dekker J, Padmore R, Henle J, Hutchinson J (2004) A mechanical basis for chromosome function. *Proceedings of the National Academy of Sciences of the United States of America* 101: 12592-12597

Kneitz B, Cohen PE, Avdievich E, Zhu L, Kane MF, Hou H Jr, Kolodner RD, Kucherlapati R, Pollard JW, Edelmann W (2000) MutS homolog 4 localization to meiotic chromosomes is required for chromosome pairing during meiosis in male and female mice. *Genes and Development* 14: 1085-1097.

Knoll A, Higgins JD, Seeliger K, Reha SJ, Dangel NJ, Bauknecht M, Schropfer S, Franklin FC, Puchta H (2012) The Fanconi anemia ortholog FANCM ensures ordered homologous recombination in both somatic and meiotic cells in *Arabidopsis*. *Plant Cell* 24: 1448-1464

Koehler KE, Hawley RS, Sherman S, Hassold T (1996) Recombination and nondisjunction in humans and flies. *Human molecular genetics* 5 Spec No: 1495-1504

Kogo H, Tsutsumi M, Ohye T, Inagaki H, Abe T, Kurahashi H (2012) HORMAD1-dependent checkpoint/surveillance mechanism eliminates asynaptic oocytes. *Genes to cells : devoted to molecular & cellular mechanisms* 17: 439-454

Kohli J, Bahler J (1994) Homologous Recombination in Fission Yeast - Absence of Crossover Interference and Synaptonemal Complex. *Experientia* 50: 295-306

Kotwaliwale CV (2012) Robustness in crossover regulation during meiosis. *Nature cell biology* 14: 335-337

Kudo NR, Wassmann K, Anger M, Schuh M, Wirth KG, Xu H, Helmhart W, Kudo H, McKay M, Maro B, Ellenberg J, de Boer P, Nasmyth K (2006) Resolution of chiasmata in oocytes requires separase-mediated proteolysis. *Cell* 126: 135-146

Kumar R, Bourbon HM, de Massy B (2010) Functional conservation of Mei4 for meiotic DNA double-strand break formation from yeasts to mice. *Genes & development* 24: 1266-1280

Kurzbauer MT, Uanschou C, Chen D, Schlogelhofer P (2012) The recombinases DMC1 and RAD51 are functionally and spatially separated during meiosis in *Arabidopsis. Plant Cell* 24: 2058-2070

Lacefield S and Murray AW (2007) The spindle checkpoint rescues the meiotic segregation of chromosomes whose crossovers are far from the centromere. *Nature Genetics* 39: 1273-1277

Lai YJ, Lin FM, Chuang MJ, Shen HJ, Wang TF (2011) Genetic Requirements and Meiotic Function of Phosphorylation of the Yeast Axial Element Protein Red1. *Molecular and cellular biology* 31: 912-923

Lake CM, Hawley RS (2013) RNF212 marks the spot. *Nature genetics* 45: 228-229

Lam WS, Yang X, Makaroff CA (2005) Characterization of *Arabidopsis thaliana* SMC1 and SMC3: evidence that AtSMC3 may function beyond chromosome cohesion. *Journal of cell science* 118: 3037-3048

Lammers JH, Offenberg HH, van Aalderen M, Vink AC, Dietrich AJ, Heyting C (1994) The gene encoding a major component of the lateral elements of synaptonemal complexes of the rat is related to X-linked lymphocyte-regulated genes. *Molecular and cellular biology* 14: 1137-1146

Lange J, Pan J, Cole F, Thelen MP, Jasin M, Keeney S (2011) ATM controls meiotic double-strand-break formation. *Nature* 479: 237-240

Langerak P, Mejia-Ramirez E, Limbo O, Russell P (2011) Release of Ku and MRN from DNA ends by Mre11 nuclease activity and Ctp1 is required for homologous recombination repair of double-strand breaks. *PLoS genetics* 7: e1002271

Lao JP, Cloud V, Huang CC, Grubb J, Thacker D, Lee CY, Dresser ME, Hunter N, Bishop DK (2013) Meiotic crossover control by concerted action of rad51-dmc1 in homolog template bias and robust homeostatic regulation. *PLoS genetics* 9: e1003978

Latypov V, Rothenberg M, Lorenz A, Octobre G, Csutak O, Lehmann E, Loidl J, Kohli J (2010) Roles of Hop1 and Mek1 in meiotic chromosome pairing and recombination partner choice in *Schizosaccharomyces pombe*. *Molecular and cellular biology* 30: 1570-1581

Lemmens BB, Johnson NM, Tijsterman M (2013) COM-1 promotes homologous recombination during *Caenorhabditis elegans* meiosis by antagonizing Ku-mediated non-homologous end joining. *Plos genetics* 9: e1003276.

Lengsfeld BM, Rattray AJ, Bhaskara V, Ghirlando R, Paull TT (2007) Sae2 is an endonuclease that processes hairpin DNA cooperatively with the Mre11/Rad50/Xrs2 complex. *Molecular cell* 28: 638-651

Li J, Hooker GW, Roeder GS (2006) Saccharomyces cerevisiae Mer2, Mei4 and Rec114 form a complex required for meiotic double-strand break formation. *Genetics* 173: 1969-1981

Li W, Chen C, Markmann-Mulisch U, Timofejeva L, Schmelzer E, Ma H, Reiss B (2004) The *Arabidopsis* AtRAD51 gene is dispensable for vegetative development but required for meiosis. *Proceedings of the National Academy of Sciences of the United States of America* 101: 10596-10601

Li XC, Schimenti JC (2007) Mouse pachytene checkpoint 2 (trip13) is required for completing meiotic recombination but not synapsis. *PLoS genetics* 3: e130

Libuda DE, Uzawa S, Meyer BJ, Villeneuve AM (2013) Meiotic chromosome structures constrain and respond to designation of crossover sites. *Nature*

Liu JG, Yuan L, Brundell E, Bjorkroth B, Daneholt B, Hoog C (1996) Localization of the N-terminus of SCP1 to the central element of the synaptonemal complex and evidence for direct interactions between the N-termini of SCP1 molecules organized head-to-head. *Experimental cell research* 226: 11-19

Liu Y, Deng Y, Li G, Zhao J (2012) Replication factor C1 (RFC1) is required for double-strand break repair during meiotic homologous recombination in *Arabidopsis*. *Plant J*

Llano E, Herran Y, Garcia-Tunon I, Gutierrez-Caballero C, de Alava E, Barbero JL, Schimenti J, de Rooij DG, Sanchez-Martin M, Pendas AM (2012) Meiotic cohesin complexes are essential for the formation of the axial element in mice. *J Cell Biol* 197: 877-885

Lo YH, Chuang CN, Wang TF (2014) Pch2 prevents mec1/tel1-mediated hop1 phosphorylation occurring independently of red1 in budding yeast meiosis. *PloS one* 9: e85687

Lobachev K, Vitriol E, Stemple J, Resnick MA, Bloom K (2004) Chromosome fragmentation after induction of a double-strand break is an active process prevented by the RMX repair complex. *Current biology : CB* 14: 2107-2112

Loidl J, Scherthan H (2004) Organization and pairing of meiotic chromosomes in the ciliate *Tetrahymena thermophila*. *Journal of cell science* 117: 5791-5801

Lorenz A, Osman F, Sun W, Nandi S, Steinacher R, Whitby MC (2012) The fission yeast FANCM ortholog directs non-crossover recombination during meiosis. *Science* 336: 1585-1588

Lorenz A, Wells JL, Pryce DW, Novatchkova M, Eisenhaber F, McFarlane RJ, Loidl J (2004a) S-pombe meiotic linear elements contain proteins related to synaptonemal complex components. *Journal of cell science* 117: 3343-3351

Lorenz A, Wells JL, Pryce DW, Novatchkova M, Eisenhaber F, McFarlane RJ, Loidl J (2004b) *S. pombe* meiotic linear elements contain proteins related to synaptonemal complex components. *Journal of cell science* 117: 3343-3351

Lukas J, Lukas C, Bartek J (2011) More than just a focus: The chromatin response to DNA damage and its role in genome integrity maintenance. *Nature cell biology* 13: 1161-1169

Luo Q, Tang D, Wang M, Luo W, Zhang L, Qin B, Shen Y, Wang K, Li Y, Cheng Z (2013) The role of OsMSH5 in crossover formation during rice meiosis. *Molecular plant* 6: 729-742

MacQueen AJ, Colaiacovo MP, McDonald K, Villeneuve AM (2002) Synapsis-dependent and -independent mechanisms stabilize homolog pairing during meiotic prophase in *C. elegans*. *Genes & development* 16: 2428-2442

Macqueen AJ, Roeder GS (2009) Fpr3 and Zip3 ensure that initiation of meiotic recombination precedes chromosome synapsis in budding yeast. *Current biology : CB* 19: 1519-1526

Maleki S, Neale MJ, Arora C, Henderson KA, Keeney S (2007) Interactions between Mei4, Rec114, and other proteins required for meiotic DNA double-strand break formation in *Saccharomyces cerevisiae*. *Chromosoma* 116: 471-486

Malik SB, Ramesh MA, Hulstrand AM, Logsdon JM, Jr. (2007) Protist homologs of the meiotic Spo11 gene and topoisomerase VI reveal an evolutionary history of gene duplication and lineage-specific loss. *Molecular biology and evolution* 24: 2827-2841

Mallela S, Latypov V, Kohli J (2011) Rec10- and Rec12-independent recombination in meiosis of *Schizosaccharomyces pombe*. *Yeast* 28: 405-421

Manfrini N, Guerini I, Citterio A, Lucchini G, Longhese MP (2010) Processing of meiotic DNA double strand breaks requires cyclin-dependent kinase and multiple nucleases. *The Journal of biological chemistry* 285: 11628-11637

Mankouri HW, Huttner D, Hickson ID (2013) How unfinished business from S-phase affects mitosis and beyond. *The EMBO journal* 32: 2661-2671

Martinez-Perez E, Schvarzstein M, Barroso C, Lightfoot J, Dernburg AF, Villeneuve AM (2008) Crossovers trigger a remodeling of meiotic chromosome axis composition that is linked to two-step loss of sister chromatid cohesion. *Genes & development* 22: 2886-2901

Martini E, Diaz RL, Hunter N, Keeney S (2006) Crossover homeostasis in yeast meiosis. *Cell* 126: 285-295

Mason JM, Arndt KM (2004) Coiled coil domains: Stability, specificity, and biological implications. *Chembiochem* 5: 170-176

Matos J, Blanco MG, Maslen S, Skehel JM, West SC (2011) Regulatory control of the resolution of DNA recombination intermediates during meiosis and mitosis. *Cell* 147: 158-172

Mazina OM, Mazin AV, Nakagawa T, Kolodner RD, Kowalczykowski SC (2004) *Saccharomyces cerevisiae* Mer3 helicase stimulates 3'-5' heteroduplex extension by Rad51; implications for crossover control in meiotic recombination. *Cell* 117: 47-56

McKim KS, Green-Marroquin BL, Sekelsky JJ, Chin G, Steinberg C, Khodosh R, Hawley RS (1998) Meiotic synapsis in the absence of recombination. *Science* 279: 876-878

McMahill MS, Sham CW, Bishop DK (2007) Synthesis-dependent strand annealing in meiosis. *PLoS biology* 5: e299

Mercier R, Jolivet S, Vezon D, Huppe E, Chelysheva L, Giovanni M, Nogue F, Doutriaux MP, Horlow C, Grelon M, Mezard C (2005) Two meiotic crossover classes cohabit in *Arabidopsis*: one is dependent on MER3,whereas the other one is not. *Current biology : CB* 15: 692-701

Merino ST, Cummings WJ, Acharya SN, Zolan ME (2000) Replication-dependent early meiotic requirement for Spo11 and Rad50. *Proceedings of the National Academy of Sciences of the United States of America* 97: 10477-10482

Mets DG, Meyer BJ (2009) Condensins Regulate Meiotic DNA Break Distribution, thus Crossover Frequency, by Controlling Chromosome Structure. *Cell* 139: 73-86

Miao C, Tang D, Zhang H, Wang M, Li Y, Tang S, Yu H, Gu M, Cheng Z (2013) Central region component1, a novel synaptonemal complex component, is essential for meiotic recombination initiation in rice. *Plant Cell* 25: 2998-3009

Milman N, Higuchi E, Smith GR (2009) Meiotic DNA double-strand break repair requires two nucleases, MRN and Ctp1, to produce a single size class of Rec12 (Spo11)-oligonucleotide complexes. *Molecular and cellular biology* 29: 5998-6005

Mimitou EP, Symington LS (2010) Ku prevents Exo1 and Sgs1-dependent resection of DNA ends in the absence of a functional MRX complex or Sae2. *The EMBO journal* 29: 3358-3369

Mimitou EP, Symington LS (2011) DNA end resection--unraveling the tail. *DNA repair* 10: 344-348

Mockel C, Lammens K, Schele A, Hopfner KP (2012) ATP driven structural changes of the bacterial Mre11:Rad50 catalytic head complex. *Nucleic acids research* 40: 914-927

Moens PB, Pearlman RE (1988) Chromatin organization at meiosis. *BioEssays* 9: 151-153

Morozumi Y, Ino R, Takaku M, Hosokawa M, Chuma S, Kurumizaka H (2012) Human PSF concentrates DNA and stimulates duplex capture in DMC1-mediated homologous pairing. *Nucleic acids research* 40: 3031-3041

Murakami H, Nurse P (2001) Regulation of premeiotic S phase and recombination-related double-strand DNA breaks during meiosis in fission yeast. *Nature genetics* 28: 290-293

Nakagawa T, Flores-Rozas H, Kolodner RD (2001) The MER3 helicase involved in meiotic crossing over is stimulated by single-stranded DNA-binding proteins and unwinds DNA in the 3' to 5' direction. *The Journal of biological chemistry* 276: 31487-31493

Nakagawa T, Kolodner RD (2002a) The MER3 DNA helicase catalyzes the unwinding of holliday junctions. *The Journal of biological chemistry* 277: 28019-28024

Nakagawa T, Kolodner RD (2002b) *Saccharomyces cerevisiae* Mer3 is a DNA helicase involved in meiotic crossing over. *Molecular and cellular biology* 22: 3281-3291

Naumova N, Imakaev M, Fudenberg G, Zhan Y, Lajoie BR, Mirny LA, Dekker J (2013) Organization of the mitotic chromosome. *Science* 342: 948-953

Neale MJ, Pan J, Keeney S (2005) Endonucleolytic processing of covalent protein-linked DNA double-strand breaks. *Nature* 436: 1053-1057

Newnham L, Jordan P, Rockmill B, Roeder GS, Hoffmann E (2010) The synaptonemal complex protein, Zip1, promotes the segregation of nonexchange chromosomes at meiosis I. *Proceedings of the National Academy of Sciences of the United States of America* 107: 781-785

Nimonkar AV, Dombrowski CC, Siino JS, Stasiak AZ, Stasiak A, Kowalczykowski SC (2012) *Saccharomyces cerevisiae* Dmc1 and Rad51 proteins preferentially function with Tid1 and Rad54 proteins, respectively, to promote DNA strand invasion during genetic recombination. *The Journal of biological chemistry* 287: 28727-28737

Nishant KT, Chen C, Shinohara M, Shinohara A, Alani E (2010) Genetic analysis of baker's yeast Msh4-Msh5 reveals a threshold crossover level for meiotic viability. *PLoS genetics* 6

Nishant KT, Plys AJ, Alani E (2008) A mutation in the putative MLH3 endonuclease domain confers a defect in both mismatch repair and meiosis in *Saccharomyces cerevisiae*. *Genetics* 179: 747-755

Nishino T, Komori K, Ishino Y, Morikawa K (2005) Structural and functional analyses of an archaeal XPF/Rad1/Mus81 nuclease: asymmetric DNA binding and cleavage mechanisms. *Structure* 13: 1183-1192

Niu H, Wan L, Baumgartner B, Schaefer D, Loidl J, Hollingsworth NM (2005) Partner choice during meiosis is regulated by Hop1-promoted dimerization of Mek1. *Molecular biology of the cell* 16: 5804-5818

Niu HY, Wan L, Busygina V, Kwon Y, Allen JA, Li X, Kunz RC, Kubota K, Wang B, Sung P, Shokat KM, Gygi SP, Hollingsworth NM (2009) Regulation of Meiotic Recombination via Mek1-Mediated Rad54 Phosphorylation. *Molecular cell* 36: 393-404

Nonomura K, Nakano M, Fukuda T, Eiguchi M, Miyao A, Hirochika H, Kurata N (2004) The novel gene HOMOLOGOUS PAIRING ABERRATION IN RICE MEIOSIS1 of rice encodes a putative coiled-coil protein required for homologous chromosome pairing in meiosis. *Plant Cell* 16: 1008-1020

Obeso D, Dawson DS (2010) Temporal characterization of homology-independent centromere coupling in meiotic prophase. *PloS one* 5: e10336

Oh SD, Lao JP, Taylor AF, Smith GR, Hunter N (2008) RecQ helicase, Sgs1, and XPF family endonuclease, Mus81-Mms4, resolve aberrant joint molecules during meiotic recombination. *Molecular cell* 31: 324-336

Ollinger R, Alsheimer M, Benavente R (2005) Mammalian protein SCP1 forms synaptonemal complex-like structures in the absence of meiotic chromosomes. *Molecular biology of the cell* 16: 212-217

Osman K, Higgins JD, Sanchez-Moran E, Armstrong SJ, Franklin FC (2011) Pathways to meiotic recombination in *Arabidopsis thaliana*. *The New phytologist* 190: 523-544

Padmore R, Cao L, Kleckner N (1991) Temporal comparison of recombination and synaptonemal complex formation during meiosis in *S. cerevisiae*. *Cell* 66: 1239-1256

Page SL, Hawley RS (2003) Chromosome choreography: The meiotic ballet. *Science* 301: 785-789

Panizza S, Mendoza MA, Berlinger M, Huang L, Nicolas A, Shirahige K, Klein F (2011) Spo11-accessory proteins link double-strand break sites to the chromosome axis in early meiotic recombination. *Cell* 146: 372-383

Parvanov ED, Ng SH, Petkov PM, Paigen K (2009) Trans-regulation of mouse meiotic recombination hotspots by Rcr1. *PLoS biology* 7: e36

Perry J, Kleckner N, Borner GV (2005) Bioinformatic analyses implicate the collaborating meiotic crossover/chiasma proteins Zip2, Zip3, and Spo22/Zip4 in ubiquitin labeling. *Proceedings of the National Academy of Sciences of the United States of America* 102: 17594-17599

Pezza RJ, Camerini-Otero RD, Bianco PR (2010) Hop2-Mnd1 condenses DNA to stimulate the synapsis phase of DNA strand exchange. *Biophysical journal* 99: 3763-3772

Pezza RJ, Voloshin ON, Vanevski F, Camerini-Otero RD (2007) Hop2/Mnd1 acts on two critical steps in Dmc1-promoted homologous pairing. *Genes & development* 21: 1758-1766

Pezza RJ, Voloshin ON, Volodin AA, Boateng KA, Bellani MA, Mazin AV, Camerini-Otero RD (2013) The dual role of HOP2 in mammalian meiotic homologous recombination. *Nucleic acids research*

Pittman DL, Cobb J, Schimenti KJ, Wilson LA, Cooper DM, Brignull E, Handel MA, Schimenti JC (1998) Meiotic prophase arrest with failure of chromosome synapsis in mice deficient for Dmc1, a germline-specific RecA homolog. *Molecular cell* 1: 697-705

Pradillo M, Lopez E, Romero C, Sanchez-Moran E, Cunado N, Santos JL (2007) An analysis of univalent segregation in meiotic mutants of *Arabidopsis thaliana*: a possible role for synaptonemal complex. *Genetics* 175: 505-511

Prieler S, Penkner A, Borde V, Klein F (2005) The control of Spo11's interaction with meiotic recombination hotspots. *Genes & development* 19: 255-269

Puizina J, Siroky J, Mokros P, Schweizer D, Riha K (2004) Mre11 deficiency in *Arabidopsis* is associated with chromosomal instability in somatic cells and Spo11-dependent genome fragmentation during meiosis. *Plant Cell* 16: 1968-1978

Qiao H, Prasada Rao HB, Yang Y, Fong JH, Cloutier JM, Deacon DC, Nagel KE, Swartz RK, Strong E, Holloway JK, Cohen PE, Schimenti J, Ward J, Hunter N (2014) Antagonistic roles of ubiquitin ligase HEI10 and SUMO ligase RNF212 regulate meiotic recombination. *Nature genetics* 46: 194-199

Qiao HY, Chen JK, Reynolds A, Hoog C, Paddy M, Hunter N (2012) Interplay between Synaptonemal Complex, Homologous Recombination, and Centromeres during Mammalian Meiosis. *PLoS genetics* 8

Ranjha L, Anand R, Cejka P (2014) The *Saccaromyces cerevisiae* Mlh1-Mlh3 heterodimer is an endonuclease that preferentially binds to Holliday junctions. *The Journal of biological chemistry*

Rasmussen SW (1976) The meotic prophase in *Bombyx mori* females analyzed by three dimensional reconstructions of synaptonemal complexes. *Chromosoma* 54: 245-293

Rattner JB, Goldsmith MR, Hamkalo BA (1981) Chromosome organization during male meiosis in *Bombyx mori. Chromosoma* 82: 341-351

Reddy KC, Villeneuve AM (2004) C. elegans HIM-17 links chromatin modification and competence for initiation of meiotic recombination. *Cell* 118: 439-452

Reynolds A, Qiao H, Yang Y, Chen JK, Jackson N, Biswas K, Holloway JK, Baudat F, de Massy B, Wang J, Hoog C, Cohen PE, Hunter N (2013) RNF212 is a dosage-sensitive regulator of crossing-over during mammalian meiosis. *Nature genetics* 45: 269-278

Roberts NY (2009) *Investigating the control of homologous chromosome pairing and crossover formation in meiosis of Arabidopsis Thaliana*, Birmingham: University of Birmingham.

Rockmill B, Voelkel-Meiman K, Roeder GS (2006) Centromere-proximal crossovers are associated with precocious separation of sister chromatids during meiosis in *Saccharomyces cerevisiae*. *Genetics* 174: 1745-1754

Roeder GS (1997) Meiotic chromosomes: it takes two to tango. *Genes & development* 11: 2600-2621

Rog O, Dernburg AF (2013) Chromosome pairing and synapsis during *Caenorhabditis elegans* meiosis. *Current opinion in cell biology* 25: 349-356

Rogacheva MV, Manhart CM, Chen C, Guarne A, Surtees J, Alani E (2014) Mlh1-Mlh3, A Meiotic Crossover and DNA Mismatch Repair Factor, is a Msh2-Msh3-Stimulated Endonuclease. *The Journal of biological chemistry*

Rogakou EP, Pilch DR, Orr AH, Ivanova VS, Bonner WM (1998) DNA double-stranded breaks induce histone H2AX phosphorylation on serine 139. *The Journal of biological chemistry* 273: 5858-5868

Roig I, Dowdle JA, Toth A, de Rooij DG, Jasin M, Keeney S (2010) Mouse TRIP13/PCH2 is required for recombination and normal higher-order chromosome structure during meiosis. *PLoS genetics* 6

Romanienko PJ, Camerini-Otero RD (1999) Cloning, characterization, and localization of mouse and human SPO11. *Genomics* 61: 170-182.

Romanienko PJ, Camerini-Otero RD (2000) The mouse Spo11 gene is required for meiotic chromosome synapsis. *Molecular cell* 6: 975-987

Ronceret A, Doutriaux MP, Golubovskaya IN, Pawlowski WP (2009) PHS1 regulates meiotic recombination and homologous chromosome pairing by controlling the transport of RAD50 to the nucleus. *Proceedings of the National Academy of Sciences of the United States of America* 106: 20121-20126

Ross KJ, Fransz P, Jones GH (1996) A light microscopic atlas of meiosis in *Arabidopsis thaliana*. *Chromosome research : an international journal on the molecular, supramolecular and evolutionary aspects of chromosome biology* 4: 507-516

Rosu S, Libuda DE, Villeneuve AM (2011) Robust crossover assurance and regulated interhomolog access maintain meiotic crossover number. *Science* 334: 1286-1289

Rosu S, Zawadzki KA, Stamper EL, Libuda DE, Reese AL, Dernburg AF, Villeneuve AM (2013) The *C. elegans* DSB-2 protein reveals a regulatory network that controls competence for meiotic DSB formation and promotes crossover assurance. *PLoS genetics* 9: e1003674

Royo H, Prosser H, Ruzankina Y, Mahadevaiah SK, Cloutier JM, Baumann M, Fukuda T, Hoog C, Toth A, de Rooij DG, Bradley A, Brown EJ, Turner JM (2013) ATR acts stage specifically to regulate multiple aspects of mammalian meiotic silencing. *Genes & development* 27: 1484-1494

Sanchez-Moran E, Armstrong SJ, Santos JL, Franklin FC, Jones GH (2002) Variation in chiasma frequency among eight accessions of *Arabidopsis thaliana*. *Genetics* 162: 1415-1422

Sanchez-Moran E, Santos JL, Jones GH, Franklin FC (2007a) ASY1 mediates AtDMC1-dependent interhomolog recombination during meiosis in *Arabidopsis*. *Genes & development* 21: 2220-2233

Sanchez-Moran E, Santos JL, Jones GH, Franklin FCH (2007b) ASY1 mediates AtDMC1-dependent interhomolog recombination during meiosis in *Arabidopsis*. *Genes & development* 21: 2220-2233

Sanchez Moran E, Armstrong SJ, Santos JL, Franklin FC, Jones GH (2001) Chiasma formation in *Arabidopsis thaliana* accession Wassileskija and in two meiotic mutants. *Chromosome research : an international journal on the molecular, supramolecular and evolutionary aspects of chromosome biology* 9: 121-128

Sartori AA, Lukas C, Coates J, Mistrik M, Fu S, Bartek J, Baer R, Lukas J, Jackson SP (2007) Human CtIP promotes DNA end resection. *Nature* 450: 509-514

Sasanuma H, Hirota K, Fukuda T, Kakusho N, Kugou K, Kawasaki Y, Shibata T, Masai H, Ohta K (2008) Cdc7-dependent phosphorylation of Mer2 facilitates initiation of yeast meiotic recombination. *Genes & development* 22: 398-410

Sasanuma H, Murakami H, Fukuda T, Shibata T, Nicolas A, Ohta K (2007) Meiotic association between Spo11 regulated by Rec102, Rec104 and Rec114. *Nucleic acids research* 35: 1119-1133

Schalk JA, Dietrich AJ, Vink AC, Offenberg HH, van Aalderen M, Heyting C (1998) Localization of SCP2 and SCP3 protein molecules within synaptonemal complexes of the rat. *Chromosoma* 107: 540-548

Schild-Prufert K, Saito TT, Smolikov S, Gu Y, Hincapie M, Hill DE, Vidal M, McDonald K, Colaiacovo MP (2011) Organization of the synaptonemal complex during meiosis in *Caenorhabditis elegans*. *Genetics* 189: 411-421

Schramm S, Fraune J, Naumann R, Hernandez-Hernandez A, Hoog C, Cooke HJ, Alsheimer M, Benavente R (2011) A novel mouse synaptonemal complex protein is essential for loading of central element proteins, recombination, and fertility. *PLoS genetics* 7: e1002088

Schvarzstein M, Wignall SM, Villeneuve AM (2010) Coordinating cohesion, co-orientation, and congression during meiosis: lessons from holocentric chromosomes. *Genes & development* 24: 219-228

Schwacha A, Kleckner N (1994) Identification of joint molecules that form frequently between homologs but rarely between sister chromatids during yeast meiosis. *Cell* 76: 51-63

Seeliger K, Dukowic-Schulze S, Wurz-Wildersinn R, Pacher M, Puchta H (2012) BRCA2 is a mediator of RAD51- and DMC1-facilitated homologous recombination in *Arabidopsis thaliana*. *The New phytologist* 193: 364-375

Shannon M, Richardson L, Christian A, Handel MA, Thelen MP (1999) Differential gene expression of mammalian SPO11/TOP6A homologs during meiosis. *FEBS Letters* 462: 329-334.

Sharif WD, Glick GG, Davidson MK, Wahls WP (2002) Distinct functions of *S. pombe* Rec12 (Spo11) protein and Rec12-dependent crossover recombination (chiasmata) in meiosis I; and a requirement for Rec12 in meiosis II. *Cell & chromosome* 1: 1

Shim EY, Hong SJ, Oum JH, Yanez Y, Zhang Y, Lee SE (2007) RSC mobilizes nucleosomes to improve accessibility of repair machinery to the damaged chromatin. *Molecular and cellular biology* 27: 1602-1613

Shin YH, Choi Y, Erdin SU, Yatsenko SA, Kloc M, Yang F, Wang PJ, Meistrich ML, Rajkovic A (2010) Hormad1 mutation disrupts synaptonemal complex formation, recombination, and chromosome segregation in mammalian meiosis. *PLoS genetics* 6: e1001190

Shin YH, McGuire MM, Rajkovic A (2013) Mouse HORMAD1 Is a Meiosis I Checkpoint Protein That Modulates DNA Double-Strand Break Repair During Female Meiosis. *Biology of reproduction* 89

Shingu Y, Mikawa T, Onuma M, Hirayama T, Shibata T (2010) A DNA-binding surface of SPO11-1, an *Arabidopsis* SPO11 orthologue required for normal meiosis. *The FEBS journal* 277: 2360-2374

Shingu Y, Tokai T, Agawa Y, Toyota K, Ahamed S, Kawagishi-Kobayashi M, Komatsu A, Mikawa T, Yamamoto MT, Wakasa K, Shibata T, Kusano K (2012) The double-stranded break-forming activity of plant SPO11s and a novel rice SPO11 revealed by a Drosophila bioassay. *BMC molecular biology* 13: 1

Shinohara A, Ogawa H, Ogawa T (1992) Rad51 protein involved in repair and recombination in *S. cerevisiae* is a RecA-like protein. *Cell* 69: 457-470.

Shinohara M, Shinohara A (2013) Multiple pathways suppress non-allelic homologous recombination during meiosis in *Saccharomyces cerevisiae*. *PloS one* 8: e63144

Siaud N, Dray E, Gy I, Gerard E, Takvorian N, Doutriaux MP (2004) Brca2 is involved in meiosis in *Arabidopsis thaliana* as suggested by its interaction with Dmc1. *The EMBO journal* 23: 1392-1401

Smagulova F, Gregoretti IV, Brick K, Khil P, Camerini-Otero RD, Petukhova GV (2011) Genome-wide analysis reveals novel molecular features of mouse recombination hotspots. *Nature* 472: 375-378

Smith AV, Roeder GS (1997) The yeast Red1 protein localizes to the cores of meiotic chromosomes. *J Cell Biol* 136: 957-967

Smolikov S, Eizinger A, Schild-Prufert K, Hurlburt A, McDonald K, Engebrecht J, Villeneuve AM, Colaiacovo MP (2007) SYP-3 restricts synaptonemal complex assembly to bridge paired chromosome axes during meiosis in *Caenorhabditis elegans*. *Genetics* 176: 2015-2025

Smolikov S, Schild-Prufert K, Colaiacovo MP (2009) A yeast two-hybrid screen for SYP-3 interactors identifies SYP-4, a component required for synaptonemal complex assembly and chiasma formation in *Caenorhabditis elegans* meiosis. *PLoS genetics* 5: e1000669

Smyth DR, Bowman JL, Meyerowitz EM (1990) Early flower development in Arabidopsis. *Plant Cell* 2: 755-767

Snowden T, Acharya S, Butz C, Berardini M, Fishel R (2004) hMSH4-hMSH5 recognizes Holliday Junctions and forms a meiosis-specific sliding clamp that embraces homologous chromosomes. *Molecular cell* 15: 437-451

Sofueva S, Yaffe E, Chan WC, Georgopoulou D, Vietri Rudan M, Mira-Bontenbal H, Pollard SM, Schroth GP, Tanay A, Hadjur S (2013) Cohesin-mediated interactions organize chromosomal domain architecture. *The EMBO journal* 32: 3119-3129

Solari AJ (2002) Primitive forms of meiosis: the possible evolution of meiosis. *Biocell : official journal of the Sociedades Latinoamericanas de Microscopia Electronica et al* 26: 1-13

Sommermeyer V, Beneut C, Chaplais E, Serrentino ME, Borde V (2013) Spp1, a member of the Set1 Complex, promotes meiotic DSB formation in promoters by tethering histone H3K4 methylation sites to chromosome axes. *Molecular cell* 49: 43-54

Spirek M, Estreicher A, Csaszar E, Wells J, McFarlane RJ, Watts FZ, Loidl J (2010) SUMOylation is required for normal development of linear elements and wild-type meiotic recombination in *Schizosaccharomyces pombe*. *Chromosoma* 119: 59-72

Stacey NJ, Kuromori T, Azumi Y, Roberts G, Breuer C, Wada T, Maxwell A, Roberts K, Sugimoto-Shirasu K (2006) *Arabidopsis* SPO11-2 functions with SPO11-1 in meiotic recombination. *Plant J* 48: 206-216

Stamper EL, Rodenbusch SE, Rosu S, Ahringer J, Villeneuve AM, Dernburg AF (2013) Identification of DSB-1, a protein required for initiation of meiotic recombination in *Caenorhabditis elegans*, illuminates a crossover assurance checkpoint. *PLoS genetics* 9: e1003679

Storlazzi A, Gargano S, Ruprich-Robert G, Falque M, David M, Kleckner N, Zickler D (2010) Recombination proteins mediate meiotic spatial chromosome organization and pairing. *Cell* 141: 94-106

Storlazzi A, Tesse S, Ruprich-Robert G, Gargano S, Poggeler S, Kleckner N, Zickler D (2008) Coupling meiotic chromosome axis integrity to recombination. *Genes & development* 22: 796-809

Strom L, Lindroos HB, Shirahige K, Sjogren C (2004) Postreplicative recruitment of cohesin to double-strand breaks is required for DNA repair. *Molecular cell* 16: 1003-1015

Strong ER, Schimenti JC (2010) Evidence Implicating CCNB1IP1, a RING Domain-Containing Protein Required for Meiotic Crossing Over in Mice, as an E3 SUMO Ligase. *Genes* 1: 440-451

Strudwick N, Brown M, Parmar VM, Schroder M (2010) Ime1 and Ime2 are required for pseudohyphal growth of *Saccharomyces cerevisiae* on nonfermentable carbon sources. *Molecular and cellular biology* 30: 5514-5530

Su SSY, Tanaka Y, Samejima I, Tanaka K, Yanagida M (1996) A nitrogen starvation-induced dormant G(0) state in fission yeast: The establishment from uncommitted G(1) state and its delay for return to proliferation. *Journal of cell science* 109: 1347-1357

Sugimoto-Shirasu K, Stacey NJ, Corsar J, Roberts K, McCann MC (2002) DNA topoisomerase VI is essential for endoreduplication in *Arabidopsis*. *Current biology : CB* 12: 1782-1786

Sun Y, Ambrose JH, Haughey BS, Webster TD, Pierrie SN, Munoz DF, Wellman EC, Cherian S, Lewis SM, Berchowitz LE, Copenhaver GP (2012) Deep genome-wide measurement of meiotic gene conversion using tetrad analysis in *Arabidopsis thaliana*. *PLoS genetics* 8: e1002968

Sym M, Engebrecht JA, Roeder GS (1993) ZIP1 is a synaptonemal complex protein required for meiotic chromosome synapsis. *Cell* 72: 365-378

Sym M, Roeder GS (1995) Zip1-induced changes in synaptonemal complex structure and polycomplex assembly. *J Cell Biol* 128: 455-466

Tesse S, Storlazzi A, Kleckner N, Gargano S, Zickler D (2003) Localization and roles of Ski8p protein in Sordaria meiosis and delineation of three mechanistically distinct steps of meiotic homolog juxtaposition. *Proceedings of the National Academy of Sciences of the United States of America* 100: 12865-12870

Town CD, Cheung F, Maiti R, Crabtree J, Haas BJ, Wortman JR, Hine EE, Althoff R, Arbogast TS, Tallon LJ, Vigouroux M, Trick M, Bancroft I (2006) Comparative genomics of Brassica oleracea and *Arabidopsis thaliana* reveal gene loss, fragmentation, and dispersal after polyploidy. *Plant Cell* 18: 1348-1359

Tsubouchi H, Roeder GS (2006) Budding yeast Hed1 down-regulates the mitotic recombination machinery when meiotic recombination is impaired. *Genes & development* 20: 1766-1775

Tsubouchi T, Macqueen AJ, Roeder GS (2008) Initiation of meiotic chromosome synapsis at centromeres in budding yeast. *Genes & development* 22: 3217-3226

Tsubouchi T, Zhao H, Roeder GS (2006) The meiosis-specific zip4 protein regulates crossover distribution by promoting synaptonemal complex formation together with zip2. *Developmental cell* 10: 809-819

Tsukuda T, Lo YC, Krishna S, Sterk R, Osley MA, Nickoloff JA (2009) INO80-dependent chromatin remodeling regulates early and late stages of mitotic homologous recombination. *DNA repair* 8: 360-369

Uanschou C, Ronceret A, Von Harder M, De Muyt A, Vezon D, Pereira L, Chelysheva L, Kobayashi W, Kurumizaka H, Schlogelhofer P, Grelon M (2013) Sufficient Amounts of Functional HOP2/MND1 Complex Promote Interhomolog DNA Repair but Are Dispensable for Intersister DNA Repair during Meiosis in *Arabidopsis*. *Plant Cell*

Uanschou C, Siwiec T, Pedrosa-Harand A, Kerzendorfer C, Sanchez-Moran E, Novatchkova M, Akimcheva S, Woglar A, Klein F, Schlogelhofer P (2007) A novel plant gene essential for meiosis is related to the human CtIP and the yeast COM1/SAE2 gene. *The EMBO journal* 26: 5061-5070

Unal E, Arbel-Eden A, Sattler U, Shroff R, Lichten M, Haber JE, Koshland D (2004) DNA damage response pathway uses histone modification to assemble a double-strand break-specific cohesin domain. *Molecular cell* 16: 991-1002

Vignard J, Siwiec T, Chelysheva L, Vrielynck N, Gonord F, Armstrong SJ, Schlogelhofer P, Mercier R (2007) The interplay of RecA-related proteins and the MND1-HOP2 complex during meiosis in *Arabidopsis thaliana*. *PLoS genetics* 3: 1894-1906

Voelkel-Meiman K, Moustafa SS, Lefrancois P, Villeneuve AM, MacQueen AJ (2012) Full-length synaptonemal complex grows continuously during meiotic prophase in budding yeast. *PLoS genetics* 8: e1002993

Wan L, de los Santos T, Zhang C, Shokat K, Hollingsworth NM (2004) Mek1 kinase activity functions downstream of RED1 in the regulation of meiotic double strand break repair in budding yeast. *Molecular biology of the cell* 15: 11-23

Wang K, Wang M, Tang D, Shen Y, Miao C, Hu Q, Lu T, Cheng Z (2012a) The role of rice HEI10 in the formation of meiotic crossovers. *PLoS genetics* 8: e1002809

Wang K, Wang M, Tang D, Shen Y, Qin B, Li M, Cheng Z (2011) PAIR3, an axis-associated protein, is essential for the recruitment of recombination elements onto meiotic chromosomes in rice. *Molecular biology of the cell* 22: 12-19

Wang Y, Cheng Z, Huang J, Shi Q, Hong Y, Copenhaver GP, Gong Z, Ma H (2012b) The DNA replication factor RFC1 is required for interference-sensitive meiotic crossovers in *Arabidopsis thaliana*. *PLoS genetics* 8: e1003039

Wang Y, Xiao R, Wang H, Cheng Z, Li W, Zhu G, Ma H (2013) The *Arabidopsis* RAD51 paralogs RAD51B, RAD51D and XRCC2 play partially redundant roles in somatic DNA repair and gene regulation. *The New phytologist*

Ward JO, Reinholdt LG, Motley WW, Niswander LM, Deacon DC, Griffin LB, Langlais KK, Backus VL, Schimenti KJ, O'Brien MJ, Eppig JJ, Schimenti JC (2007) Mutation in mouse hei10, an e3 ubiquitin ligase, disrupts meiotic crossing over. *PLoS genetics* 3: e139

Watanabe Y, Nurse P (1999) Cohesin Rec8 is required for reductional chromosome segregation at meiosis. *Nature* 400: 461-464

Weinstein A (1918) Coincidence of Crossing over in DROSOPHILA MELANOGASTER (AMPELOPHILA). *Genetics* 3: 135-172

Wilkins AS, Holliday R (2009) The evolution of meiosis from mitosis. *Genetics* 181: 3-12

Wojtasz L, Cloutier JM, Baumann M, Daniel K, Varga J, Fu J, Anastassiadis K, Stewart AF, Remenyi A, Turner JM, Toth A (2012) Meiotic DNA double-strand breaks and chromosome asynapsis in mice are monitored by distinct HORMAD2-independent and -dependent mechanisms. *Genes & development* 26: 958-973

Wojtasz L, Daniel K, Roig I, Bolcun-Filas E, Xu H, Boonsanay V, Eckmann CR, Cooke HJ, Jasin M, Keeney S, McKay MJ, Toth A (2009) Mouse HORMAD1 and HORMAD2, two conserved meiotic chromosomal proteins, are depleted from synapsed chromosome axes with the help of TRIP13 AAA-ATPase. *PLoS genetics* 5: e1000702

Woltering D, Baumgartner B, Bagchi S, Larkin B, Loidl J, de los Santos T, Hollingsworth NM (2000) Meiotic segregation, synapsis, and recombination checkpoint functions require

physical interaction between the chromosomal proteins Red1p and Hop1p. *Molecular and cellular biology* 20: 6646-6658

Wu HY, Burgess SM (2006) Two distinct surveillance mechanisms monitor meiotic chromosome metabolism in budding yeast. *Current biology : CB* 16: 2473-2479

Yamada S, Ohta K, Yamada T (2013) Acetylated Histone H3K9 is associated with meiotic recombination hotspots, and plays a role in recombination redundantly with other factors including the H3K4 methylase Set1 in fission yeast. *Nucleic acids research* 41: 3504-3517

Yamamoto M (1996a) The molecular control mechanisms of meiosis in fission yeast. *Trends in biochemical sciences* 21: 18-22

Yamamoto M (1996b) Regulation of meiosis in fission yeast. *Cell structure and function* 21: 431-436

Yang S, Yuan Y, Wang L, Li J, Wang W, Liu H, Chen JQ, Hurst LD, Tian D (2012a) Great majority of recombination events in *Arabidopsis* are gene conversion events. *Proceedings of the National Academy of Sciences of the United States of America* 109: 20992-20997

Yang Y, Ishino S, Yamagami T, Kumamaru T, Satoh H, Ishino Y (2012b) The OsGEN-L protein from *Oryza sativa* possesses Holliday junction resolvase activity as well as 5'-flap endonuclease activity. *Journal of biochemistry* 151: 317-327

319

Yant L, Hollister JD, Wright KM, Arnold BJ, Higgins JD, Franklin FC, Bomblies K (2013) Meiotic adaptation to genome duplication in *Arabidopsis arenosa*. *Current biology : CB* 23: 2151-2156

Yin Y, Cheong H, Friedrichsen D, Zhao Y, Hu J, Mora-Garcia S, Chory J (2002) A crucial role for the putative *Arabidopsis* topoisomerase VI in plant growth and development. *Proceedings of the National Academy of Sciences of the United States of America* 99: 10191-10196

Youds JL, Mets DG, McIlwraith MJ, Martin JS, Ward JD, ONeil NJ, Rose AM, West SC, Meyer BJ, Boulton SJ (2010) RTEL-1 Enforces Meiotic Crossover Interference and Homeostasis. *Science* 327: 1254-1258

Yu H, Wang M, Tang D, Wang K, Chen F, Gong Z, Gu M, Cheng Z (2010) OsSPO11-1 is essential for both homologous chromosome pairing and crossover formation in rice. *Chromosoma* 119: 625-636

Yuan L, Yang X, Ellis JL, Fisher NM, Makaroff CA (2012) The *Arabidopsis* SYN3 cohesin protein is important for early meiotic events. *Plant J* 71: 147-160

Zakharyevich K, Ma Y, Tang S, Hwang PY, Boiteux S, Hunter N (2010) Temporally and biochemically distinct activities of Exo1 during meiosis: double-strand break resection and resolution of double Holliday junctions. *Molecular cell* 40: 1001-1015

Zakharyevich K, Tang S, Ma Y, Hunter N (2012) Delineation of joint molecule resolution pathways in meiosis identifies a crossover-specific resolvase. *Cell* 149: 334-347

Zanders S, Alani E (2009) The pch2Delta mutation in baker's yeast alters meiotic crossover levels and confers a defect in crossover interference. *PLoS genetics* 5: e1000571

Zanders S, Sonntag Brown M, Chen C, Alani E (2011) Pch2 modulates chromatid partner choice during meiotic double-strand break repair in *Saccharomyces cerevisiae*. *Genetics* 188: 511-521

Zhang C, Song Y, Cheng ZH, Wang YX, Zhu J, Ma H, Xu L, Yang ZN (2012) The *Arabidopsis thaliana* DSB formation (AtDFO) gene is required for meiotic double-strand break formation. *Plant Journal* 72: 271-281

Zhang J, Pawlowski WP, Han F (2013) Centromere Pairing in Early Meiotic Prophase Requires Active Centromeres and Precedes Installation of the Synaptonemal Complex in Maize. *Plant Cell*

Zhang L, Kim KP, Kleckner NE, Storlazzi A (2011) Meiotic double-strand breaks occur once per pair of (sister) chromatids and, via Mec1/ATR and Tel1/ATM, once per quartet of chromatids. *Proceedings of the National Academy of Sciences of the United States of America* 108: 20036-20041

Zhang X, Henriques R, Lin SS, Niu QW, Chua NH (2006) Agrobacterium-mediated transformation of *Arabidopsis thaliana* using the floral dip method. *Nature Protocols* 1: 641-646.

Zickler D, Kleckner N (1998) The leptotene-zygotene transition of meiosis. *Annual review of genetics* 32: 619-697

Zickler D, Kleckner N (1999) Meiotic chromosomes: integrating structure and function. *Annual review of genetics* 33: 603-754

Appendix

Appendix 1. T-DNA insertion mutant lines

Mutant line	Gene number	Allele	WT primer set	T-DNA primer set
Atasy1	At1G67370	Salk_144182	ASY1F-ASY1R	LB1.3F-ASY1R
Atasy3	At2G46980	Salk_143676	ASY3F-ASY3R	LB1.3F-ASY3R
Atsyn1	At5G05490	Salk_091193	SYN1F- SYN1R	LB1.3F-SYN1R
Atspo11-1-4	At3G13170	WiscDsLox_461-464J19	SPO114F-SPO114R	WSF-SPO114F
Atatr	At5G40820	Salk_032841	ATRF-ATRR	LB1.3F-ATRR
Atatm	At3G48190	Salk_089805	ATMF-ATMR	LB1.3F-ATMR
Atprd3	At1G01690	GABI677D06	PRD3F-PRD3R	GABILB-PRD3F
Atrad51	At5G20850	Sail_873_C08	RAD51F-RAD51R	SailLB-RAD51R
Atpch2-1	At4g24710	Sail_1187_C06	PCH21F-PCH21R	SailLB-PCH21R
Atpch2-2	At4g24710	SALK_031449	PCH22F-PCH22R	LB1.3F-PCH22R
Atpch2-3	At4g24710	SALK_130138	PCH23F-PCH23R	LB1.3F -PCH23R
Atdmc1	AT3G22880	Feldmann line 3668	DMC1C-	DMC1A-

			DMC1D	DMC1B
Atmsh5	At3g20475	SALK_110240	MSH5F- MSH5R	LB1.3F – MSH5R

Table 1.1. List of T-DNA insertion mutant lines

WT and T-DNA primer sets were used to discriminate between wild-type, heterozygote

and homozygote plants for the insertion of the T-DNA. WT primer set amplified a

genomic region of the gene of interest only if it does not contain a T-DNA inserted. T-

DNA primer set amplified a region comprising the left border of the T-DNA and the

sequence of the gene of interest adjacent to the left border of the T-DNA inserted

Appendix 2. Growth media

All media were prepared with MilliQ water and sterilized by autoclave.

Autoclave was carried out at 15 psi at 121 °C for 20 min.

2.1. Bacterial growth media

<u>LB</u>

Bacto-tryptone   10 g

Bacto-yeast extract   5 g

NaCl   10 g

Adjusted pH to 7.0 with 1 M NaOH

Made up to 1 L with MilliQ water

Sterilised by autoclaving

LA

Bacto-tryptone	10 g
Bacto-yeast extract	5 g
NaCl	10 g
Bacto-agar	15 g

Adjusted pH to 7.0 with 1 M NaOH

Made up to 1 L with MilliQ water

Sterilised by autoclaving

SOB

Bacto-tryptone	20 g
Bacto-yeast extract	5 g
NaCl	0.50 g
KCl	0.187 g

Adjusted pH to 7.0 with 1 M NaOH

Made up to 980 ml with MilliQ water

Sterilised by autoclaving

Added the following filter-sterilised solutions:

1M $MgCl_2$ 10 ml

1M MgSO$_4$ 10 ml

SOC

Bacto-tryptone	20 g
Bacto-yeast extract	5 g
NaCl	0.50 g
KCl	0.187 g

Adjusted pH to 7.0 with 1 M NaOH

Made up to 960 ml with MilliQ water

Sterilised by autoclaving

Added the following filter-sterilised solutions:

1M MgCl$_2$	10 ml
1M MgSO$_4$	10 ml
1M glucose	20 ml

Stock solution antibiotics

100 mg/ml Ampicillin

Ampicillin (SIGMA)   1 g

Made up to 10 ml of MilliQ water

Filter-sterilised through a 0.2 μm filter

50 mg/ml Kanamycin

Kanamycin (SIGMA)   0.5 g

Made up to 10 ml of MilliQ water

Filter-sterilised through a 0.2 μm filter

50 mg/ml Rifampicin

Rifampicin (SIGMA)   0.5 g

Made up to 10 ml of DMSO

Filter-sterilised through a 0.2 μm filter

2.2. Yeast growth media

<u>YPDA broth</u>

Difco peptone   20 g
Yeast extract   10 g
Glucose   20 g
Adenine hemisulfate   30 mg

Adjusted pH to 6.5 with 1 M NaOH

Made up to 1 L with MilliQ water

Sterilised by autoclaving

<u>YPDA agar</u>

Difco peptone   20 g

Yeast extract	10 g
Agar	20 g
Glucose	20 g
Adenine hemisulfate	30 mg

Adjusted pH to 6.5 with 1 M NaOH

Made up to 1 L with MilliQ water

Sterilised by autoclaving

SD dropout broth

1sachet Ready-To-Go yeast media pouches (Clontech) was used with 500 ml MilliQ water

Adjusted pH to 5.8 with 1 M NaOH

Sterilised by autoclaving

SD drop-out agar

1 sachet Ready-To-Go yeast media pouches (Clontech) was used with 500 ml MilliQ water

Adjusted pH to 5.8 with 1 M NaOH

Sterilised by autoclaving

2.3. Plant media

MS media

Murashige and Skoog	2.2 g
Agar	10.0 g

Made up to 1 L with MilliQ water

Adjusted pH to 5.8 with 1 M KOH

Sterilised by autoclaving

Stock solution glufosinate ammonium

50 mg/ml glufosinate ammonium (SIGMA)	50 mg

Made up to 1 ml of MilliQ water

Appendix 3. Reagent preparation

All buffers and solutions were made with MilliQ water

3.1. Protein electrophoresis and western blotting solution

SDS-PAGE

Per Biorad gel	RESOLVING		STACKING
	10%	12%	
MilliQ water	4.0ml	3.3ml	1.7ml
(30%/0.8% w/v) Acryl/Bis-acrylamide	3.3ml	4.0ml	0.4ml
Tris	2.5ml	2.5ml	0.3ml
10% (w/v) SDS	0.1ml	0.1ml	25 μl
10% (w/v) ammonium persulfate	0.1ml	0.1ml	25 μl
TEMED	4.0μl	4.0μl	2.5 μl

Table 3.1. Components of resolving and stacking gels and their amounts.

For running solution, Tris solution was made at 1.5M, pH8.0

For stacking solution, Tris solution was made at 1M, pH6.0

5X SDS loading dye:

Tris-HCl (2M, pH6.8) (v/v)	67.5%
SDS (w/v)	10 %
Glycerol (w/v)	50 %
β-mercaptoethanol (w/v)	5 %
bromphenol blue	few grains

5X ELFO buffer

Tris (w/v)	1.5%
Glycine (w/v)	7.2%
SDS (w/v)	0.5%

Adjusted pH to 8.3 with 1 M HCl.

Coomassie stain solution

Coomassie blue R-250 (w/v)	0.1%
Methanol (v/v)	45%
Glacial acetic acid (v/v)	45%
MilliQ water (v/v)	10%

Coomassie destain solution

Methanol (v/v)	20%
Glacial acetic acid (v/v)	7%
MilliQ water (v/v)	63%

Ponceau S stain

Ponceau S (w/v)	0.1%

| Glacial acetic acid (v/v) | 1.0 % |
| MilliQ water (v/v) | 98.9% |

Protein transfer buffer

Glycine (w/v)	1.4%
Tris (w/v)	0.3%
Methanol (v/v)	20%
MilliQ water (v/v)	78.3%

Adjusted pH to 8.3 with 1 M HCl

10X TBST Buffer

NaCl (w/v)	8.0%
KCl (w/v)	0.2%
Tris (w/v)	3.0%
Tween 20 (v/v)	1.0 %
MilliQ water (v/v)	88.0 %

Adjusted pH to 7.4 with 1 M HCl

Blocking buffer

| Dried skimmed milk powder (w/v) | 5.0 % |
| 1X TBST buffer (v/v) | 95.0 % |

IP buffer

Tris-HCl pH 7.5	20 mM
NaCl	150 mM
Glycerol	1 ml
EDTA	2 mM
Complete protease inhibitor cocktail (Roche)	1 tablet

Made up to 10 ml with BPC water grade

Filter-sterilised through a 0.2 μm filter

TCA buffer

Tris-HCl (pH 8.0)	20 mM
Ammonium acetate	50 mM
EDTA	2 mM
Phenylmethyl-sulfonyl fluoride	1 mM
Complete protease inhibitor cocktail (Roche)	1 tablet

Made up to 10 ml with BPC water grade

Filter-sterilised through a 0.2 μm filter

TCA-Laemmli loading buffer

SDS/glycerol stock solution	480 μl

Tris/EDTA stock solution	400 μl
β mercaptoethanol	50 μl
Phenylmethyl-sulfonyl fluoride	0.35 mg
Complete protease inhibitor cocktail	1 tablet
BPC water grade	30 μl

SDS/glycerol stock solution

SDS (w/v)	2.1 M
Glycerol (v/v)	3.5 ml
Tris base	83.3 mM
Bromophenol blue	few grains

Made up to 12 ml with BPC water grade.

Filter-sterilised through a 0.2 μm filter

Tris/EDTA stock solution

Tris base	200 mM
EDTA	20 mM

Made up to 10 ml with BPC water grade

Filter-sterilised through a 0.2 μm filter

Elution buffer

Glycine	50 mM
NaCl	150 mM
BSA (SIGMA) (w/v)	10 %

Adjusted pH to 2.4 with 1 M NaOH.

3.2. DNA extraction and DNA electrophoresis gel

Extraction buffer

2M Tris-HCl pH 9.5	2.5 ml
1M EDTA	500 μl
2M KCl	6.25 ml

Made up to 50 ml with MilliQ water

Dilution buffer

3 % bovine serum albumin (w/v, SIGMA)

TBE

Tris-HCl	44.5 mM
Boric acid	44.5 mM

EDTA   1.0 mM

6X DNA loading buffer

Glycerol (v/v)   30 %

Bromophenol blue   few grains

Xylene cyanol FF (w/v)   0.25 %

1 X PIM

Leupeptin (10 mg/ml in DMSO)   1 μl

Pepstatin (10 mg/ml in DMSO)   1 μl

Chymostatin (10 mg/ml in DMSO)   1 μl

MilliQ water   997 μl

3.3. Cytology

Fixative solution

Ethanol (v/v)   75 %

Glacial acetic acid (v/v)   25 %

Alexander's stain solution

Ethanol   10 ml

Malachite green (1% in 95% Ethanol)	1 ml
Fuchsin acid (1% in MilliQ water)	5 ml
Orange G (1% in MilliQ water)	0.5 ml
Phenol	5 g
Glacial acetic acid	2 ml
Chloral hydrate	5 g
Glycerol	25 ml
MilliQ water	50 ml

Citrate buffer

Citric acid	44.5 mM
Sodium citrate	55.5 mM

Stock digestion medium

Cellulose (SIGMA)	100 mg
Pectolysase (SIGMA)	100 mg
Citrate buffer	10 ml

Enzyme solution for DAPI-stained chromosome spread

Stock digestion medium	333 µl
Citrate buffer	667 µl

DAPI Counterstaining solution

DAPI (SIGMA) (1 mg/ml in MilliQ water)   10 μl

Vectashield mounting medium (Vector)   1 ml

20X SSC

NaCl   3 M

Trisodium citrate   300 mM

Adjusted pH to 7.0 with 1 M HCl.

Pepsin solution

MilliQ water   99.8 ml

Hcl 5M   0.2 ml

Pepsin   10 mg

Hybridisation solution

Detran sulphate   1 g

Deionised formamide   5 ml

20x SCC   1 ml

MilliQ water   7 ml

Filter-sterilised through a 0.2 μm filter

<u>4T</u>

20X SSC	20 ml
Tween 20	50 µl
MilliQ Water	100 ml

<u>PBST</u>

Phosphate saline buffer (Oxoid)	1 tablet
Triton X100	100 µl
MilliQ Water	100 ml

<u>EM digestion mix</u>

Cytohelicase	0.1 g
Sucrose	0.375 g
Polyvinylpyrollidone	0.25 g

Made up to 25 mL with MilliQ water

Filter-sterilised through a 0.2 µm filter

<u>EM block</u>

BSA	0.1 g
PBST	10 ml

Filter-sterilised through a 0.2 μm filter

Appendix 4. Primer sequences

Primer	Nucleotide sequence (5'to 3')	Tm (°C)	PCR technique
pGAD-ASY3 1-793 F	CAGATTACGCTCATATGAGCGACTATAGAAGCTTC	68.3	cloning
pGAD-ASY3 1-793 R	CACCCGGGTGGAATTTCAATCATCCCTCAAACATTCTG	71.6	cloning
pGBK-ASY3 1-793 F	AGGAGGACCTGCATATGAGCGACTATAGAAGCTTC	70.6	cloning
pGBK-ASY3 1-793 R	GGATCCCCGGGAATTTCAATCATCCCTCAAACATTCTG	71.6	cloning
pGAD-ASY3 1-510 R	CACCCGGGTGGAATTTCAATCATCCCTCAAACATTCTG	71.6	cloning
pGBK-ASY3 1-510 R	GGATCCCCGGGAATTTCAATCATCCCTCAAACATTCTG	71.6	cloning
pGAD-ASY3 280 R	CACCCGGGTGGAATTCAGCGACCTAAGTTGGCACCAGC	75.0	cloning
pGBK-ASY3 280 R	GGATCCCCGGGAATTCAGCGACCTAAGTTGGCACC	75.0	cloning
pGAD-ASY3	CAGATTACGCTCATGAAGGCTTGGGAAGGGCTGTT	71.8	cloning

623-793 F			
pGBK-ASY3 623-793 F	AGGAGGACCTGCATGAAGGCTTGGGAAGGGCTGTT	74.2	cloning
pGAD-ASY1 F	CAGATTACGCTCATATGGTGATGGCTCAGAAGCTGAA	70.6	cloning
pGAD-ASY1 R	CACCCGGGTGGAATTCAATTAGCTTGAGATTTCTGACG CTT	72.4	cloning
pGBK-ASY1 F	AGGAGGACCTGCATATGGTGATGGCTCAGAAGCTGAA	72.8	cloning
pGBK-ASY1 R	GGATCCCCGGAAATTCAATTAGCTTGAGATTTCTGACG CTT	71.4	cloning
pGAD-PRD3 F	CAGATTACGCTCATATGAAGATGAATATT	59.6	cloning
pGAD-PRD3 R	CACCCGGGTGGAATTTCAGTTAATTATTAT	62.7	cloning
pGBK-PRD3 F	AGGAGGACCTGCATATGAAGATGAATATT	62.4	cloning
pGBK-PRD3 R	GGATCCCCGGGAATTTCAGTTAATTATTAT	62.7	cloning
T7 F	TAATACGACTCACTATAGGGC	55.9	sequencing
ASY3 genome F1	GGTCTCCGAGATCGTCTCATCGG	66.0	sequencing
ASY3 genome F2	GGTGCCAACTTAGGTCGCAAGTGC	66.1	sequencing

342

ASY3 genome F3	CCTCTCAAGGGACAACAGGCC	63.7	sequencing
ASY3 genome F4	GCCGAAACAAGATTACAAGAGC	58.4	sequencing
ASY1 genome F1	AGCAGAGATCACTGAGCAGG	59.4	sequencing
ASY1 genome F2	ACGCTAAAGGTCAAGAGCGTGC	62.1	sequencing
ASY1 genome F3	ATGGACAGGATGACCCAAGAGG	62.1	sequencing
PRD3 genome F1	TCTTGAAACTGAACGCATACAGC	58.9	sequencing
PRD3 genome F2	ACCACAATTTCCGAGAAATCC	55.9	sequencing
SailLB	TTCATAACCAATCTCGATACAC	54.7	genotyping
GABILB	ATATTGACCATCATACTCATTGC	55.3	genotyping
LB1.3F	ATTTTGCCGATTTCGGAAC	52.4	genotyping
WSF	AACGTCCGCAATGTGTTATTAAGTTGTC	62.2	genotyping
ASY1F	CAATAACACAGACCCTTCATC	55.9	genotyping
ASY1R	CTCTGTTCAAGTTCTCTCAG	55.3	genotyping
ASY3F	AGGAGATGCTTCTGGAGAAC	57.3	genotyping
ASY3R	CTGGTGCCAACTTAGGTCGC	61.4	genotyping
SYN1F	CTTCTTAAGGATGGCCGCTAC	59.8	genotyping
SYN1R	CCACTTTTATGGGCAATGAAG	55.9	genotyping

SPO114F	GAGGATATCCAGATGTCTC	54.5	genotyping
SPO114R	AGGAGAGCTTACTTCACGAC	57.3	genotyping
ATRF	GAATTCTCTACTTCAAGGGTTCCG	61.0	genotyping
ATRR	CCACATTTGGACGGCTGGTCAGC	66.0	genotyping
ATMF	CATCTTCCAACACCATCTCAATGGG	63	genotyping
ATMR	GAAGAACGAACTGCTTCCTTTACCC	63	genotyping
PRD3F	GTGACATCATGCAAGCCAATCGAGGAAC	66.6	genotyping
PRD3R	CTGAATCTCTCTGGTGAACGTGTGACAG	66.6	genotyping
RAD51F	TTCAGGATGGTGTCTCAGAGC	59.8	genotyping
RAD51R	ATGCCAAGGTTGACAAGATTG	55.9	genotyping
ASY1TAF	CGCTAAAGGTCAAGAGCGTG	59.4	genotyping
ASY1TAR	CTCTCTGGTGTCTTGTCTCTC	59.8	genotyping
PCH21F	CAGTGCAAATAGCCGTCGCTGAG	64.2	genotyping
PCH21R	CTCACATGGTCCTTCTTCAATGAGC	63.0	genotyping
PCH22F	CCATCCGGTGCAACTCCAGGTC	65.8	genotyping
PCH22R	CCATCTTCCTCCACCATCTCTTGG	64.4	genotyping
PCH23F	GGATTATTCTTTTGCACGGACCACC	63.0	genotyping
PCH23R	GTCCGATCACTTCACAACTATTGGTG	63.2	genotyping
DMC1A	CCTGCAATGGTCTCATGATGCATAC	63.0	genotyping
DMC1B	GATGCAATCGATATCAGCCAATTTTAGAC	62.4	genotyping
DMC1C	AGGTACTCTGTCTCTCAATG	55.3	genotyping
DMC1D	ACTAATCCTTCGCGTCAGCAATGC	62.7	genotyping
MSH5F	AACCGATCGTCATTTGTTCTG	55.9	genotyping

MSH5R	CACTAAGGCCTGCTGAATTTG	57.9	genotyping

Table 4.1. List of primer sequences and their annealing temperature

Appendix 5. Vector list

NAME	SUPPLIER	RESISTANCE GENE	USE
pGADT7	Clontech	Kanamycin	Yeast two hybrid
pGBKT7	clontech	Ampicillin	Yeast two hybrid
pEG100	Provided by Eduardo Corredor	Kanamycin	*Arabidopsis* transformation
pDrive	Qiagen	Ampicillin/ Kanamycin	Cloning

Table 5.1.: List of vectors used during this study

Appendix 6. List of publication and presentation

6.1. Publication

Ferdous M., Higgins JD., Osman K., **Lambing C.**, Roitinger E., Mechtler K., Armstrong SJ., Perry R., Pradillo M., Cuñado N., and Franklin FCH (2012). Inter-homolog crossing-

over and synapsis in Arabidopsis meiosis are dependent on the chromosome axis protein AtASY3, **PLoS Genetics.**

6.2. Presentations

April 2011: **Graduate Research School Symposium**, Birmingham, UK. **Poster presentation** - ASY3, a novel component of the meiotic chromosome axes, is required for chromosome synapsis and crossover formation in *Arabidopsis thaliana*

April 2011: **British Meiosis meeting**, Sheffield, UK. **Poster presentation** - ASY3, a novel component of the meiotic chromosome axes, is required for chromosome synapsis and crossover formation in *Arabidopsis thaliana*

June 2011: **Doctoral Researcher Conference**, national meeting, Birmingham, UK. **Poster presentation** - ASY3, a novel component of the meiotic chromosome axes, is required for chromosome synapsis and crossover formation in *Arabidopsis thaliana*

February 2012: **Short Talks, School of Biosciences Seminar,** Birmingham, UK. **Talk –** Phosphorylation of AtASY1 is required to ensure inter-homologue crossover formation in *Arabidopsis.*

March 2012: **British Meiosis meeting**, Birmingham, UK. **Talk –** Phosphorylation of AtASY1 is required to ensure inter-homologue crossover formation in *Arabidopsis.*

May 2012: **EMBO Workshop**, Genetic stability and change: genome maintenance mechanisms with plants. Roscoff, France. **Talk** – Phosphorylation of AtASY1 is required to ensure inter-homologue crossover formation in *Arabidopsis.*

June 2012: **Gordon Research Seminar**, Meiosis. New London, USA. **Poster presentation** - Phosphorylation of AtASY1 is required to ensure inter-homologue crossover formation in *Arabidopsis.*

June 2012: **Gordon Research Conference**, Meiosis, New London, USA. **Poster presentation –** Analysis of meiotic chromosome axis organization in *Arabidopsis thaliana* using super-resolution microscopy.

March 2013. **British Meiosis Meeting**, Cambridge, UK. **Talk** – Multiple mechanisms link chromosome axis morphogenesis to ASY1 localisation during early prophase I in *Arabidopsis.*

September 2013. **EMBO Conference on Meiosis,** Dresden, Germany. **Poster –** Phosphorylation of AtASY1-T295 is required for the correct association of AASY1 with the chromosome axis and formation of inter-homologue crossovers in *Arabidopsis thaliana.*

March 2014. **British Meiosis Meeting**, Edinburgh, UK. **Talk** – Coordinated chromosome axis remodeling by PCH2 is essential for CO assurance and interference in plants.

April 2014: **Graduate Research School Symposium**, Birmingham, UK. <u>**Talk** – Coordination between chromosome axis morphogenesis and homologous recombination in *Arabidopsis* meiosis.</u>

Inter-Homolog Crossing-Over and Synapsis in *Arabidopsis* Meiosis Are Dependent on the Chromosome Axis Protein AtASY3

Maheen Ferdous[1,9], **James D. Higgins**[1,9], **Kim Osman**[1], **Christophe Lambing**[1], **Elisabeth Roitinger**[2], **Karl Mechtler**[2,3], **Susan J. Armstrong**[1], **Ruth Perry**[1], **Mónica Pradillo**[4], **Nieves Cuñado**[4], **F. Chris H. Franklin**[1]*

1 School of Biosciences, University of Birmingham, Birmingham, United Kingdom, 2 Institute of Molecular Pathology (IMP), Vienna, Austria, 3 Institute of Molecular Biotechnology (IMBA), Vienna, Austria, 4 Departamento de Génetica, Facultad de Biología, Universidad Complutense de Madrid, Madrid, Spain

Abstract

In this study we have analysed AtASY3, a coiled-coil domain protein that is required for normal meiosis in *Arabidopsis*. Analysis of an *Atasy3-1* mutant reveals that loss of the protein compromises chromosome axis formation and results in reduced numbers of meiotic crossovers (COs). Although the frequency of DNA double-strand breaks (DSBs) appears moderately reduced in *Atasy3-1*, the main recombination defect is a reduction in the formation of COs. Immunolocalization studies in wild-type meiocytes indicate that the HORMA protein AtASY1, which is related to Hop1 in budding yeast, forms hyper-abundant domains along the chromosomes that are spatially associated with DSBs and early recombination pathway proteins. Loss of AtASY3 disrupts the axial organization of AtASY1. Furthermore we show that the AtASY3 and AtASY1 homologs BoASY3 and BoASY1, from the closely related species *Brassica oleracea*, are co-immunoprecipitated from meiocyte extracts and that AtASY3 interacts with AtASY1 via residues in its predicted coiled-coil domain. Together our results suggest that AtASY3 is a functional homolog of Red1. Since studies in budding yeast indicate that Red1 and Hop1 play a key role in establishing a bias to favor inter-homolog recombination (IHR), we propose that AtASY3 and AtASY1 may have a similar role in *Arabidopsis*. Loss of AtASY3 also disrupts synaptonemal complex (SC) formation. In *Atasy3-1* the transverse filament protein AtZYP1 forms small patches rather than a continuous SC. The few AtMLH1 foci that remain in *Atasy3-1* are found in association with the AtZYP1 patches. This is sufficient to prevent the ectopic recombination observed in the absence of AtZYP1, thus emphasizing that in addition to its structural role the protein is important for CO formation.

Introduction

Meiotic recombination is initiated by the formation of Spo11-catalysed DSBs during early prophase I [1]. Each break is resected to produce 3′ single-stranded DNA tails which then interact with the RecA homologs Rad51 and Dmc1 to form nucleoprotein filaments. The filament on one side of the break then invades the homologous duplex DNA on either of the two non-sister chromatids resulting in strand displacement to form a displacement loop (D-loop). Extension of the invading strand via DNA synthesis increases the size of the D-loop, thus enabling the capture of the 3′-end of the DNA from the other side of the DSB. Further DNA synthesis and ligation of the DNA ends leads to the formation of two four-way junctions termed a double-Holliday junction (dHj) that, on resolution, results in the formation of a CO (reviewed in [2]).

An important feature of meiotic recombination is its close coordination with the alignment, pairing and synapsis of homologous chromosomes during prophase I (reviewed in [3]).

Mutants that are defective in chromosome axis or SC morphogenesis exhibit a profound effect on recombination and subsequent CO formation. For example, during meiosis in budding yeast IHR predominates over inter-sister chromatid recombination, this bias being in part dependent on the chromosome axis proteins Hop1 and Red1 [4]. The Hop1-related proteins AtASY1 and Hormad1/2 are thought to perform the equivalent role in *Arabidopsis* and mouse respectively [5–7]. It is proposed that AtASY1 is essential for AtDMC1-dependent IHR. In the absence of AtASY1, the association of AtDMC1 with the early recombination intermediates appears compromised such that virtually all IHR is aborted [8]. Mutation of the budding yeast SC transverse filament gene *ZIP1* results in a failure of CO-designated intermediates to progress to form COs [9]. CO formation is also affected, albeit in a distinct manner, in the corresponding *Arabidopsis* and rice mutants [10,11]. In the case of *Arabidopsis* lacking the Zip1 homolog, AtZYP1, there is a moderate reduction in CO frequency which is accompanied by the occurrence of recombination between non-homologous chromosomes. In rice, mutation of the *ZEP1* gene

Author Summary

Homologous recombination (HR) during prophase I of meiosis leads to the formation of physical connections, known as chiasmata, between homologous chromosomes (homologs). Chiasmata are essential for accurate homolog segregation at the first meiotic division. HR is initiated by the formation of DNA double-strand breaks (DSBs). As DNA replication prior to meiosis results in the duplication of each homolog to form two identical sister chromatids, a DSB in one sister chromatid could potentially be repaired using the other as the repair template rather than one of the two non-sister chromatids of the homolog. If this route were predominant, the formation of chiasmata would be disfavored and chromosome segregation would be compromised. However, during meiosis there is a strong bias towards inter-homolog recombination (IHR). In this study we have identified AtASY3, a component of the proteinaceous axes that organize the chromosomes during meiosis in *Arabidopsis*. We find that AtASY3 interacts with AtASY1, a previously identified axis protein that is essential for crossover formation. We show that loss of AtASY3 disrupts the axis-organization of AtASY1. This results in a substantial reduction in chiasmata, and there is extensive chromosome mis-segregation. We propose that loss of AtASY3 affects the efficiency of the inter-homolog bias.

leads to an apparent increase in CO/chiasma frequency. The interrelationship between recombination proteins and meiotic chromosome organization is further emphasized in a study in the filamentous fungus *Sordaria macrospora* [12]. This revealed that, in addition to their previously described recombination functions, Mer3, Msh4 and Mlh1 have roles in ensuring accurate juxtaposition of the homologous chromosomes. Nevertheless, understanding the functional interrelationship between the recombination machinery and the chromosome axes and SC and the extent to which it is conserved between species has proved challenging. Although the structural organization of meiotic chromosomes is conserved, the chromosome axis and SC proteins exhibit a high level of primary sequence divergence. This limits the efficacy of straightforward homology searches as a route to identification of homologues in different species [13] and raises the question of how functionally related these proteins may be.

As one approach to overcome this problem we have begun to make an inventory of proteins present in meiocytes from *Arabidopsis* and the closely related species, *Brassica oleracea*, in order to analyze novel meiotic proteins and identify meiotic protein complexes ([14], KO, KM, ER and FCHF unpublished). Used in combination with homology searches this has enabled us to identify an *Arabidopsis* meiosis-specific coiled-coil protein, AtASY3. Analysis of AtASY3 has revealed that it is a component of the chromosome axes during meiotic prophase I. We demonstrate that loss of AtASY3 compromises AtASY1 localization leading to a reduced level of CO formation and a defect in chromosome synapsis. Our study provides further insights into the role of chromosome axis-associated proteins and the SC in the control of CO formation.

Results

Reduced fertility and meiotic defects in plants lacking the coiled-coil protein AtASY3

Analysis of proteins from *B. oleracea* meiocytes by mass spectrometry (MS) resulted in the detection of 4 peptides with homology to the predicted product of the *Arabidopsis* gene,

At2g46980 (Figure S1A). We noted that At2g46980 (referred to hereafter as *AtASY3*) is predicted to encode an 88 kDa protein with a coiled-coil domain in its C-terminus region (Figure S1B). A database search revealed that the predicted coiled-coil protein was most closely related to a rice meiotic gene PAIR3 (25.6% identity) and had weak homology to Red1 from budding yeast (16.4% identity) [15–18]. RT-PCR analysis indicated that *AtASY3* was transcribed in reproductive tissues but not in vegetative tissues suggesting a potential role during the reproductive stage of development (Figure S1C). Thus we decided to characterize *AtASY3* further, to determine whether it encoded a meiotic protein and to establish its role.

We obtained three T-DNA insertion lines of *AtASY3* from the Nottingham Arabidopsis Stock Centre (NASC) (Figure S1B). Molecular characterization of each line confirmed the positions of the T-DNA insertions within *AtASY3* (Figure S2). Homozygous plants from each line showed normal vegetative growth but fertility was reduced by around 75% (Figure S3A).

The reduction in fertility was consistent with a defect in meiosis. To confirm this, DAPI-stained chromosome spread preparations from pollen mother cells (PMCs) were examined by fluorescence microscopy. Since the three lines were cytologically indistinguishable, the analysis of *Atasy3-1* is presented in Figure 1 and *Atasy3-2* and *Atasy3-3* are shown in Supplementary Figure S3B. Chromosome behavior was apparently normal from G2 through early prophase I (Figure 1A, 1G). However, normal pachytene nuclei were not observed (Figure 1B, 1H). As the chromosomes began to condense during late diplotene/diakinesis it became clear that a proportion of the homologous chromosome pairs had failed to form chiasmata (Figure 1C, 1I). This was confirmed by the presence of univalent chromosomes at metaphase I leading to mis-segregation at both meiotic divisions resulting in the formation of aneuploid tetrads (Figure 1D–1F, 1J–1L).

That the meiotic phenotype was due to mutation of *AtASY3* was confirmed by an allelism test in which a homozygous *Atasy3-1/Atasy3-2* double mutant was found to exhibit meiotic defects indistinguishable from the parental lines (Figure S3A–S3C) and a complementation test in which a full length *AtASY3* cDNA cloned under the control of the *AtDMC1* promoter in pPF408 [19], was found to restore normal meiosis in *Atasy3-1* (Figure S3D–S3I).

Cytological analysis of AtASY3 and AtASY1 localization during meiotic prophase I in wild type

The distribution of AtASY3 was studied by immunolocalization on chromosome spread preparations of wild-type PMCs using anti-AtASY3 antibody (Figure 2). AtASY3 foci were first detected on the chromatin at late G2 together with accumulation of the protein in the nucleolus (Figure 2A). At leptotene the nucleolar signal of AtASY3 disappeared and the protein was detected along the chromosome axes (Figure 2B). This persisted through zygotene and pachytene during which partial colocalization with the SC transverse filament protein AtZYP1 [10] was observed (Figure 2C–2F).

In wild-type meiocytes at the transition from late G2 to leptotene, which is cytologically typified by a prominent centralized nucleolus, numerous chromatin-associated foci and short stretches of AtASY1 staining were observed (Figure 2G). By leptotene these developed into a linear, yet not entirely uniform, signal along the axes. Analysis using deconvolution software (see Materials and Methods) revealed that the variation in signal intensity at leptotene arises because AtASY1 is distributed along the axes as a series of diffuse hyper-abundant patches or domains separated by stretches of lower abundance (Figure 2H). This is accentuated at pachytene when the DAPI-stained chromosomes appear as thick, rope-like structures. At this stage the AtASY1
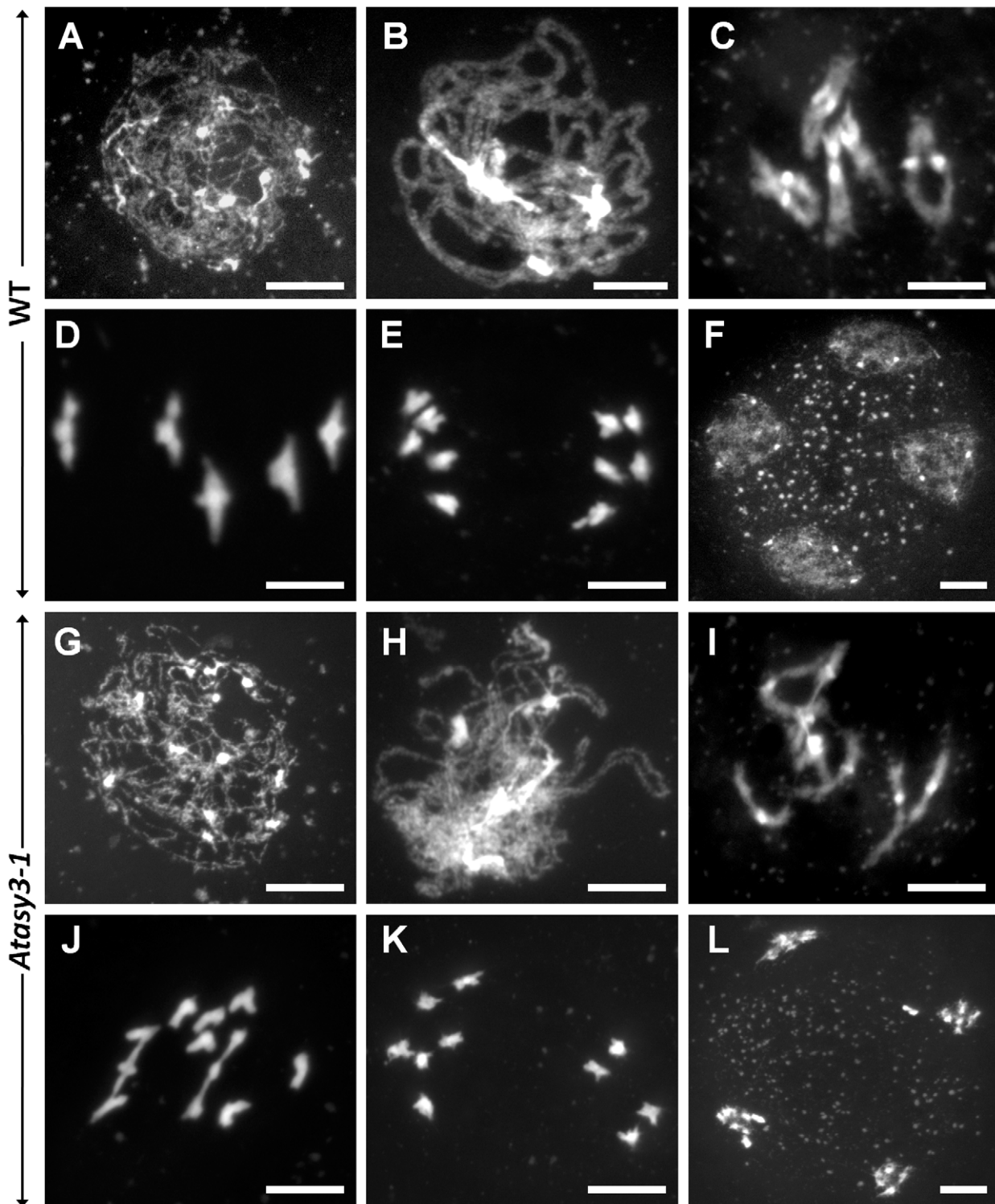
Figure 1. Meiotic stages. From wild-type (A–F) and *Atasy3-1* (G–L) pollen mother cells. (A,G) Leptotene. (B,H) Pachytene. (C,I) Diakinesis. (D,J) Metaphase I. (E,K) Dyad. (F,L) Tetrad. Early prophase I stages in *Atasy3-1* are similar to that of wild-type, however, at pachytene (H) homologous chromosomes fail to undergo full synapsis in *Atasy3-1*. Some univalents are present at diakinesis (I) and metaphase I (J) in *Atasy3-1* which can lead to chromosome mis-segregation at meiotic divisions and give rise to unbalanced dyad (K) and tetrad (L) nuclei. Bar, 10 μm.
doi:10.1371/journal.pgen.1002507.g001

signal is depleted along the axis and the domains become foci-like in appearance (Figure 2I). The foci appear relatively evenly distributed and consistent in number (Mean number of foci per nucleus = 160; n = 10). The tendency for AtASY1 to form domains along the axis is supported by electron microscopy (EM) studies in the plant *Crepis capillaris*. Immunologold localization of ASY1 in

Figure 2. Immunolocalization of AtASY3 and AtASY1. Immunolocalization of AtASY3 (red) on DAPI stained (blue) wild-type meiocytes during meiotic prophase I (A–F). (A) Late G2, (B) Leptotene, (C) Zygotene, (D) Pac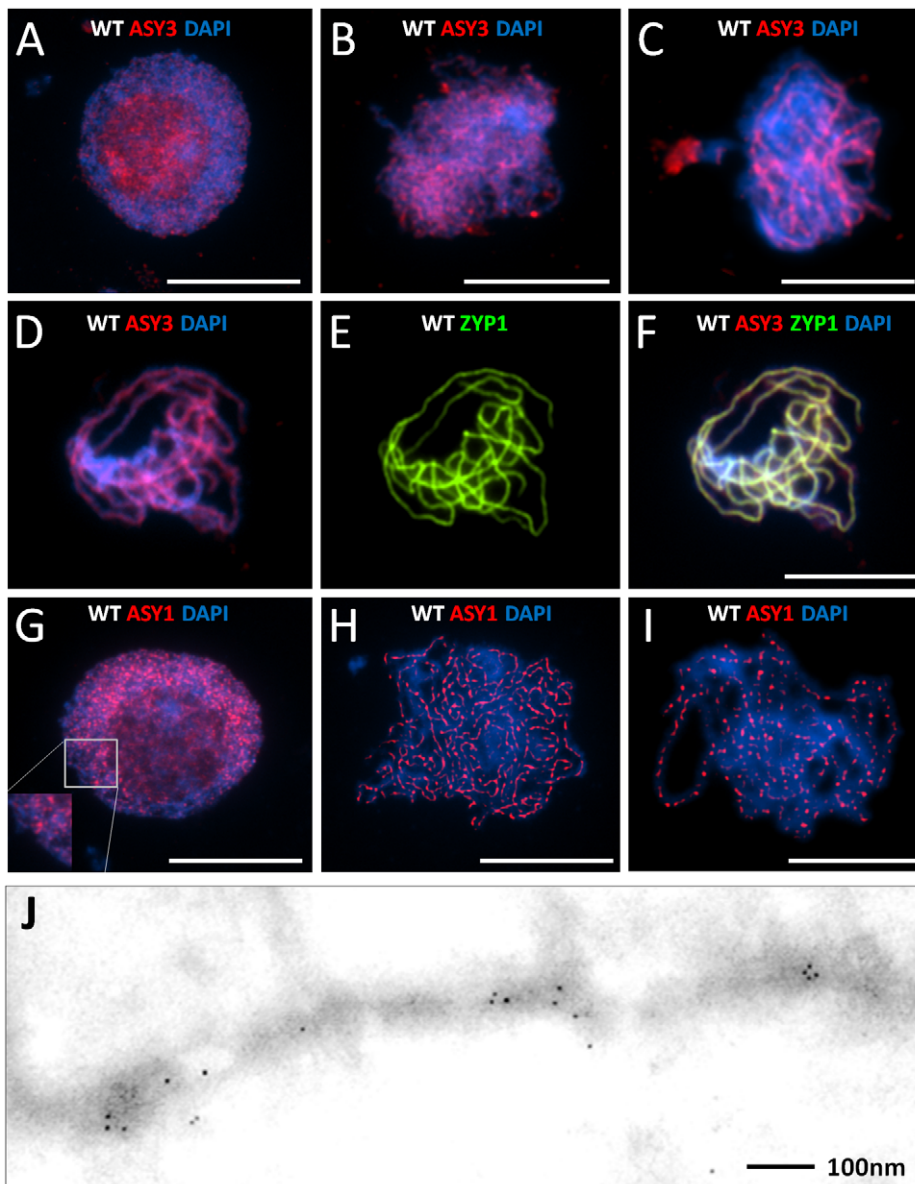hytene, dual localization with AtZYP1 (green) (E) and merged image (F). Immunolocalization of AtASY1 (red) on DAPI stained wild-type meiocytes during prophase I (G–I). (G) Late G2, (H) Leptotene (deconvoluted image), (I) Pachytene (deconvoluted image). Bar, 10 μm. (J) Immunogold labelling of AtASY1 on *Crepis capillaris* at meiotic prophase I. Bar 100 nm.
doi:10.1371/journal.pgen.1002507.g002

chromosome spread preparations of *C. capillaris* meiocytes reveals that the gold particles form discrete axis-associated clusters rather than an evenly distributed signal (Figure 2J).

Organization of the chromosome axis proteins and synaptonemal complex in *Atasy3-1*

Application of anti-AtASY3 antibody to prophase I spread preparations of chromosomes from *Atasy3-1* PMCs did not result in any AtASY3 signal (Figure 3A). This confirmed the specificity of the anti-AtASY3 antibody and supported the RT-PCR analysis which indicated that the *AtASY3* transcript was absent in the mutant lines (Figure S1D).

Since AtASY3 localized to the chromosome axes during prophase I, we investigated the effect of loss of the protein in

Atasy3-1 on other axis components. Immunolocalization of the cohesin proteins AtSMC3 and AtSYN1, the *Arabidopsis* ortholog of the budding yeast meiotic cohesin Rec8 [20,21], on spread preparations of *Atasy3-1* PMCs was indistinguishable from wild-type. Both proteins were detected as linear chromosome axis-associated signals during prophase I (Figure 3B–3E), suggesting global sister chromatid cohesion is present. In contrast, localization of AtASY3 was dependent on the cohesin complex, as it was completely disrupted in an *Atsyn1* mutant (Figure 3F).

Localization of AtASY1 in *Atasy3-1* meiocytes at late G2/early leptotene was similar to wild-type, with numerous chromatin-associated foci and short stretches of signal observed (Figure 3G). As prophase I progressed, AtASY1 co-localized with the axes. However, rather than forming a linear signal with the underlying
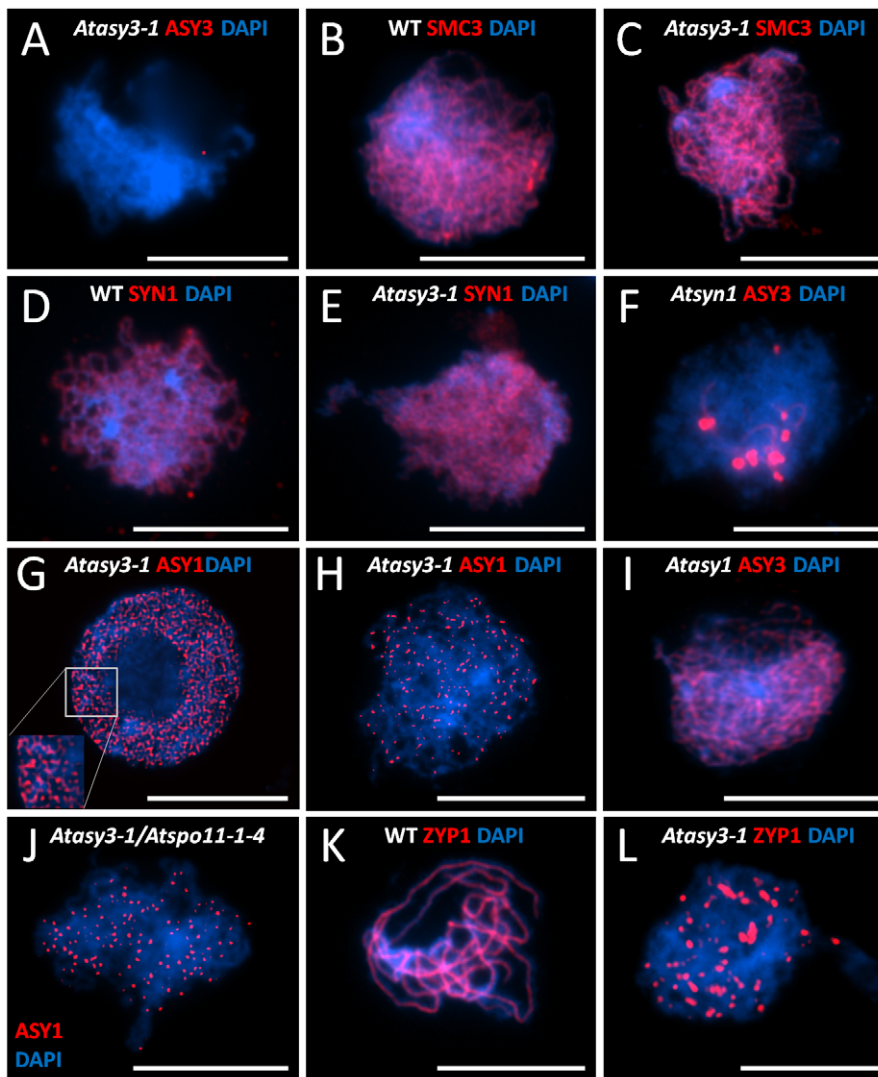
Figure 3. Immunolocalisation of chromosome axis proteins on *Arabidopsis* wild-type and chromosome axis mutants. At prophase I (A) AtASY3 (red) on *Atasy3-1*, (B) AtSMC3 (red) on wild-type and (C) *Atasy3-1*, (D) AtSYN1 (red) on wild-type and (E) *Atasy3-1*. (F) AtASY3 (red) on an *Atsyn1* mutant, G) AtASY1(red) on *Atasy3-1* at late G2 and (H) at late prophase I, (I) Immunolocalization of AtASY3 (red) on an *Atasy1* mutant at leptotene, (J) AtASY1(red) on an *Atspo11-1-4/Atasy3-1* mutant at late prophase I, (K) Immunolocalization of AtZYP1 (red) on wild-type at pachytene and (L) on *Atasy3-1* at late prophase I. DNA is stained with DAPI (blue) for all. Bar, 10 µm.
doi:10.1371/journal.pgen.1002507.g003

domain organization observed in wild-type, the protein was detected as discrete, evenly-distributed foci which persisted until the chromosomes began to condense at the end of prophase I (Figure 3H). These appeared rather heterogeneous in shape and size. The mean number of the AtASY1 foci was 69 per nucleus (n = 30), but there was considerable variation between individual nuclei, with the number ranging from 39–115.

In contrast to the aberrant localization of AtASY1 in *Atasy3-1*, that of AtASY3 in an *Atasy1* mutant was indistinguishable from wild-type. This suggests that while normal localization of AtASY1 is dependent on AtASY3, this relationship is not reciprocal (Figure 3I). The same situation has been observed in budding yeast where Hop1 loading requires Red1 but not vice-versa [22].

Previously we have shown that the association of AtASY1 with the chromosome axes is independent of AtSPO11-induced DSB formation [8]. Consistent with this we observed that the axis-associated AtASY1 foci remained in an *Atasy3-1/Atspo11-1-4* double mutant (Figure 3J). As anticipated, the double mutant

failed to form chiasmata, confirming that those detected in *Atasy3-1* are DSB-dependent (Figure S4B A,B).

As the initial cytological analysis of *Atasy3-1* indicated a defect in chromosome synapsis we investigated this in more detail. In wild-type meiocytes, the SC transverse filament protein, AtZYP1, polymerized to form the linear central region of the SC, such that at pachytene each pair of homologous chromosomes was fully synapsed (Figure 3K) [10]. In *Atasy3-1* the linearization of AtZYP1 to form a continuous SC did not occur. In most cases the AtZYP1 signals remained as foci or on occasion formed short stretches that were often abnormally thick and distorted in appearance. In some instances these structures could represent the accumulation of polycomplexes, nucleating at sites where AtZYP1 was unable to polymerize correctly along the lateral elements of the paired homologs (Figure 3L).

That SC formation was disrupted in *Atasy3-1* was supported by the analysis of silver-stained chromosome spread preparations using electron microscopy. In wild-type, fully synapsed homolo-

gous chromosomes were observed at pachytene (Figure 4A). In chromosome spread preparations of the *Atasy3* mutants using the same conditions the nuclei were diffuse and the chromosome axes could not be readily discerned (Figure 4B). However, by modifying the chromosome spreading conditions (see Materials and Methods) it was possible to detect nuclei where more extensive regions of axis were visible (Figure 4C). In some cases these were aligned, although the spacing often appeared variable. These observations support the immunolocalization studies that indicated that SC formation was disrupted. They also suggest that although chromosome axes are formed in *Atasy3-1*, there is likely some structural defect, possibly making them more susceptible to fragmentation by the chromosome spreading procedure. Alternatively, axis formation may be incomplete in the mutant.

Chiasma frequency is significantly reduced in *Atasy3* mutants

To quantify the reduction in COs in the *Atasy3* mutants we analysed the chiasma frequency and distribution in 50 *Atasy3-1* PMCs. This revealed nuclei containing 0–6 chiasmata with an overall mean chiasma frequency of 3.3 (Figure 1J, Figure S4A, Table S1). Similar results were obtained for *Atasy3-2* (3.17 n = 50) and *Atasy3-3* (3.32 n = 50). These observations contrast with wild-type nuclei which contain 8–12 chiasmata with an overall mean of 9.76 [23]. Inspection of the chiasma distribution in the *Atasy3* mutants revealed that 74.8% of the residual chiasmata were localized to the distal regions of the chromosomes. This figure is unchanged from that of wild-type (73.8% n = 50) (Table S1).

To further analyze the functional relationship between AtASY3 and AtASY1 we constructed an *Atasy3-1/Atasy1* double mutant and compared the effect on chiasma formation to that in the *Atasy3-1* and *Atasy1* single mutants. This revealed a reduction in the mean chiasma frequency from 3.3 (n = 50) observed in *Atasy3-1* to 1.78 (n = 50; $P < 10^{-7}$) in *Atasy3-1/Atasy1*, but no significant difference between the double mutant and *Atasy1* (1.88 n = 50; P = 0.681) (Figure S4B C,D). Thus AtASY1 is epistatic to AtASY3 with regard to CO formation, whereas the relationship is reversed in terms of protein loading. A similar relationship exists for DSB formation and Red1 and Hop1 loading in budding yeast [22,24]. Whereas Hop1 loading is greatly reduced in a *red1* mutant, but not

vice-versa, a *hop1* mutant exhibits a stronger defect in DSB formation. Our data suggest that the higher CO frequency in *Atasy3-1* as compared to *Atasy3-1/Atasy1* may be attributable to the AtASY1 foci that remain in the single mutant, but that this is insufficient to promote wild-type levels of COs. However, this interpretation assumes that immunolocalization detects all the axis-associated AtASY1 that is present in *Atasy3-1*.

In budding yeast a group of proteins referred to as ZMM, comprising Zip1, Zip2, Zip3, Zip4, Msh4, Msh5 and Mer3, are crucial for the formation of interference-sensitive COs [9]. Homologs of the *ZMM* genes have been identified in *Arabidopsis* where their mutation results in a ~85% reduction in CO formation [reviewed in 25]. The remaining COs (~15%) exhibit a random numerical distribution based on a Poisson analysis [26,27]. Since loss of AtASY3 resulted in a substantial reduction in chiasmata/COs we surmised that the protein was required for the formation of normal levels of *ZMM*-dependent COs. To investigate this, an *Atasy3-1/Atmsh4* double mutant was constructed and the chiasma frequency determined to establish if loss of AtASY3 resulted in any reduction in chiasmata over that observed in *Atmsh4*. In a survey of 30 metaphase I nuclei from the *Atasy3-1/Atmsh4* line no chiasmata were detected, whereas the mean chiasma frequency in the *Atmsh4* mutant was 1.1 (n = 30) (Figure S4B E,F). This indicates that AtASY3 has a role in the formation of all meiotic COs.

Loss of AtASY3 affects DSB formation and localization of recombination pathway proteins

To address the basis for the reduced chiasma formation in *Atasy3-1*, we began by investigating the level of DSB formation in the mutant. The meiosis-specific histone H2AX is rapidly phosphorylated in chromatin surrounding the site of a DSB [28,29,30]. This phosphorylated form, γH2AX, can be detected by immunolocalization as foci in chromosome spread preparations from meiocytes. In wild-type nuclei a mean of 160.8 (n = 5) γH2AX foci were detected at leptotene (Figure 5A). In *Atasy3-1* the corresponding number was 114.2 (n = 5) (Figure 5B). This suggested that the formation of DSBs was significantly reduced in the *Atasy3-1* mutant (P<0.01). However, based on these observations we cannot exclude the possibility that the observed
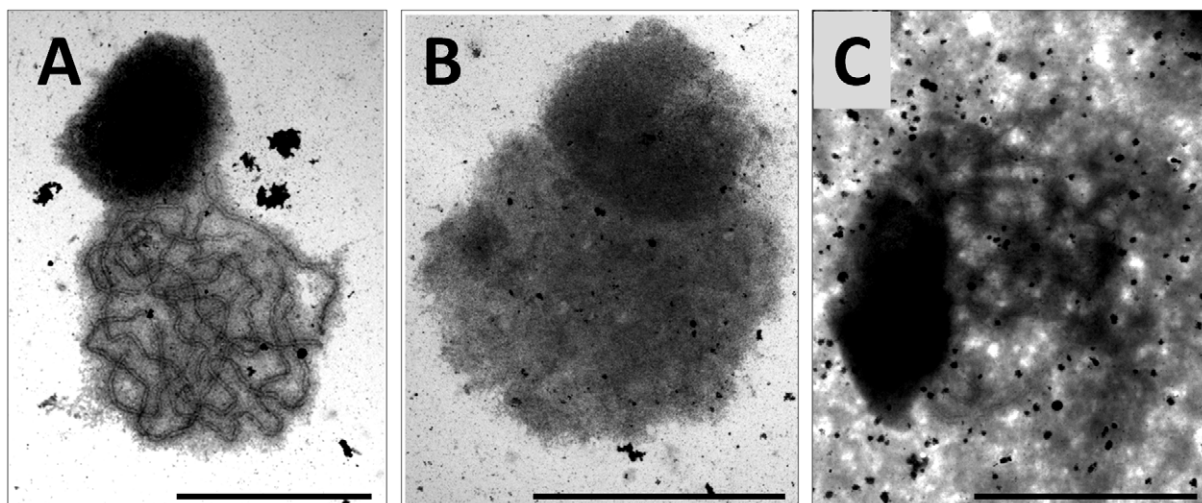

Figure 4. Electron micrographs of silver stained meiotic prophase I nuclei in wild-type and *Atasy3-1*. (A) wild-type, (B) *Atasy3-1* (C) *Atasy3-1* (modified method) showing aligned stretches of axis (arrow). Bar, 10 µm.
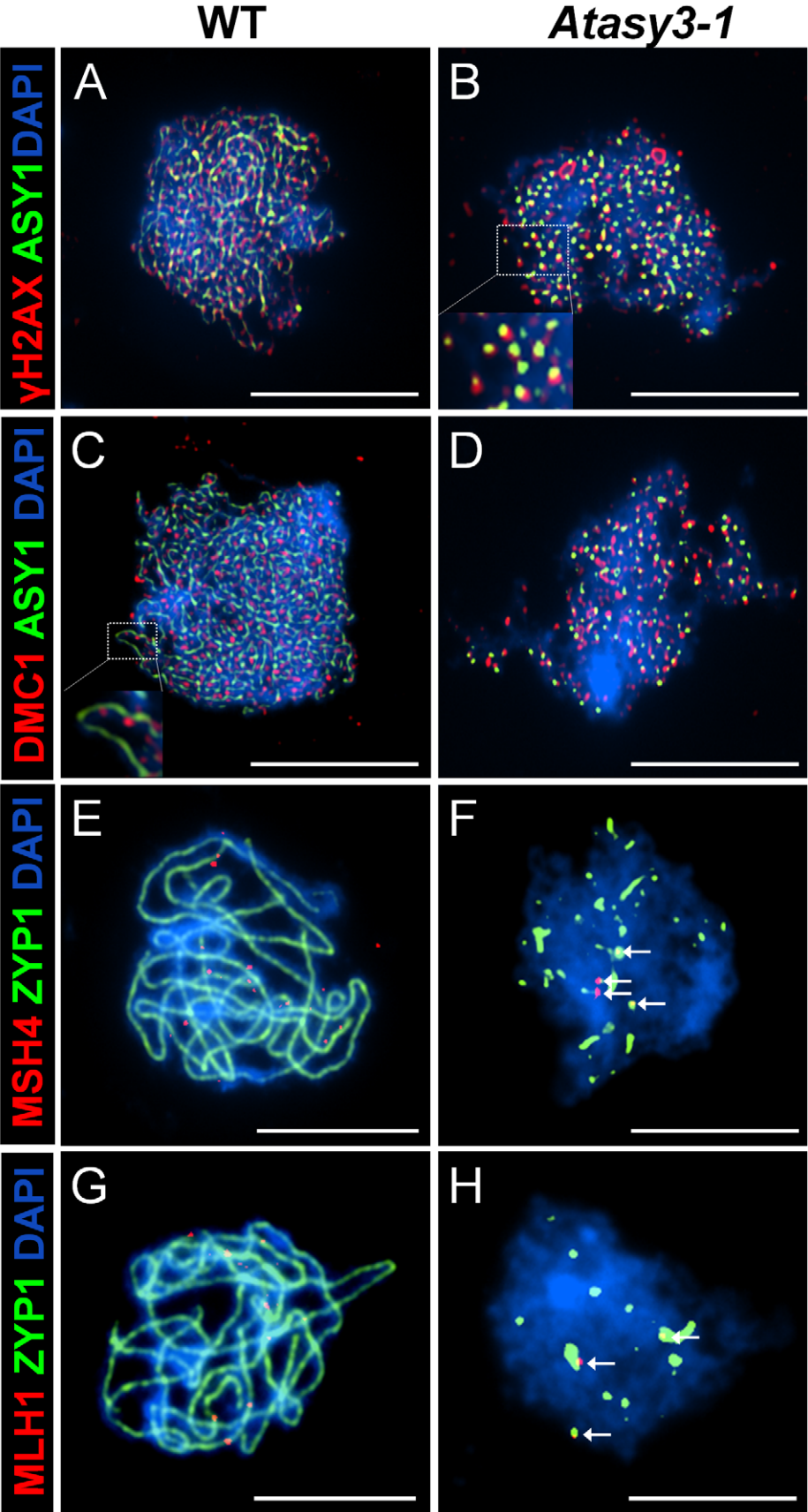doi:10.1371/journal.pgen.1002507.g004

Figure 5. Dual immunolocalisation of AtASY1 and AtZYP1 with recombination pathway proteins in wild-type and *Atasy3-1* meiotic prophase I nuclei. (A) AtASY1 (green) and γH2AX (red) on wild-type and (B) *Atasy3-1* at leptotene, (C) AtASY1 (green) and AtDMC1 (red) on wild-type and (D) on *Atasy3-1* at leptotene. (E) AtZYP1 (green) and AtMSH4 (red) on wild-type and (F) on *Atasy3-1* (AtMSH4 arrowed). (G) AtZYP1 (green) and AtMLH1 (red) on wild-type and (H) on *Atasy3-1* (AtMLH1 arrowed). DAPI (blue) for all. Bar, 10 μm.
doi:10.1371/journal.pgen.1002507.g005

difference in the number of foci in the mutant compared to wild-type was due to an accelerated turn-over of DSBs. It also assumes that H2AX is phosphorylated at all DSBs in the mutant.

Immunolocalization of AtDMC1 and AtRAD51 [31,32] revealed a significant reduction in the number of foci observed in *Atasy3-1* at leptotene relative to wild-type. In the case of AtDMC1, the figures for *Atasy3-1* and wild-type were 106.8 (n = 5) and 143.8 (n = 5) (P = 0.02) respectively (Figure 5C, 5D). For AtRAD51, the mean number of foci in *Atasy3-1* was 99.8 (n = 5) compared to 141 (n = 5) (P<0.01) in wild-type meiocytes (Figure S5A, S5B). Although the numbers of AtDMC1 and AtRAD51 foci only indirectly reflect the number of DSBs, these figures are consistent with the decrease in γH2AX foci observed in *Atasy3-1*.

The MutS homolog AtMSH4 is required for the formation of normal levels of interference sensitive COs [23]. In wild-type, AtMSH4 foci accumulate on the chromosomes at leptotene and these gradually reduce in number through zygotene. By early pachytene only a few remain and they continue to dissociate from the chromatin such that by late pachytene they have disappeared [23]. Similarly, in this study we observed a mean of 140 (n = 5) AtMSH4 foci in wild-type nuclei at leptotene which gradually reduced to around 10 foci detectable at early pachytene (Figure S5C; Figure 5E). A similar pattern of turnover of AtMSH4 foci was observed in *Atasy3-1*. However, the peak number of foci observed at each stage was lower than in wild-type. At leptotene a mean of 109.8 (n = 5) foci were recorded (Figure S5D). The foci reduced in number to between 0–4 at early pachytene and were found to associate with the stretches of AtZYP1 protein present in *Atasy3-1* (Figure 5F).

The MutL homologue, AtMLH1, is thought to mark the sites of COs/chiasmata [33]. Dual-immunolocalization of AtMLH1 and AtZYP1 on chromosome spread preparations revealed 8–12 AtMLH1 foci (mean = 9.8, n = 10) in wild-type nuclei at pachytene (Figure 5G). In *Atasy3-1* this was significantly reduced to a mean of 3.2 AtMLH1 foci (P<0.001; n = 10) per nucleus which is consistent with the observed chiasma frequency. These foci invariably co-localized with the patches of AtZYP1 that remained in the *Atasy3-1* meiocytes (Figure 5H).

These observations reveal a coordinate reduction in the number of γH2AX, AtDMC1, AtRAD51 and early AtMSH4 foci to around 60% of the number observed in wild-type. However, there must be an additional defect or defects since the overall number of crossovers, based on AtMLH1 foci and chiasma counts, is only around 30% of the wild-type level. Nevertheless, there is no overall repair defect as there is no evidence of chromosome fragmentation. Previously we have reported that loss of AtASY1 also leads to a major defect in CO formation, but with no obvious defect in DSB formation suggesting that DSBs occur at or near the wild-type level [8]. This was based on immunolocalization of γH2AX foci in squash preparations of meiocytes at early prophase I. Since our analysis of *Atasy3-1* was carried out using chromosome spread preparations we decided to determine the number of γH2AX foci in *Atasy1* using the same approach. This revealed that the mean number of γH2AX foci was 129.5 (n = 10) (Figure S5E, S5F). Thus as previously [8], there is no evidence of a major depletion of γH2AX foci in *Atasy1*, but a slight reduction cannot be excluded (P = 0.12).

Interplay between the recombination and chromosome axis proteins

Dual localization of γH2AX and AtASY1 in wild-type nuclei revealed the γH2AX foci were adjacent to the hyper-abundant domains of AtASY1 and showed a slight tendency to overlap (Figure 5A). This observation is consistent with the proposal that the nascent DSB is tethered to the chromosome axis more or less coincident with its formation [4,34,35]. Similarly dual localization of AtDMC1 and AtASY1 revealed a close association of the AtDMC1 foci with the AtASY1-stained axis, but the signals were largely distinct and did not overlap (Figure 5C).

Despite the fact that AtASY1 was present as discrete foci rather than hyper-abundant domains in *Atasy3-1*, these were virtually all (97.4% n = 5) found in association with a γH2AX signal (Figure 5B). In a control designed to detect fortuitous co-localization (see Materials and Methods) this figure was 39% (n = 5). However, in the sample of cells analysed the mean number of γH2AX foci was greater than the number of AtASY1 foci (114.2 versus 87.8 respectively, n = 5). Hence, not all of the γH2AX foci co-localize with AtASY1 in *Atasy3-1*. The AtASY1 foci in *Atasy3-1* were also found in association with the AtDMC1 foci (95%, n = 5) (Figure 5D). However, in this case, unlike in wild-type, there was a tendency for signals to overlap. Hence it would appear that the two proteins end up localized at the same sites on the chromosomes but their spatial relationship may be perturbed in the absence of AtASY3.

We have previously shown that the stable association of AtDMC1 foci to the chromosome axes during early prophase I requires AtASY1 [8]. Since AtASY1 localization is disrupted in *Atasy3-1*, we investigated the localization of AtDMC1 in *Atasy3-1* in more detail. The chronology of AtDMC1 localization was determined by carrying out the immunolocalization of the protein together with prior BrdU pulse-labeling of the PMCs during meiotic S-phase as described previously [8]. This revealed that in *Atasy3-1*, *Atasy1* and wild-type maximum numbers of AtDMC1 foci accumulated on the chromosomes around 12 h following the BrdU-pulse. However, at 24 h while numerous AtDMC1 foci still remained in both *Atasy3-1* and wild-type, they were entirely absent in *Atasy1* (Figure S6). These data indicate that the rapid loss of AtDMC1 foci observed in *Atasy1* does not occur in *Atasy3-1*. That turnover of AtDMC1 foci in *Atasy1* is more rapid than in wild-type could suggest that some normal barrier to progression is absent, such that recombination proceeds but CO-designation is defective. Since the initial rate of accumulation of AtDMC1 is normal in *Atasy3-1* it would suggest that the reduced number of foci in the mutant may reflect a reduction in DSBs rather than an increase in turnover. Furthermore, it suggests that despite the overall depletion of AtASY1, the residual protein is sufficient to ensure that the temporal localization of AtDMC1 is similar to that in wild-type meiocytes.

AtASY3 and AtASY1 and their Brassica homologs are able to interact

The finding that normal axis-association of AtASY1 was dependent on AtASY3 combined with the observation that the two proteins co-localized during prophase I suggested both a functional and possibly a direct physical inter-relationship between

them. To obtain evidence that AtASY3 and AtASY1 may be components of a meiotic complex and possibly interact *in planta* we conducted a co-immunoprecipitation (CoIP) experiment using anti-AtASY1 antibody. Since extracting protein in sufficient quantities from *Arabidopsis* meiocytes is impractical due to the small size of the anthers, we used meiocyte extracts from *B. oleracea*. In previous studies we have shown that an anti-AtASY1 antibody recognizes the corresponding *Brassica* protein, BoASY1, which shares 83% amino acid sequence identity with AtASY1 [36]. Similarly, analysis of *BoASY3* from *B. oleracea* indicated that it encodes a protein with 77% sequence identity with its *Arabidopsis* counterpart (Figure S7) and that it localized to the chromosome axes during prophase I of meiosis (Figure S8). Co-immunoprecipitating proteins were identified by MS of tryptic peptides followed by searches against a combined *Brassica* database containing the BoASY1 and BoASY3 full-length sequences (see Materials and Methods for details). BoASY1 was identified as the top hit with 40 unique peptides corresponding to 397/599 amino acids (65% coverage) and BoASY3 as the second hit with 28 peptides corresponding to 297/776 amino acids (38% coverage) (Figure S9A). Both proteins were absent from the control sample. Thus it would seem probable that BoASY1 and BoASY3 are components of a complex and given the close conservation with *Arabidopsis*, is likely the case for AtASY1 and AtASY3.

To determine if the proteins can directly interact, the full-length cDNAs of each gene were cloned as in-frame fusions with the *GAL4* DNA binding domain (DBD) and the *GAL4* activator domain (AD) in the yeast two hybrid plasmids pGBKT7 and pGADT7 respectively. Plasmids encoding the AtASY1-DBD and AtASY3-AD fusions and the reciprocal pair of constructs were co-transformed into yeast. At the same time control transformations,

where one of the constructs was replaced by the corresponding empty vector, were also carried out. All plasmid combinations enabled the transformed yeast to grow on synthetic dropout medium (-Leu/-Trp) that selected the auxotrophic markers on the cloning vectors. When the plasmid combinations were tested on low stringency selective plates (-Leu/-Trp/-His) the yeast cells containing AtASY1 and AtASY3 as reciprocal DBD/AD fusions enabled significant growth at all dilutions. Some slight growth was also detected in controls containing the AtASY1-DBD and AtASY3-AD plasmids. However, under higher stringency selection (-Leu/-Trp/-His/-Ade) growth was entirely restricted to the combinations carrying both genes (Figure 6). Further experiments with a series of plasmids in which truncated regions of AtASY3 were fused to the GAL4 activator domain indicated that the interaction of AtASY3 with AtASY1 was dependent on amino acid residues 623–793 of AtASY3 which correspond to the predicted coiled-coil region (Figure 6). These data suggested that AtASY1 and AtASY3 can interact and likely do so *in planta*.

Discussion

AtASY3 is a component of the meiotic chromosome axes in *Arabidopsis*

We have identified AtASY3, a chromosome axis protein that is required for normal levels of COs and SC formation in *Arabidopsis*. AtASY3 is predicted to contain a coiled-coil domain towards the C-terminus. This structural feature is found in other meiotic proteins, such as Red1 in budding yeast, SCP3/Cor1 in mammals and OsPAIR3 in rice, that are components of the axial regions of the SC, yet on the basis of amino acid sequence homology are reported to have no close homologs in other species
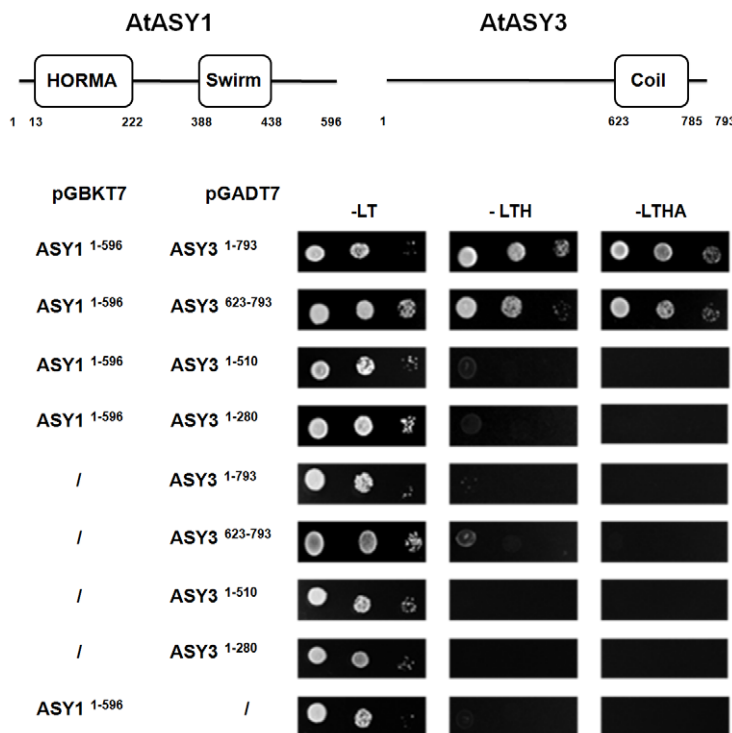
Figure 6. Yeast two-hybrid analysis of AtASY3 and AtASY1 with schematic illustration of predicted domains and relative positions of amino acid residues. Plasmid constructs were co-transformed into Y2HGold yeast cells before plating on SD -Leu/-Trp (-LT), SD -Leu/-Trp/-His (-LTH) and SD -Leu/-Trp/-His/-Ade (-LTHA). Growth on –LTH and –LTHA confirms a protein-protein interaction between AtASY1 and AtASY3 that is dependent on AtASY3 residues 623–793.
doi:10.1371/journal.pgen.1002507.g006

[15,16,18,37,38]. AtASY3 appears similar in this respect. Although it shares 77% sequence identity with BoASY3 from the closely related *B. oleracea*, the level of sequence identity with Red1 and OsPAIR3 is limited, at 16.4% and 25.6% respectively. This sequence divergence appears to be a recurrent feature of proteins that are components of the chromosome axes.

DSBs appear reduced and crossover formation is compromised in *Atasy3-1*

In *Arabidopsis* the level of DSBs may be inferred from the number of γH2AX and/or AtDMC1 or AtRAD51 foci detected in meiocytes at early prophase I [8]. Our data suggested a consistent reduction in DSBs from 150–160 in wild-type meiocytes to about 100 in *Atasy3-1*, an overall reduction of around 33%. However, as DSB detection is indirect, we cannot formally rule out the possibility that not all DSBs are detected in the mutant. Nevertheless, as the number of γH2AX foci is very similar to those of the strand-exchange proteins this seems a reasonable conclusion.

The physical association of the recombination machinery and the chromosome axes has been known for many years [3,34,39]. Recent studies in budding yeast indicate that the DSB machinery becomes tethered to the chromosome axes prior to break formation and that the axis components Red1 and Hop1 are required for this [4,35]. Analysis of *red1* mutants has revealed a defect in DSB formation [40–42]. It is conceivable that AtASY3 may play a similar role in axis organization that is crucial to enable normal levels of DSB formation. The reduction in foci corresponding to γH2AX and the strand-exchange proteins is consistent with a scenario whereby DSB formation occurs in the context of the axis, rather than the recombination complex associating with the axis following break formation, as in the latter instance, a reduction in γH2AX foci would not be anticipated. However, it remains possible that depletion of AtASY3 may induce a change in chromatin structure that in turn results in a reduction in DSBs.

Although DSB formation appears to be significantly reduced in *Atasy3-1*, any reduction due to the loss of AtASY1 appears more marginal. This is in broad agreement with our earlier study [8]. It is worth noting that this difference mirrors chromosome axis formation in the two mutants. Whereas loss of AtASY3 disrupts the axes, the *Atasy1* mutant has clearly defined axes, albeit with some minor discontinuities, seemingly indicating the importance of the chromosome axes for efficient DSB formation [43]. However, it contrasts with observations in budding yeast and mouse, where mutants lacking Hop1 and HORMAD respectively exhibit strongly reduced numbers of DSBs [44,45]. At present the basis and significance of this difference remains unknown. It may reflect an underlying difference in the control of DSB formation, although the formation of DSBs in *hop1* and *red1* mutants in different budding yeast strains also shows some variation [40,46].

A reduction in the mean chiasma/CO frequency to around 30% of the wild-type level was observed in all *Atasy3* lines. Analysis of the *Atmsh4/Atasy3-1* double mutant indicates that loss of AtASY3 compromises the formation of COs which are subject to CO interference, and also non-interfering COs. This would suggest that AtASY3 plays a crucial role at an early stage in the recombination pathway. A reduction in CO formation is also a characteristic of mutants in the axis-associated proteins Red1 and OsPAIR3 [18,24,40,41]. A recent study in budding yeast has indicated that loss of Red1 results in a conversion from inter-homolog bias to inter-sister bias for DSB repair. It is proposed that this is due to a loss of constraint on Rec8 loading at the recombination site, thus favoring inter-sister recombination [4]. It

is conceivable that a similar situation arises through the loss of AtASY3. If so, this could explain why there is a proportionally greater reduction in CO formation in *Atasy3-1* than might be expected from the apparent reduction in DSBs. Simple extrapolation would suggest that if the ratio of COs to non-COs was maintained in the mutant, the mean CO/chiasma frequency would be 6–7 rather than the 3.5 observed. This implies that there is a loss of inter-homolog bias and that a greater proportion of the DSBs are repaired via another route such as inter sister-chromatid exchange. Alternatively, loss of AtASY3 may result in preferential processing of some or all of the recombination intermediates to favor non-COs rather than COs. At present the data does not enable us to distinguish between these possibilities.

The observation that 75.7% of the chiasmata that remain in *Atasy3-1* are sub-telomeric/distal is consistent with previous studies in *Arabidopsis* showing that the telomeres cluster on the nucleolus during early prophase I and as a result the sub-telomeric regions of the homologous chromosomes are placed in proximity [47]. A similar situation was observed in *Atasy1* where virtually all the residual chiasmata are distal [48].

Axis-association of AtASY1 is AtASY3-dependent and occurs in the absence of DSB formation

Deconvolution of the linear AtASY1 signal in wild-type meiocytes at leptotene through early pachytene revealed that it comprises evenly-spaced axis-associated domains of hyper-abundance interspersed with more lightly staining regions. This organization was supported by immunogold studies in meiocytes from *C. capillaris*. The number of AtASY1 domains appeared quite consistent, at around 160 per nucleus. The organization of AtASY1 is highly reminiscent of that of Hop1 which has been observed to form domains of alternating hyper-abundance and lower-abundance in budding yeast at early pachytene [49,50]. Loss of AtASY3 resulted in a significant effect on the distribution of AtASY1, such that axis-associated foci were observed during prophase I. These were fewer in number than the AtASY1 domains observed in wild-type and this varied from cell to cell ranging from 39–115 in the sample examined. Nevertheless, dual-localization studies with γH2AX and AtDMC1 indicated that these AtASY1 foci coincided with sites of recombination. However, further investigation will be required to determine whether or not localization of AtASY1 at the axial region still occurs with normal spatial specificity in *Atasy3-1*. Studies in budding yeast initially reported that localization of the AtASY1 homolog, Hop1, was dependent on the chromosome axis protein Red1 [22]. However, more recently it was suggested that while normal levels of Hop1 loading require Red1, some Hop1 is loaded at the sites of DSBs independently [46]. Our observations suggest a similar relationship between AtASY1 and AtASY3.

In wild-type, the AtASY1-abundant regions along the axes at prophase I correlated both spatially and numerically with the γH2AX and AtDMC1 foci, suggesting that the DSBs are positioned within AtASY1-enriched domains. This is consistent with the proposed role of AtASY1 in promoting IHR [8]. Interestingly, whereas the γH2AX and AtASY1 signals over-lapped, the AtDMC1 signal was adjacent to, but did not merge with the AtASY1 signal. Further study will be required to explore the significance of this observation. It appears that a similar spatial relationship between DSBs and AtASY1 is maintained in *Atasy3-1* as virtually all the AtASY1 foci in the mutant co-localize with γH2AX. Thus, it suggests that recruitment of AtASY1 and the recombination machinery to the axial region is spatially coordinated. However, these may not be interdependent events since localization of AtASY1 in the *Atspo11-1-4* null mutant

appears, based on immunofluorescence, normal [8]. Similarly in this study, examination of AtASY1 localization in an *Atasy3-1/Atspo11-1-4* double mutant suggests that the AtASY1 foci observed in *Atasy3-1* are still formed and associated with the axial region. Nevertheless, further studies will be required to establish if the AtASY1 domains observed in *Atspo11-1-4* and *Atasy3-1/Atspo11-1-4* are identical to those in the wild-type. If so, then it suggests that AtASY1 is initially recruited to predetermined chromosomal regions that also encompass DSB hotspots, possibly establishing a spatial relationship favoring IHR. Alternatively, it is conceivable that the AtASY1 domain formation observed in wild-type may be guided or influenced by DSB formation or the pre-DNA break recombinosome complex. Studies in budding yeast have also led to the proposal that the interhomolog bias is established before DSB formation with enforcement of the bias occurring at the transition from the nascent DSB to a joint molecule recombination intermediate [41].

Although the majority of the AtASY1 foci in *Atasy3-1* were associated with γH2AX foci at early prophase I, there were additional γH2AX signals that did not colocalize. If loss of DSBs and the destabilization of AtASY1 localization observed in *Atasy3-1* occurs stochastically, then, given that formation of AtASY1 foci and DSBs does not appear to be co-dependent, one would expect to see a similar proportion of γH2AX and AtASY1 foci that were not associated with one another. As this does not appear to be the case, it seems possible that a sub-set of DSBs occur in regions that are not associated with AtASY1. It may simply be that although the AtASY1 foci that persist in *Atasy3-1* correspond to the position of the domains observed in wild-type they are substantially smaller. Hence a proportion of the γH2AX foci no longer co-localize despite the normal spatial recruitment of the recombination complexes to the chromatin. Alternatively, some DSBs may occur in regions of lower AtASY1 abundance. Previously, it has been proposed in budding yeast that some DSBs are formed at random sites that are not associated with DSB hotspots [41]. Hence, if the AtASY1 domains are coincident with hotspots, which would seem logical, this may also be the case in *Arabidopsis*.

Evidence suggests that AtASY3 and Red1 share functional similarities

Despite amino acid sequence variation it has been suggested that Red1 and SCP3/Cor1 may be structural analogs [15]. Nevertheless, to date a functional ortholog of Red1 in a multi-cellular organism has not been reported. However, the studies described here suggest that AtASY3 has at least some functional similarity to Red1. The most compelling evidence arises from the close functional interrelationships that both proteins share with their corresponding HORMA domain proteins. Loss of Red1 and AtASY3 proteins results in a disruption of Hop1 and AtASY1 localization respectively, during prophase I [22]. In budding yeast Red1 has been shown to interact with Hop1 in co-immunoprecipitation experiments [46]. Yeast two-hybrid studies have shown that the 290 amino acids at the C-terminus of Red1 are essential for the interaction with Hop1. This part of the protein is predicted to form a coiled-coil domain. In this study MS analysis of proteins that were co-immunoprecipitated from *Brassica* meiocytes using an anti-AtASY1 antibody revealed a likely interaction between BoASY1 and BoASY3, the homologs of AtASY1 and AtASY3 respectively. That AtASY3 and AtASY1 can directly interact was confirmed by yeast two-hybrid analysis. Moreover further study revealed that the C-terminal of AtASY3 that contains a predicted coiled-coil region is essential for the interaction between the two proteins. Studies indicate that Red1 is required for normal levels of DSB formation. This also appears to be the case for AtASY3,

although this effect does not appear as pronounced in *Atasy3-1* as that in a *red1* mutant where a reduction in DSB formation to ~25% of wild-type has been reported [42].

It seems likely that PAIR3 in rice may also be a functional homolog of Red1. While a direct interaction with the rice HORMA domain protein OsPAIR2 has not yet been demonstrated, localization of OsPAIR2 is OsPAIR3 dependent and an *Ospair3* mutant has a similar phenotype to that of *Atasy3-1* [17,18].

SC nucleation is sufficient to prevent aberrant ectopic recombination

In addition to its structural role within the SC, the budding yeast protein Zip1 has been shown to play a key role in meiotic recombination [51,52]. Zip1 together with other members of the ZMM group of proteins, Zip2, Zip3, Zip4, Msh4, Msh5 and Mer3, is crucial for the formation of interference-dependent COs [51]. In *Arabidopsis* loss of AtZYP1 only results in a modest reduction in chiasma frequency to about 80% of the wild-type level. However, many of the remaining chiasmata occur between ectopic chromosome regions, possibly between duplicated sequences that amount to around 60% of the *Arabidopsis* genome [10]. The studies described here revealed that loss of AtASY3 had a profound effect on the formation of the SC. In most nuclei it appeared that alignment of the chromosome axes was extensively disrupted and immunolocalization studies with the transverse filament protein AtZYP1 indicated little evidence of normal SC assembly. In general, nuclei contained a mixture of AtZYP1 foci or occasional short stretches which appeared abnormally thickened and deformed. Although *Atasy3-1* is essentially asynaptic, there is no evidence of the non-allelic recombination observed in plants lacking AtZYP1. The bivalents that remained in the *Atasy3-1* meiocytes at metaphase I comprised homologous chromosomes and there was no evidence of multivalent formation. Immunolocalization studies revealed a reduction in AtMLH1 foci that reflected the reduction in chiasmata in *Atasy3-1*. These AtMLH1 foci, which are thought to localize to CO sites [33], were invariably associated with the residual AtZYP1 present in the mutant. Hence, it would appear that the presence of AtZYP1 at the site of recombination is important for the prevention of non-allelic recombination, but extensive SC polymerization is not required. This finding provides further evidence that in addition to SC formation, AtZYP1 plays an important role in the formation of COs in *Arabidopsis*.

In summary, these studies provide further insight into meiotic CO formation. Moreover they emphasize that despite the lack of sequence homology between the chromosome axes components from different species, it seems likely that a close functional relationship remains.

Materials and Methods

Plant material and nucleic acid extraction

A. thaliana ecotype Columbia (0) was used for wild-type analysis. T-DNA insertion lines SALK_143676, SALK_050971 and SAIL_423_H01 were obtained from NASC for mutant analysis [53]. Plants were grown, material harvested and nucleic acid extractions were performed as previously described by Higgins *et al.* [23].

T-DNA insertion site mapping

The T-DNA insertion site of the mutant lines was confirmed as previously described [23] (Figure S2). Details of the primers used are presented in Table S2.

Complementation of Atasy3-1

Primers ASY3-CM-F1 and ASY3-CM-R1 (Table S2) were used to amplify the entire AtASY3 coding sequence with flanking 5′ and 3′ UTR regions from cDNA clone pda 19140 (Riken, Japan). The PCR product was cloned into the binary vector pPF408 [19] using SpeI sites incorporated into the primers. The construct was confirmed by sequencing. The binary plasmid construct was introduced into *Agrobacterium tumefaciens* LBA 4404 and plants transformed as previously described [23].

RNA extraction and RT–PCR

RNA extraction and RT-PCR was carried out as previously described [54]. Details of the primers are given in Table S2.

Nucleic acid sequencing

Nucleotide sequencing was carried out by the Genomics and Proteomics Unit, School of Biosciences, University of Birmingham, UK.

Antibody production

Primers ASY3-AB-F1 and ASY3-AB-R1 (Table S2) were used to amplify a 702bp fragment comprising amino acid residues 560 to 793 of *AtASY3* from cDNA clone pda 19140 (Riken, Japan). The PCR product was cloned into the expression vector pET21b (Novagen) using *NdeI* and *XhoI* sites incorporated into ASY3-AB-F1 and ASY3-AB-R1 respectively. Recombinant His-tagged protein was isolated from *E. coli* BL21 (Novagen) under native conditions using Ni-agarose following the manufacturer's protocol (QIAGEN). Polyclonal antiserum against the recombinant protein was raised in rabbit (BioGenes GmbH, Germany).

Cytological procedures

Cytological studies were carried out as previously described [23]. The following antibodies were used: anti-AtASY3 (rabbit, 1/200 dilution) anti-AtASY1 (rabbit/rat, 1/1000 dilution), anti-AtMSH4 (rabbit, 1/500 dilution), anti-AtZYP1 (rabbit/rat, 1/500 dilution), anti-AtSMC3 (rabbit 1/500 dilution), anti-AtSYN1 (rabbit 1/500 dilution), anti-AtDMC1 (rabbit 1/500 dilution), anti-AtRAD51 (rabbit, 1/500 dilution), anti-AtMLH1 (rabbit/rat, 1/200 dilution) and anti-γH2AX (ser 139, catalog no. 07-164 Upstate Biotechnology; rabbit, 1/100 dilution) [10,23,55]. Microscopy was carried out using a Nikon 90i Fluorescence Microscope (Tokyo, Japan). Image capture, image analysis and processing were conducted using NIS-Elements-F software (Nikon, Tokyo, Japan). Image deconvolution was carried out using the function "Mexican hat". This allows better discrimination of the signals. This function performs filtration on the intensity component (or on every selected component - when working with multichannel images) of an image using convolution with 5×5 kernel. Mexican Hat kernel is defined as a combination of Laplacian kernel and Gaussian kernel it marks edges and also reduces noise. In double-staining experiments the level of chance overlap of foci was assessed using the misorientation method whereby one of the two images is rotated through180 degrees following which colocalizing foci are counted as previously described [56].

Electron microscopy and immunogold labeling was performed as previously described [36,57] except for the modified *Atasy3* chromosome spread protocol where the detergent was Triton X-100 0.1%+Lipsol 0.05% and the digestion time was increased to 7 min.

Chiasma counts were carried out as previously described [58]. Chromosome spread preparations from PMCs at metaphase I were examined by light microscopy after fluorescence *in situ* hybridization (FISH) using 45S and 5S rDNA probes. The use of FISH enabled the identification of individual chromosomes. The overall shape of individual bivalents allowed the number and position of individual chiasmata to be determined and this was also informed by the position of the FISH signals.

Statistical procedures

The statistical procedures were carried out as described previously [23].

Proteomic analysis of Brassica meiocytes

AtASY3 peptides were initially identified in meiocyte extracts prepared from *Brassica oleracaea var. alboglabra* A12DHd as previously described [14]. Co-IP experiments were conducted on meiocytes extracted from the same material. Protein extraction was under non-denaturing conditions at 4°C. Briefly, tissue was powdered by grinding in liquid nitrogen, resuspended in IP Buffer (20 mM Tris-HCl pH 7.5, 150 mM NaCl, 10% glycerol, 2 mM EDTA, 0.1% NP40, protease inhibitor cocktail (Roche, #11836170001), phosphatase inhibitor (Thermo Scientific #78420)) and cell debris removed by centrifugation. Protein extracts were used immediately. Antibodies were cross-linked to Affi-Prep Protein A beads (Bio-Rad, #156-0006) using DMP (Sigma #D8388) and pre-eluted with glycine to remove any non-cross-linked antibody. Meiocyte extracts were pre-cleared by incubation with non-specific IgG. Parallel Co-IPs were carried out using affinity purified anti-AtASY1 antibody and an unrelated antibody as a control. Following washing to remove non-specific proteins, bound proteins were glycine-eluted, trypsin-digested and analysed on an LTQ-Orbitrap Velos mass spectrometer (Thermo Fisher Scientific). Since a complete sequence of the *Brassica oleracea* genome is currently unavailable, protein identification was carried out against a combined *Brassica rapa/napus/oleracea* database, downloaded from NCBI (http://www.ncbi.nlm.nih.gov) in 2010, into which the BoASY1 and BoASY3 full-length sequences had been manually inserted. For details of the MS analysis see Figure S9B.

Yeast 2-hybrid analysis

Yeast two-hybrid screens were performed according to the Yeastmaker Yeast transformation System 2 manual (Clontech, USA). Briefly, Y2HGold yeast cells were co-transformed with pGADT7 and pGBKT7 using the polyethylene glycol/lithium acetate method. The co-transformed yeasts were grown in SD -Leu/-Trp, SD -Leu/-Trp/-His and SD -Leu/-Trp/-His/-Ade for testing protein-protein interaction through the activation of the two reporter genes *His3* and *Ade2*. The strength of the interaction was assayed by drop test using serial dilutions of mid-exponential-phase cultures. 3 µl drops of undiluted, 10- and 100-fold diluted culture were spotted on the selective agar medium and incubated at 30°C for 2 days. Details of the primers used for plasmid construction are shown in Table S2. Plasmid constructs are as shown in Figure 6.

Supporting Information

Figure S1 A. Peptides from *Brassica oleracea* meiocytes with homology to gene At2g46980 *(AtASY3)* identified by mass spectrometry. Peptides were identified in two independent experiments using the procedure described in Sanchez-Moran *et al.*, 2005 Cytogenet and Genome Res. 109:181–189 [14]. The *Arabidopsis* TAIR database was used for peptide identification. B. (i) Diagrammatic representation of the 793 aa, 88 kDa AtASY3

protein indicating the relative position of the putative coiled-coil domain (black box). (ii) Map of the ~3.5 kb At2g46980 locus showing the exon/intron organization of *AtASY3*. The exons are represented by numbered black boxes. The triangles indicate the T-DNA insertion sites in *Atasy3-1*, *Atasy3-2* and *Atasy3-3*. C. Expression analysis of *AtASY3* using semi-quantitative RT-PCR indicates that in wild-type (WT) expression is highest in bud tissue (B) with a low level present in open flowers (F). Expression is not detected in stem (S) or leaf (L). *AtASY3* expression is absent in the *Atasy3-1*, *Atasy3-2* and *Atasy3-3* mutants. *AtGAPD* was used as an expression control.
(PDF)

Figure S2 Nucleotide sequencing of the T-DNA insertion sites in *Atasy3-1*, *Atasy3-2* and *Atasy3-3*.
(PDF)

Figure S3 A. Fertility in *Atasy3-1* is reduced compared to wild-type Col 0. (A) wild-type, (B) *Atasy3-1*, (C) wild-type silique, (D) *Atasy3-1* silique. Bar 10 mm. *Atasy3-1* exhibited a reduction in mean silique length of 37% (n = 50) and a reduction in seed-set of 73% (n = 50). B. Representative meiotic stages of *Atasy3-2* (A–F) and *Atasy3-3* (G–L). Leptotene (A,G); pachytene (B,H); diakinesis (C,I); metaphase (D,J); dyad (E,K) tetrad (F,L). Bar, 10 μm. C. An allelism test was carried out by reciprocally crossing heterozygous *Atasy3-1* and *Atasy3-2*. Cytological analysis of *Atasy3-1/Atasy3-2* reveals asynapsis at pachytene (A) and univalents in metaphase I (B). This leads to mis-segregation at meiotic divisions resulting in the subsequent formation of unbalanced tetrads (C). Bar, 10 μm. Fertility in an *Atasy3-1* complementation line (F) was restored to the normal level observed in wild-type (D) in contrast to that of *Atasy3-1* (E). Bar, 10 mm. Cytological analysis confirmed that normal meiosis was restored in the *Atasy3-1* complementation line. Homologous chromosomes underwent normal synapsis in pachytene (G). A full complement of five bivalents was observed in metaphase I (H). These underwent normal segregation leading to the formation of balanced tetrads (I). Bar, 10 μm.
(PDF)

Figure S4 A. Chromosome spread preparations from PMCs at metaphase I were examined by light microscopy after fluorescence *in situ* hybridization (FISH) using 45S (green) and 5S (red) rDNA probes. The use of FISH enabled the identification of individual chromosomes. The overall shape of individual bivalents allowed the number and position of individual chiasmata to be determined and this was also informed by the position of the FISH signals. For full details of the chiasma scoring procedure see: Sanchez-Moran *et al.* (2002) Genetics 162: 1415–1422 [58]. Analyses of metaphase I nuclei of wild-type (A) a-b. Rod bivalents, single interstitial chiasma in the long arm Chr. 2 and Chr. 4 respectively; c-e. Ring-bivalents, 2 chiasmata Chr. 1, Chr 5 and Chr.3 respectively. *Atasy3-1* (B) a. Chr. 5 rod bivalent distal chiasma; b. Chr. 1 rod bivalent distal chiasma, c. Chr. 4 rod bivalent single short arm chiasma. Analysis indicated that mean chiasma frequency in *Atasy3-1* was significantly reduced to 3.40 in contrast to wild-type, which had an overall mean chiasma frequency of 9.84. Bar, 10 μm. B. Cytological analyses of metaphase I chromosome spreads indicated the presence of univalents in *Atasy3-1/Atspo11-1-4* (A). No chiasmata were observed in this double mutant in contrast to wild-type (B), where five bivalents were observed in all of the metaphase I cells analysed. This confirms that the chiasmata in *Atasy3-1* are DSB-dependent. Comparison of the mean chiasma frequency of *Atasy3-1/Atasy1* (C) and *Atasy1* (D) revealed no significant difference between the double mutant and the latter suggesting a close functional relationship between AtASY3 and AtASY1. Analysis of 30 metaphase I nuclei from *Atasy3-1/Atmsh4*

(E) shows that the double mutant fails to form chiasmata in contrast to *Atmsh4* (F), in which a mean chiasma frequency of 1.1 (n = 30) was observed. Bar, 10 μm.
(PDF)

Figure S5 Immunolocalization of recombination proteins in *Atasy3-1* and γH2AX *in Atasy1*. Immunolocalization of AtRAD51 (red) on DAPI stained (blue) wild-type (A) and *Atasy3-1*(B) meiocytes at early prophase I. (C) and (D) show corresponding images for AtMSH4. In both cases there is a reduction in foci in the *Atasy3-1* mutant. Immunolocalization of γH2AX (red) on DAPI stained (blue) meiocytes from wild-type (E) and *Atasy1* (F). *(see main text for details). Bar*, 10 μm.
(PDF)

Figure S6 Time-course analysis of AtDMC1 (red) localization in wild-type (WT), *Atasy1* and *Atasy3-1*. The study revealed that AtDMC1 foci in *Atasy3-1* are stabilized and persist at least up to 24 h post BrdU (green) pulse-labeling at S phase before gradually decreasing to very low numbers by 30 h. This observation was similar to that in WT but contrast with that of *Atasy1*, where AtDMC1 foci are destabilized soon after loading and their numbers decrease rapidly at ~18 h. Almost all of AtDMC1 foci in *Atasy1* were lost by 24 h post BrdU pulse labeling as previously reported by Sanchez-Moran *et al.* 2007 [8].
(PDF)

Figure S7 Sequence alignment of AtASY3 and BoASY3. The proteins exhibit 77% sequence identity.
(PDF)

Figure S8 Immunolocalization of BoASY3 protein using anti-AtASY3 antibody to wild-type *Brassica oleracea* chromosome spread preparations from meiocytes at leptotene, zygotene and pachytene. The BoASY3 protein localises to meiotic chromosomes as numerous foci in leptotene and gradually polymerizes to form a continuous linear signal by pachytene. The localisation of BoASY3 is indistinguishable to that of AtASY3 in *Arabidopsis*. BoASY3 could not be detected using pre-immune anti-AtASY1 antiserum. Bar, 10 μm.
(PDF)

Figure S9 A. BoASY3 sequence showing protein coverage following co-immunoprecipitation with BoASY1 and MS analysis (highlighted yellow). B. Mass spectrometry conditions.
(PDF)

Table S1 Chiasma counts for *Atasy3-1* and wild-type. A. *Atasy3-1* mean chiasma frequency 3.3 (n = 50). Proportion of distal chiasma = 74.8%. B. *Arabidopsis* (Col-0) wild-type mean chiasma frequency 9.76 (n = 50). Proportion of distal chiasma = 73.8%. The proportion of distal chiasmata is not significantly different in the mutant.
(PDF)

Table S2 Primer sequences used during the study. Primers 1–8 were used for confirming T-DNA insertions sites; primers 9–12 were used for the analysis of *AtASY3* expression; Primers 13 and 14 were used for complementation studies; primers 15 and 16 were used for the production of recombinant AtASY3 for antibody production. Primers 17–22 were for yeast two-hybrid studies. The regions amplified are indicated; F/R denotes forward and reverse.
(PDF)

Acknowledgments

Author Contributions

References

1. Keeney S, Giroux CN, Kleckner N (1997) Meiosis-specific DNA double-strand breaks are catalyzed by Spo11, a member of a widely conserved protein family. Cell 88: 375–384.
2. Neale MJ, Keeney S (2006) Clarifying the mechanics of DNA strand exchange in meiotic recombination. Nature 442: 153–158.
3. Kleckner N (2006) Chiasma formation: chromatin/axis interplay and the role(s) of the synaptonemal complex. Chromosoma 115: 175–194.
4. Kim KP, Weiner BM, Zhang LR, Jordan A, Dekker J, et al. (2010) Sister Cohesion and Structural Axis Components Mediate Homolog Bias of Meiotic Recombination. Cell 143: 924–937.
5. Caryl AP, Armstrong SJ, Jones GH, Franklin FCH (2000) A homologue of the yeast HOP1 gene is inactivated in the Arabidopsis meiotic mutant asy1. Chromosoma 109: 62–71.
6. Shin YH, Choi Y, Erdin SU, Yatsenko SA, Kloc M, et al. (2010) Hormad1 Mutation Disrupts Synaptonemal Complex Formation, Recombination, and Chromosome Segregation in Mammalian Meiosis. Plos Genetics 6.
7. Wojtasz L, Daniel K, Roig I, Bolcun-Filas E, Xu HL, et al. (2009) Mouse HORMAD1 and HORMAD2, Two Conserved Meiotic Chromosomal Proteins, Are Depleted from Synapsed Chromosome Axes with the Help of TRIP13 AAA-ATPase. Plos Genetics 5.
8. Sanchez-Moran E, Santos JL, Jones GH, Franklin FCH (2007) ASY1 mediates AtDMC1-dependent interhomolog recombination during meiosis in Arabidopsis. Genes & Development 21: 2220–2233.
9. Borner GV, Kleckner N, Hunter N (2004) Crossover/noncrossover differentiation, synaptonemal complex formation, and regulatory surveillance at the leptotene/zygotene transition of meiosis. Cell 117: 29–45.
10. Higgins JD, Sanchez-Moran E, Armstrong SJ, Jones GH, Franklin FCH (2005) The Arabidopsis synaptonemal complex protein ZYP1 is required for chromosome synapsis and normal fidelity of crossing over. Genes Dev 19: 2488–2500.
11. Wang M, Wang KJ, Tang D, Wei CX, Li M, et al. (2010) The Central Element Protein ZEP1 of the Synaptonemal Complex Regulates the Number of Crossovers during Meiosis in Rice. Plant Cell 22: 417–430.
12. Storlazzi A, Gargano S, Ruprich-Robert G, Falque M, David M, et al. (2010) Recombination Proteins Mediate Meiotic Spatial Chromosome Organization and Pairing. Cell 141: 94–106.
13. Page SL, Hawley RS (2004) The genetics and molecular biology of the synaptonemal complex. Annual Review of Cell and Developmental Biology 20: 525–558.
14. Sanchez-Moran E, Mercier R, Higgins JD, Armstrong SJ, Jones GH, et al. (2005) A strategy to investigate the plant meiotic proteome. Cytogenet Genome Res 109: 181–189.
15. de los Santos T, Hollingsworth NM (1999) Red1p, a MEK1-dependent phosphoprotein that physically interacts with Hop1p during meiosis in yeast. Journal of Biological Chemistry 274: 1783–1790.
16. Thompson EA, Roeder GS (1989) Expression and DNA sequence of RED1, a gene required for meiosis I chromosome segregation in yeast. Molecular & General Genetics 218: 293–301.
17. Wang KJ, Wang M, Tang D, Shen Y, Qin BX, et al. (2011) PAIR3, an axis-associated protein, is essential for the recruitment of recombination elements onto meiotic chromosomes in rice. Molecular Biology of the Cell 22: 12–19.
18. Yuan WY, Li XW, Chang YX, Wen RY, Chen GX, et al. (2009) Mutation of the rice gene PAIR3 results in lack of bivalent formation in meiosis. Plant Journal 59: 303–315.
19. Siaud N, Dray E, Gy I, Gerard E, Takvorian N, et al. (2004) Brca2 is involved in meiosis in Arabidopsis thaliana as suggested by its interaction with Dmc1. Embo Journal 23: 1392–1401.
20. Bai XF, Peirson BN, Dong FG, Xue C, Makaroff CA (1999) Isolation and characterization of SYN1, a RAD21-like gene essential for meiosis in Arabidopsis. Plant Cell 11: 417–430.
21. Lam WS, Yang XH, Makaroff CA (2005) Characterization of Arabidopsis thaliana SMC1 and SMC3: evidence that AtSMC3 may function beyond chromosome cohesion. Journal of Cell Science 118: 3037–3048.
22. Smith AV, Roeder GS (1997) The yeast Red1 protein localizes to the cores of meiotic chromosomes. Journal of Cell Biology 136: 957–967.
23. Higgins JD, Armstrong SJ, Franklin FCH, Jones GH (2004) The Arabidopsis MutS homolog AtMSH4 functions at an early step in recombination: evidence for two classes of recombination in Arabidopsis. Genes & Development 18: 2557–2570.
24. Rockmill B, Roeder GS (1990) Meiosis in asynaptic yeast. Genetics 126: 563–574.
25. Osman K, Higgins JD, Sanchez-Moran E, Armstrong SJ, Franklin FCH (2011) Pathways to meiotic recombination in Arabidopsis thaliana. New Phytologist 190: 523–544.
26. Copenhaver GP, Housworth EA, Stahl FW (2002) Crossover interference in Arabidopsis. Genetics 160: 1631–1639.
27. Higgins JD, Buckling EF, Franklin FCH, Jones GH (2008) Expression and functional analysis of AtMUS81 in Arabidopsis meiosis reveals a role in the second pathway of crossing-over. Plant Journal 54: 152–162.
28. Paull TT, Rogakou EP, Yamazaki V, Kirchgessner CU, Gellert M, et al. (2000) A critical role for histone H2AX in recruitment of repair factors to nuclear foci after DNA damage. Current Biology 10: 886–895.
29. Rogakou E, Pilch D, Orr A, Ivanova U, Bonner W (1998) DNA double-stranded breaks induce histone H2AX phophorylation on serine 139. J Biol Chem 273: 5858–5868.
30. Shroff R, Arbel-Eden A, Pilch D, Ira G, Bonner WM, et al. (2004) Distribution and dynamics of chromatin modification induced by a defined DNA double-strand break. Current Biology 14: 1703–1711.
31. Klimyuk VI, Jones JDG (1997) AtDMC1, the Arabidopsis homologue of the yeast DMC1 gene: Characterization, transposon-induced allelic variation and meiosis-associated expression. Plant Journal 11: 1–14.
32. Li WX, Chen CB, Markmann-Mulisch U, Timofejeva L, Schmelzer E, et al. (2004) The Arabidopsis AtRAD51 gene is dispensable for vegetative development but required for meiosis. Proceedings of the National Academy of Sciences of the United States of America 101: 10596–10601.
33. Jackson N, Sanchez-Moran E, Buckling E, Armstrong SJ, Jones GH, et al. (2006) Reduced meiotic crossovers and delayed prophase I progression in AtMLH3-deficient Arabidopsis. Embo Journal 25: 1315–1323.
34. Blat Y, Protacio RU, Hunter N, Kleckner N (2002) Physical and Functional Interactions among Basic Chromosome Organizational Features Govern Early Steps of Meiotic Chiasma Formation. Cell 111: 791–802.
35. Panizza S, Mendoza MA, Berlinger M, Huang L, Nicolas A, et al. (2011) Spo11-Accessory Proteins Link Double-Strand Break Sites to the Chromosome Axis in Early Meiotic Recombination. Cell 146: 372–383.
36. Armstrong SJ, Caryl AP, Jones GH, Franklin FC (2002) Asy1, a protein required for meiotic chromosome synapsis, localizes to axis-associated chromatin in Arabidopsis and Brassica. J Cell Sci 115: 3645–3655.
37. Dobson MJ, Pearlman RE, Karaiskakis A, Spyropoulos B, Moens PB (1994) Synaptonemal complex proteins: occurrence, epitope mapping and chromosome disjunction. Journal of Cell Science 107: 2749–2760.
38. Lammers JHM, Offenberg HH, Vanaalderen M, Vink ACG, Dietrich AJJ, et al. (1994) The gene encoding a major component of the lateral elements of synaptonemal complexes of the rat is related to X-linked lymphocyte-regulated genes. Molecular and Cellular Biology 14: 1137–1146.
39. Carpenter ATC (1975) Electron-microscopy of meiosis in Drosophila melanogaster females: II: The recombination nodule - a recombination-associated structure at pachytene? Proceedings of the National Academy of Sciences of the United States of America 72: 3186–3189.
40. MaoDraayer Y, Galbraith AM, Pittman DL, Cool M, Malone RE (1996) Analysis of meiotic recombination pathways in the yeast Saccharomyces cerevisiae. Genetics 144: 71–86.
41. Schwacha A, Kleckner N (1997) Interhomolog bias during meiotic recombination: Meiotic functions promote a highly differentiated interhomolog-only pathway. Cell 90: 1123–1135.
42. Xu LH, Weiner BM, Kleckner N (1997) Meiotic cells monitor the status of the interhomolog recombination complex. Genes & Development 11: 106–118.
43. Pradillo M, Lopez E, Romero C, Sanchez-Moran E, Cunado N, et al. (2007) An analysis of univalent segregation in meiotic mutants of Arabidopsis thaliana: A possible role for synaptonemal complex. Genetics 175: 505–511.
44. Schwacha A, Kleckner N (1994) Identification of joint molecules that form frequently between hmologs but rarely between sister chromatids during yeast meiosis. Cell 76: 51–63.
45. Daniel K, Lange J, Hached K, Fu J, Anastassiadis K, et al. Meiotic homologue alignment and its quality surveillance are controlled by mouse HORMAD1. Nature Cell Biology 13: 599–U232.
46. Woltering D, Baumgartner B, Bagchi S, Larkin B, Loidl J, et al. (2000) Meiotic segregation, synapsis, and recombination checkpoint functions require physical interaction between the chromosomal proteins Red1p and Hop1p. Molecular and Cellular Biology 20: 6646–6658.
47. Armstrong SJ, Jones GH (2001) Female meiosis in wild-type Arabidopsis thaliana and in two meiotic mutants. Sexual Plant Reproduction 13: 177–183.
48. Ross KJ, Fransz P, Armstrong SJ, Vizir I, Mulligan B, et al. (1997) Cytological characterization of four meiotic mutants of Arabidopsis isolated from T-DNA_transformed lines. Chromosome res 5: 551–559.
49. Boerner GV, Barot A, Kleckner N (2008) Yeast Pch2 promotes domainal axis organization, timely recombination progression, and arrest of defective recombinosomes during meiosis. Proceedings of the National Academy of Sciences of the United States of America 105: 3327–3332.
50. Joshi N, Barot A, Jamison C, Boerner GV (2009) Pch2 Links Chromosome Axis Remodeling at Future Crossover Sites and Crossover Distribution during Yeast Meiosis. Plos Genetics 5.

51. Boerner GV, Kleckner N, Hunter N (2004) Crossover/noncrossover differentiation, synaptonemal complex formation, and regulatory surveillance at the leptotene/zygotene transition of meiosis. Cell 117: 29–45.
52. Storlazzi A, Xu LZ, Schwacha A, Kleckner N (1996) Synaptonemal complex (SC) component Zip1 plays a role in meiotic recombination independent of SC polymerization along the chromosomes. Proceedings of the National Academy of Sciences of the United States of America 93: 9043–9048.
53. Alonso JM (2003) Genome-wide insertional mutagenesis of Arabidopsis thaliana (vol 301, pg 653, 2003). Science 301: 1849–1849.
54. Chen Z, Higgins JD, Hui JTL, Li J, Franklin FCH, et al. (2011) Retinoblastoma protein is essential for early meiotic events in Arabidopsis. Embo Journal 30: 744–755.
55. Mercier R, Armstrong SJ, Horlow C, Jackson NP, Makaroff CA, et al. (2003) The meiotic protein SWI1 is required for axial element formation and recombination initiation in Arabidopsis. Development 130: 3309–3318.
56. Gasior SL, Wong AK, Kora Y, Shinohara A, Bishop DK (1998) Rad52 associates with RPA and functions with Rad55 and Rad57 to assemble meiotic recombination complexes. Genes & Development 12: 2208–2221.
57. Lopez E, Pradillo M, Romero C, Santos JL, Cunado N (2008) Pairing and synapsis in wild type Arabidopsis thaliana. Chromosome Research 16: 701–708.
58. Sanchez-Moran E, Armstrong SJ, Santos JL, Franklin FCH, Jones GH (2002) Variation in chiasma frequency among eight accessions of Arabidopsis thaliana. Genetics 162: 1415–1422.